

**CHIRALITY TRANSFER IN 5-*EXO* CYCLIZATIONS
OF AXIALLY CHIRAL *O*-IODOANILIDES**

by

Andre J. B. Lapierre

B. Sc., McMaster University, 2000

Submitted to the Graduate Faculty of
Arts and Sciences in partial fulfillment
of the requirements for the degree of
Doctor of Philosophy

University of Pittsburgh

2005

UNIVERSITY OF PITTSBURGH
FACULTY OF ARTS AND SCIENCES

This dissertation was presented

by

Andre J. B. Lapierre

It was defended on

December 6th, 2005

and approved by

Dr. Kay Brummond

Dr. Theodore Cohen

Dr. Michael Mokotoff

Dr. Dennis Curran
Dissertation Director

To my wife and family,

CHIRALITY TRANSFER IN 5-EXO CYCLIZATIONS OF AXIALLY CHIRAL *O*-IODOANILIDES

Andre J. B. Lapierre, Ph.D.

University of Pittsburgh, 2005

Stereoselective 5-*exo* radical and Heck cyclizations of axially chiral *o*-iodoanilides to enantioenriched oxindoles and dihydroindolones are described. Mechanisms for the transfer of chirality from the atropisomeric anilides to the newly formed stereocenters in the cyclic products are proposed and supported with physical data. Additionally, the N-aryl bond rotation barriers for eight *o*-iodoanilides are reported.

A series of axially chiral *N*-allyl-*o*-iodoanilides were cyclized under room temperature radical conditions to dihydroindolones with good to excellent chirality transfer (74–97 %). Cyclization rate constant data is presented to rationalize the regioselective preference for *N*-allyl over *N*-acryloyl cyclization when an *o*-methyl group is present. X-ray crystallography was used to assign absolute configurations to a cyclization precursor/product pair. Radical 5-*exo* cyclizations of axially chiral *o*-iodoanilides bearing branched, bulky *N*-substituents are covered. The bulkiness of *N*-substituents permitted the resolution of a series of novel *o*-iodoanilides lacking a second *ortho* substituent. Radical cyclizations of these *o*-iodoanilides transferred this transient axial chirality into a new stereocenter in the oxindole products with high fidelity (78–92 %). The first Heck cyclizations of axially chiral *o*-iodoanilides with chirality transfer (84–89 %) are described. X-ray crystallographic data is presented for one anilide cyclization precursor with studies to elucidate the mechanism of chiral transfer.

TABLE OF CONTENTS

PREFACE	xvi
1. AXIALLY CHIRAL ANILIDES	1
1.1. Axial Chirality	1
1.2. Stereochemical Designations of Axially Chiral Groups	2
1.3. Atropisomerism.....	2
1.4. Tertiary Anilide Conformers	3
1.4.1. Restricted N-CO Bond Rotation	3
1.4.2. Tertiary Anilides E/Z Preferences.....	4
1.5. Restricted N-Aryl Bond Rotation	5
1.6. Synthetic Approaches to Enantioenriched Axially Chiral Anilides (Stoichiometric)	6
1.7. Synthetic Approaches to Enantioenriched Axially Chiral Anilides (Catalytic)	9
1.8. Chromatographic Access to Enantioenriched Axially Chiral Anilides.....	10
2. MEMORY OF CHIRALITY	12
2.1. Background.....	12
2.2. Memory of Chirality in Radical Chemistry	14
2.3. Chirality Transfer in Radical Cyclizations of Axially Chiral Acrylanilides	17
3. RADICAL CYCLIZATIONS OF AXIALLY CHIRAL <i>N</i>-ALLYL-<i>O</i>-IODOANILIDES 20	
3.1. Introduction.....	20
3.2. Precursor and Product Preparation.....	22
3.3. Resolution and Rotation Barriers of Precursors.....	23
3.4. Chirality Transfer in Radical Cyclizations of <i>N</i> -Allyl- <i>o</i> -Iodoanilides.....	26
3.5. Determination of Absolute Configuration.....	28
3.6. Preliminary Model of Chirality Transfer.....	30
3.7. Regioselectivity, Competitive Cyclizations.....	32
3.8. Cyclization Rate Constant Measurements	35
3.9. Conclusions.....	37
4. RELAYING ASYMMETRY OF TRANSIENT ATROPISOMERS OF <i>O</i>-IODOANILIDES	38
4.1. Background.....	38
4.2. Resolution of Chiral Auxiliary-based Atropisomers.....	41
4.3. Enantiomeric Series.....	46
4.4. Determination of Absolute Configuration of Cyclization Precursors and Products.....	50
4.5. Conclusion	53
5. ASYMMETRIC HECK-MIZOROKI CYCLIZATIONS OF <i>O</i>-IODOANILIDES ATROPISOMERS	54
5.1. Introduction.....	54
5.2. Heck-Mizoroki Reaction	55

5.3.	Precursor Preparation, Resolution.....	58
5.4.	Chirality Transfer in Heck Cyclizations.....	61
5.5.	Synthesis of Second Generation Precursor.....	64
5.6.	Racemic Synthesis of Esermethole.....	65
5.7.	Resolution and Recrystallization of Second Generation Precursor.....	66
5.8.	Stereochemistry.....	70
5.9.	Conclusion.....	71
6.	EXPERIMENTAL	72
6.1.	General Information.....	72
6.2.	General Procedures.....	74
6.2.1.	General procedure for acylation of anilines (I).....	74
6.2.2.	General procedure for N-allylation of anilides (II).....	74
6.2.3.	General procedure for thermally initiated radical cyclization of anilides (III).....	75
6.2.4.	General procedure for Et ₃ B initiated radical cyclization of N-allyl anilides (IV) ...	75
6.2.5.	General procedure for Et ₃ B initiated radical cyclizations of acrylanilides (V).....	76
6.3.	Compound Data for Chapter 3.....	76
6.3.1.	<i>N</i> -(2-Iodo-4,6-dimethylphenyl)benzamide (not shown in text):.....	76
6.3.2.	<i>N</i> -(2-Iodo-4,6-dimethylphenyl)-4-bromobenzamide (not shown in text):.....	77
6.3.3.	<i>N</i> -(2-Iodo-4,6-dimethylphenyl)-2-phenylacetamide (not shown in text):.....	77
6.3.4.	<i>N</i> -(2-Iodo-4,6-dimethylphenyl)-3-phenylpropionamide (not shown in text):.....	78
6.3.5.	<i>rac-N</i> -Allyl- <i>N</i> -(2-iodo-4,6-dimethylphenyl)benzamide (56a):.....	78
6.3.6.	<i>rac-N</i> -(2-Iodo-4,6-dimethylphenyl)- <i>N</i> -(3-methylbut-2-enyl)-4-bromobenzamide (56b):	79
6.3.7.	<i>rac-N</i> -Allyl- <i>N</i> -(2-iodo-4,6-dimethylphenyl)-2-phenylacetamide (56c):.....	80
6.3.8.	<i>rac-N</i> -(2-Iodo-4,6-dimethylphenyl)- <i>N</i> -(3-phenylallyl)-2-phenylacetamide (56d):..	81
6.3.9.	<i>rac-N</i> -But-2 <i>E</i> -enyl- <i>N</i> -(2-iodo-4,6-dimethylphenyl)-2-phenylacetamide (56e):.....	81
6.3.10.	<i>rac-N</i> -(2-Iodo-4,6-dimethylphenyl)- <i>N</i> -(3-methylbut-2-enyl)-2-phenylacetamide (56f):	82
6.3.11.	<i>rac-N</i> -Allyl- <i>N</i> -(2-iodo-4,6-dimethylphenyl)-3-phenylpropionamide (56g):.....	83
6.3.12.	<i>rac-N</i> -Allyl- <i>N</i> -(2-iodo-4,6-dimethylphenyl)- <i>trans</i> -crotonamide (56h):.....	84
6.3.13.	Phenyl-(3,5,7-trimethyl-2,3-dihydroindol-1-yl)methanone (57a):.....	84
6.3.14.	(4-Bromophenyl)-(3-isopropyl-5,7-dimethyl-2,3-dihydroindol-1-yl)methanone (57b):	85
6.3.15.	1-(3-5,7-Trimethyl-2,3-dihydroindol-1-yl)-2-phenylethanone (57c):.....	86
6.3.16.	1-(3-Benzyl-5,7-dimethyl-2,3-dihydroindol-1-yl)-2-phenylethanone (57d):.....	86
6.3.17.	1-(3-Ethyl-5,7-dimethyl-2,3-dihydroindol-1-yl)-2-phenylethanone (57e):.....	87
6.3.18.	1-(3-Isopropyl-5,7-dimethyl-2,3-dihydroindol-1-yl)-2-phenylethanone (57f):.....	88
6.3.19.	1-(3-Methyl-5,7-dimethyl-2,3-dihydroindol-1-yl)-3-phenylpropanone (57g):.....	88
6.3.20.	1-(3-Methyl-5,7-dimethyl-2,3-dihydroindol-1-yl)but-2-enone (57h):.....	89
6.3.21.	<i>rac-N</i> -Allyl- <i>N</i> -(2-iodophenyl)- <i>trans</i> -crotonamide (71b-1):.....	90
6.3.22.	<i>N</i> -Allyl-2-iodo-4,6-dimethylaniline (75):.....	90
6.3.23.	3,5,7-Trimethyl-2,3-dihydroindole (76):.....	91
6.4.	Compound Data for Chapter 4.....	92
6.4.1.	<i>N</i> -Cyclohexyl- <i>p</i> -toluidine (108):.....	92
6.4.2.	<i>N</i> -Cyclohexyl-2-iodo-4-methylaniline (not shown in text):.....	93
6.4.3.	<i>N</i> -Cyclohexyl- <i>N</i> -(2-iodo-4-methylphenyl)-but-2 <i>E</i> -enamide (<i>rac</i> -109):.....	93

6.4.4.	(2-Iodophenyl)-isopropylamine (111):.....	94
6.4.5.	<i>N</i> -(2-Iodophenyl)- <i>N</i> -isopropylacrylamide (<i>rac</i> -112):	95
6.4.6.	3-Ethyl-1-cyclohexyl-5-methyl-1,3-dihydroindol-2-one (114):	96
6.4.7.	3-Methyl-1-isopropyl-1,3-dihydroindolin-2-one (115):.....	97
6.5.	Compound Data for Chapter 5.....	97
6.5.1.	<i>N</i> -(2-Iodo-4,6-dimethylphenyl)-2-methyl-2 <i>E</i> -butenamide (153a):.....	97
6.5.2.	<i>N</i> -(2-Iodo-4,6-dimethylphenyl)- <i>N</i> ,2-dimethyl-2 <i>E</i> -butenamide (154a):	98
6.5.3.	<i>N</i> -(2-Bromo-4,6-dimethylphenyl)- <i>N</i> ,2-dimethyl-2 <i>E</i> -butenamide (154b):	99
6.5.4.	<i>N</i> -(2-Iodo-4-methyl-6-trimethylsilylphenyl)- <i>N</i> ,2-dimethyl-2 <i>E</i> -butenamide (<i>rac</i> -156a): 100	
6.5.5.	4-Bromo-2,6-diiodoaniline (not shown in text):	101
6.5.6.	4-Bromo-2,6-diiodo- <i>N,N</i> -bis(trimethylsilyl)aniline (158):	101
6.5.7.	4-Bromo-2-iodo- <i>N</i> -methyl- <i>N</i> ,6-bis-(trimethylsilyl)aniline (not shown in text): ...	102
6.5.8.	<i>N</i> -(4-Bromo-2-iodo-6-trimethylsilylphenyl)- <i>N</i> ,2-dimethyl-2 <i>E</i> -butenamide (<i>rac</i> -156b): 103	
6.5.9.	1,3,5,7-Tetramethyl-1-vinyl-1,3-dihydroindol-2-one (<i>rac</i> -159):.....	104
6.5.10.	Methyl 4-(<i>tert</i> -butyldiphenylsilyloxy)-2-methylbut-2 <i>E</i> -enoate (not shown in text): 105	
6.5.11.	4-Bromo-2-chloroaniline (166):.....	105
6.5.12.	4-Bromo-2-chloro-6-iodoaniline (167):.....	106
6.5.13.	<i>N</i> -(4-Bromo-2-chloro-6-iodophenyl)-4-(<i>tert</i> -butyldiphenylsilyloxy)- <i>N</i> ,2-methylbut-2 <i>E</i> -enamide (169):.....	107
6.5.14.	<i>N</i> -(4-Bromo-2-chloro-6-iodophenyl)-4-(<i>tert</i> -butyldiphenylsilyloxy)- <i>N</i> ,2-dimethylbut-2 <i>E</i> -enamide (164):.....	108
6.5.15.	(<i>S</i>)-5-Bromo-3-(2-(<i>tert</i> -butyldiphenylsilyloxy)vinyl)-7-chloro-1,3-dimethylindolin-2-one (170):	109
6.5.16.	(<i>S</i>)-5-Bromo-7-chloro-1,2-dihydro-3-(2-oxoethyl)-1,3-dimethyl-2-oxo-[3 <i>H</i>]indole (163): 110	
6.5.17.	(3 <i>aS-cis</i>)-5-Bromo-7-chloro-1,3 <i>a</i> ,8-trimethyl-1,2,3,3 <i>a</i> ,8,8 <i>a</i> -hexahydro-pyrrolo[2,3- <i>b</i>]indole (<i>S-cis</i> -171):	111
6.5.18.	(<i>rac-cis</i>)-7-Chloro-5-methoxy-1,3 <i>a</i> ,8-trimethyl-1,2,3,3 <i>a</i> ,8,8 <i>a</i> -hexahydro-pyrrolo[2,3- <i>b</i>]indole (not shown in text):.....	112
6.5.19.	<i>rac</i> -esermethole (<i>rac</i> -162):	113
6.6.	Resolution of Compounds by Chiral HPLC	113
6.6.1.	Analytical method	113
6.6.2.	Semi-preparative method.....	114
6.7.	Measurement of <i>N</i> -Aryl Bond Rotation Barriers.....	114
6.7.1.	General Procedure for <i>N</i> -Aryl Bond Rotation Barrier Measurement	114
6.8.	Rate Constant Studies.....	118
7.	SUPPLEMENTARY DATA	121
7.1.	Select ¹ H and ¹³ C NMR.....	121
7.2.	X-ray Crystallography Data.....	210
	APPENDIX	246
	BIBLIOGRAPHY	249

LIST OF TABLES

Table 3-1 - Preparation of Cyclization Substrates.....	23
Table 3-2 - Thermal Equilibration Data for 56b	24
Table 3-3 - Summary of Radical Cyclizations of Anilides 56a-g	28
Table 4-1 - Diastereoselective Cyclizations of o-Iodoacrylanilide 96	43
Table 4-2 - Diastereoselective Cyclizations of o-Iodoacrylanilide 103	46
Table 4-3 - Summary of Radical Cyclizations of 109 and 112.....	50
Table 5-1 - Summary of Heck Cyclizations of Anilides Enantioenriched 154.....	63
Table 6-1 – Thermal Equilibration Data for 56b.....	115
Table 6-2 – Thermal Equilibration Data for (<i>M</i>)-56b.....	116
Table 6-3 – Thermal Equilibration Data for (<i>M</i>)-56a.....	116
Table 6-4 – Thermal Equilibration Data for (<i>M</i>)-56c.....	117
Table 6-5 – Thermal Equilibration Data for (<i>M</i>)-56g.....	117
Table 6-6 – Thermal Equilibration Data for (<i>M</i>)-109.....	117
Table 6-7 – Thermal Equilibration Data for (<i>P</i>)-112.....	118
Table 6-8 – Thermal Equilibration Data for (<i>P</i>)-154a.....	118
Table 6-9 – Thermal Equilibration Data for FEE-164.....	118
Table 6-10 - Rate Constant Data for 81	119
Table 6-11 - Rate Constant Data for 85.....	120

LIST OF EQUATIONS

Equation 3-1 - Calculation of the N-Aryl Bond Rotation Barrier of 56b	25
Equation 6-1 - Calculation of N-Aryl Bond Rotation Barrier of (<i>M</i>)-56b.....	116

LIST OF FIGURES

Figure 1.1 - Enantiomers of 2,3-Pentadiene.....	1
Figure 1.2 - Assigning Stereochemical Designations to Axially Chiral Molecules.....	2
Figure 1.3 - Atropisomeric Pair of 2,2'-Dinitro-6,6'-diphenic Acid Enantiomers.....	3
Figure 1.4 – Rotational Isomers and Resonance Structures of Tertiary Amides.....	4
Figure 1.5 - Conformers of <i>N</i> -Methylacetanilide.....	4
Figure 1.6 – The First Axially Chiral Anilide Reported.....	5
Figure 1.7 - Rotational barrier of Selected Axially Chiral Anilides.....	6
Figure 3.1 - Possible Radical Cyclizations of Axially Chiral <i>N</i> -Allyl- <i>o</i> -Iodoanilides.....	22
Figure 3.2 - Thermal Equilibration Plot for 56b.....	24
Figure 3.3 - Rotation Barriers of Four Axially Chiral Anilides 56a-c,g.....	26
Figure 3.4 - Transfer of Chirality in Axially Chiral <i>N</i> -Allyl- <i>o</i> -Iodoanilides.....	27
Figure 3.5 – ORTEP Diagrams of (<i>M</i>)-56b.....	29
Figure 3.6 – ORTEP Diagrams of (<i>R</i>)-57b.....	30
Figure 3.7 - Rationalization of Observed Stereochemistry for <i>N</i> -Allyl and <i>N</i> -Acryloyl Anilides.....	31
Figure 3.8 - Radical Cyclizations of <i>o</i> -Bromoanilides Lacking <i>ortho</i> Substituents.....	33
Figure 3.9 - Cyclization Rate Constant Measurements for 56i and 78.....	35
Figure 3.10 - Cyclization Rate Constants.....	36
Figure 3.11 - Transition State Analysis.....	37
Figure 4.1 –Radical Cyclization with Stereoselection Controlled by Chiral Auxiliary.....	39
Figure 4.2 – Radical Cyclization of Anilide 91 with Low Stereoselection.....	40
Figure 4.3 - Oxindole Natural Products.....	41
Figure 4.4 - Mechanistic Proposal.....	44
Figure 4.5 - Proposed Series Enantiomeric <i>o</i> -Iodoanilides.....	47
Figure 4.6 - ORTEP Diagram of (<i>M</i>)-112.....	51
Figure 4.7 - ORTEP Diagram of (<i>M</i>)-109.....	51
Figure 4.8 - Assignment of Absolute Configurations of 115 and 116.....	53
Figure 5.1 – Aryl Iodide as a Precursor to Radical or Heck-Mizoroki Cyclizations.....	54
Figure 5.2 - Heck Reaction Catalytic Cycle.....	55
Figure 5.3 - Proposed Cationic and Neutral Heck Pathways.....	57
Figure 5.4 - β -Hydride Elimination Leading to Loss ($R = H$) or Retention ($R \neq H$) of Chirality.....	58
Figure 5.5 - Comparison of Rotation Barriers of 46 and 154a.....	61
Figure 5.6 – Proposed Retrosynthesis of Esermethole 162.....	64
Figure 5.7 – <i>N</i> -Aryl Bond Rotation Barrier of 164.....	67
Figure 5.8 - ORTEP Diagram of Anilide <i>rac</i> -164.....	68
Figure 5.9 - Chromatogram of (<i>E</i>)-170/(<i>Z</i>)-170.....	69
Figure 5.10 - Transition State Proposals.....	71
Figure 6.1 – Thermal Equilibration of 56b.....	114
Figure 6.2 – Thermal Equilibration Plot for 56b.....	115
Figure 6.3 - Rate Constant Plot for 81.....	119
Figure 6.4 - Rate Constant Plot for 85.....	120
Figure 7.1 - ORTEP of (<i>M</i>)-56b.....	210

Figure 7.2 - ORTEP of (<i>R</i>)-57b.....	216
Figure 7.3 - ORTEP of (<i>M</i>)-109.....	223
Figure 7.4 - ORTEP of (<i>M</i>)-112.....	230
Figure 7.5 - ORTEP of <i>rac</i> -164.....	236

LIST OF SCHEMES

Scheme 1.1 - Taguchi's Chiral Pool Approach to Axially Chiral <i>o-t</i> -Butylanilides.....	7
Scheme 1.2 - Enantioenriched Anilides via Asymmetric Crystallization	8
Scheme 1.3 - Uemura's Method: Enantiotopic Lithiation of Chromium Complexes.....	9
Scheme 1.4 - Pd-catalyzed Enantioselective Allylation of Secondary Anilides.....	10
Scheme 1.5 - Taguchi's Catalytic Asymmetric N-Arylation Methodology.....	10
Scheme 1.6 – Chiral Stationary Phase of (<i>S,S</i>)-Whelk O 1 HPLC Columns.....	11
Scheme 2.1 - Marquet's Confirmation of Leuchs' Observation	12
Scheme 2.2 - Seebach's Original Observation	13
Scheme 2.3 - Fuji's Substrate Designed to Relay Chiral Information.....	14
Scheme 2.4 - Photoinduced Norrish-Yang Cyclization Demonstrates Memory of Chirality.....	15
Scheme 2.5 - Proposed Mechanism for Giese's Norrish-Yang Cyclization	16
Scheme 2.6 – Trapping of a Cyclic Radical with Retention of Configuration	17
Scheme 2.7 - Transfer of Chirality in Axially Chiral <i>o</i> -Iodoacrylanilides	19
Scheme 3.1 - An Unexpected Cyclization Result	20
Scheme 3.2 - A Possible Mechanism for the Formation of 50	21
Scheme 3.3 - Regioselectivity Reversal Affected by <i>ortho</i> Substitution	34
Scheme 3.4 - Synthesis of Authentic Sample of 57h.....	34
Scheme 4.1 – Comparison of Cyclization of Anilides 8 (Curran) and 91a (Hypothetical).....	40
Scheme 4.2 - Synthesis of (<i>S</i>)-phenethylamine-derived <i>o</i> -Iodoacrylanilide 96.....	42
Scheme 4.3 - Synthesis of L-Valine-derived <i>o</i> -Iodoacrylanilide 103	45
Scheme 4.4 – Initial Unsuccessful Attempts at N-Arylation of 106.....	47
Scheme 4.5 - Synthesis of Branched N-Alkyl- <i>o</i> -Iodoanilides	48
Scheme 5.1 – Stereoselective Heck Cyclizations with (<i>R</i>)-(+)-BINAP	56
Scheme 5.2 - Preparation of Anilides <i>rac</i> -154a,b	59
Scheme 5.3 - Preparation of Anilides <i>rac</i> -156a,b	60
Scheme 5.4 - Heck Cyclizations of <i>rac</i> -154a.....	62
Scheme 5.5 - Radical Cyclizations of Related Anilide 160.....	63
Scheme 5.6 - Synthesis of Anilide <i>rac</i> -164	65
Scheme 5.7 - Racemic Synthesis of <i>rac</i> -Esermethole	66
Scheme 5.8 - Heck Cyclization of Anilide (+)-164 and Attempted Elaboration to Desoxyeseroline.....	69

LIST OF ABBREVIATIONS

Ac	acetyl
AIBN	2,2'-azobisisobutyronitrile
BINAP	2,2'- <i>bis</i> -(diphenylphosphino)-1,1'-binaphthyl
BTMA•ICl₂	benzyltrimethylammonium dichloroiodate
<i>n</i>-BuLi	<i>n</i> -butyl lithium
<i>t</i>-BuOK	potassium <i>tert</i> -butoxide
calcd	calculated
d	day(s)
dba	dibenzylidene acetone
DBU	1,8-diazabicyclo[5.4.0]undec-7-ene
DMA	dimethylacetamide
DMAP	4-dimethylaminopyridine
DMSO	dimethylsulfoxide
dr	diastereomeric ratio
EDCI	1-ethyl-3-(3-dimethylaminopropyl)carbodiimide
ee	enantiomeric excess
equiv	equivalents
er	enantiomeric ratio
eV	electron volt(s)
FEE	first eluting enantiomer
GC	gas chromatography
HPLC	high pressure liquid chromatography

hr	hour(s)
HRMS	high resolution mass spectrometry
I.D.	inner diameter
IR	infrared spectroscopy
LAH	lithium aluminum hydride
LDA	lithium diisopropylamide
LRMS	low resolution mass spectrometry
μM	micromolar
MeI	methyl iodide
min	minute(s)
mM	millimolar
MsCl	methylsulfonyl chloride
<i>m/z</i>	mass/charge ratio
NaOMe	sodium methoxide
NBS	<i>N</i> -bromosuccinimide
NMP	<i>N</i> -methylpyridine
NMR	nuclear magnetic resonance
OAc	acetate
Ph	phenyl
PMP	1,2,2,6,6-pentamethylpiperidine
ppm	parts per million
pyr	pyridine
Rt	retention time

s	second(s)
SEE	second eluting enantiomer
TBAF	tetrabutylammonium fluoride
TBDPSCI	<i>tert</i> -butylchlorodiphenylsilane
TEA	triethylamine
Tf	trifluoromethylsulfate
THF	tetrahydrofuran
TLC	thin layer chromatography
TMS	trimethylsilyl
UV	ultraviolet

PREFACE

Let me take this opportunity to credit my advisor Prof. Dennis Curran with helping me reach this stage in my education. His steady guidance, intellect, and enthusiasm had a definite impact on my research and development as a scientist. I owe him a lifetime of gratitude. My only regret during my stay at Pittsburgh was not having the chance to experience his excellent teaching skills in a true class setting. Yet, he has still taught me much.

I have also benefited from the diverse Curran group members who passed through the 11th floor labs over the past five years. Many of the working relationships have morphed into friendships that I value greatly. Thank you all.

The department technical staff tackled each of the instrumental problems that I encountered in the course of my research. In particular I would like to thank Greg Meisner, Lance Kennelty and David Emala for their help. As well, I need to point out the contributions of Steve Geib; his X-ray crystallography expertise played a critical role in the success of my projects.

Lastly, I need to thank Profs. Kay Brummond, Ted Cohen and Michael Mokotoff for their service on my doctoral committee.

1. AXIALLY CHIRAL ANILIDES

1.1. Axial Chirality

A molecule is chiral when the geometrical placement of its atoms in three-dimensional space is such that it cannot be superimposed on its mirror image. Chiral molecules with one stereogenic center meet this requirement by having four differing groups attached to a shared or common atom. In the case of axially chiral molecules, the element of asymmetry is an axis within the molecule.¹ A classic example of axial chirality is an allene that has differing pairs of substituents at each end (Figure 1.1).

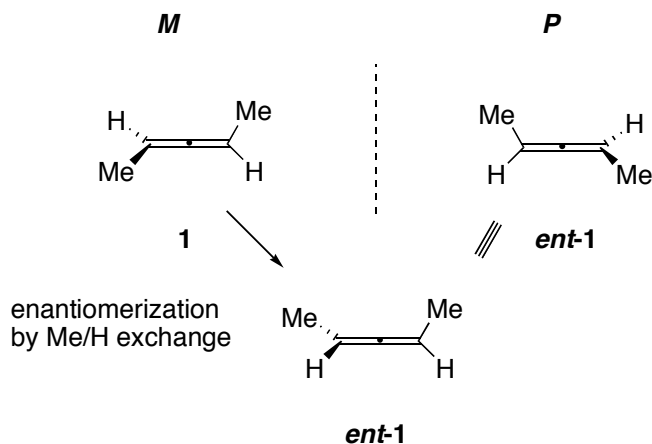


Figure 1.1 - Enantiomers of 2,3-Pentadiene

In 2,3-pentadiene **1**, each methyl group is oriented 90° from the plane formed by the other methyl group and the carbons of the allene. Conceptually, enantiomerization of **1** to *ent-1* is possible by exchanging the methyl group and the hydrogen atom at one end of the molecule. However, the energy barrier to this exchange is prohibitively high.

1.2. Stereochemical Designations of Axially Chiral Groups

Designations of *M* and *P* are often used to describe configurations of molecules with chiral axes.¹ For this designation, only the ligands of highest priority at either end of the axis are considered. When the molecule is viewed down the length of the chiral axis (the choice of end is arbitrary), if the turn from priority ligand in front to the priority ligand in the rear is clockwise, then the designation is *P* (Figure 1.2). Correspondingly, counterclockwise represents *M*.

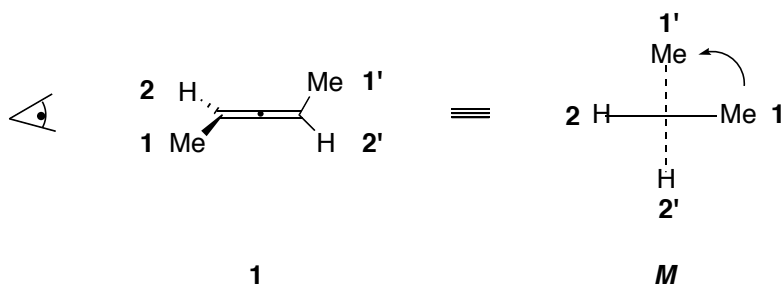


Figure 1.2 - Assigning Stereochemical Designations to Axially Chiral Molecules

1.3. Atropisomerism

Atropisomers (from the Greek *a* and *tropos*, meaning “not” and “turn”) are a sub-category of axially chiral molecules whose chirality exists by virtue of restricted rotations around a formal single bond. Eliel has suggested that atropisomers are “stereoisomers resulting from restricted rotation about single bonds where the rotational barrier is high enough to permit isolation.”² The pioneering example of atropisomerism dates back to 1922, when George Christie and James Kenner resolved the two enantiomers of 2,2'-dinitro-6,6'-diphenic acid **2** by an asymmetric recrystallization (Figure 1.3).³ Similar to the methyl-bearing termini of 2,3-butadiene, each phenyl ring in 2,2'-dinitro-6,6'-diphenic acid is oriented roughly perpendicular to the plane formed by the other phenyl ring. By virtue of the placement of the two rings and their differential substitution with respect to the axis along the C-C bond connecting the two phenyl

rings, the molecule is chiral. Conversion of (*M*)-**2** to (*P*)-**2** is achieved by rotating 180° about the C-C bond connecting the phenyl rings.

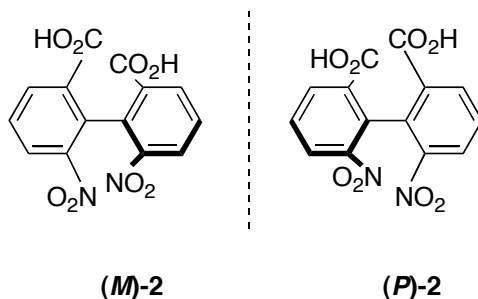


Figure 1.3 - Atropisomeric Pair of 2,2'-Dinitro-6,6'-diphenic Acid Enantiomers

Oki put forth the arbitrary definition that a rotational isomer must have a half-life of at least 1000 s for the molecule to be considered to exhibit atropisomerism.⁴ The temperature dependence of this definition is a weak point. For example, an atropisomer with a 1000 s lifetime at -100 °C would only have a fleeting existence at ambient temperature. A more apt criterion for atropisomerism is to consider the energetic barrier to rotation. For example, a rotation barrier of approximately 21.8 kcal/mol (90.9 kJ/mol) translates to a half-life of about 1000 s (just under 17 min) at ambient temperature. Thus, to conveniently handle atropisomers at room temperature, rotation barriers above ~22 kcal/mol (~92 kJ/mol) are needed.

1.4. Tertiary Anilide Conformers

1.4.1. Restricted N-CO Bond Rotation

Tertiary amides exhibit restricted rotation about their N-CO bonds. The N-CO bond of anilides, as in most amides, has significant π character as a result of nitrogen lone pair delocalization

towards the electronegative oxygen (Figure 1.4). The additional contributions of the resonance forms with π bonding **3A**, **3B** increase the barrier to N–CO rotation significantly.

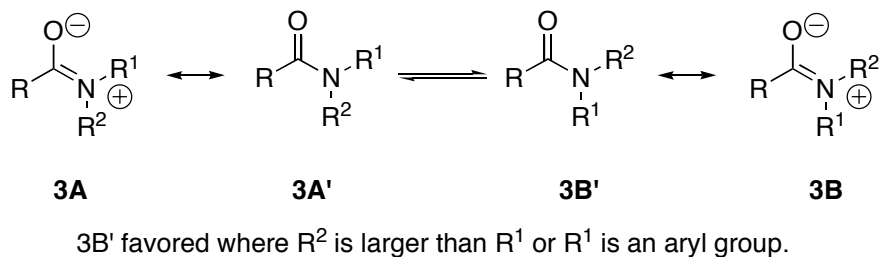


Figure 1.4 – Rotational Isomers and Resonance Structures of Tertiary Amides

1.4.2. Tertiary Anilides E/Z Preferences

If R¹ and R² (Figure 1.4) differ in size, then the energy levels of the two conformers, **3A'** and **3B'**, will not be equally populated. The conformation **3B'** in which the larger group is syn to oxygen is more favored for steric reasons. Tertiary anilides are an exception to this generalization because of the possibility of N-aryl bond rotation, which places the aromatic ring perpendicular to the plane of the amide and relieves steric interactions. For example, amide **4** in pyridine exhibits a 99.5/0.5 preference for the *E* isomer (Figure 1.5).⁵ This conformational preference has been supported by crystallographic data and theoretical calculations.⁶

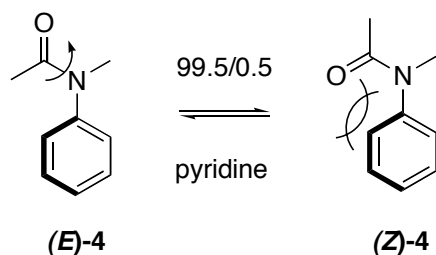


Figure 1.5 - Conformers of *N*-Methylacetanilide

1.5. Restricted N-Aryl Bond Rotation

It has been long known that tertiary anilides exhibit restricted rotation about the N-aryl bond. Following the discovery of biaryl atropisomerism in 1922, researchers sought out other classes of optically active compounds that exhibit restricted rotation.⁷ If the N-aryl bond rotation barrier is sufficiently high, then the separation and laboratory manipulations of anilide enantiomers at ambient temperatures would be possible. In 1928, Mills published the first example of an axially chiral anilide **5** (Figure 1.6).⁸

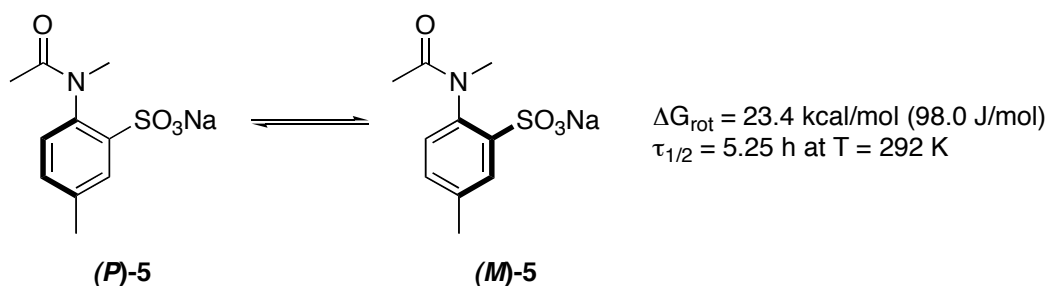


Figure 1.6 – The First Axially Chiral Anilide Reported

In the years ensuing Mill's discovery, a number of axially chiral anilides have been synthesized by our group⁹ and others.¹⁰⁻¹⁷ By late 2005, the N-aryl bond rotation barrier has been quantified for numerous substrates. A gallery of 32 representative anilides and related compounds sorted by ascending rotation barriers is diagrammed in the Appendix (page 246).

Substitution at positions flanking the chiral axis affect the magnitude of the rotation barrier. If an *ortho* substituent is sufficiently large or if two different, medium-sized *ortho* substituents are present, then an anilide can have a rotational barrier high enough to allow separation and laboratory manipulations of enantiomers at ambient temperatures. For example, the chiral *o*-iodoacrylamide **8** has a rotation barrier of 30.8 kcal/mol (129.0 kJ/mol), which translates to a

half-life of over 175 years at 20 °C (Figure 1.7). The *ortho* methyl group alone does not result in a large rotational barrier; anilide **6** racemizes in seconds under typical laboratory conditions.¹¹ In the case of anilide **7**, a single *ortho* *tert*-butyl group is sufficiently bulky enough to enable a barrier of 29.1 kcal/mol (121.8 kJ/mol).

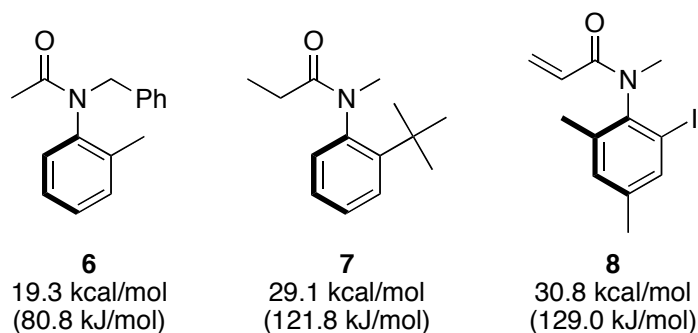
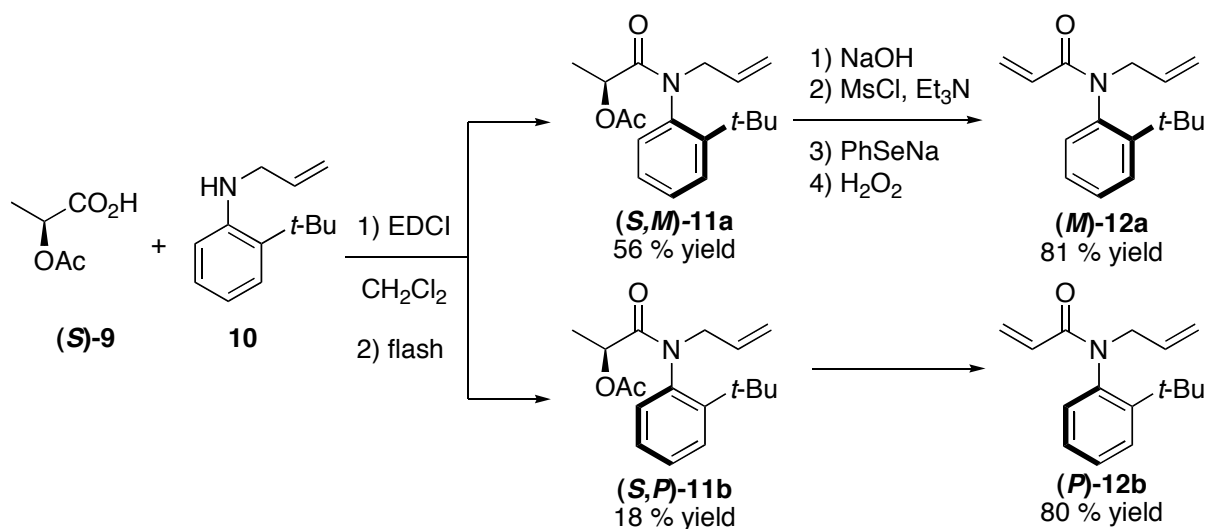


Figure 1.7 - Rotational barrier of Selected Axially Chiral Anilides

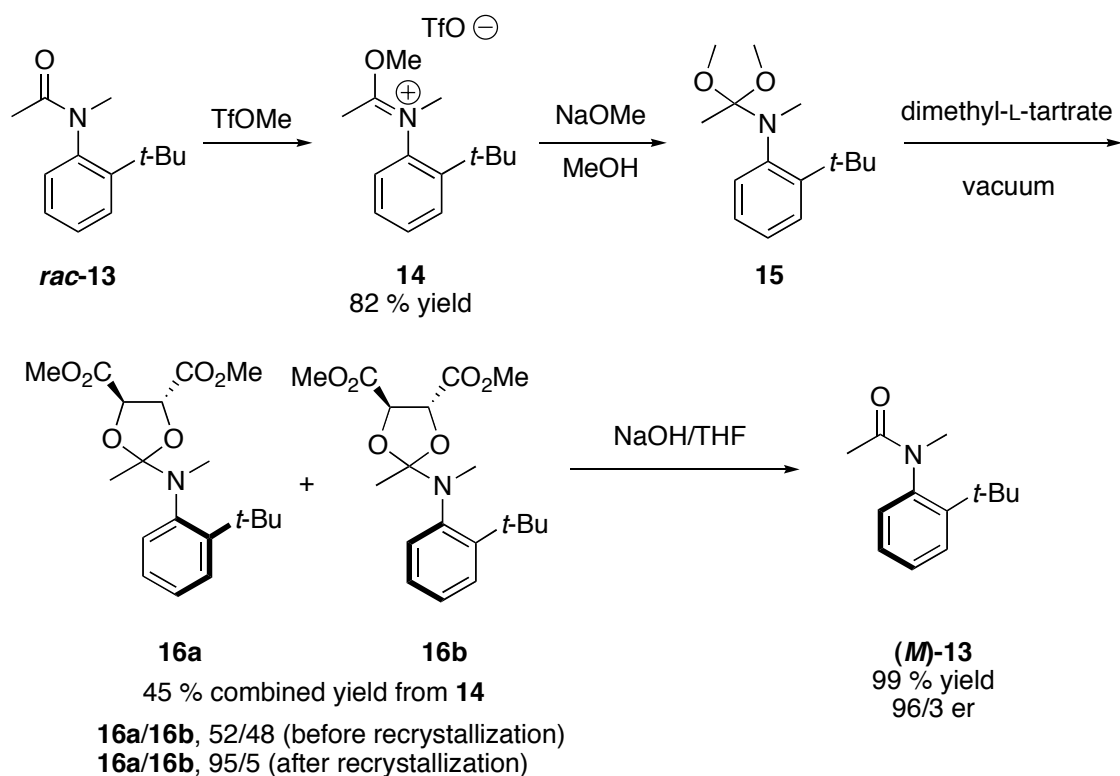
1.6. Synthetic Approaches to Enantioenriched Axially Chiral Anilides (Stoichiometric)

To date, only a few synthetic approaches exist for the preparation of enantioenriched samples of axially chiral anilides. The earliest known methodology was put forth by Taguchi and coworkers in 1998.¹² In it, the chiral pool reagent lactic acid **9** was coupled with *N*-allyl aniline **10** to generate a separable mixture of diastereomers **11a**, **11b** (Scheme 1.1). The acetoxy group was subsequently removed by a four-step process to yield corresponding acrylamide enantiomers **12a**, **12b** with ees as high as 97 %. A modification of this method by Simpkins used SmI_2 to reductively deoxygenate the acetate (not shown).¹³



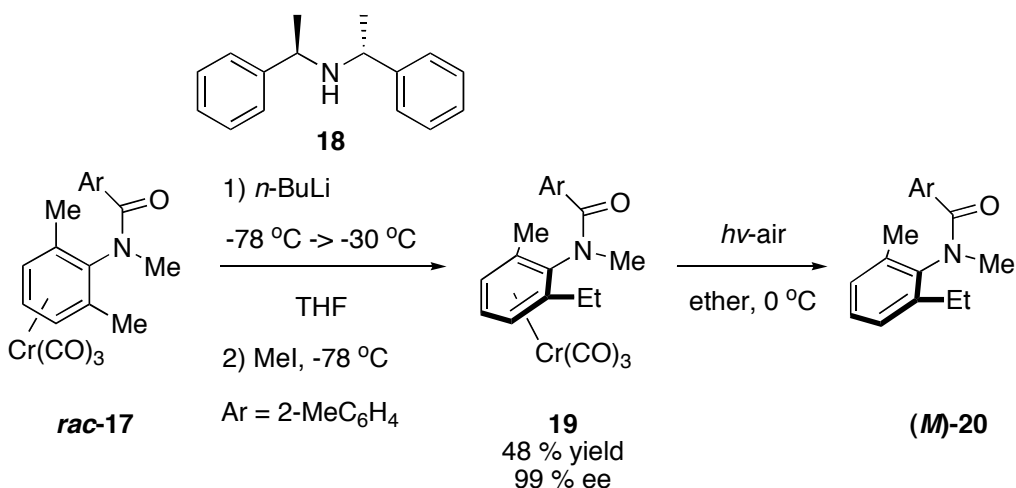
Scheme 1.1 - Taguchi's Chiral Pool Approach to Axially Chiral *o*-*t*-Butylanilides

A conceptually different approach developed by Ates and Curran relies on the crystallization-induced asymmetric transketalization of amide ketals (Scheme 1.2).^{9c} Beginning with *rac*-**13**, the dimethyl ketal **15** was formed in two steps; ketal **15** was subjected to trans-ketalization with dimethyl L-tartrate to give a 52/48 mixture of atropisomers **16a**, **16b**. When the mixture was slowly crystallized, the ratio of **16a/16b** was increased to 95/5 in what is likely a crystallization-induced asymmetric transformation. Hydrolysis of the amide ketals regenerates anilide (*M*)-**13** with 96.5/3.5 er. That the er of **13** is roughly equivalent to the dr of the starting mixture of **16a/16b** indicates that hydrolysis of the ketal occurs faster than the N-aryl bond rotation.



Scheme 1.2 - Enantioenriched Anilides via Asymmetric Crystallization

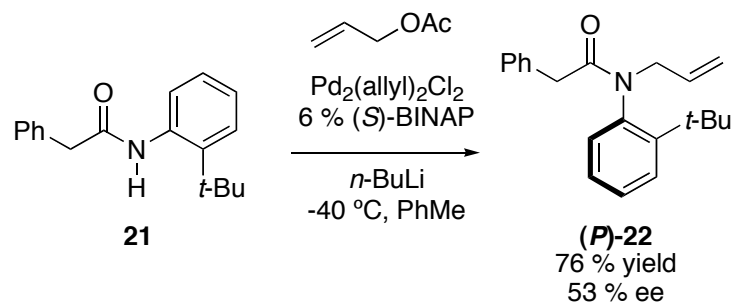
An elegant protocol by Uemura includes the enantiotopic lithiation of prochiral methyl groups in tricarbonylchromium complexes of *N*-benzoyl-*N*-methyl-2,6-dimethylaniline *rac*-**17** by a chiral lithium amide from amine **18**, followed by quenching of the benzylic anion with methyl iodide to generate **19** with ees as high as 99 % (Scheme 1.3). Subsequent exposure of the chromium complex **19** to light and air allowed the isolation of the axially chiral anilide (*M*)-**20** with no loss of enantiopurity.¹⁴



Scheme 1.3 - Uemura's Method: Enantioselective Lithiation of Chromium Complexes

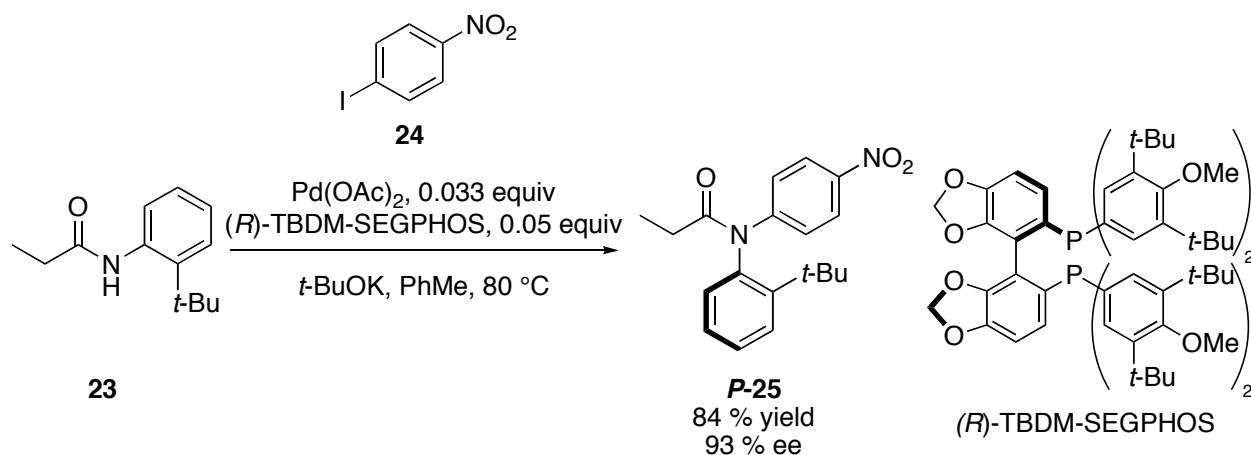
1.7. Synthetic Approaches to Enantioenriched Axially Chiral Anilides (Catalytic)

A common feature of the methodologies thus far is that they all rely on a stoichiometric amount of a chiral species. Dr. Jun Terauchi developed the first catalytic enantioselective methodology in our labs in 2000.^{9f} Deprotonation of a prochiral, secondary anilide **21** generates an anionic intermediate that reacts preferentially with one enantiotopic face of a chiral Pd π -allyl complex (Scheme 1.4). In the best example, a 76 % yield of **22** was obtained in 53 % ee. Soon after, the Taguchi group published a nearly identical approach, albeit with lower ees obtained.¹⁵ Taken together, these examples represent the first examples of catalytic asymmetric syntheses of axially chiral anilides.



Scheme 1.4 - Pd-catalyzed Enantioselective Allylation of Secondary Anilides

Earlier in 2005, Taguchi reported an extension to the N-allylation approach. When secondary anilide **23** and 1-iodo-4-nitrobenzene **24** were treated with base and in the presence of catalytic Pd coordinated with the (*R*)-TBDM-SEGPHOS chiral ligand, anilide **25** was produced in high yield and 93 % ee.¹⁶ Surprisingly, despite the high temperatures required for the reaction to occur over 2 to 6 h, products were isolated without racemization.

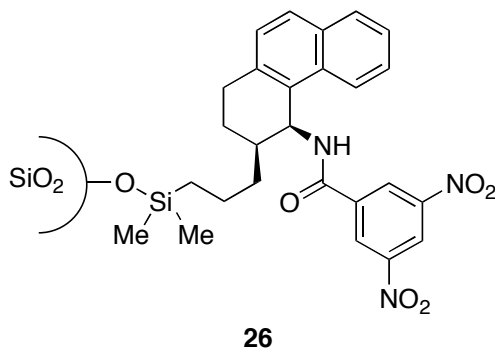


Scheme 1.5 - Taguchi's Catalytic Asymmetric N-Arylation Methodology

1.8. Chromatographic Access to Enantioenriched Axially Chiral Anilides

Although a wide variety of methodologies for the synthesis of axially chiral anilides have been published, a common feature that they lack is substrate generality. When an appropriate

asymmetric synthesis is not available for a substrate, the best option is often to prepare the compound in racemic form and then separate small quantities (10–100 mg) into enantiomers using commercial chiral HPLC columns.¹⁷ Regis Technologies's (*S,S*)-Whelk-O 1 product in particular, is a workhorse column in our research. This column has a covalently bound chiral stationary phase **26** that presents “a semi-rigid framework holding a π -acidic 3,5-dinitrobenzamide group perpendicular to a π -basic polynuclear aromatic group.”¹⁸ The amide N-H group acts as a hydrogen bond donor and is situated in the cleft formed by the two aromatic systems. The Whelk-O 1 column is capable of resolving enantiomers of a wide variety of chiral systems. The Whelk-O 1 column is capable of resolving enantiomers of a wide variety of chiral compounds, but is particularly suited for those possessing 1) Lewis basic functionality and 2) aromatic ring(s). While a chromatographic approach is more general, it can be labor intensive when the separation between enantiomers is poor.

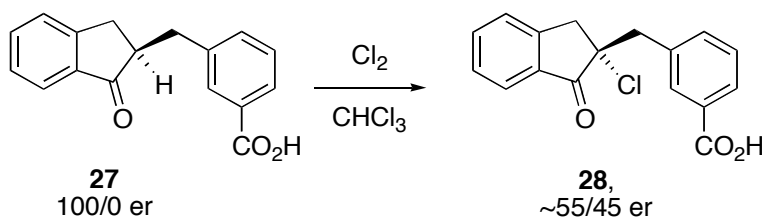


Scheme 1.6 – Chiral Stationary Phase of (*S,S*)-Whelk O 1 HPLC Columns

2. MEMORY OF CHIRALITY

2.1. Background

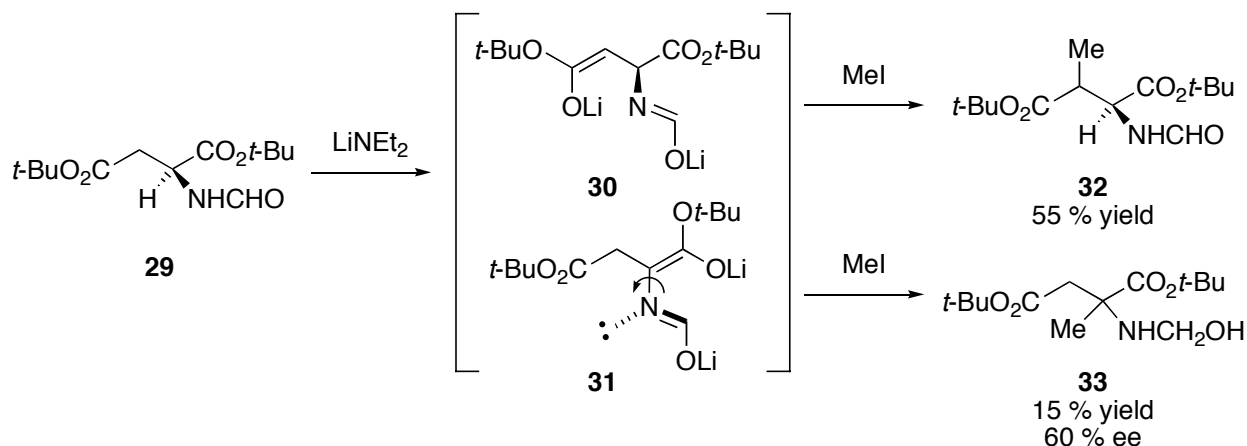
In 1913, Leuch reported a curious result. When he treated an optically active ketone **27**, by virtue of an α chiral center, with chlorine to effect an α chlorination, the resulting product **28** retained optical activity.¹⁹ This result was counterintuitive to thinking at the time because the enol intermediate was believed to be achiral and therefore, unable to influence stereoselection in subsequent steps. Apparently, despite the loss of a chiral center a mechanism existed to translate chiral information to the product. Half a century later, Marquet repeated Leuch's experiment and confirmed that the α chlorinated product **28** did indeed possess non-zero, albeit diminished, ee (Scheme 2.1).²⁰



Scheme 2.1 - Marquet's Confirmation of Leuchs' Observation

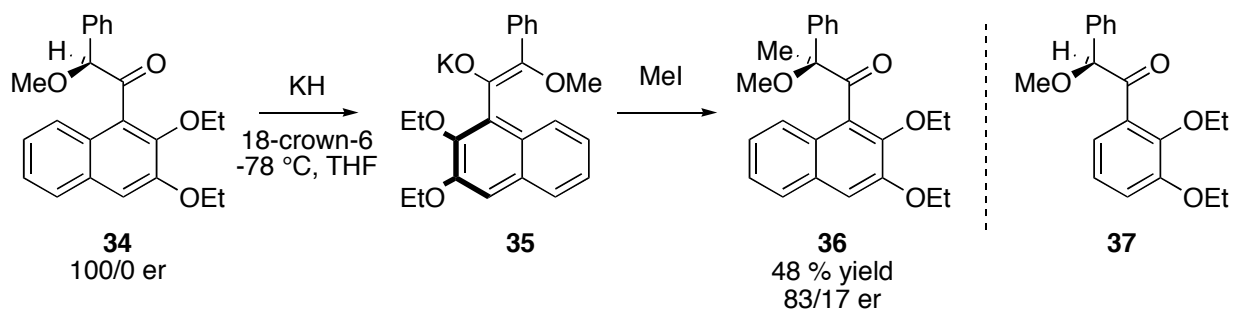
Fifteen years later, Seebach and co-workers reported a related result. While attempting the β methylation of aspartate derivative **29** by a double lithiation procedure, they observed the expected β methylated product **32** along with 15 % of the α methylated side product **33**.²¹ Contrary to expectations, the er side product was not 50/50 but 80/20 (Scheme 2.2). Like Leuch's result, a seemingly achiral intermediate, in this case an enolate, produced non-racemic product. Clearly, the intermediate must be chiral. Seebach postulated that double deprotonation

of **29** could result in an enolate **31** with transient axial chirality, about the bond highlighted with an arrow, that could influence the facial approach of the electrophile to the reactive site and result in a moderate transfer of chirality to the product **33**.



Scheme 2.2 - Seebach's Original Observation

A decade later, Fuji described the first substrate designed to exhibit and exploit the dynamic behavior that Seebach observed (Scheme 2.3). When enolate **35**, formed by the deprotonation of chiral naphthyl ketone **34** (100/0 er) at $-78\text{ }^\circ\text{C}$, was quenched with methyl iodide, the resulting α -methyl product **36** was isolated with an 83/17 er.²² Despite the loss of the sole stereocenter, chirality is relayed to the product **36**. The key insight was the use of a naphthyl group to act as a surrogate for the original chiral information. Upon deprotonation of **34**, the chiral information is 'stored' in the axially chiral enolate **35** that directs the stereoselection during the alkylation step. To eliminate the possibility that aggregates between the achiral enolate and chiral precursor were responsible for the stereoselection observed, a control experiment was conducted. When phenyl ketone **37** was submitted to identical methylation conditions the resulting product was racemic, presumably because the intervening axially chiral intermediate (not shown) did not have a sufficiently long enough lifetime to delay racemization prior to alkylation.



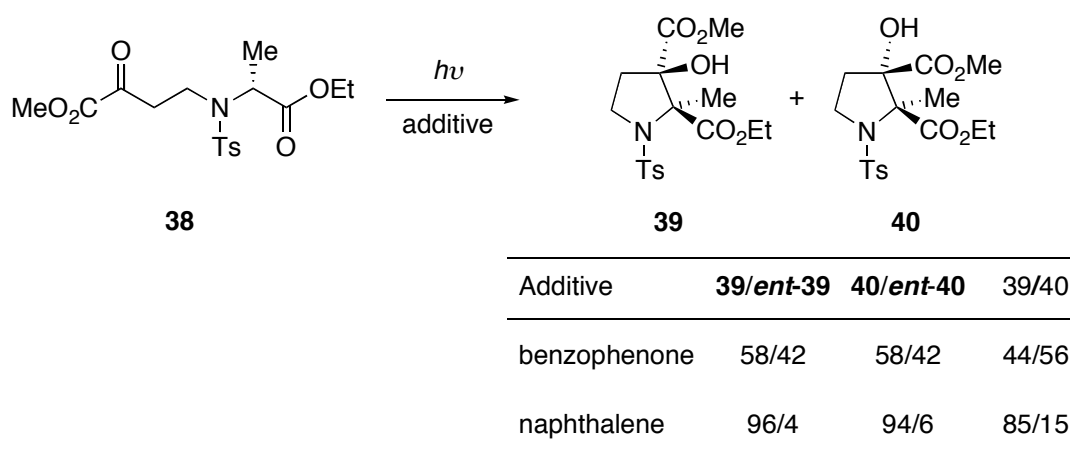
Scheme 2.3 - Fuji's Substrate Designed to Relay Chiral Information

Three years later, Fuji demonstrated a stereoselective α alkylation of phenylalanine derivatives based on the same idea. Whereas, in the previous example (Scheme 2.3), the naphthyl group served as a source of asymmetry in the axially chiral intermediate, the latter work exploited size differences between nitrogen protecting groups to influence the stereoselection on the reaction.²³ Fuji coined the name “memory of chirality” to describe this “principle.”²⁴ The term memory evokes the ‘capacity of a substance to return to a previous state or condition after having been altered.’²⁵ Initially Fuji narrowly defined as a reaction where “central chirality at a carbon α to a carbonyl group is preserved as transient axial chirality of the intermediate enolate and is then regenerated as central chirality in the reaction product.” Two recent reviews document subsequent work over the past decade that demonstrates that this phenomenon is not restricted to enolate chemistry²⁶ or axially chiral intermediates.²⁷

2.2. Memory of Chirality in Radical Chemistry

In the years following Fuji’s initial report²² other examples of memory of chirality in enolates appeared in the literature.²⁶ Yet, there are no reasons why memory of chirality phenomenon should be solely the domain of anion chemistry. One of the earliest examples of a radical

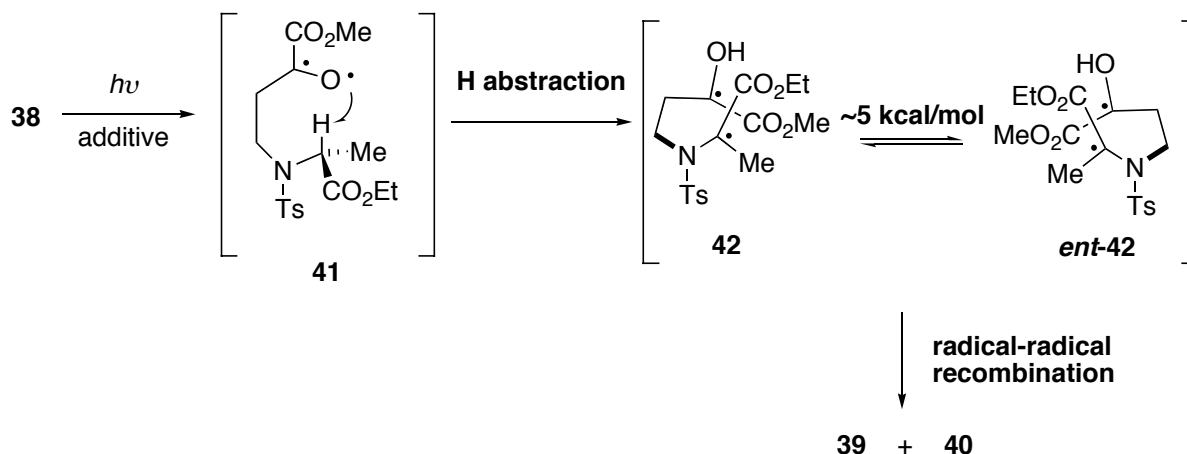
reaction that demonstrates memory of chirality behavior came from the labs of Giese. In 1999, Giese and co-workers described the photoinduced Norrish-Yang cyclization of a protected alanine derivative **38** to proline derivatives **39** and **40**.²⁸ The initially formed diradical **41** undergoes a 1,6-H abstraction to generate another diradical **42** (Scheme 2.5). This event happens concomitantly with loss of chirality at the α center due to the tiny barrier to inversion of acyclic radicals.²⁹ Radical-radical recombination generates diastereomeric cyclic products, **39** and **40**. When additive benzophenone was used as a triplet sensitizer the products were isolated with low ee (see Scheme 2.4, entry 1). In contrast, when triplet quencher naphthalene was used as an additive **39** and **40** were produced with significant retention of chirality.



Scheme 2.4 - Photoinduced Norrish-Yang Cyclization Demonstrates Memory of Chirality

Key intermediate **42** possesses transient axial chirality, a necessary outcome of the conformation required for the hydrogen transfer. The rotation barrier about the C–C bond highlighted in **42** (Scheme 2.5) is estimated to be 5 kcal/mol (21 kJ/mol). But, radical-radical recombination has an even lower activation barrier, approximately 2 kcal/mol (8 kJ/mol), and ring closure outpaces other conformational events that would lead to scrambled stereochemistry in the products. An explanation for the effect of the additive is tied to the relative reaction rates of the spinisomers.

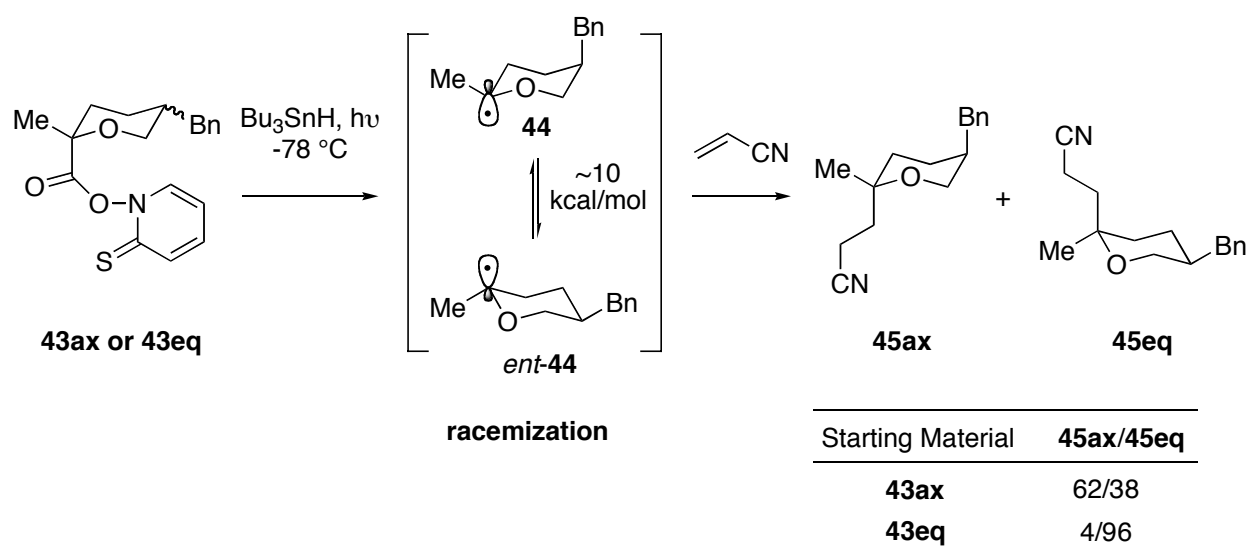
A triplet radical is slower to recombine because of the additional requirement of spin relaxation prior to ring closure (Scheme 2.5). The singlet radical is correspondingly more reactive and ring closure is significantly faster than conformation changes within the intermediate (**42**).



Scheme 2.5 - Proposed Mechanism for Giese's Norrish-Yang Cyclization

A year prior, Rychnovsky and co-workers reported the successful trapping of a cyclic radical with retention of configuration (Scheme 2.6).³⁰ Photoinduced decarboxylation of optically active *N*-hydroxypyridine-2-thione esters **43** produces tetrahydropyran radical **44** which can racemize through ring inversion. If the intermediate **44** can be trapped by an electrophile before ring inversion (estimated barrier of 10 kcal/mol or 42 kJ/mol) occurs, then an optically active product **45** will be formed. Like previous examples, an intermediate with fleeting chirality is transformed into a more stable chirality. What distinguishes this example from ones previously discussed, is that the molecule retains its type of asymmetry throughout the reaction, which is in conflict with the guiding idea put forth by Fuji.²² Is this not also an example of memory of chirality, or is the definition too exclusive? A more encompassing definition was recently put forth by Zhao and Carlier:^{26b} “a ‘memory of chirality’ reaction can be defined as a formal substitution at an sp^3 stereogenic center that proceeds stereospecifically, even though the reaction

proceeds by trigonalization of that center, and despite the fact that no other permanently chiral elements are present in the system.” Yet, Rychnovsky’s work also does not meet this criterion because of the presence of the benzyl stereocenter throughout the process. We offer an even broader definition that covers Rychnovsky’s observations: a ‘memory of chirality’ reaction can be defined as the stereospecific formation of an sp^3 stereogenic center, despite the reaction proceeding through a metastable chiral intermediate formed during the destruction of the initial chirality at the reactive site.



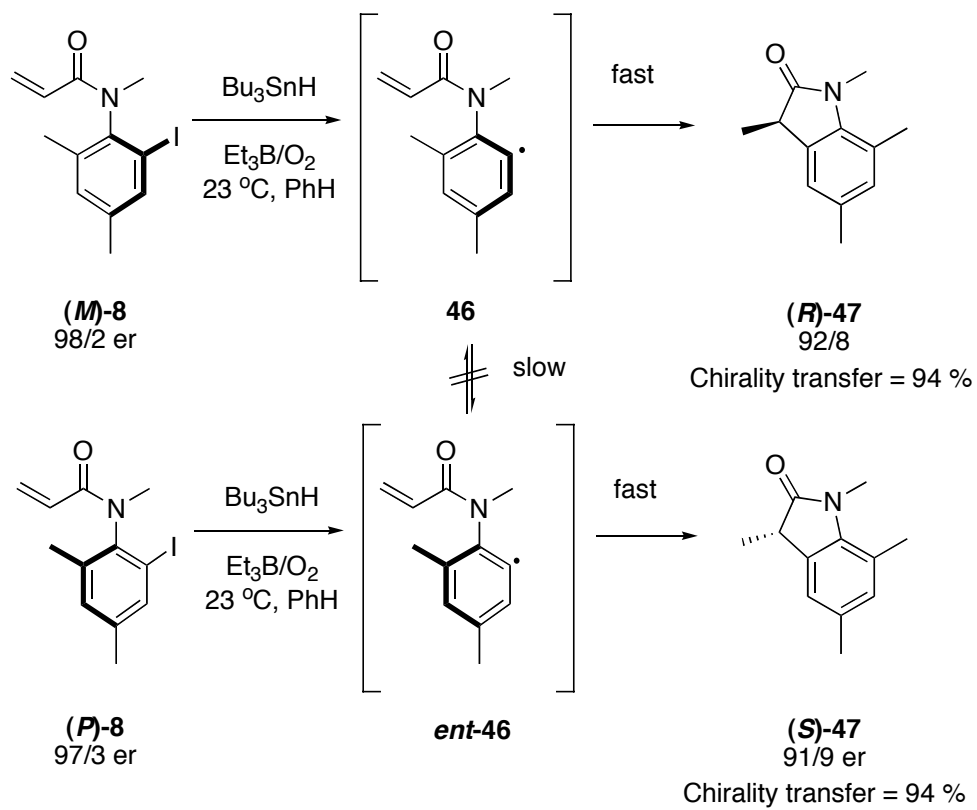
Scheme 2.6 – Trapping of a Cyclic Radical with Retention of Configuration

2.3. Chirality Transfer in Radical Cyclizations of Axially Chiral Acrylanilides

Past research from our group has revealed reactions that share some of the attributes of those in Rychnovsky’s report. For over a decade, our group has studied axially chiral anilides and benzamides and their use in stereochemical transformations.^{9,17} In 1999, our group reported on the radical cyclization of enantioenriched *o*-iodoacrylanilides **8**. Acrylanilide **8** is a stable atropisomer with a N-aryl bond rotation barrier of 30.8 kcal/mol (129.0 kJ/mol).^{9c} Iodine

abstraction of (*M*)-**8** (98/2 er) by a tin radical produces **46**, which might be expected to racemize (**46** → *ent*-**46**) under the reaction conditions because of the drastic loss of the bulk in the *ortho* position. In fact, the 5-*exo* oxindole product (*R*)-**47** was isolated significantly enantioenriched (92/8 er). The chirality transfer for the radical cyclization of (*M*)-**8** to (*R*)-**47** is 94 %. The cyclization of **8** was found to proceed with high levels of chirality transfer, because the rate of the cyclization, about $8 \times 10^7 \text{ s}^{-1}$ based on a comparable substrate,^{9g} surpasses that of any competing bond rotations. Like the Rychnovsky example (Scheme 2.6) the transition from the stable chirality of the starting material to the transient chirality of the intermediate occurs without a change in the source of chiral information (stereocenter → stereocenter, chiral axis → chiral axis). What sets the latter work apart is that the axial chirality of **8** is ultimately transferred to a new stereocenter in **47**; the chirality is not ‘remembered.’ Although the above cyclization does not constitute a ‘memory of chirality’ process, like the other transformations in this chapter, it proceeds with a metastable chiral intermediate under non-equilibrium conditions.

We use the term chirality transfer to describe the fidelity of the transfer of stereochemical information for memory/transfer of chirality reactions. Chirality transfer is calculated by dividing the amount of the major enantiomer in the product by the amount of the major enantiomer in the starting material (in the above example, $92/98 = 94 \%$). Thought of in another way, chirality transfer is the yield, not excess, of the major enantiomer one would expect to isolate from the reaction of an enantiopure sample. Qualitatively, it is a measure of the partitioning of enantiomeric intermediates between two diastereomeric transition states.

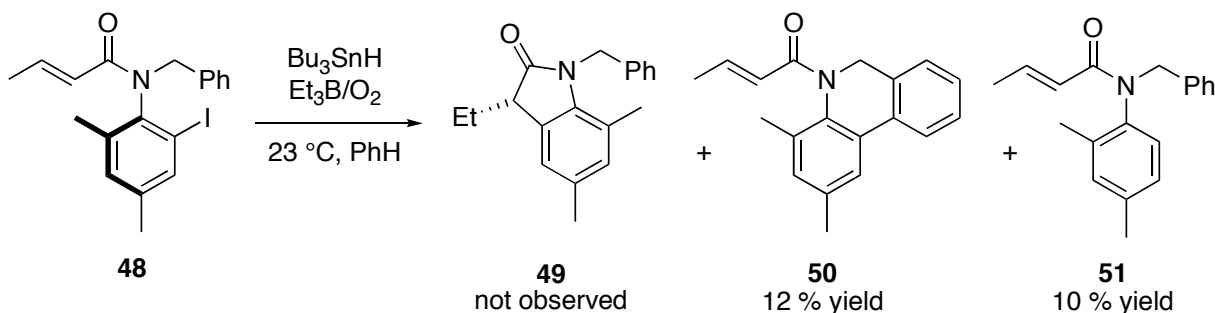


Scheme 2.7 - Transfer of Chirality in Axially Chiral *o*-Iodoacrylanilides

3. RADICAL CYCLIZATIONS OF AXIALLY CHIRAL *N*-ALLYL-*O*-IODOANILIDES

3.1. Introduction

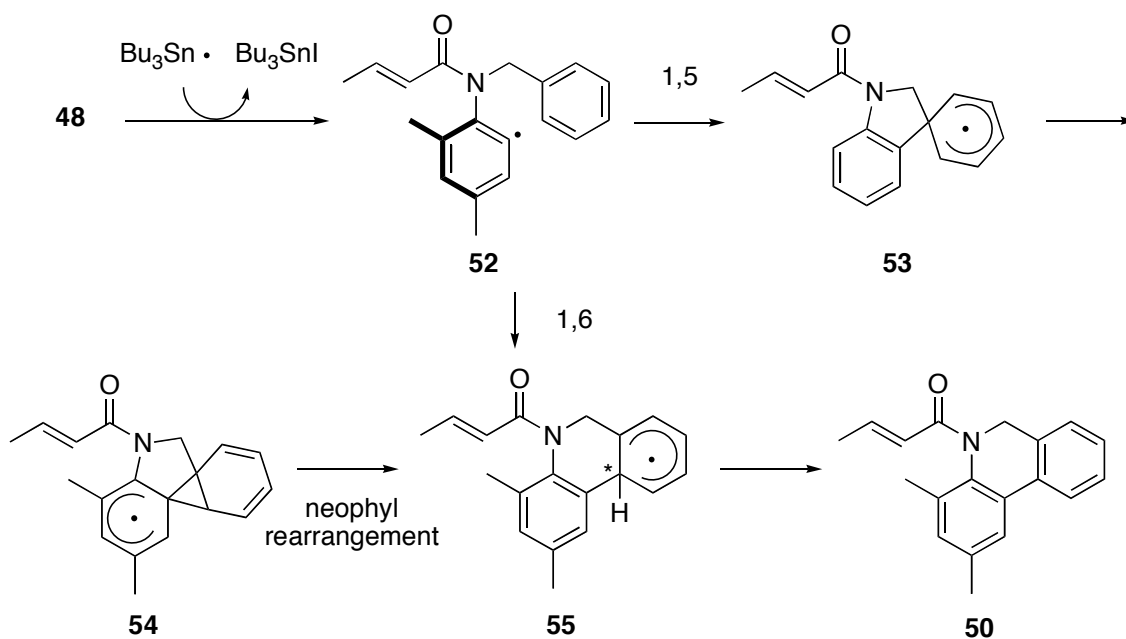
The radical cyclization of *N*-acryloyl anilide **8** to provide **47** (Scheme 2.7) is an example of an intramolecular reaction that occurs with excellent chirality transfer (> 90 %).^{9c} In this reaction, the intermediate aryl radical **46** must have a much lower barrier of rotation than its precursor **8**, but its barrier to cyclization is even lower yet, so racemization of the intermediate radical is not a significant reaction. In the course of this investigation, Christine H.-T. Chen submitted iodoanilide **48** to the standard radical cyclization conditions. Instead of the expected oxindole product **49**, phenanthroline **50** was produced in 12 % yield along with the reduced product **51** (Scheme 3.1).³¹



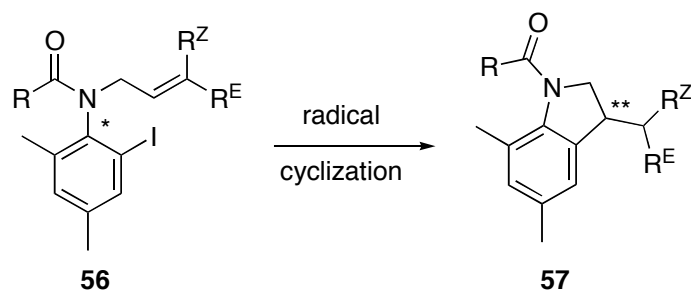
Scheme 3.1 - An Unexpected Cyclization Result

A possible mechanism for the formation of **50** is suggested in Scheme 3.2. Although, the yield of **50** is low, this striking result implies that aryl radical attack on the pendant benzyl group is faster than the expected 5-*exo* radical cyclization onto the crotonoyl group, itself known to be a rapid process.³² In the same study^{9c} the rate of cyclization (k_{cyc}) of the *N*-ethyl analogue of **48**

was measured to be $7.8 \times 10^7 \text{ sec}^{-1}$. If the 1,6 cyclization is occurring, then the newly formed stereocenter (*) in **55** is ultimately destroyed along with any possible data on chirality transfer. (The 1,5 pathway can only lead to achiral products.) The observation that cyclization onto the N-benzyl group occurs faster than cyclization onto the crotonyl group hints that suitable axially chiral iodoanilides with a pendant N-allyl group instead of a benzyl one will cyclize with chirality transfer. Based on this hint, we set out to study this class of radical cyclizations, shown generally in Figure 3.1.



Scheme 3.2 - A Possible Mechanism for the Formation of 50

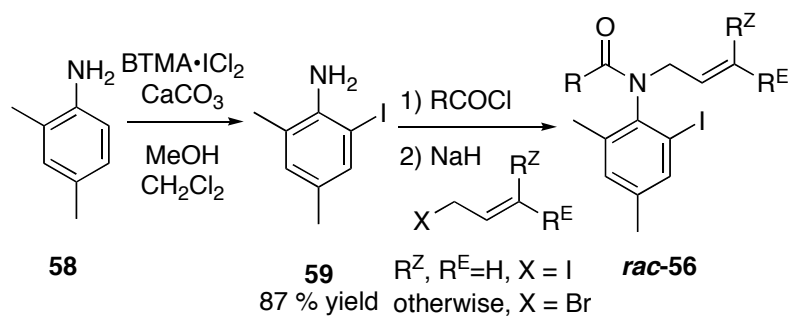


Axial chirality (*) in **56** transferred to new stereocenter (**) in **57**.

Figure 3.1 - Possible Radical Cyclizations of Axially Chiral *N*-Allyl-*o*-Iodoanilides

3.2. Precursor and Product Preparation

There are no available asymmetric methods to prepare axially chiral anilides such as **56**. As such, cyclization precursors **56a-i** were synthesized in racemic form (Table 3-1) and chiral preparative HPLC was used to resolve each enantiomeric pair of atropisomers. The synthesis of cyclization precursors **56a-i** began with the *ortho* iodination of 2,4-dimethylaniline (**58** → **59**). A two-step sequence of *N*-acylation of **59** followed by *N*-allylation generated the nine anilides **56a-i** employed in this study. Aniline **59** was submitted to modified Schotten-Baumann conditions with a series of acyl chlorides to produce secondary anilides (not shown) in yields ranging from 47–100 %. Addition of a secondary anilide to a slurry of sodium hydride in THF, followed by the appropriate allylating agent generated **56a-i** in 35–100 % yield. Racemic samples of **56a-g** were cyclized using standard tin hydride mediated conditions to prepare *rac*-**57a-g**, used as racemic standards for chiral HPLC analysis.



	R	R ^Z	R ^E	% yield ^a
56a	Ph	H	H	35
56b	<i>p</i> -BrC ₆ H ₄	Me	Me	54
56c	PhCH ₂	H	H	50
56d	PhCH ₂	H	Ph	47
56e	PhCH ₂	H	Me	20
56f	PhCH ₂	Me	Me	37
56g	PhCH ₂ CH ₂	H	H	74
56h	CH ₃ CH=CH	H	H	20
56i	Me	Me	Me	69

^a Overall yield of final two steps.

Table 3-1 - Preparation of Cyclization Substrates

3.3. Resolution and Rotation Barriers of Precursors

To access enantioenriched samples of **56a-g**, racemic samples were resolved on a semi-preparative (*S,S*)-Whelk-O 1 column (25 cm x 10.0 mm I.D.), eluting with 10–40 % *i*PrOH in hexanes (8–10 mL/min). Typical injection amounts were between 40 to 80 mg and about one hundred milligrams of both enantiomers of each precursor were regularly isolated. The ees of the enantioenriched samples **56a-g** were measured by analytical chiral HPLC and fell reliably in the range of 96–99 %. The racemic products **57a-g** were injected into an analytical (*S,S*)-Whelk-O 1 column and each pair of enantiomers was well resolved, allowing a quantitative analysis of chirality transfer experiments by chiral HPLC.

The N-aryl bond rotation barriers for four representative precursors **56a-c,g** were measured in a thermal equilibration experiment. A solution of an enantioenriched sample of **56b** in 9/1 hexanes/*i*PrOH was placed in a sealable tube and heated at 114 °C (387 K). Periodically,

aliquots were removed and their ee measured by chiral HPLC analysis. A plot of the logarithmic decrease in ee versus time (e.g. **56b**: plot Figure 3.2, data Table 3-2) showed the expected first order rate of racemization. The value of the slope corresponds to the rate of racemization (k_{rac}); this value is divided in half to correct for the fact that only one of every two rotation events result in an observable racemization event. Using the Arrhenius kinetics, k_{rac} was translated into a free energy barrier to rotation for *p*-bromobenzamide **56b**, 30.7 kcal/mol or 128.3 kJ/mol (Equation 3-1).

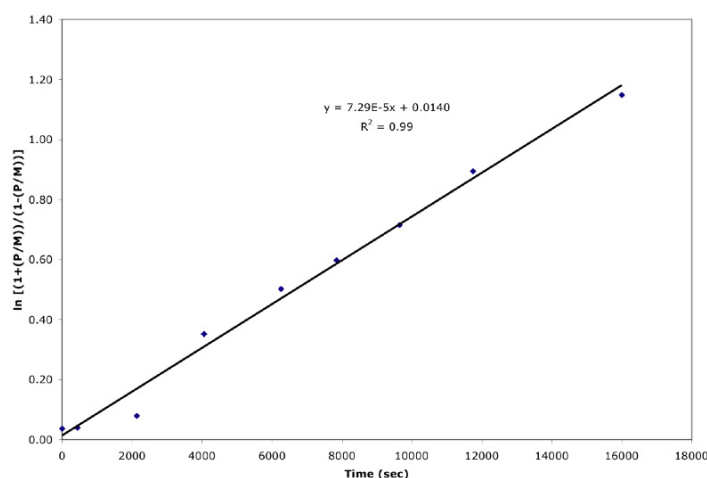


Figure 3.2 - Thermal Equilibration Plot for 56b

(M)-56b		T = 387 K
Time (min)	%	ee
0	96	
36	92	
68	70	
104	61	
131	55	
161	49	
196	41	
267	32	

Table 3-2 - Thermal Equilibration Data for 56b

$$\ln \left[\frac{1 + [P-56b]/[M-56b]}{1 - [P-56b]/[M-56b]} \right] = k_{\text{rac}}^{\ddagger} + c$$

$$2k_{\text{rac}} = 7.29 \times 10^{-5} \text{ s}^{-1} \quad (\text{slope} = k_{\text{rac}} \text{ or } 2k_{\text{rot}})$$

$$k_{\text{rot}} = \text{slope}/2 = (7.29 \times 10^{-5} \text{ s}^{-1})/2 = 3.65 \times 10^{-5} \text{ s}^{-1}$$

$$K_{\text{rot}}^{\ddagger} = k_{\text{rac}}^{\ddagger} h / kT = \frac{(3.65 \times 10^{-5} \text{ s}^{-1}) (6.626 \times 10^{-34} \text{ Js})}{(1.381 \times 10^{-23} \text{ J/K}) (387 \text{ K})}$$

$$K_{\text{rot}}^{\ddagger} = 4.52 \times 10^{-18} \text{ substitute into } \Delta G^{\ddagger} = -RT \ln K^{\ddagger}$$

$$\Delta G_{\text{rot}}^{\ddagger} = 128.314 \text{ kJ/mol or } \mathbf{30.7 \text{ kcal/mol}}$$

Equation 3-1 - Calculation of the N-Aryl Bond Rotation Barrier of 56b

Not surprisingly, the barrier of related benzamide **56a** was comparable, 29.7 kcal/mol or 124.3 kJ/mol (Figure 3.3). Phenacetyl **56c** and phenethyl **56g** amides exhibited slightly higher rotation barriers of 32.6 (136.5 kJ/mol) and 32.7 kcal/mol (136.9 kJ/mol), respectively. All of these barriers are sufficiently high enough to allow handling of these compounds under typical laboratory conditions.

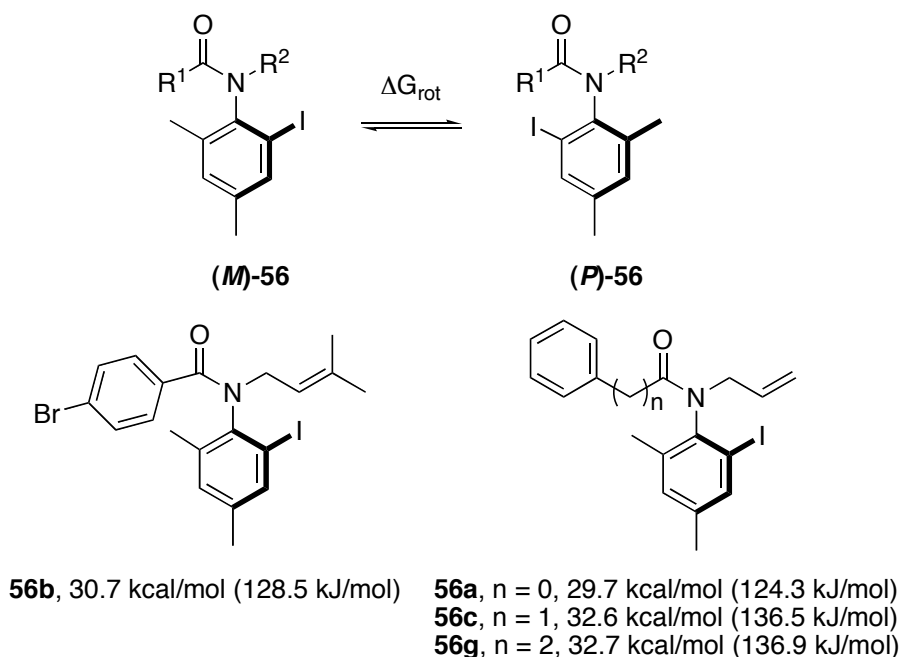


Figure 3.3 - Rotation Barriers of Four Axially Chiral Anilides 56a-c,g

3.4. Chirality Transfer in Radical Cyclizations of *N*-Allyl-*o*-Iodoanilides

To measure the chirality transfer of the cyclization, enantioenriched samples of precursors **56a-g** were submitted to room temperature tin hydride mediated radical cyclization conditions. For example, a sample of anilide (*M*)-**56c** (98.5/1.5 er, Figure 3.4) was dissolved in benzene that had been aerated beforehand by exposure to the atmosphere for at least 10 min. Bu_3SnH (1.5 equiv, 0.01 M) was added to the solution, followed by triethylborane (1.0 equiv) to initiate the reaction.³³ After the reaction was judged to be complete by TLC (<5 min), the reaction was worked up and the crude material was purified by silica gel flash chromatography to give dihydroindolone (*R*)-**57c** in 53 % yield. The er of (*R*)-**57c** was measured by chiral HPLC and found to be 93.5/6.5. The opposite enantiomer, (*P*)-**56c** (99.5/0.5 er), produced dihydroindolone (*S*)-**57c** in 54 % yield and 96.5/3.5 er. The levels of chirality transfer exhibited were 95 % and 97 % respectively. That chirality transfers occurs in these reaction demonstrates that the

intermediate radicals **60** and *ent*-**60** do not interconvert by N-aryl bond rotation under the reactions conditions. Instead, rapid radical 5-*exo* cyclization traps the axial chirality of **56** in a new stereocenter in **57**.

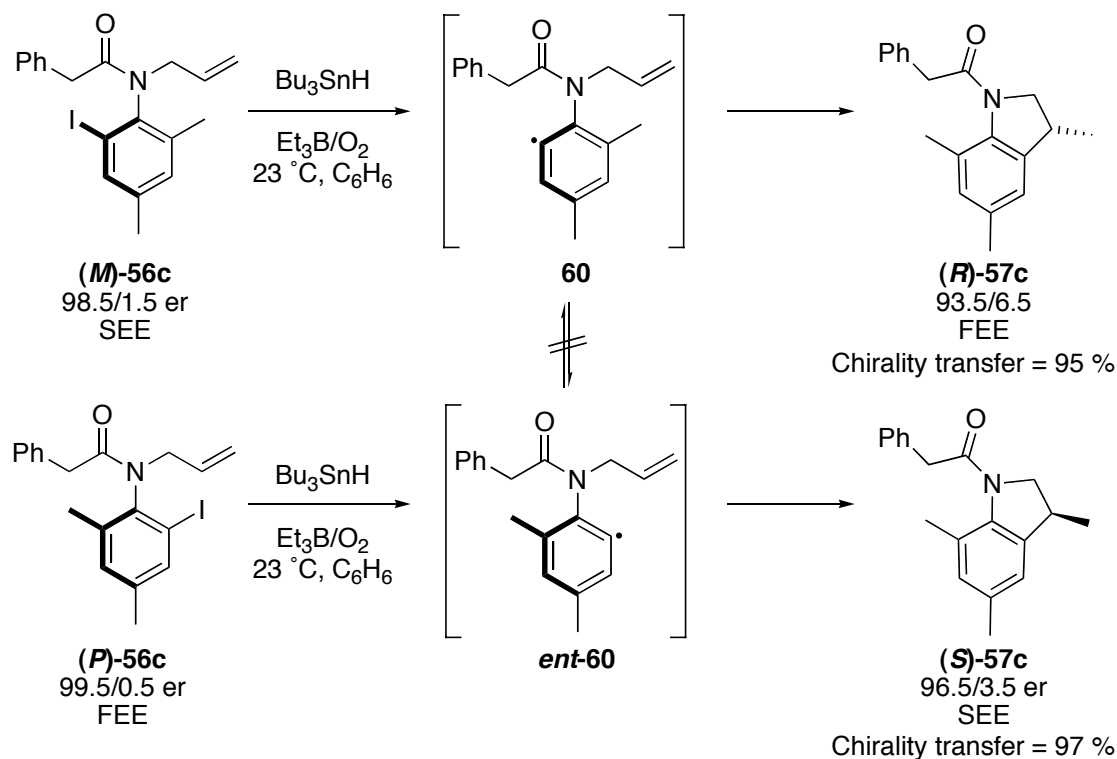
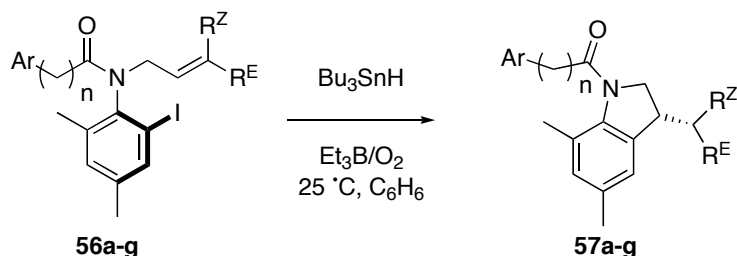


Figure 3.4 - Transfer of Chirality in Axially Chiral *N*-Allyl-*o*-Iodoanilides

Table 3-3 summarizes the cyclization data for all precursors **56a-g**. Yields of **57** were good to excellent (67–95 %), although substrates **56c,d** were exceptions (40–54 %, entries 5/6 and 7/8). Substitution about the alkene radical acceptor impacted the level of chirality transfer observed. Substrates with no substitution or with a single *E*-substituent in the terminal alkene position cyclized with high levels of chirality transfer (87–97 %, Entries 1/2, 5/6, 7/8, 9/10 and 13/14). Marginally lower levels of chirality transfer (74–80 %) were observed for substrates bearing terminal *Z*-substituents (Entries 3/4 and 11/12).



Entry	Precursor	Elution Order _{SM}	Ar	n	R ^Z	R ^E	er _{SM}	Product	Elution Order _P	%Yield ^b	er _P	% Chirality Transfer
1	(+)- 56a	FEE	Ph	0	H	H	99.5/0.5	(+)- 57a	FEE	95	93/7	93
2	(-)- 56a	SEE	Ph	0	H	H	99.5/0.5	(-)- 57a	SEE	92	93.5/6.5	94
3	(+)-(P)- 56b ^a	FEE	4-BrC ₆ H ₄	0	Me	Me	99.5/0.5	(+)-(S)- 57b ^a	SEE	72	74/26	74
4	(-)-(M)- 56b ^a	SEE	4-BrC ₆ H ₄	0	Me	Me	99/1	(-)-(R)- 57b ^a	FEE	95	73.5/26.5	74
5	(-)- 56c	FEE	Ph	1	H	H	99.5/0.5	(-)- 57c	SEE	54	96.5/3.5	97
6	(+)- 56c	SEE	Ph	1	H	H	98.5/1.5	(+)- 57c	FEE	53	93.5/6.5	95
7	(-)- 56d	FEE	Ph	1	H	Ph	99.5/0.5	(-)- 57d	SEE	40	87/13	87
8	(+)- 56d	SEE	Ph	1	H	Ph	99/1	(+)- 57d	FEE	50	88/12	89
9	(-)- 56e	FEE	Ph	1	H	Me	99.5/0.5	(-)- 57e	SEE	77	89.5/10.5	90
10	(+)- 56e	SEE	Ph	1	H	Me	99.5/0.5	(+)- 57e	FEE	71	91.5/8.5	92
11	(-)- 56f	FEE	Ph	1	Me	Me	99.5/0.5	(-)- 57f	SEE	79	80/20	80
12	(+)- 56f	SEE	Ph	1	Me	Me	99.5/0.5	(+)- 57f	FEE	81	79/21	79
13	(-)- 56g	FEE	Ph	2	H	H	98/2	(-)- 57g	SEE	67	92.5/7.5	94
14	(+)- 56g	SEE	Ph	2	H	H	99.5/0.5	(+)- 57g	FEE	74	95/5	95

^a Absolute configuration assigned by X-ray crystallography.

^b Isolated yield after chromatography.

Table 3-3 - Summary of Radical Cyclizations of Anilides 56a-g

3.5. Determination of Absolute Configuration

The absolute configuration of precursor (-)-**56b** (second eluting enantiomer) was determined by X-ray crystallography using the anomalous dispersion method by Dr. Steve Geib. The crystal structure of (-)-**56b** in Figure 3.5 shows it to possess the *M* configuration. The plane of the amide bond in precursor **56b** is nearly perpendicular to the plane of the aryl ring (84°), a common feature of tertiary anilides.⁶ As predicted,⁵ the aryl ring is trans to the amide oxygen.

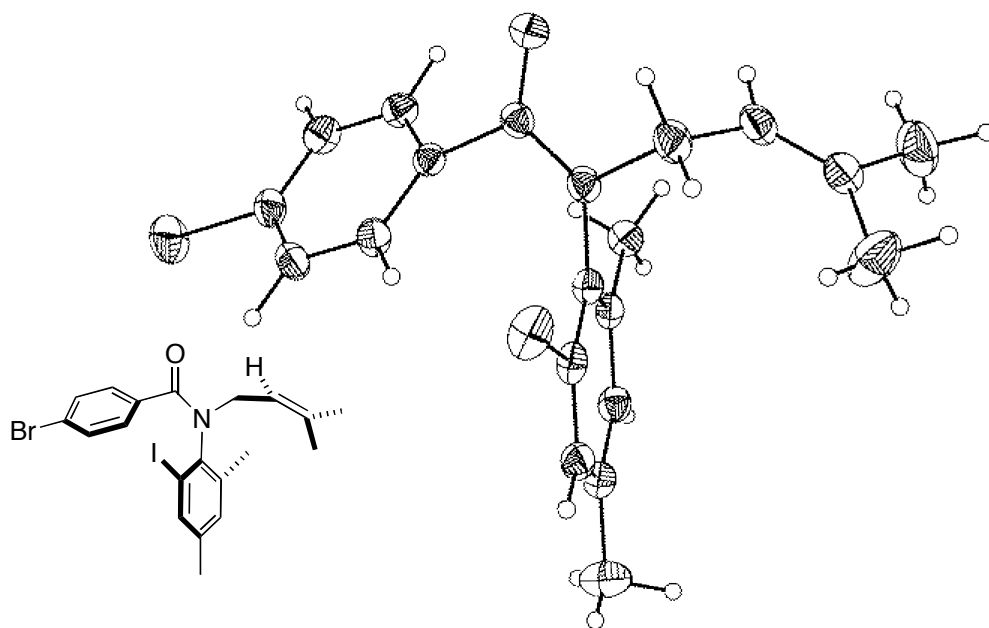


Figure 3.5 – ORTEP Diagrams of (M)-56b

The X-ray crystal structure of (–)-(*R*)-**57b** (first eluting enantiomer) differs in that the N-Ar group is now nearly cis to the carbonyl oxygen (angle 10°) while the N-CH₂ group is nearly trans (angle 150°). The unusual amide bond geometry is likely the outcome of the severe strain that is imposed by the *o*-methyl group in the standard amide geometry.

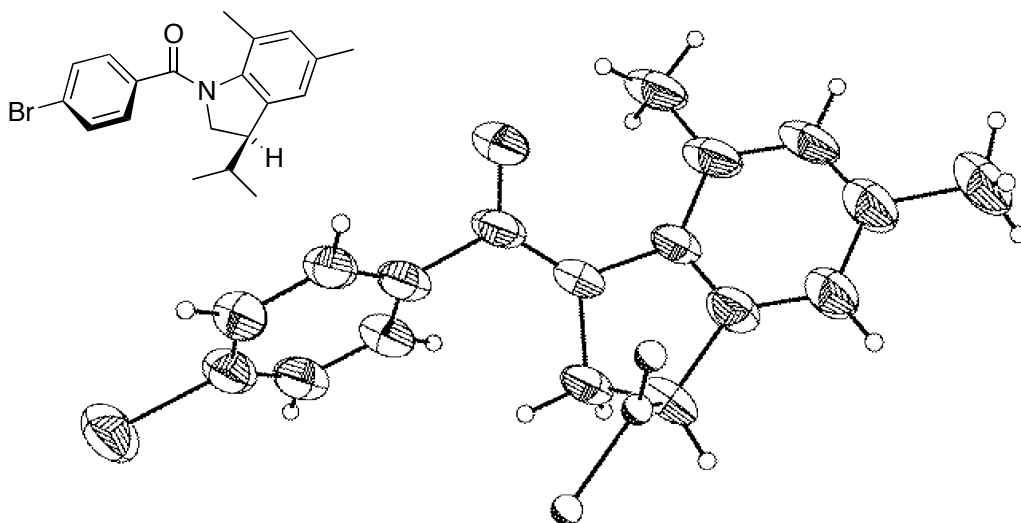


Figure 3.6 – ORTEP Diagrams of (*R*)-57b

Having established the absolute configurations of anilide (*M*)-56b and dihydroindolone (*R*)-57b we examined the possibility of assignment of the absolute configurations of the remaining compounds, relying on optical rotation and chiral HPLC data. A couple of trends were noted, *e.g.* for all seven enantiomeric pairs, the dextrorotatory enantiomer of the precursor yielded the dextrorotatory enantiomer of the product, and vice versa. Secondly, the first eluting enantiomer of the precursor on a (*S,S*)-Whelk O 1 chiral HPLC column gave the second eluting enantiomer of the product, and vice versa. The exception to the latter trend was benzamide 56a/57a (FEE → FEE, SEE → SEE). Unfortunately, based on the above information it is not possible to make strong conclusions about the configurations of the remaining precursors/products.

3.6. Preliminary Model of Chirality Transfer

Having confirmed that (*M*)-56b cyclizes faithfully to (*R*)-57b, a preliminary model of chirality transfer in N-allyl cyclizations was proposed (Figure 3.7, upper). When aryl radical **61** is formed, the aniline ring is in a perpendicular orientation with respect to the plane of the amide bond. N-aryl bond rotation in **61** positions the radical for attack on the allyl group. Also, a C–C

bond rotation away from the radical (**61** → **62**) exposes the reactive alkene face. This model for cyclization stands in stark contrast to our current model for cyclization of N-acryloyl anilides^{9e,h,i} (Figure 3.7, lower). In it, a cyclization of radicals like **64** that proceeds with twisting of the acryloyl group towards the aryl radical (**64** → **65**), accounts for the configurations of the final products.

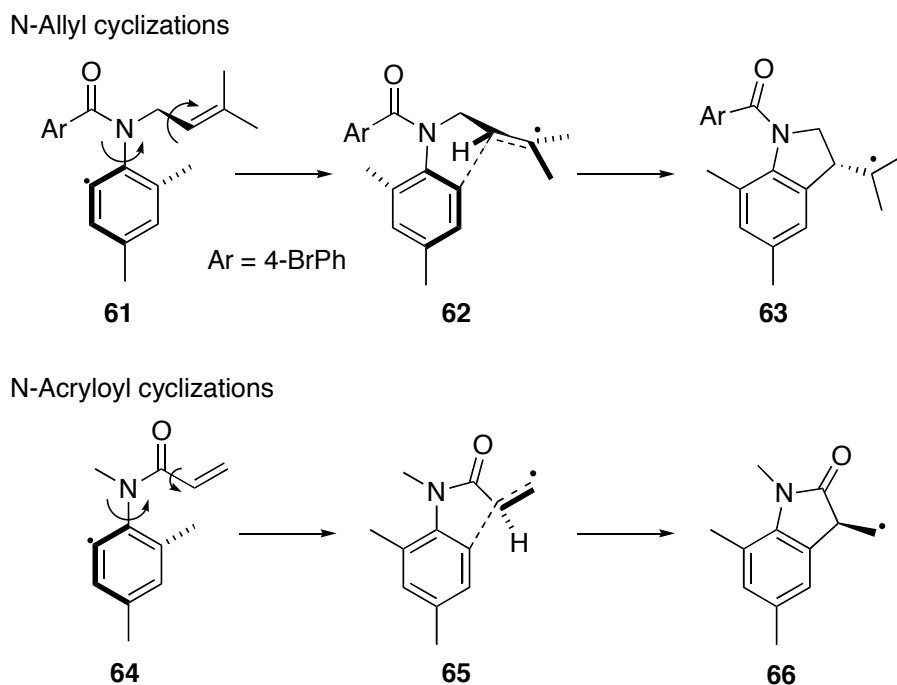


Figure 3.7 - Rationalization of Observed Stereochemistry for N-Allyl and N-Acryloyl Anilides

Apparently, the disparate cyclization models are the result of the differing conformational properties of the two systems. In the N-acryloyl systems, π -conjugation between the carbonyl group and the alkene in **64** rigidifies the conformation about the OC–C bond. In contrast, C–C bonds in N-allyl groups possess greater conformational flexibility that can accommodate a different mode of twisting of the alkene group. To date, the configurations of the N-acryloyl precursors and the products from their cyclizations have been established by a combination of

X-ray crystallography and optical rotation calculations and measurements for multiple substrates.^{9c,h,i} In contrast, stereochemical data for N-allyl cyclizations rests on a single pair of crystal structures (Figure 3.5, Figure 3.6). Further confirmations of configurations of other precursors/products pairs in the N-allyl series would allow a more authoritative comparison of the two modes of cyclization.

3.7. Regioselectivity, Competitive Cyclizations

Radical cyclizations of racemic *o*-bromoanilides lacking a second *ortho* substituent have been studied previously (Figure 3.8).³⁴⁻³⁷ In a 1988 methodology study, Bowman and co-workers generated aryl radicals under standard tin hydride conditions that cyclized onto the N-acryloyl group to yield oxindoles **68**.³⁴ Earlier that same year, Dittami and Ramanathan published a study of the analogous N-allyl cyclizations. In it, they observed that cyclization of anilides **69** provided dihydroindolones **70**.³⁵ When Jones and Storey submitted anilides **71**,³⁶ a substrate possessing both types of alkene radical acceptors, under the same radical conditions, only cyclization to the crotonoyl group to give oxindole **72** was observed.³⁸ Jones attributed this exclusivity to conformational preferences of starting material that biased **71** towards N-acryloyl cyclization. In particular, local minima that placed the aryl ring at 60° to the amide plane (Br proximal to the N-acryloyl side) were proposed and supported by MM2 calculations. When the system was modeled again using improved parameters by us,³⁹ a minimum was predicted with the aryl ring aligned nearly perpendicular. Furthermore, this conformational preference was supported by crystallographic data of related anilides.⁶

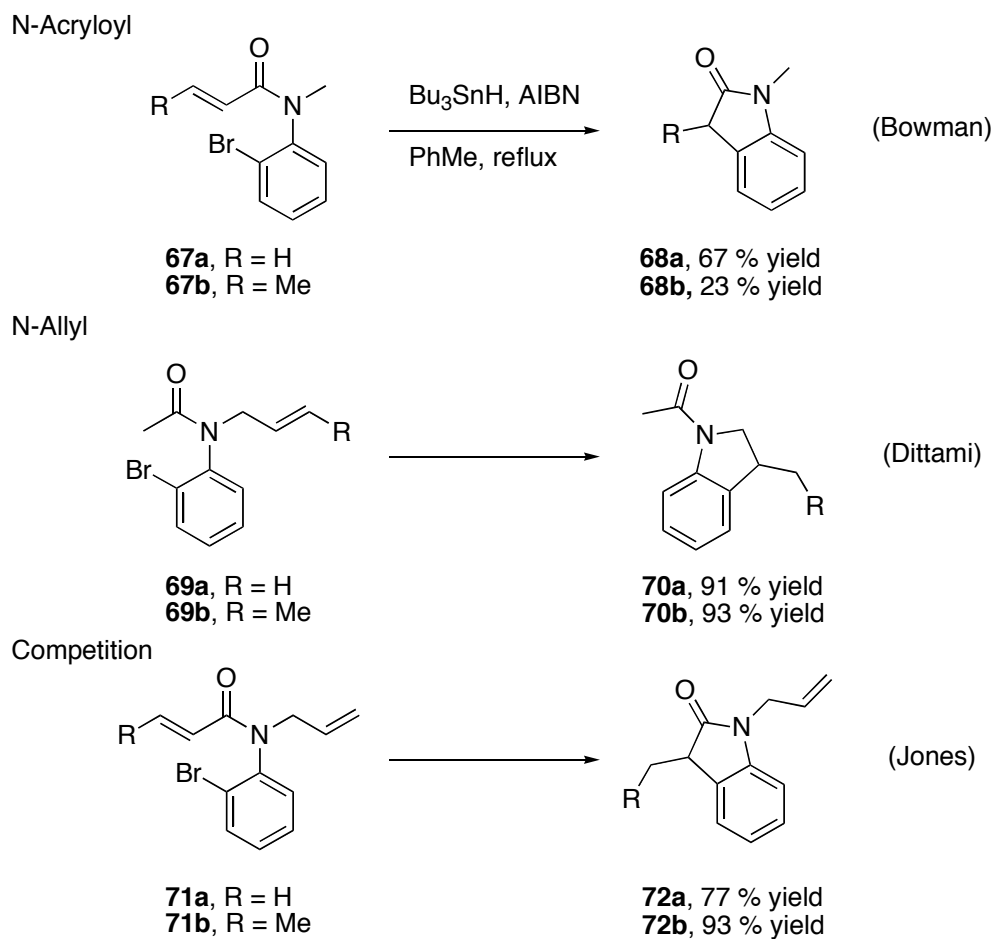
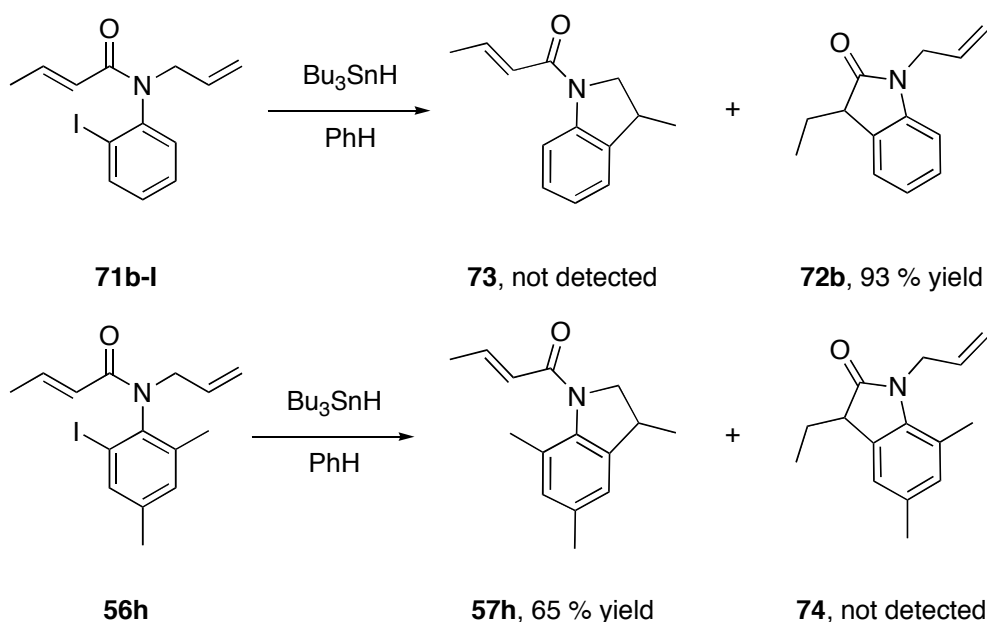


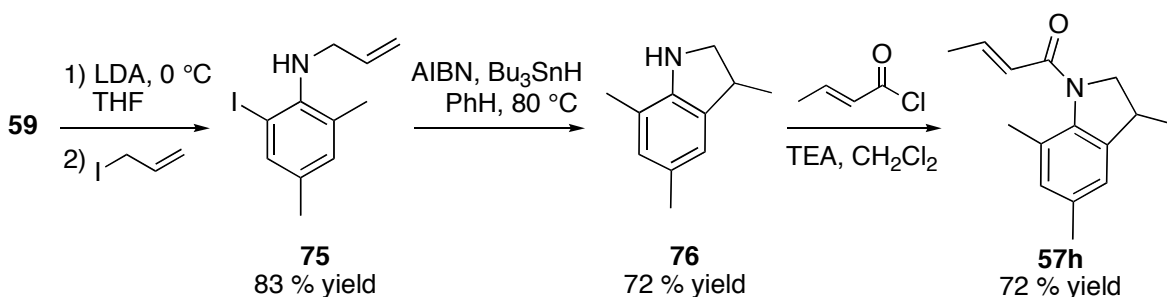
Figure 3.8 - Radical Cyclizations of *o*-Bromoanilides Lacking *ortho* Substituents

The unexpected regioselectivity in the cyclization of **48** (Scheme 3.1) appeared *prima facie* in conflict with Jones' results (**71** → **72**, Figure 3.8). As a direct comparison to the Jones internal competition experiment, we studied the cyclization of analogous anilide **rac-56h** (Scheme 3.3). Like Jones' compound **73**, anilide **56h** has identical N-crotonoyl and N-allyl groups in place as radical acceptors. Unlike **73**, the aryl ring of **56h** has an *ortho* methyl group in lieu of a hydrogen atom. There is also an additional *para* methyl group, but it is likely too far removed from the reactive center to influence reactivity. Similarly, the use of an iodide as radical precursor over a bromide is also considered inconsequential. When **56h** was cyclized, it

produced dihydroindolone **57h** in 65 % isolated yield, resulting from cyclization to the N-allyl group. The ^1H NMR spectrum of the crude product matched an authentic sample of **57h** prepared by an alternative route (Scheme 3.4). Furthermore, the ^1H NMR spectrum of the crude product did not reveal any signals corresponding to the expected product **74**, the outcome of cyclization to the N-crotonoyl group. To verify Jones' structural assignment, the *o*-iodoanilide analog of **71b** was prepared and cyclized, which provided exclusively oxindole **72b** in 93 % yield; dihydroindolone **73** was not detected (Scheme 3.3). Clearly, the identity of the *ortho* substituent greatly impacts the regioselectivity of the cyclization.



Scheme 3.3 - Regioselectivity Reversal Affected by *ortho* Substitution



Scheme 3.4 - Synthesis of Authentic Sample of 57h

3.8. Cyclization Rate Constant Measurements

To better understand the change in regioselectivity, we measured the cyclization rate constants of **56h** (N-allyl) and **78** (N-acryloyl) by standard competition kinetics.⁴⁰ Samples of **56i** and **78** were cyclized at 80 °C at varying concentrations of tin hydride. The molar ratios of cyclized to reduced product (**57i/77**, **79/80**) were measured by GC against an internal standard. Data for these experiments are shown in Figure 3.9 and the calculated rate constants are summarized in Figure 3.10.[†] The rate constant for cyclization of **83** was found to be $3.0 \times 10^9 \text{ s}^{-1}$, almost 40 times larger than that for cyclization of **85** ($7.8 \times 10^7 \text{ s}^{-1}$). We also attempted to measure the rate constant for cyclization of radical **81**. When anilide **71b-I** was cyclized at 80 °C only trace amounts of the reduced product were detectable by GC, even when the reaction was conducted at the highest tin hydride concentrations. Based on these observations, we estimate a lower limit for the cyclization rate constant of radical **81** at about 10^{10} s^{-1} .

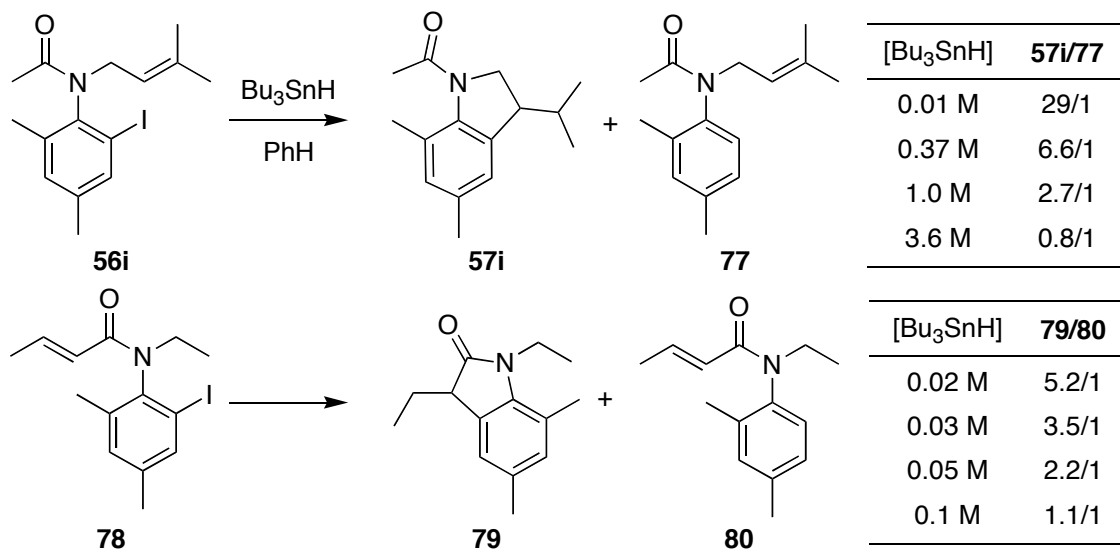


Figure 3.9 - Cyclization Rate Constant Measurements for **56i** and **78**

[†] A fuller treatment of this data can be found in Section 6.8 (page 118).

A comparison of the two N-acryloyl examples reveals the dampening effect of *ortho* substitution on the speed of cyclizations. The presence of the *o*-methyl group slowed the rate of cyclization by approximately two orders of magnitude (**85** → **86**) versus the unsubstituted process (**81** → **82**). In contrast, in the case of N-allyl cyclization (**83** → **84**), the slowdown was less dramatic, allowing that process to overtake competing N-acryloyl cyclization in **56h** (Scheme 3.3).

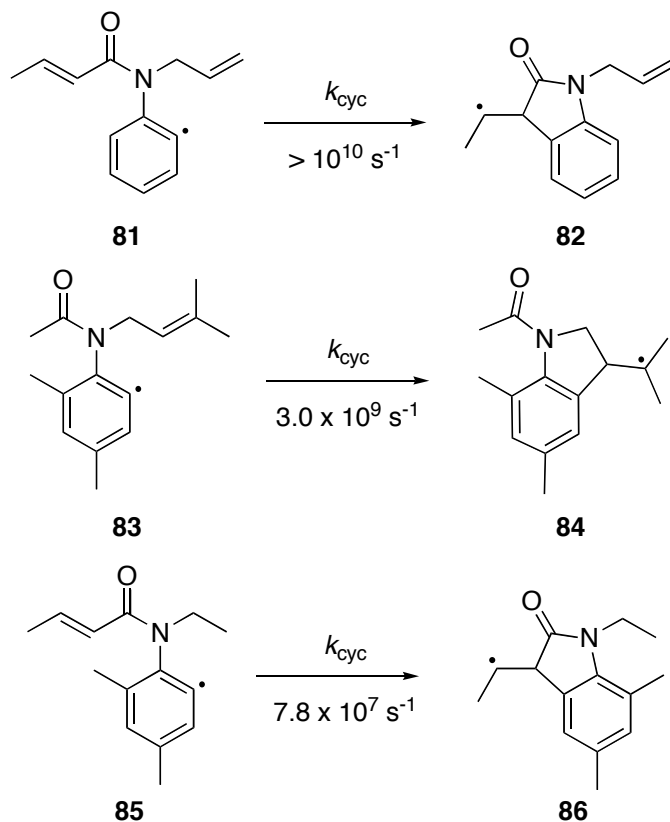


Figure 3.10 - Cyclization Rate Constants

A proposal for the role of *o*-methyl group in the slowdown of the N-acryloyl cyclization is diagrammed in Figure 3.11. Cyclization to the N-acryloyl group probably requires significant co-planarity between the aniline ring and the amide group (**87** → **88a**), forcing a steric interaction between the *o*-methyl group and methylene of the N-allyl group that increases the energetic barrier to the process. In contrast, the N-allyl group, not being strained by resonance,

is more flexible and can extend out towards the attacking radical (**87** → **88b**). The net outcome is less twisting of the aryl group is necessary and steric interactions between the *o*-methyl group and the N-acryloyl group are avoided.

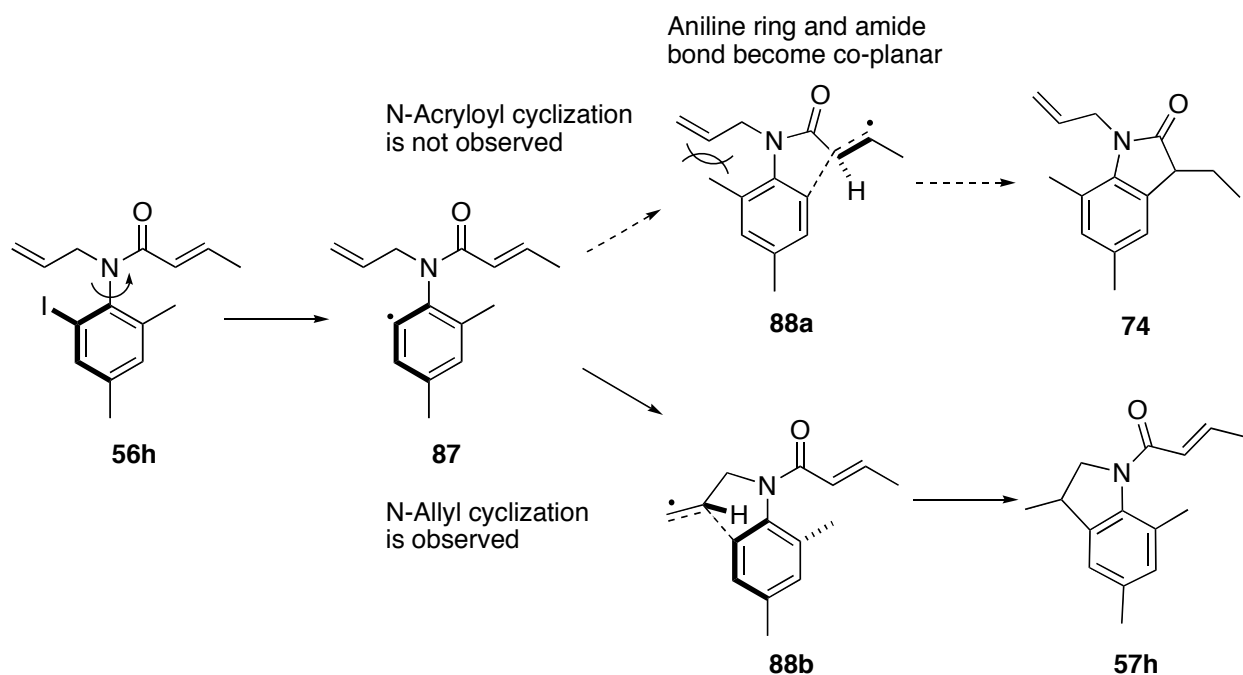


Figure 3.11 - Transition State Analysis

3.9. Conclusions

In summary, intrigued by the results a ‘failed’ reaction, a study axially chiral *N*-allyl-*o*-iodoanilides revealed that they can be cyclized under radical conditions to the product dihydroindolones with high levels of chirality transfer (74–97 %). Based on a pair of X-ray crystal structures a preliminary model has been proposed to predict the mechanism of chirality transfer. A series of rate constants measurements were used to elucidate the role of *ortho* substitution in the unanticipated reversal from N-acryloyl cyclization to N-allyl cyclization. As well, the N-aryl bond rotation barriers of four anilides were quantified (29.7–30.7 kcal/mol or 124.3–136.9 kJ/mol).

4. RELAYING ASYMMETRY OF TRANSIENT ATROPISOMERS OF *O*- IODOANILIDES

4.1. Background

Radicals were initially viewed by the synthetic community as unsuitable for enantioselective reactions because of their highly reactive nature. This misconception has since subsided under growing evidence of enantioselective radical processes.⁴¹ In the 1980s, researchers in the radical community began to apply techniques of stereoselection brought over from the domains of ionic and pericyclic chemistry to radical reactions.⁴² In 1989, Porter and co-workers reported the successful 15-*endo* radical cyclization of **89**.⁴³ All four possible diastereomers of **90** were observed; the *endo/exo* ratio was found to be 8/1. While the *exo* products (not shown) exhibited no stereoselection, the *endo* products were isolated in an 18/1 diastereomeric ratio, with **90** being the major component. The key to the stereoselection is the C₂-symmetric amide auxiliary, a strategy that had been used before successfully in enolate and cycloaddition chemistry.⁴⁴ The auxiliary influences the face of attack of the intermediate radical at the α alkene position. That no stereoselection is observed at the β position is likely because the auxiliary is too distant from the reaction site to have any influence.

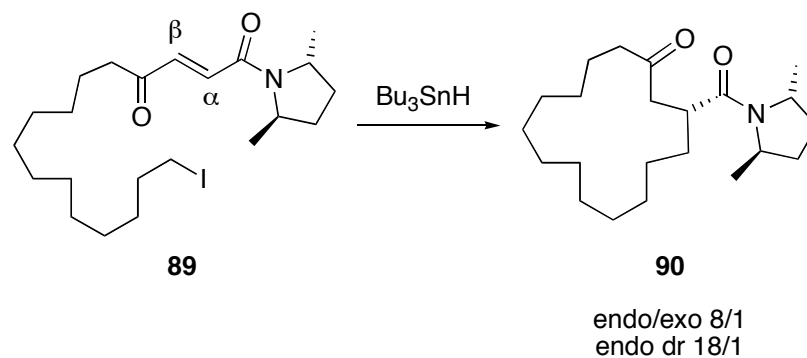


Figure 4.1 –Radical Cyclization with Stereoselection Controlled by Chiral Auxiliary

Not all uses of chiral auxiliaries resulted in high stereoselection. Also in 1989, Jones and co-workers reported on the radical cyclizations of *o*-haloacrylanilides bearing chiral N-substituents **91** as part of their program towards the synthesis of oxindole and indole-derived natural products (Figure 4.2).⁴⁵ Jones and McCarthy reasoned that the chiral substituents should induce stereoselectivity during their radical cyclization to form oxindoles **92**. In fact, only low levels of asymmetric induction were observed in the cyclization products **92**.⁴⁶ For example, cyclization of *N*-2-phenylethyl acrylanilide **91a** with Bu_3SnH in toluene at 105 °C provided dihydroindolone **92a** as a 51/49 mixture of stereoisomers. When vicinal methyl groups were introduced to the alkene (**91b**), the dr of the product (**92b**) rose to 69/31. Jones reasoned that the additional steric bulk interacted with the chiral auxiliary in the transition state, thereby helping to differentiate the diastereotopic faces of the alkene. The failure to observe useful levels of stereoselection though, suggests that the chiral center is unable to influence the attack of the aryl radical and the two diastereomeric transition states are near in energy.

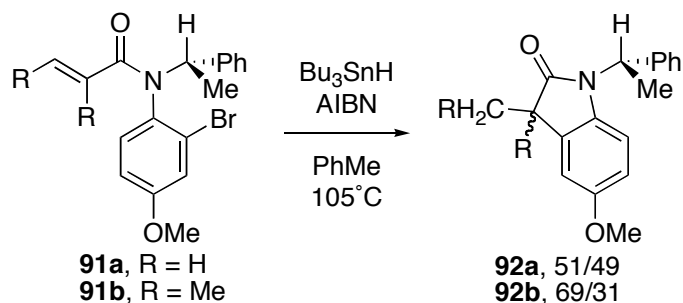
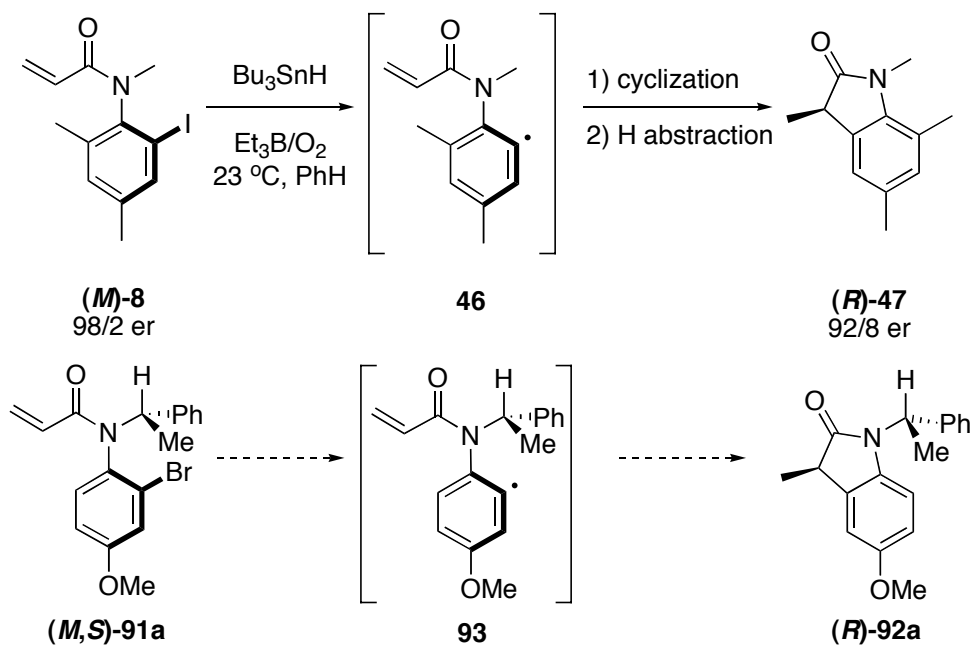


Figure 4.2 – Radical Cyclization of Anilide 91 with Low Stereoselection

Jones noted broadening of signals in the ^1H NMR of **91**, a feature he attributed to restricted rotation about the N-aryl bond. If **91a** could be resolved into its diastereomeric atropisomers, we believed it would be possible to cyclize them separately to the corresponding oxindole *e.g.* (*M,S*)-**91a** \rightarrow **93** \rightarrow **92a** (Scheme 4.1) in a process analogous to the cyclization of enantiomeric (*M*)-**8**.^{9c} We began a research project to prepare and resolve diastereomeric anilides like **91** and to evaluate whether they too can be cyclized under radical conditions to the corresponding oxindole with transfer of axial chirality to the newly formed stereocenter.



Scheme 4.1 – Comparison of Cyclization of Anilides 8 (Curran) and 91a (Hypothetical)

Another reason for studying the stereoselective cyclizations of anilides like **91** is that the products lack an *ortho* substituent. In comparison, the cyclization **8** → **47** yields a product with a methyl group in the 7-position, an unseen substitution pattern in the oxindole class of natural alkaloids. This feature may make this class of anilides better suited for the synthesis of natural oxindole alkaloids such as (–)-horsfiline⁴⁵ and spirotryprostatin B (Figure 4.3).⁴⁷

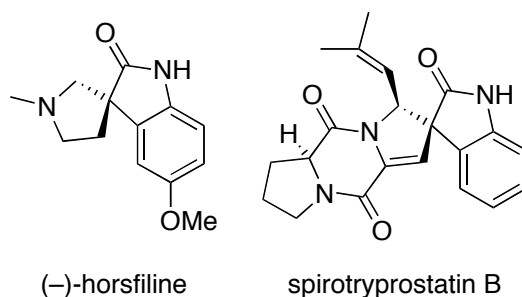
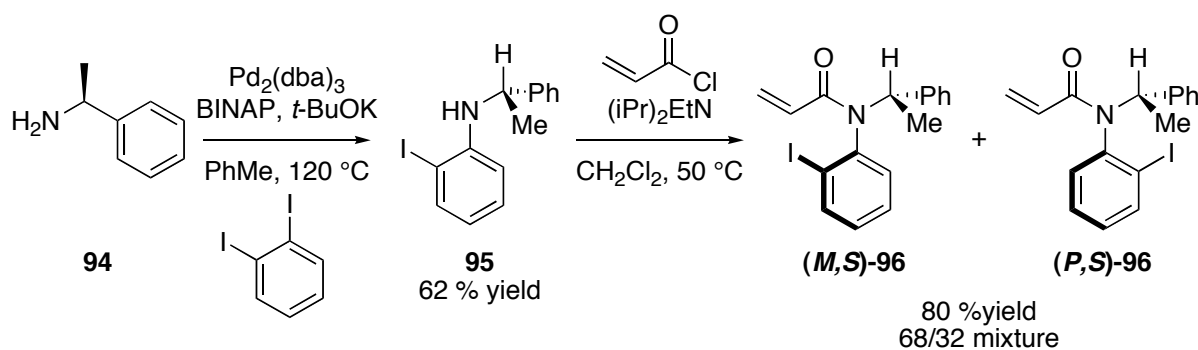


Figure 4.3 - Oxindole Natural Products

4.2. Resolution of Chiral Auxiliary-based Atropisomers

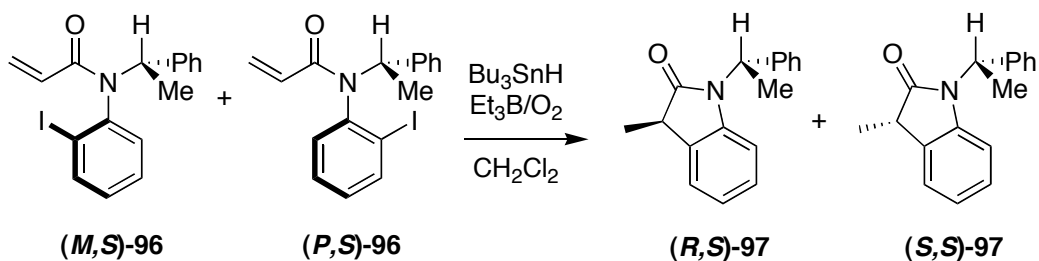
To address this question, co-worker Dr. Marc Petit prepared iodoacrylanilide **95** from 1,2-diodobenzene **94** in a two-step procedure (Scheme 4.2). A Buchwald-Hartwig coupling between (*S*)-phenethylamine **93** and 1,2-diodobenzene formed aniline **95** in 62 % yield. Acylation of **95** produced a mixture of atropisomers (*M,S*)-**96**/*(P,S)*-**96** in a 68/32 ratio, as determined by NMR spectroscopic studies at room temperature. Although the atropisomers of **95** were not separable by silica gel flash chromatography, resolution of the diastereomers was possible using preparative chiral HPLC ((*S,S*)-Whelk-O 1). At the time of this work, this was the first known example of resolution of mono-*ortho*-substituted anilides, except when the *ortho*-substituent is *tert*-butyl.^{9a,b} Dr. Petit was able to resolve **96** into its atropisomeric components (*M,S*)-**96** and (*P,S*)-**96** by preparative HPLC experiments. The isolated major diastereomer

(*M,S*)-**96** equilibrates to a 68/32 (*M,S*)-**96**/*(P,S)*-**96** mixture, the *N*-aryl bond rotation barrier was found to be 23.0 kcal/mol or 96.3 kJ/mol ($\tau_{1/2}$ = 156 min at 25 °C). Because the barrier to equilibration is exceedingly low, care must be taken to minimize the exposure of enriched samples of (*M,S*) or (*P,S*)-**96** to sources of heat during handling.



Scheme 4.2 - Synthesis of (*S*)-phenethylamine-derived *o*-Iodoacrylanilide **96**

Mixtures of **96** were cyclized at a number of different temperatures, as summarized in Table 4-1. When an equilibrium mixture of **96** was submitted to standard radical cyclization at 110 °C (entry 1), a 50/50 ratio of products (*R,S*)-**97** and (*S,S*)-**97** was obtained. Anilide **96** differs in halide (Br → I) and *ortho* substitution (OMe → H) from **89a**, but because the cyclization result is consistent with Jones' observation, we believe that these changes to be immaterial to the stereoselectivity. When the reaction temperature was lowered, the diastereomeric ratio of **97** increased until plateauing at 84/16 (−25 °C) (entries 2–5). Diastereomerically enriched samples of **96** were obtained by preparative chiral HPLC. When a mixture in a 91/9 ratio of (*M,S*)-**96**/*(P,S)*-**96** was cyclized at −78 °C, (*R,S*)-**97** and (*S,S*)-**97** were obtained in a 95/5 ratio, while a mixture in a 2/98 ratio gave (*R,S*)-**97**/*(S,S)*-**97** in 16/84 ratio (entries 6–7). In comparison, each atropisomer of **96** cyclizes to a different stereoisomer of oxindole **97**, but the cyclization of the major atropisomer (*M,S*)-**96** is more selective than that of the minor (*P,S*)-**96**.



96 $(M,S)/(P,S)$	Temp. (°C)	97 $(R,S)/(S,S)$	% Yield
68/32	110	50/50	82
68/32	20	78/22	79
68/32	0	81/19	76
68/32	-25	84/16	82
68/32	-78	84/16	73
91/9	-78	95/5	84
2/98	-78	16/84	76

Table 4-1 - Diastereoselective Cyclizations of *o*-Iodoacrylanilide **96**

A mechanistic proposal to rationalize the results in Table 4-1 is offered in Figure 4.4. Tributyltin radical abstracts an iodine atom from **96** to form a mixture of diastereomeric radicals **98 α** , **98 β** , initially in a ratio comparable to the diastereomeric ratio of **96**. There are two relevant pathways for radicals **98**, cyclization or N-aryl bond rotation. Because of the loss of a bulky iodine atom, radicals **98 α** , **98 β** are now more susceptible to interconversion by rotation and subsequent loss of stereochemical sense. Radical cyclization of **98** produces **99**, which leads to oxindole **97** after hydrogen abstraction from tributyltin hydride. We hypothesize that the varying stereoselection with temperature can be explained by how the rates of rotation compare with those of cyclization. At higher temperatures, the rates of interconversion between the diastereomeric

radical intermediates (k_r and k_r') compete with the rates of cyclization ($k_{c\alpha}$ and $k_{c\beta}$).[‡] The net result is poor stereoselection because the sense of stereochemistry in axis is scrambled prior to cyclization. In contrast, at temperatures equal to or below 20 °C, the level of stereoselectivity actually exceeds that of the initial rotamer ratio (68/32) (entries 2–5). At lower temperatures the interconversion of radicals **98 α** ,**98 β** is suppressed and each radical cyclizes with its own selectivity in favor of opposite stereoisomers of **99**. Radical **98 β** cyclizes to (*R,S*)-**99** with high fidelity, while **98 α** cyclizes predominately to (*S,S*)-**99** but with approximately 20 % leakage to (*R,S*)-**99**. This leakage accounts for the observation that the product ratios differ from the starting atropisomer ratios when **98 β** is present in significant amounts.

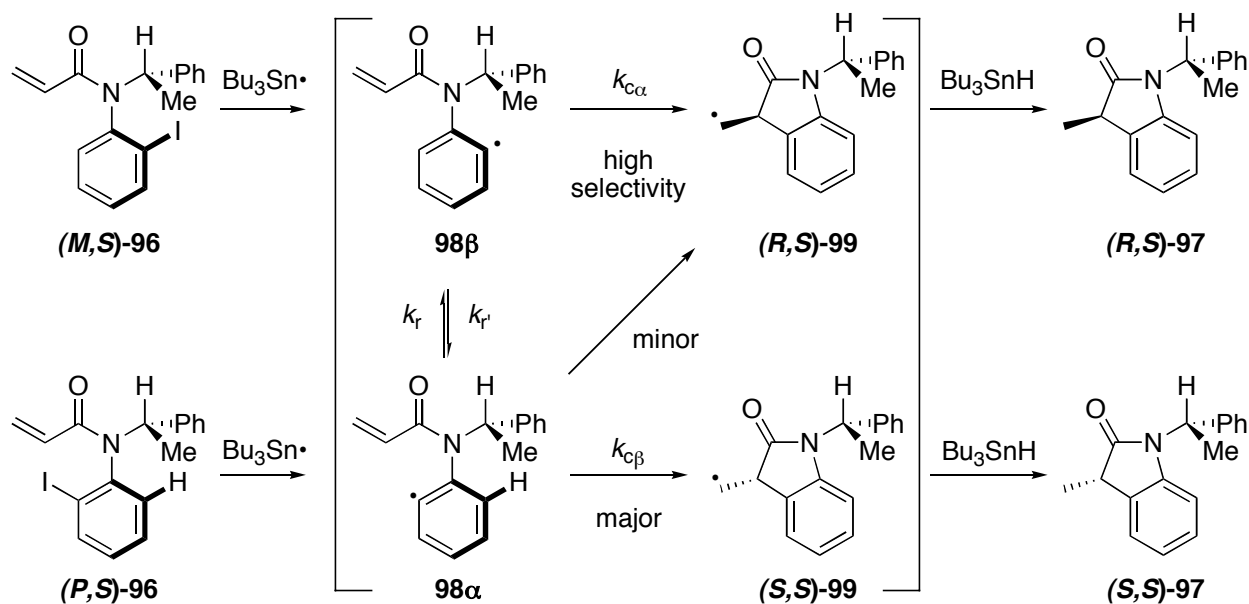
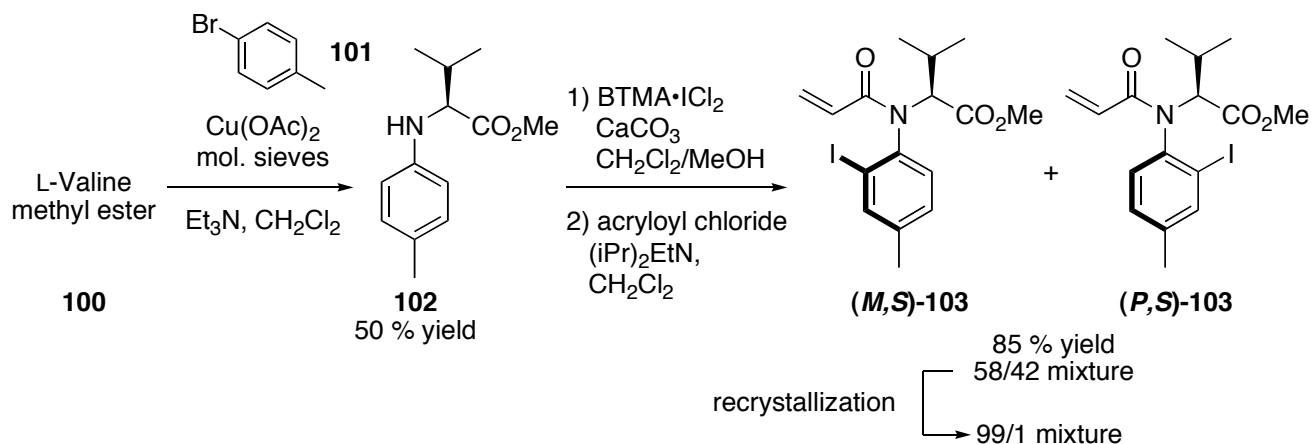


Figure 4.4 - Mechanistic Proposal

[‡] Based on control experiments, we do not believe that diastereoselective iodine abstraction is a possibility. A series of cyclization experiments at varying substoichiometric amounts of Bu_3SnH showed that (*M,S*)-**96** and (*P,S*)-**96** were consumed at about equal rates.

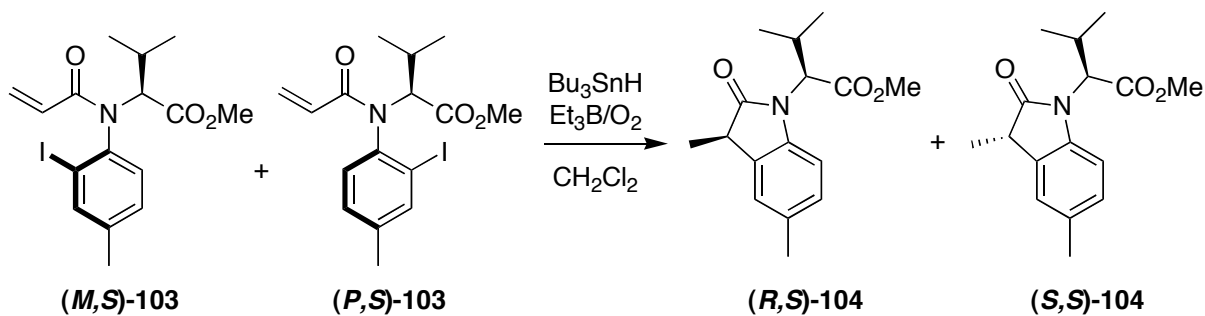
Dr. Petit next prepared iodoanilide **103** from L-valine **100**. Initial attempts to couple L-valine with diiodobenzene **94** under Pd-catalyzed conditions were unsuccessful (not shown), presumably for steric reasons, so a three step synthesis of **103** was employed (Scheme 4.3). First, L-valine **100** and *p*-bromotoluene **101** were coupled in a Cu-catalyzed reaction⁴⁸ to produce aniline **102** in 50 % yield. The iodinating agent benzyltrimethylammonium dichloriodide was used to install an *ortho* iodine atom. Subsequent acylation with acryloyl chloride yielded anilide **103**. At ambient temperature, anilide **103** exists as a 58/42 equilibrium mixture of (*M,S*) and (*P,S*) rotamers, which were separable by preparative HPLC. More conveniently, slow crystallization of the equilibrium mixture from hexanes deposited exclusively (*M,S*)-**103** in a crystallization-induced asymmetric transformation. The barrier to rotation from the major (*M,S*) to minor diastereomer (*P,S*) of **103** was measured to be 24.3 kcal/mol (101.7 kJ/mol). The absolute configuration of the (*M,S*)-**103** was established by X-ray crystallography.



Scheme 4.3 - Synthesis of L-Valine-derived *o*-Iodoacrylanilide **103**

Cyclization of a 99/1 mixture of rotamers (*M,S*)-**103**/(*P,S*)-**103** faithfully provided (*R,S*)-**104** (94/6–97/3), while cyclization of a 97/3 mixture enriched in (*P,S*)-**103** faithfully provided (*S,S*)-**104** (91/9). A sample of (*R,S*)-**104** was recrystallized; X-ray analysis of the resulting single

crystal allowed an unambiguous assignment of the absolute configuration of **104** to be assigned. The transfer of chirality observed for **103** → **104** is consistent with the stereochemical model proposed for previous results in an enantiomeric series (Scheme 2.7).^{9c,h}



103 (<i>M,S</i>)/(<i>P,S</i>)	Temp. (°C)	104 (<i>R,S</i>)/(<i>S,S</i>)	% Yield	% Chirality Transfer
99/1	25	94/6	73	95
99/1	0	94/6	82	95
99/1	-78	97/3	76	98
3/97	25	9/91	79	94
3/97	-78	9/91	82	94

Table 4-2 - Diastereoselective Cyclizations of *o*-Iodoacrylanilide **103**

4.3. Enantiomeric Series

The successful resolution and selective cyclization of diastereomeric atropisomers such as **93** and **103** suggested that analogous enantioselective transformations were possible. We postulated that a key feature that enabled the resolution of anilides **96** and **103** was the use of branched N-alkyl groups to increase the N-aryl bond rotation barrier. Based on the success of **96** and **103**, we attempted to prepare and resolve a series of racemic *o*-iodoanilides with branched N-alkyl groups (Figure 4.5). Each N-alkyl group was chosen for its bulkiness and synthetic accessibility. Anilide **105c** is particularly promising because, unlike **105a,b**, the N-diphenylmethyl group is potentially removable at a later stage by a reductive hydrogenation procedure.

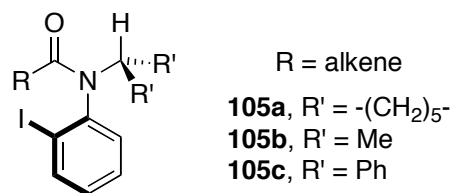
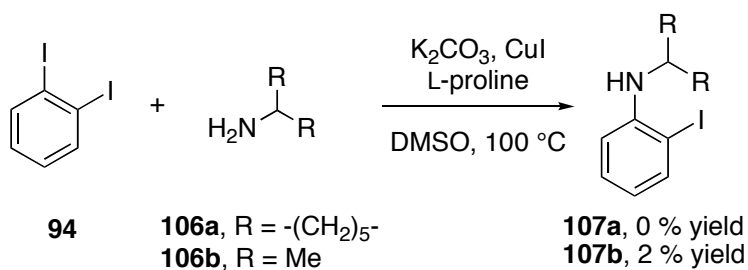


Figure 4.5 - Proposed Series Enantiomeric *o*-Iodoanilides

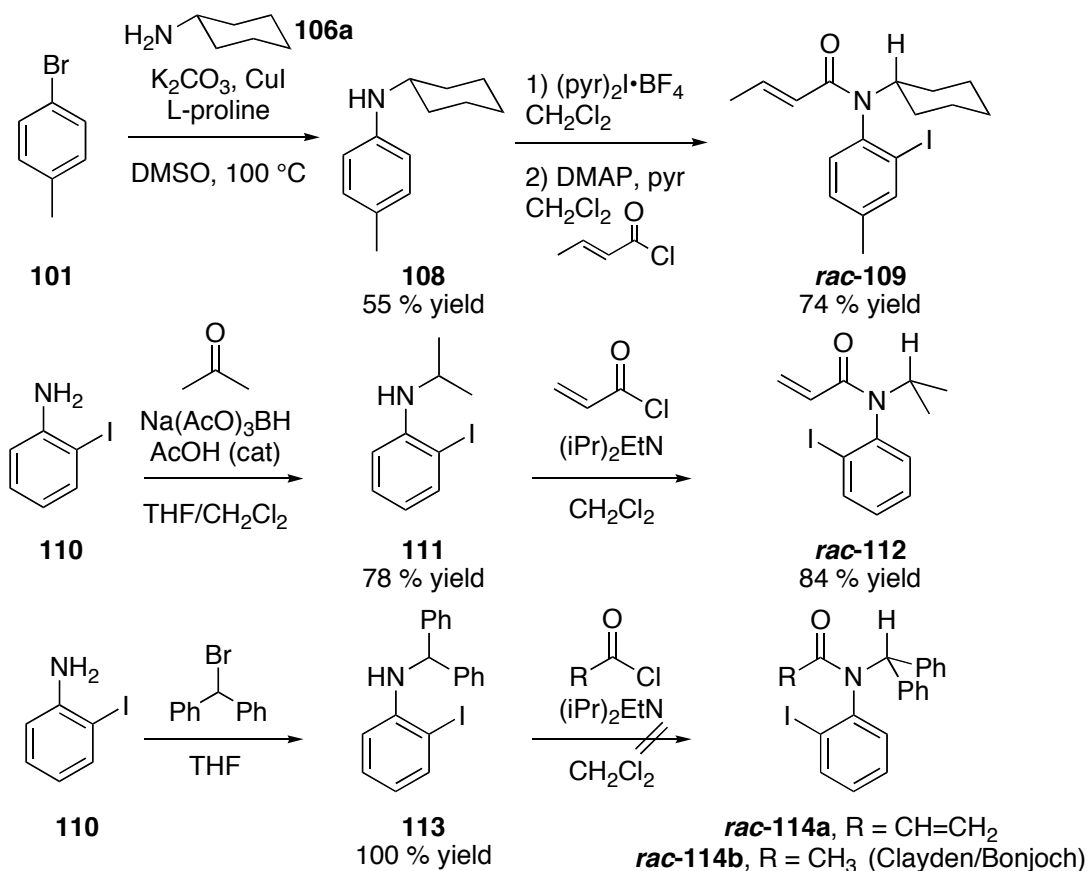
Our initial synthetic approach to this class of anilides relied on a modified Ullman reaction⁴⁹ between the amines **106** and 1,2-diiodobenzene **94** (Scheme 4.4). Unfortunately, the reactions with cyclohexylamine **106a** and isopropylamine **106b** proceeded with little or no yield. We attributed this failure to steric congestion at the reaction site by the neighboring iodine atom.



Scheme 4.4 – Initial Unsuccessful Attempts at N-Arylation of 106

Changing plans, for the cyclohexyl substrate we opted for the approach used for the synthesis of anilide **103** (Scheme 4.3). Coupling of cyclohexyl amine to *p*-bromotoluene generated aniline **108** in 55 % yield (Scheme 4.5). Iodination with dipyridine iodonium tetrafluoroborate⁵⁰ cleanly installed the requisite iodine atom. Acylation of **108** with crotonoyl chloride under the standard acylation procedure was unsuccessful, possibly due to the bulky nature of the cyclohexyl group on the nitrogen. Ultimately, acylation of **108** in the presence of excess DMAP (2 equiv), pyridine (3 equiv), and crotonoyl chloride (3 equiv) produced *rac*-**109** in 74 % yield. To prepare isopropyl substrate **112**, we opted for a reductive amination between 2-iodoaniline **110** and acetone, which cleanly produced aniline **111** in 78 % yield (Scheme 4.5). Acylation of

2-iodoaniline **110** with acryloyl chloride yielded the desired anilide *rac*-**112** in racemic form. Attempted synthesis of the diphenylmethyl precursor **114a** began with the alkylation of 2-iodoaniline **110** with diphenylmethyl bromide to give **113** (Scheme 4.5). Unfortunately, the attempted acylation of **113** gave only decomposition products. Similarly, recently published attempts by Clayden and co-workers to acetylate the same substrate, during a study of related axially chiral anilides, met with failure.⁵¹ Lacking a viable method to construct the amide bond, efforts to prepare anilide **114a** were abandoned.



Scheme 4.5 - Synthesis of Branched N-Alkyl-*o*-Iodoanilides

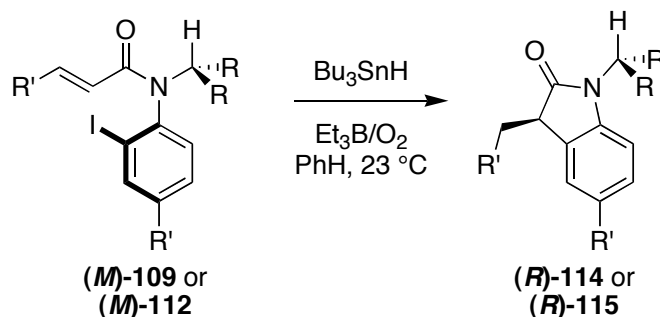
The enantiomers **109** and **112** were separated by using a (*S,S*)-Whelk O 1 chiral preparative HPLC column (25 cm x 10.0 mm I.D.) eluting with 9/1 hexanes/*i*PrOH.¹⁷ Typical injections

sizes were 25–100 mg and recovery averaged over 90 %. The peaks of **109** were partially overlapped ($T_r = 13.9$ and 15.2 min), while the peaks of **112** exhibited baseline separation ($T_r = 11.3$ and 13.2 min). To minimize racemization, fractions were cooled to $0\text{ }^\circ\text{C}$ prior to rapid concentration *in vacuo*. The % ee of the recovered samples of **109** and **112** were typically greater than 80 %.

We suspected that crystalline samples of **109** and **112** would not be susceptible to racemization at room temperature. This suspicion was confirmed by keeping an 83 % ee crystalline sample of (*P*)-**109** at room temperature. After 1 week, the ee was measured at 81 %, unchanged within experimental error. In contrast, enantioenriched samples of (*P*)-**109** in solution were observed to racemize in minutes at room temperature. We attribute the disparity in these results to conformational stability derived from packing forces in the crystal lattice. The N-aryl bond rotation barriers of **109** and **112** were measured by dissolving their respective samples at room temperature and periodically analyzing an aliquot by chiral HPLC to measure the decaying % ee. Standard plots of the data showed the expected first order rate of racemization and provided rotation barriers of 23.1 (96.7) and 22.8 kcal/mol (95.5 kJ/mol) for **109** and **112**, respectively.

With the enantioenriched radical precursors **109** and **112** prepared, tin hydride mediated cyclizations were conducted to measure the level of chirality transfer. Triethylborane (1.0 equiv) was added to an aerated benzene solution of the *o*-iodoanilide and Bu_3SnH (1.1 equiv, 0.01 M) to initiate the reaction.³³ In all cases, the reactions were complete before any progress could be monitored by TLC. Radical cyclization of (*M*)-**109** (91/9 er) yielded (*R*)-**114** in a 71/29 er (% 78 chirality transfer) (Table 4-3, entry 1). The chirality transfer of the opposite enantiomer cyclization was slightly higher (69 %, entry 2). Enantiomers of the isopropyl analogue **112** also

were observed to cyclize with faithful transfer of chirality to its oxindole product (**115**, entries 3/4). The levels of chirality transfer observed for **112** are comparable to those for related acrylanilide substrates in previous studies.^{9c,h} The crotonoyl substrate **109** exhibited slightly lower levels of chirality transfer than **112**, consistent with observations that substitution about the alkene lowers the fidelity of the cyclization.⁹



Precursor	R	R'	er_{SM}	Elution Order	Product	er_{Prod}	Elution Order	% Yield	% Chirality Transfer
(M)-109	-(CH ₂) ₅ -	Me	91/9	FEE	(R)-114	71/29	SEE	81	78
(P)-109	-(CH ₂) ₅ -	Me	86/14	SEE	(S)-114	75/25	FEE	85	87
(M)-112	Me	H	83/17	SEE	(R)-115	76/24	SEE	85	92
(P)-112	Me	H	86/14	FEE	(S)-115	75/25	FEE	78	87

Table 4-3 - Summary of Radical Cyclizations of 109 and 112

4.4. Determination of Absolute Configuration of Cyclization Precursors and Products

The second eluting enantiomer of **109** was recrystallized by quickly dissolving an enantioenriched sample in hexanes at room temperature before cooling the solution to approximately -15 °C. Similarly, a sample of the first eluting enantiomer of **112** was recrystallized by this procedure, but 1-heptene was used as the solvent instead. In both cases, single crystals of **109** and **112** were obtained. The absolute configuration of **109** and **112** were secured by X-ray crystallography using the anomalous dispersion method by Dr. Steve Geib. In

both cases, the *M* enantiomer was observed. The crystal structures of (*M*)-**109** and (*M*)-**112** are shown in Figure 4.6 and 4.7 respectively. The aniline ring in **112** is nearly perpendicular to the plane of the amide bond (89.5°). As expected, the amide is *trans* and the acryloyl group is in an *s-cis* conformation. The isopropyl group in **112** is twisted away from the iodine atom (Figure 4.6). The crystal structure of **109** closely matches that of **112**. Unlike **112**, the aniline ring in **109** is slightly more tilted (80°) towards the plane of the amide bond (Figure 4.7).

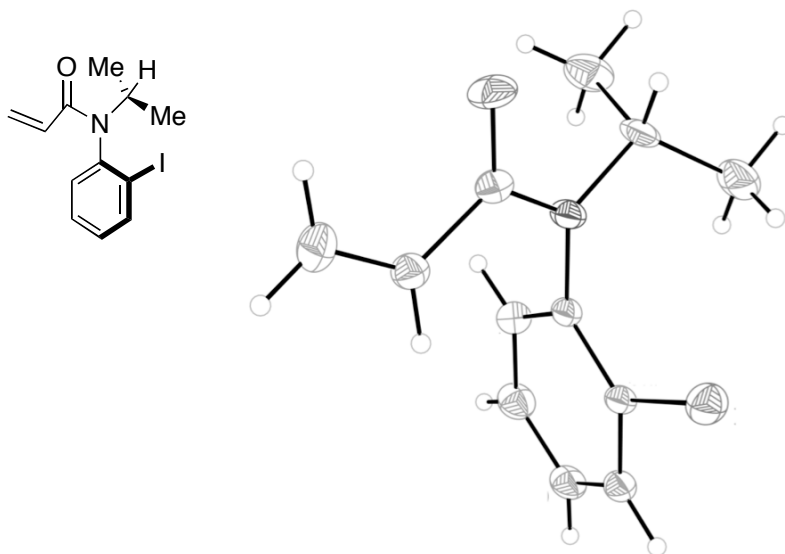


Figure 4.6 - ORTEP Diagram of (*M*)-112

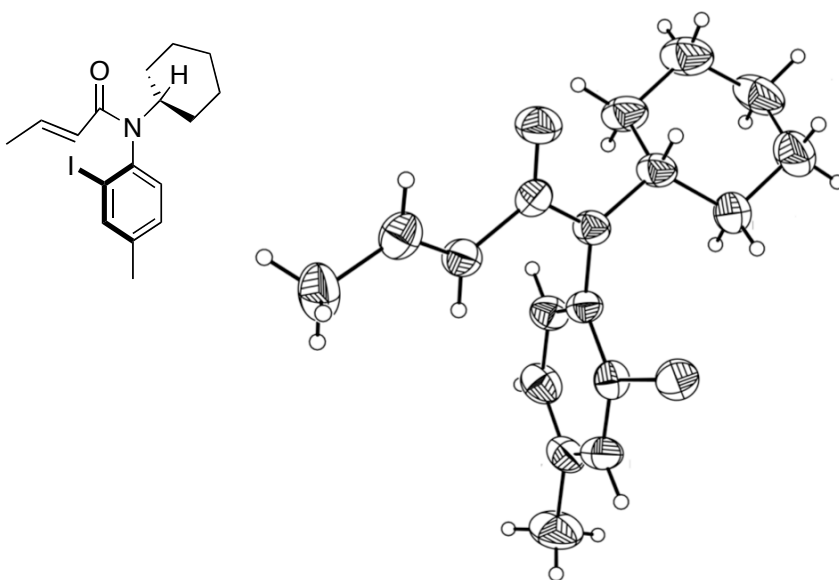


Figure 4.7 - ORTEP Diagram of (*M*)-109

When the respective *M* enantiomers of **109** and **112** were cyclized, in each case the dextrorotatory enantiomers of the resulting cyclized products, **115** and **116** respectively, were obtained. Additionally, the oxindoles **115/116** isolated from the cyclization of (*M*)-**109** and (*M*)-**112** were both found to be the first eluting enantiomer (FEE) by chiral HPLC ((*S,S*)-Whelk-O 1). Unfortunately, we lacked direct information about the absolute configuration of **115/116**. Because **115/116** lack heavy atoms, they are unsuitable for assignment of absolute configurations by X-ray analysis. In order to assign an absolute configuration to the cyclized products, we compared optical rotation and elution order data with related oxindoles **117** and **118** of known absolute configuration (Figure 4.8). In earlier work,^{9h} the second eluting enantiomer of oxindole **117** was found to have an *R* configuration at the α stereocenter by X-ray analysis. Optical rotation measurements of (*R*)-**117** showed it to be dextrorotatory. Likewise, the second eluting enantiomer of substrate **118** is dextrorotatory. This was the predicted sign of optical rotation by calculation for (*R*)-**118**.^{9d} By analogy, we conclude that the cyclization of (*M*)-**109** and (*M*)-**112** gave (*R*)-**115** and (*R*)-**116**, respectively. Furthermore, this model for cyclization is consistent with the stereochemical model previously discussed in the diastereomeric series (Figure 4.4).

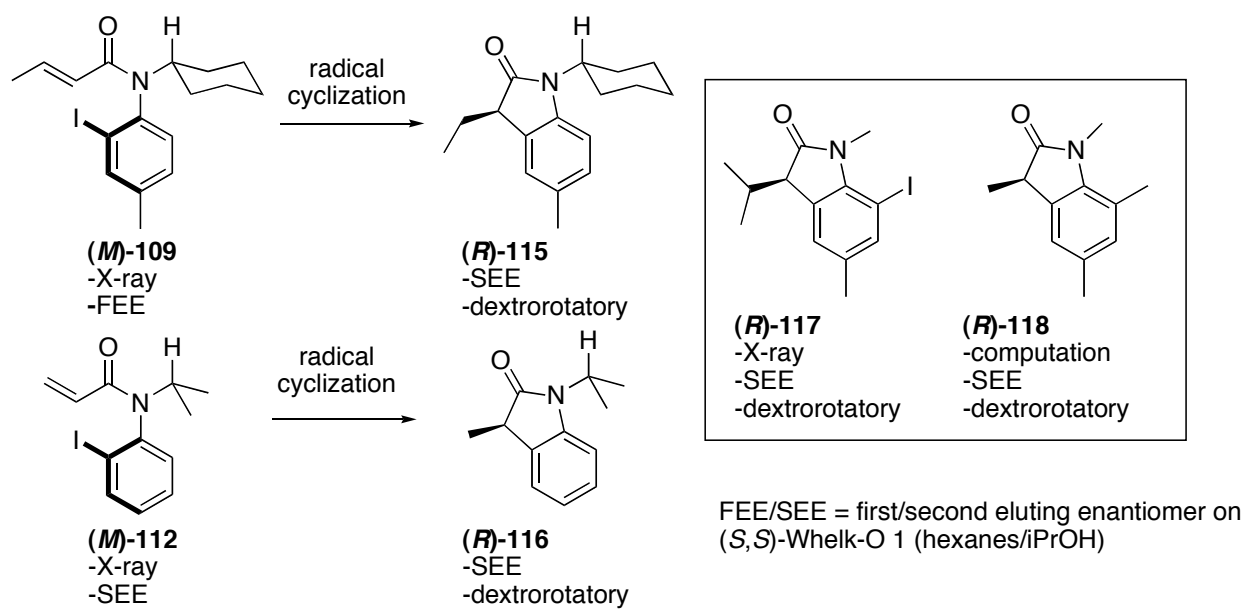


Figure 4.8 - Assignment of Absolute Configurations of 115 and 116

4.5. Conclusion

The results show the enantiomeric and diastereomeric *o*-iodoanilides atropisomers bearing only a hydrogen atom at the other *ortho*-position can be resolved and handled under ambient laboratory conditions. The asymmetry present in these transient atropisomers can then be locked into a stereocenter by a subsequent radical cyclization, which occurs with good to excellent levels of chirality transfer (78–92 %). Because the precursors lack a second *ortho* substituent, the potential exists to use these compounds in the stereoselective syntheses of natural oxindole alkaloids.

5. ASYMMETRIC HECK-MIZOROKI CYCLIZATIONS OF *O*-IODOANILIDE ATROPISOMERS

5.1. Introduction

Work in our labs has demonstrated that axially chiral *o*-iodoacrylanilides can be reliably cyclized under radical conditions with transfer of chirality to a newly formed stereocenter (Scheme 2.7). This transformation (**120** → **121**) is possible because rapid radical cyclization occurs before N-aryl bond rotation can erode the sense of axial chirality. An analogous organometallic 5-*exo* cyclization process (**123** → **126**) is a Heck-Mizoroki reaction. In addition to acting as a precursor to a radical, an aromatic iodide **123** could also undergo C–I bond insertion by a Pd species to generate hypothetical organometallic intermediate **124**. Could a Heck-Mizoroki cyclization of a suitably substituted axially chiral *o*-iodoanilide also occur with transfer of chirality?

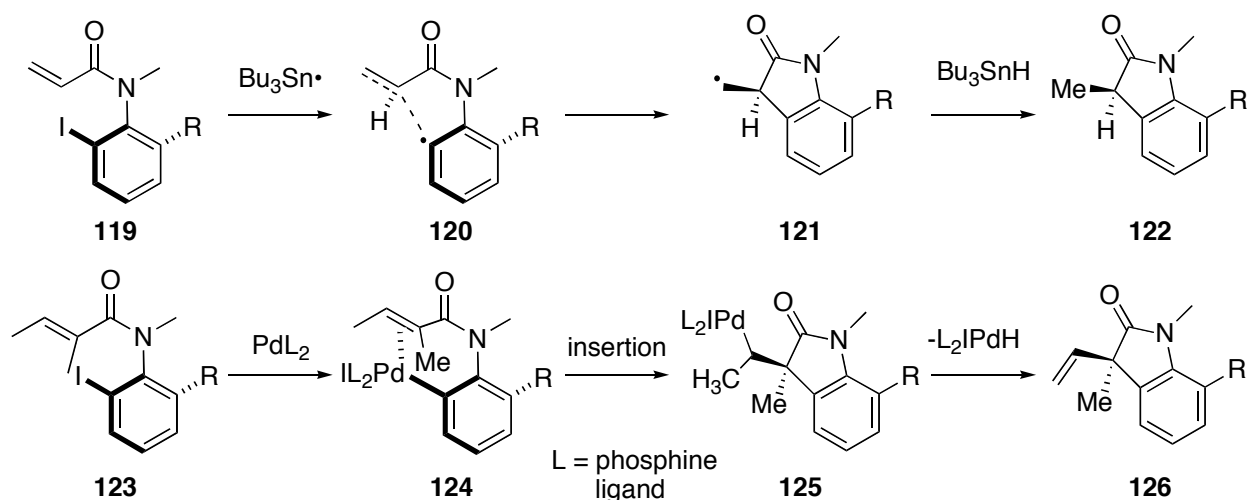


Figure 5.1 – Aryl Iodide as a Precursor to Radical or Heck-Mizoroki Cyclizations

5.2. Heck-Mizoroki Reaction

The Mizoroki–Heck reaction was discovered independently by Mizoroki⁵² and Heck⁵³ in the early 1970s. The Heck-Mizoroki reaction is more commonly known as the Heck reaction because of his fundamental work that developed the reaction into a general method of chemistry.⁵⁴ The classic Heck reaction is a Pd-catalyzed arylation of alkenes. Key steps of the reaction cycle include oxidative addition (**129** → **130**) of the Pd into an Ar-X bond (*e.g.* X = Br, I, or OTf) and addition of the formed ArPdX intermediate to unsaturated bonds (**132** → **133**) (Figure 5.2).

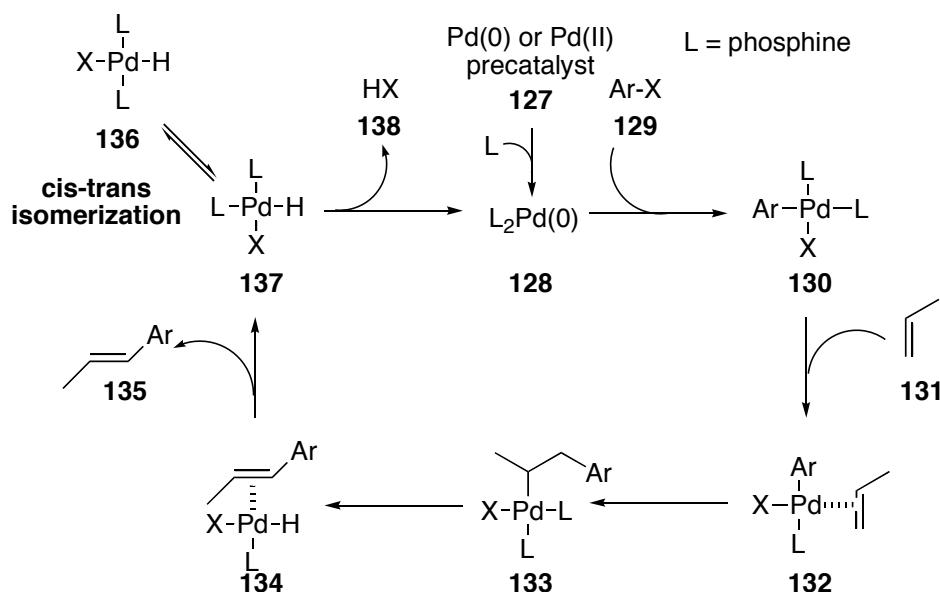
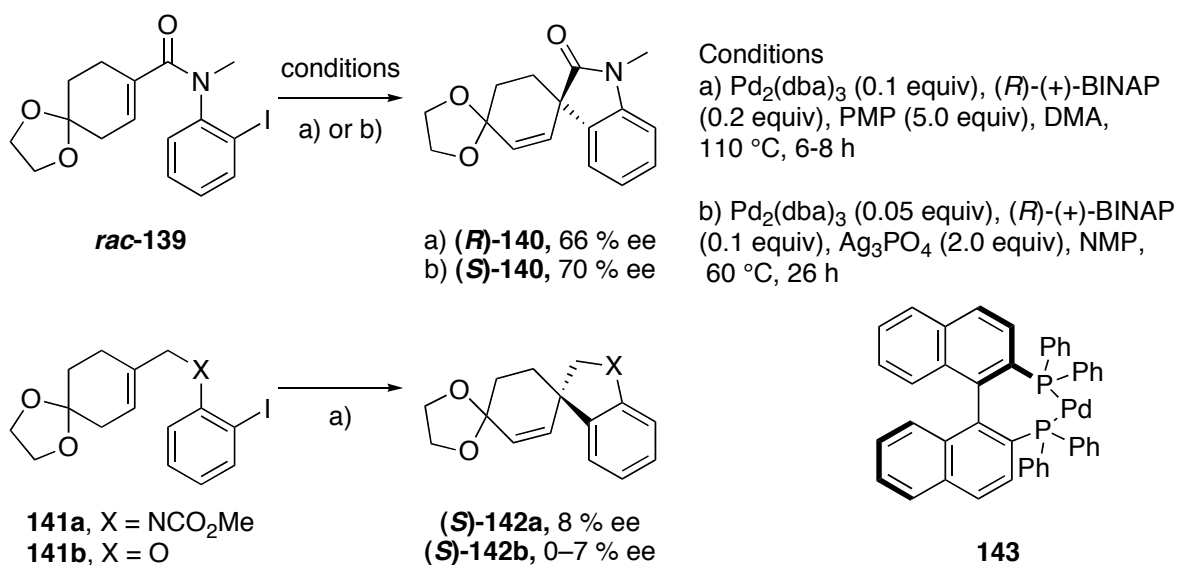


Figure 5.2 - Heck Reaction Catalytic Cycle

In 1989, Shibasaki and co-workers reported pioneering examples of enantioselective Heck reactions for the synthesis of fused ring systems such as decalins,^{55,56} hydrindans,⁵⁷ indolizines,⁵⁸ diquinanes,⁵⁹ and related natural products. The Overman group has done important work,⁶⁰ including the first Heck reactions to generate asymmetric quaternary centers, on enantioselective intramolecular Heck reactions of *o*-iodoanilides that use chiral phosphine

ligands as the source of asymmetry (Scheme 5.1).⁶¹ In a typical experiment,⁶² *rac*-**139** was exposed to catalyst **143**, preformed from Pd₂(dba)₃ and (*R*)-(+)-BINAP, in dimethylacetamide at 80 °C and produced (*R*)-**140** with 66 % ee. Interestingly, replacement of the amine base with Ag salts gave (*S*)-**140** in 70 % ee, a reversal in the stereoselection of the process. When the scope of this reaction was tested with anilide **141a** and phenolic ether **141b** little or no enantioselectivity was observed in the spirocyclic products (*S*)-**142a,b**. The latter results suggest that the conformational features of the substrate **139** play a role in the stereoselection of the process.



Scheme 5.1 – Stereoselective Heck Cyclizations with (*R*)-(+)-BINAP

Based on the above results and other mechanistic observations[§] Overman outlined the following 'neutral' and 'cationic' pathways (Figure 5.3) to begin to rationalize the observed changes in

[§] a) Reactions conducted with a BINAP analog synthetically modified to be monoligating occurred with poor stereoselection. Therefore, the stereodifferentiating step must involve a catalytic complex with a bidentate Pd-BINAP complex. b) Enantioselectivity is insensitive to solvent. c) The product ee correlates with the ee of BINAP used; therefore, a monomeric Pd-BINAP complex is responsible for stereoselection.

stereoselection. He proposed that the reactions where tertiary amines are used as the HI scavenger proceed through a neutral reaction pathway. After oxidative insertion into an aryl halide (**143a**) to form **144a**, the tethered alkene coordinates to Pd in the apical position and produces square pyramid complex **145**. Displacement of the halide anion (**145** → **146**) followed by migratory insertion (**146** → **147**) irreversibly locks in the new stereocenter (*). The cationic pathway can be accessed by oxidative insertion in the analogous aryl triflate (**143b** → **144b**). Because the triflate anion is fully dissociated⁶³ square planar complex **148** is formed that leads to the opposite configuration of intermediate **149**.

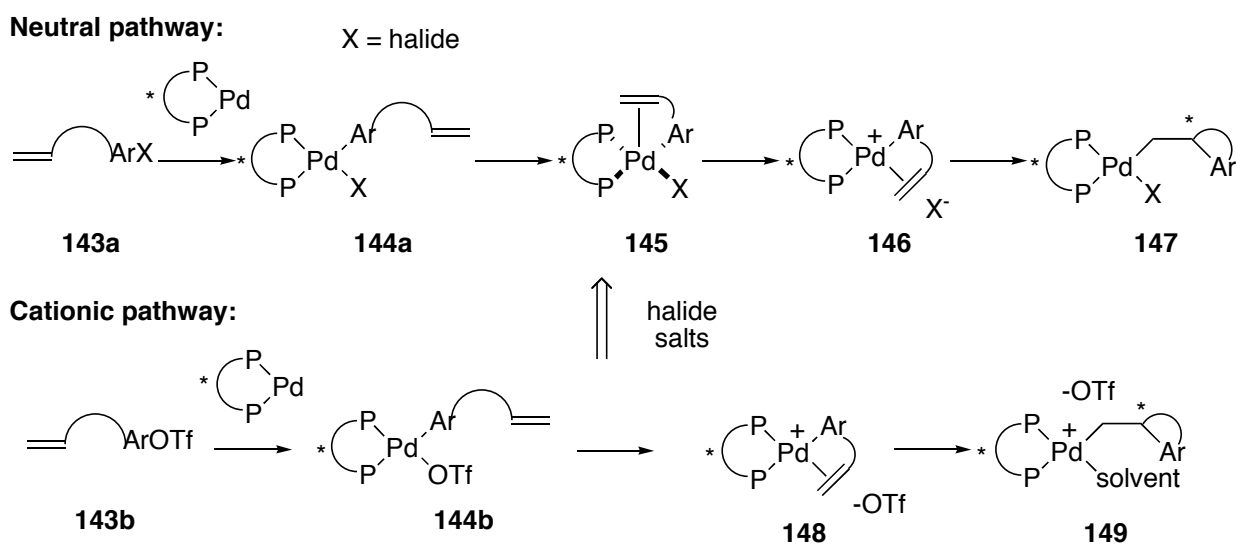


Figure 5.3 - Proposed Cationic and Neutral Heck Pathways

Two steps may be responsible for the stereoselectivity of the reaction: halide displacement by the alkene (**145** → **146**) or oxidative addition (**143** → **144**). Overman wrote^{62b} that the latter “could be the enantioselective step if the intermediates undergoing oxidative addition were the diastereomeric Pd-BINAP alkene complex.” The strongest evidence against the oxidative step is the observation that cyclizations of aryl triflates in the presence of added halide salts gave configurations of the product consistent with those from neutral reactions. From this it was

concluded that halide salts shunt intermediate from the cationic to the neutral pathway and the stereoselective step is further downstream.

5.3. Precursor Preparation, Resolution

With the aim of better understanding the mechanism of chirality transfer during Heck cyclizations of *o*-iodoanilides, we wanted to evaluate whether the reactions could occur enantioselectively without an external source of asymmetry. Suitable substrates to test this premise would be axially chiral *o*-iodoanilides with enantiomers that are resolvable and possessing a sufficiently high barrier to rotation to permit handling at room temperature. Furthermore, an α substituent is necessary to avoid β -hydride elimination in presumed intermediate **150** to form the more stable α,β trisubstituted alkene (**151**) instead of the terminal alkene (**152**). Formation of **151** would result in the destruction of the newly formed α stereocenter and loss of stereochemical information (Figure 5.4).

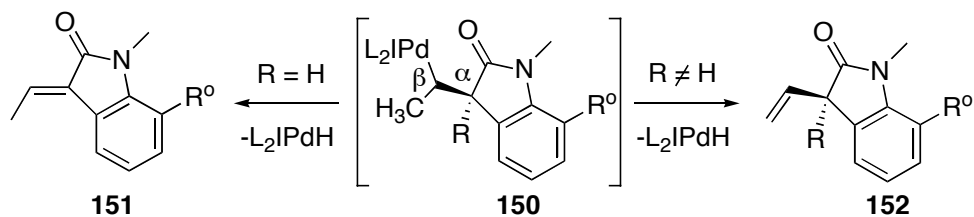
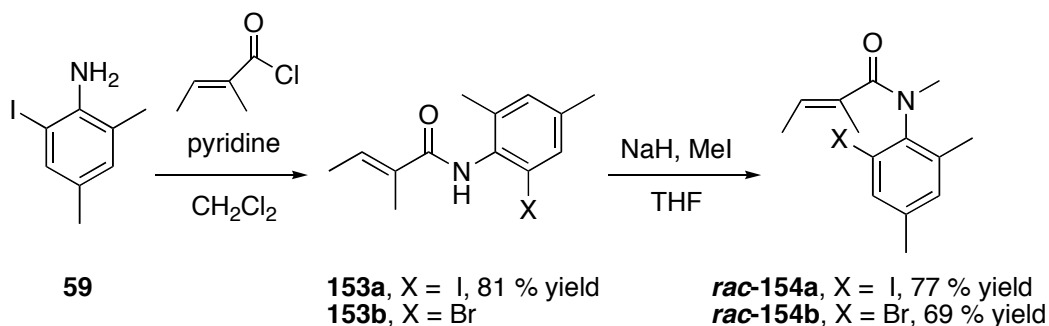


Figure 5.4 - β -Hydride Elimination Leading to Loss ($R = H$) or Retention ($R \neq H$) of Chirality

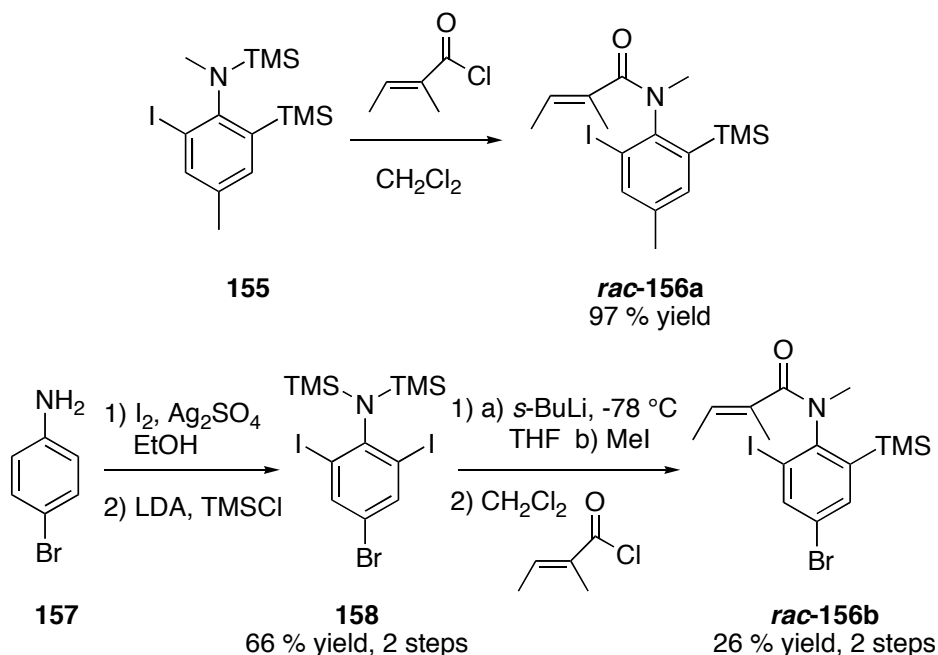
We prepared a series of four possible anilide substrates to investigate this cyclization reaction (Scheme 5.2). Iodoaniline **59** was first acylated with tigloyl chloride in the presence of

pyridine^{**} to form **153a** in 81 % yield. Deprotonation of **153a** with sodium hydride, followed by quenching with methyl iodide gave *rac*-**154a** in 62 % yield. The bromo homolog *rac*-**154b** was prepared in a similar fashion (69 % yield) from a sample of **153b** previously prepared by Dr. Weidong Liu. Treatment of aniline **155**, graciously donated by Dr. Marc Petit,⁹ⁱ with tigloyl chloride produced *o*-trimethylsilylanilide *rac*-**156a** cleanly in 97 % yield (Scheme 5.3). The *p*-bromo homolog of **156a** was synthesized in four steps from aniline **157**. Double electrophilic iodination of the *ortho* positions yielded 4-bromo-2,6-diidoaniline (not shown). Double treatment of the latter with LDA at -78 °C followed by TMSCl, achieved N,N-bissilylation to give aniline **158** in 66 % yield over two steps. Exposure of **158** to *sec*-butyllithium triggers lithium halogen exchange with concomitant transfer of one of the silyl groups to the *ortho* position. Quenching the resulting anion with methyl iodide gives the *N*-methyl-*N*-trimethylsilyl derivative (not shown). Reaction of the latter aniline with tigloyl chloride generates *rac*-**156b** in 26 % yield over two steps.



Scheme 5.2 - Preparation of Anilides *rac*-154a,b

^{**} When triethylamine, diisopropylethylamine, or 4-dimethylaminopyridine were used as bases, the β - γ migrated alkene product was observed. Presumably, the migration of the alkene is indicative of ketene formation.



Scheme 5.3 - Preparation of Anilides *rac*-156a,b

The enantiomers of *rac*-**154a** were resolvable by injection onto a chiral HPLC column ((*S,S*)-Whelk O 1). Unfortunately, the enantiomers of *rac*-**154b** and *rac*-**156a,b** were not resolvable by using available chiral HPLC columns ((*S,S*)-Whelk O 1, Chiralcel OD) and their further use in this study was discontinued. The enantiomers of **154a** were separated by using a (*S,S*)-Whelk O 1 chiral preparative HPLC column (25 cm x 10.0 mm I.D.) eluting with 8/2 hexanes/*i*PrOH.¹⁷ Typical injections amounts were 50 mg and combined recovery of enantioenriched atropisomers averaged over 80 %. The rotation barrier of the anilide **154a** was measured by racemizing a sample at 90 °C in 9/1 hexanes/*i*PrOH, and the decrease in ee was measured as a function of time by chiral HPLC analysis. A standard plot of this data showed the expected first order rate of racemization, and provided a rotation barrier of 27.5 kcal/mol (115.1 kJ/mol). The value for N-aryl bond rotation barrier of **154a** is about 3 kcal/mol lower than observed for acrylanilide **46** (Figure 5.5). Presumably, steric interactions in **154a** between the α methyl group and the aniline ring causes the alkene to twist out of plane with respect to the amide carbonyl group and thereby

present a smaller substituent for the iodine or methyl group of the anilide to rotate past in the transition state (Figure 5.5, right).

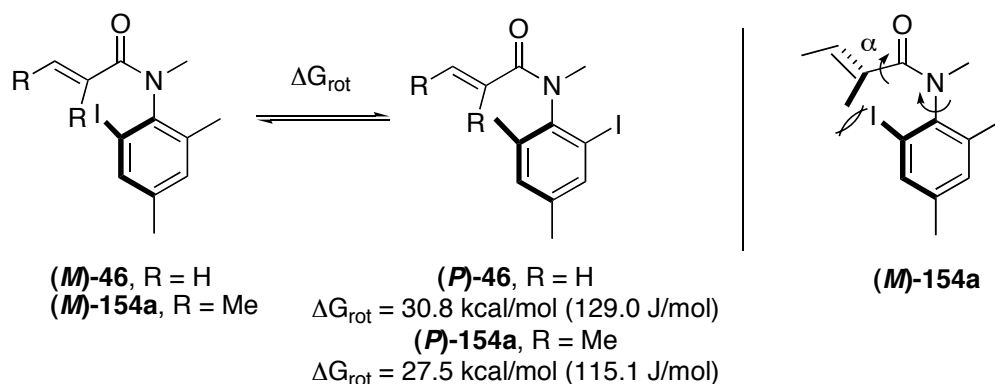


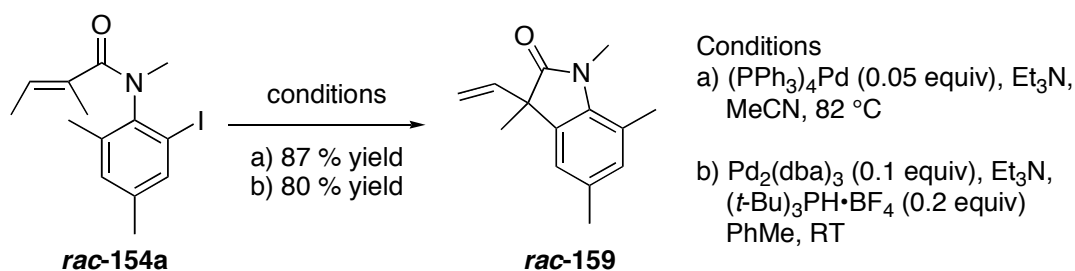
Figure 5.5 - Comparison of Rotation Barriers of 46 and 154a

5.4. Chirality Transfer in Heck Cyclizations

When a sample of *rac*-**154a** was treated with $(\text{PPh}_3)_4\text{Pd}$, prepared *in situ*, in the presence of an amine base in refluxing MeCN, the expected racemic oxindole product *rac*-**159** was obtained in 87 % yield (Scheme 5.4). When product *rac*-**159** was injected into an analytical (*S,S*)-Whelk-O 1 chiral column, each enantiomers was well resolved, thereby permitting a convenient quantitative analysis of a chirality transfer experiments by HPLC.

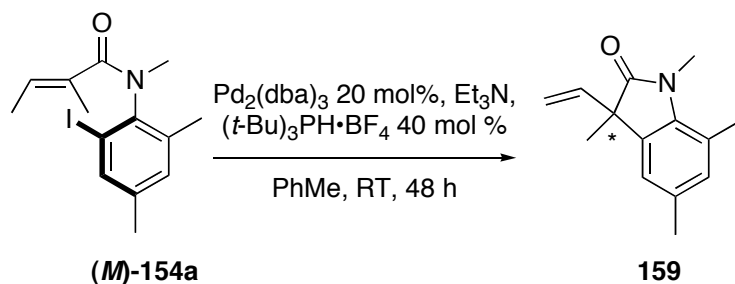
However, at 80 °C, an enantiopure sample of **154a** has a half-life of just over an hour. Consequently, any attempt to conduct a Heck cyclization of **154a** at elevated temperatures would occur with the ee of **154a** diminishing during the course of the reaction. One way to avoid this fate would be to perform the reaction at temperature low enough to suppress the racemization pathway but permitting the cyclization. Unfortunately, this also has the effect of slowing an already sluggish Heck reaction.^{61b} Taking a cue from work by Hartwig on room temperature

Heck reactions,⁶⁴ we used conditions employing bulky alkyl phosphine ligands. Bulky phosphine ligands demonstrated greater catalytic activity in Heck reactions, perhaps because their electron-rich nature increases the electron density on the Pd center, promoting the oxidative addition step. Additionally, bulky phosphines have a greater tendency to dissociate from the Pd complex, which can promote one or more steps of the catalytic cycle (Figure 5.2). The use of *tert*-butyl phosphine along with large amounts of catalyst (40 mol % in Pd) achieved complete conversion to *rac*-**159** at room temperature over a 48 h period.



Scheme 5.4 - Heck Cyclizations of *rac*-**154a**

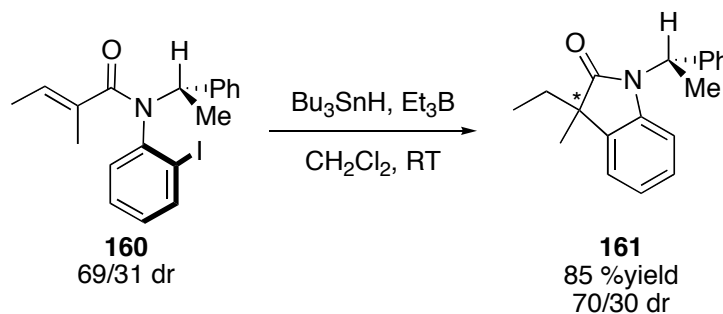
When an enantioenriched sample of anilide (*M*)-**154a** was submitted to the room temperature Heck-Mizoroki conditions the product oxindole was obtained in 85 % yield and chirality transfer (Table 5-1, entry 1). The opposite enantiomer, (*P*)-**154a**, was cyclized with a similar level of chirality transfer (89 %, entry 2). Because anilide **154a** has a half-life of over four months at ambient temperature any *in situ* racemization during the reaction would be insignificant. The chirality transfer observed for **154a** → **159** is slightly lower than previous radical cyclizations (**160** → **161**) with the same alkene substitution pattern (Scheme 5.5).⁶⁵



Note: Absolute configurations of the products are unassigned.

Precursor	er_{SM}	Elution Order	Product	er_P	Elution Order	% Yield	% Chirality Transfer
(M)-(-)-154a	93/7	FEE	(+)-159	79/21	SEE	85	85
(P)-(+)-154a	96/4	SEE	(-)-159	85/15	FEE	88	89

Table 5-1 - Summary of Heck Cyclizations of Anilides Enantioenriched 154



Note: Absolute configuration of product is unknown.

Scheme 5.5 - Radical Cyclizations of Related Anilide 160

The absolute configuration of **154a** is tentatively assigned based on its structural similarity to **8**.^{††} It was observed that the levorotatory enantiomers of **8** and **154a** both elute first by chiral HPLC ((*S,S*)-Whelk O 1). Unfortunately, we failed to obtain single-crystal samples of **154a**, a waxy solid, via slow recrystallization in a number of solvents. This prevented us from securing definitively the absolute configuration of **154a** by X-ray crystallography. Oxindole **159**, lacking a heavy atom, is not suitable for assignment of absolute configuration by X-ray analysis.

^{††} The absolute configuration of a synthetic precursor to **8** was definitively established by X-ray crystallography.^{9c}

Attempts to derivatize **159** to an X-ray suitable compound were unsuccessful. Without knowledge of the absolute configuration of both the precursor and cyclized product, we cannot propose a transition state to rationalize the observed stereoselection.

5.5. Synthesis of Second Generation Precursor

A novel cyclization substrate **164** was proposed with the idea that it be elaborated into the eseroline class of natural products⁶⁶ with well-established absolute configurations (Figure 5.6). Using this approach, the absolute configuration of the stereocenter formed during cyclization could be assigned by comparing the sign of optical rotation. Consistent with the previous cyclization substrate, *o*-iodoanilide **164** should be resolvable into its enantiomers. Substrate **164** differs from **154a** in that the 3-siloxy group offers a functional group handle for further synthetic elaboration following the procedures of Fuji (Figure 5.6).⁶⁷ Substitution of the bromide with a methoxy group and reductive removal of *o*-chloride would yield natural product esermethole **162**. Secondly, replacing the 6-iodo-2,4-dimethyl aniline core with a trihalogenated core may increase crystallinity and potentially improve the chances of growing a single crystal for X-ray analysis.

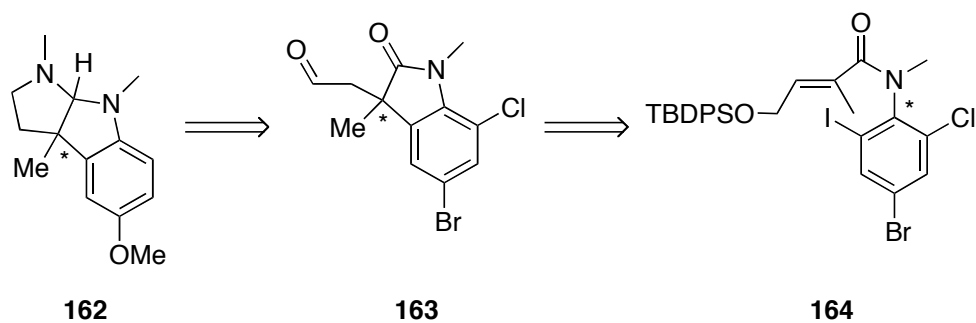
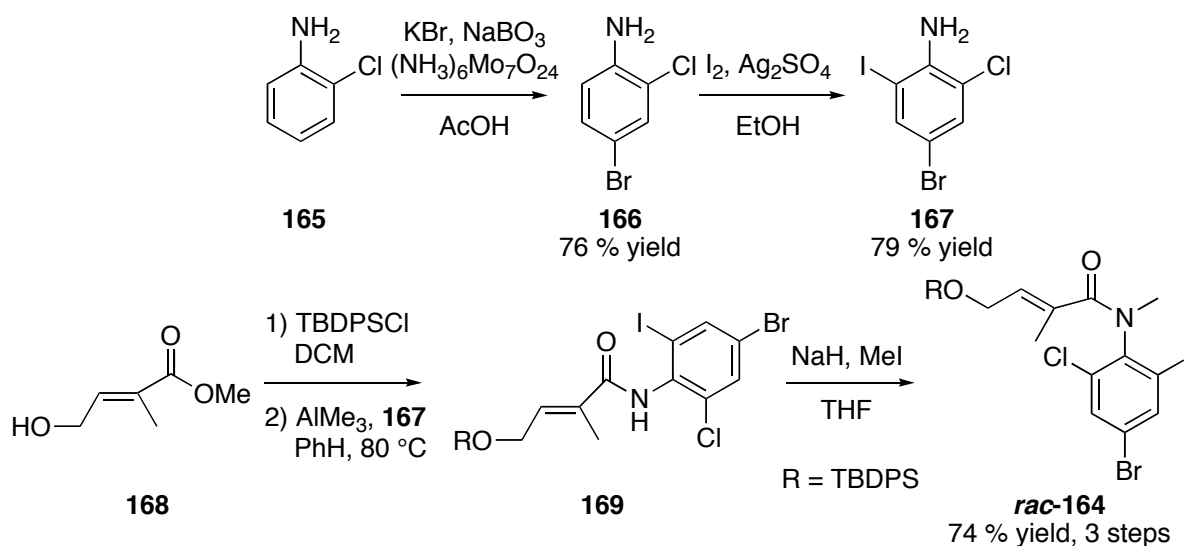


Figure 5.6 – Proposed Retrosynthesis of Esermethole **162**

Synthesis of **164** (Scheme 5.6) began with the preparation of aniline **167**. Electrophilic bromination of 2-chloroaniline **165**, followed by iodination generated aniline **167** in 60 % yield (2 steps). Preparation of the acyl fragment began with known hydroxy ester **168**.⁶⁸ Silylation of **168** with TBDPSCI protects the hydroxy group during subsequent steps. Reaction of silyloxy ester (not shown) with aniline **167**, pre-treated with AlMe_3 , under refluxing conditions produced secondary anilide **169**.⁶⁹ Deprotonation of anilide **169** with sodium hydride and quenching with methyl iodide produces the desired cyclization precursor *rac*-**164** in 74 % yield (three steps).

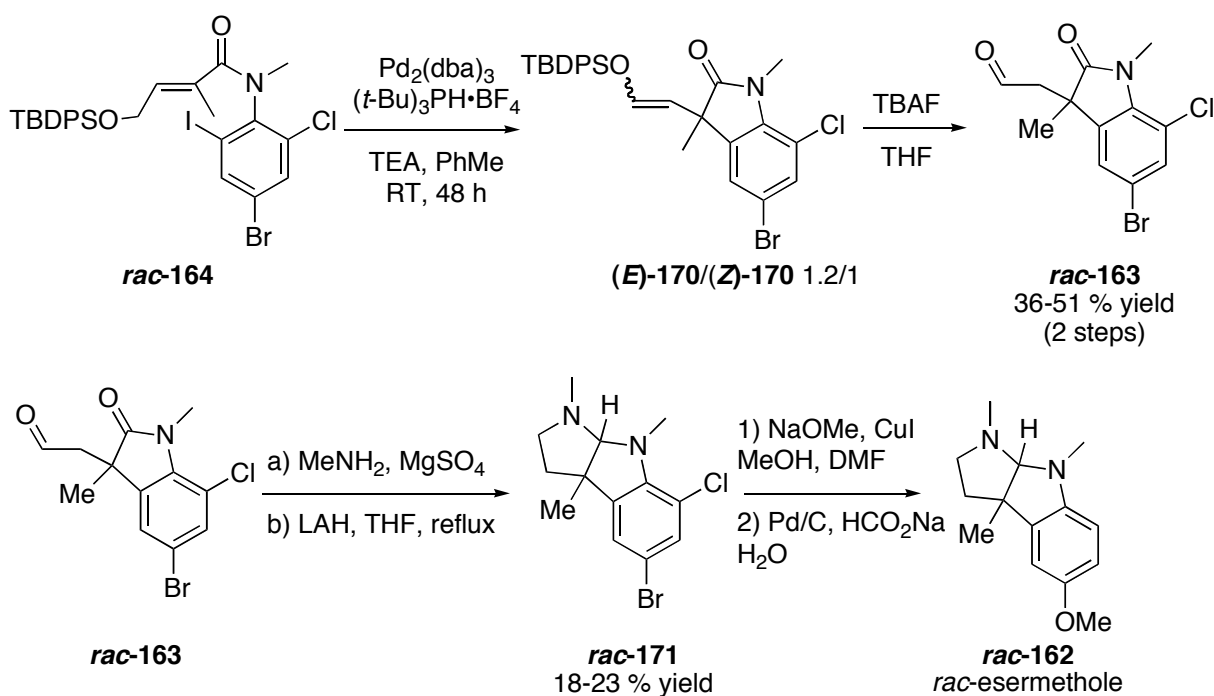


Scheme 5.6 - Synthesis of Anilide *rac*-164

5.6. Racemic Synthesis of Esermethole

The synthesis of esermethole **162** was first executed in a racemic manner. Heck cyclization of *rac*-**164** gave a 1.2/1 mixture of the alkene *E/Z* isomers of **170**. The crude product of this reaction was redissolved in THF and treated with TBAF to remove the silyl group and reveal the aldehyde functionality of *rac*-**163**; yields of the aldehyde ranged from 36–51 %. Aldehyde *rac*-**163** was reacted with methyl amine for *in situ* imine formation. Adding lithium aluminum

hydride and refluxing the reaction mixture gave *rac*-**171** in poor yields (18–23 %). A side-product of the reaction was the debrominated homolog **172**. Coupling of sodium methoxide with *rac*-**171** under Cu-catalyzed conditions, installed the desired methoxy group in the *para* position, producing 7-chloroesermethole (not shown). A reductive hydrodechlorination on a small scale (< 2 mg), catalyzed by Pd/C and using sodium formate as the hydride source, gave *rac*-esermethole (*rac*-**162**). Comparison of the crude ¹H NMR spectrum of *rac*-**162** to literature reports^{62b} confirmed the formation of the desired product.



Scheme 5.7 - Racemic Synthesis of *rac*-Esermethole

5.7. Resolution and Recrystallization of Second Generation Precursor

The enantiomers **164** were separated by using a (*S,S*)-Whelk O 1 chiral preparative HPLC column (25 cm x 10.0 mm I.D.) eluting with 98/2 hexanes/*i*PrOH.¹⁷ Typical injections sizes were 35 mg and recovery averaged only 25 % due to aggressive peak shaving. The N-aryl bond rotation barrier of **164** was measured by racemizing an enantioenriched sample. An

enantioenriched sample of anilide **164** (92 % ee) was heated at 80 °C in 9/1 hexane/iPrOH, and the decrease in ee was measured as a function of time by chiral HPLC analysis. A standard plot of this data showed the expected first order rate of racemization, and provided a rotation barrier of 26.7 kcal/mol (111.8 kJ/mol).

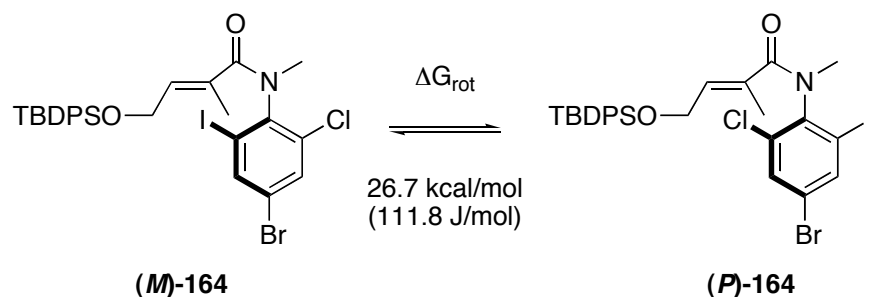


Figure 5.7 – N-Aryl Bond Rotation Barrier of 164

In order to assign the absolute configuration, we attempted to prepare enantiomerically pure single crystals of **164** for X-ray analysis. Attempts to recrystallize enriched samples by dissolution and slow evaporation of the solvent were unsuccessful or resulted in racemic crystals. Additionally, a highly enantioenriched (>98 % ee) sample of the second eluting enantiomer of **164** formed X-ray suitable crystals upon cooling at approximately -15 °C. Unfortunately, these crystals were also found to be racemic. Attempts to crystallize the desilylated derivative (not shown) were also unsuccessful.

Despite failing to assign the absolute configuration of **164**, the crystal structure of *rac*-**164** contains information about the alkene conformation (Figure 5.8). The α,β unsaturated carbonyl group is in an approximate *s-trans* conformation with the alkene twisted 38° from the plane of carbonyl group (C=C–C=O). The *s-trans* conformation is consistent with observations made of similar tigloyl derivatives in the crystal state.⁷⁰ The torsion angle between the plane of the amide

bond and that of aniline ring (OC–N–C–Cl) in **164** is more acute (67°) than is typically observed for tertiary anilides, with the iodine edge tilted towards the alkene group. Unusually, a small torsion angle (13°) exists between the carbonyl group and the N-aryl bond (O=C–N–C). The phenyl rings of the TBDPS group are slightly distorted, presumably as a result of the low quality of the crystal.

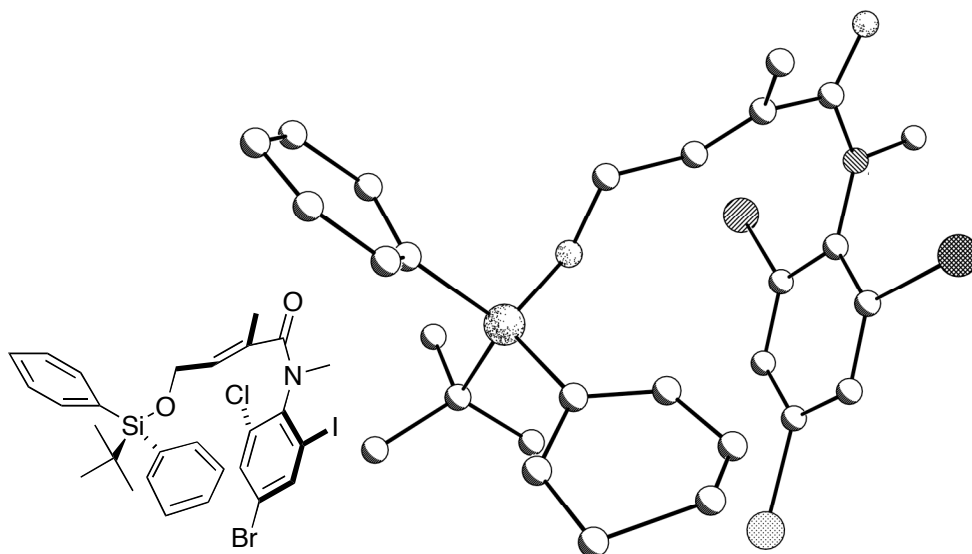
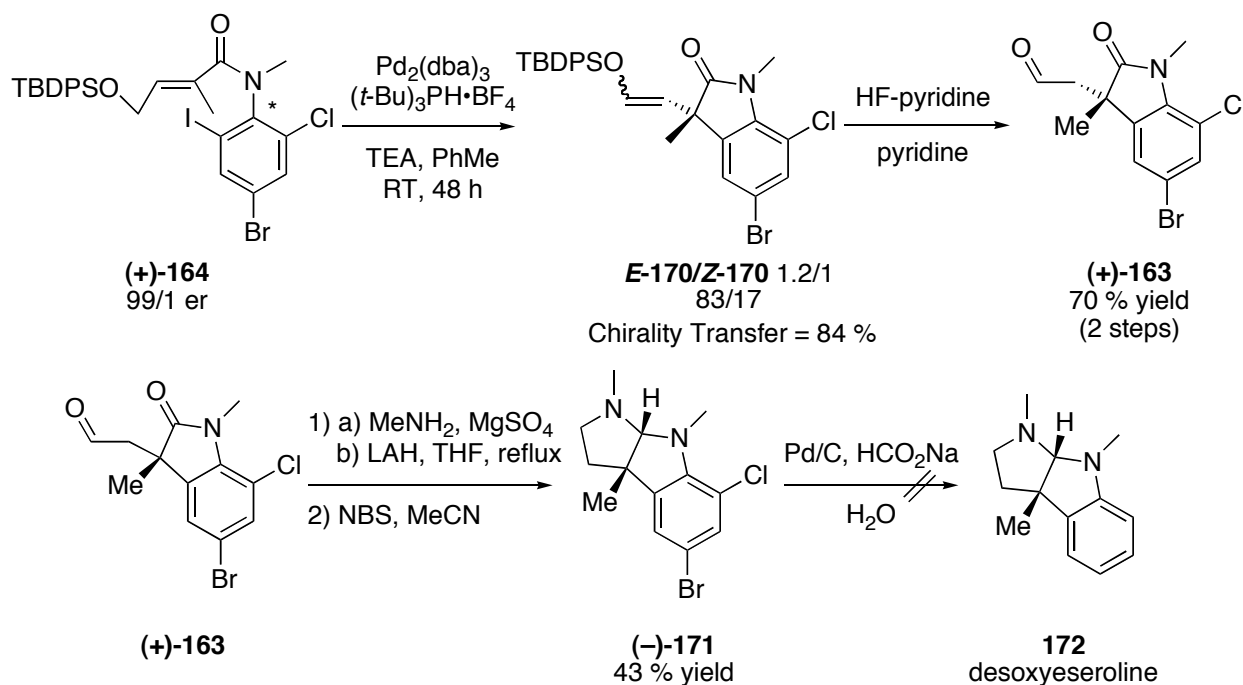


Figure 5.8 - ORTEP Diagram of Anilide *rac*-164

When the second eluting enantiomer of anilide **164** (99/1 er) was submitted to room temperature Heck conditions, oxindole **170** was obtained as a 1.2/1 mixture of alkene isomers (Scheme 5.8). By chiral HPLC, both geometrical isomers of **170** were found to be first eluting and with 83/17 er (Figure 5.9). The level of chirality transfer (84 %) in the cyclization is comparable to that of **154a** (Table 5-1). Treatment of the mixture with HF-pyridine gave aldehyde (+)-**163** in 70 % yield from **164**. A reductive amination cyclization with methylamine generated the heterocycle tricyclic core. Crude ^1H NMR and GC analysis revealed a mixture of the desired product and the debrominated by-product⁷¹ (~1/1). Treatment of the crude mixture of products with NBS in acetonitrile gave pure (–)-**171**. Faced with limited amounts of (–)-**171** (<5 mg) a double

hydrodehalogenation was attempted in hopes of preparing related alkaloid desoxyeseroline (**172**). Unfortunately, the reaction was unsuccessful and the desired product **172** was not obtained.



Scheme 5.8 - Heck Cyclization of Anilide (+)-164 and Attempted Elaboration to Desoxyeseroline

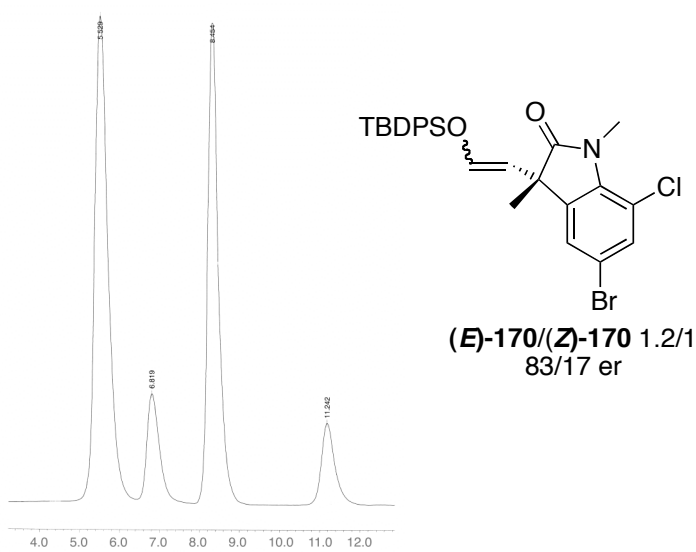


Figure 5.9 - Chromatogram of (E)-170/(Z)-170

5.8. Stereochemistry

Although the desired synthetic target was not obtained, we can draw tentative conclusions about the stereochemistry obtained in the Heck cyclization. The optical rotation of **171** was found to be levorotatory. When compared with the optical activity of numerous related eseroline derivatives⁷² we can tentatively assign the absolute configuration of the stereocenter generated in **170** as *S*.

Lacking an absolute configuration assignment for the Heck cyclization precursor (+)-**164** we are left to speculate on how the stereochemical information is transferred to the new stereocenter in the product **170**. Based on the available information we propose the following two possible mechanisms to account for the stereochemistry observed in the cyclization of **164**. If the configuration of **164** is *M*, then the cyclization must proceed through the *s-trans* rotamer (Figure 5.10, top), the rotamer observed in the crystal state (Figure 5.8). Subsequent Pd-insertion into the C-I bond ((*M*)-**164** → (*M*)-**173**) forms the penultimate cyclization intermediate. Unlike in earlier radical cyclizations of *o*-iodoanilides,^{9c,g,h} formation of the key intermediate (**173**) may actually occur with an increase in the N-aryl bond rotation barrier because of the bulkiness of the Pd atom and bound ligands. As such, we believe *in situ* racemization (*M* → *P*) is unlikely to occur under the reaction conditions. Insertion of the Pd-C bond across the alkene ((*M*)-**173** → **174**) transfers the chirality of the axis to the new α stereocenter. Subsequent β -hydride elimination produces the (*R*)-**170** as a mixture of *E/Z* isomers, depending on the C-C rotamer at the time. If the starting configuration is *P*, the analogous cyclization process ((*P*)-**164** → (*P*)-**173**) must proceed via the *s-cis* rotamer, leading to common intermediate **174**.

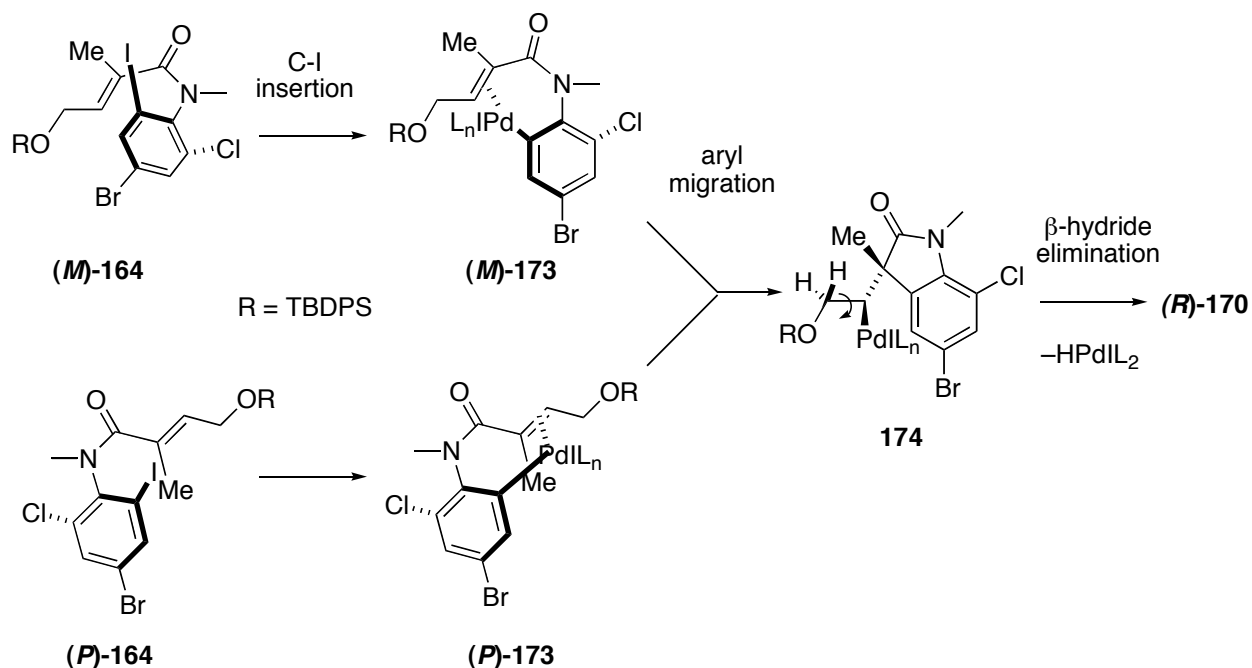


Figure 5.10 - Transition State Proposals

5.9. Conclusion

The results demonstrate, for the first time, that axially chiral *o*-iodoanilides can be cyclized under Pd-catalyzed conditions with transfer of chirality to the newly formed stereocenter without an external chiral source. Like their radical counterparts, Heck cyclizations of enantioenriched *o*-iodoanilides proceeded with significant (84–89 %) levels of chirality transfer. This interesting observation supports the idea that oxidative addition may be the stereodifferentiating step in Pd-catalyzed enantioselective cyclizations of racemic anilides.

6. EXPERIMENTAL

6.1. General Information

Unless otherwise noted, all reactions were run under an argon atmosphere. All reactions were performed in oven-dried glassware that was cooled under argon. Benzoyl chloride, phenyl acetyl chloride, dihydrocinnamoyl chloride, 4-bromobenzoyl chloride, *trans*-crotonyl chloride, 2,4-dimethyl aniline, benzyltrimethylammonium dichloroiodate, tributyl tin hydride, triethyl borane (1.0 M in hexanes), sodium hydride (95 % dispersion in oil), allyl iodide, crotonyl bromide, 4-bromo-2-methyl-2-butene, cinnamyl bromide, 2-iodoaniline, pyridine, 4-dimethylaminopyridine, Cu(I) iodide, *p*-bromotoluene, L-proline, cyclohexylamine, diisopropylethylamine, sodium triacetoxyborohydride, methyl iodide, trimethylaluminum (2.0 M in hexanes), $(\text{NH}_3)_6\text{Mo}_7\text{O}_{24}\cdot(\text{H}_2\text{O})_4$, potassium bromide $\text{NaBO}_3\cdot(\text{H}_2\text{O})_4$, Ag_2SO_4 , *tert*-butyldiphenylchlorosilane, sodium formate, tris(dibenzylideneacetone)-dipalladium(0)-chloroform adduct, and 10 % Pd/C were purchased from Aldrich and used without modification, save for the following exceptions. Phenylacetyl chloride and distilled prior to use. 2,4-Dimethyl aniline was dissolved in diethyl ether, filtered through a pad of silica gel to remove colored baseline impurities, and concentrated *in vacuo*. Triethyl amine was purchased from Fisher Scientific and used without modification. $\text{Pd}(\text{OAc})_2$, *tert*-butylphosphonium tetrafluoroborate were purchased from Strem Chemicals and used without modification. Acryloyl chloride and methylamine (2.0 M in THF) were purchased from Acros and used without further modification. Lithium aluminum hydride was purchased from Alfa Aesar and used without further modification. 2-Iodo-4,6-dimethylaniline **59** was prepared according to Kajigaesi's procedure.⁷³

Methyl 4-hydroxy-2-methylbut-2*E*-enoate **168**,⁶⁸ *N*-allyl-2-Iodo-4,6-dimethylaniline **77**,⁷⁴ and *N*-allyl-2-iodoaniline⁷⁵ were prepared according to previous reported procedures. Air and moisture sensitive chemicals were handled using standard syringe techniques. THF, toluene, benzene, and diethyl ether were distilled from sodium/benzophenone under argon. Dichloromethane was distilled from calcium hydride under argon. Alternatively, each solvent, except benzene, was dried by passing them through columns of activated alumina.

¹H and ¹³C NMR spectra were recorded on Bruker Avance DPX 300 (300 MHz), Avance 300 (300 MHz), and Avance DRX 500 (500 MHz) NMR spectrometers. Chemical shifts (δ) are reported in ppm relative to TMS using the residual solvent proton resonance of CDCl₃ (7.27 ppm) or the CDCl₃ carbon peak (77.0 ppm). In reporting data, the following abbreviations were employed: s = singlet, d = doublet, m = multiplet, p = pentet, sex = sextet, o = octet, bs = broad singlet, dd = doublet of a doublet, ddd = doublet of a doublet of a doublet, dddd = doublet of a doublet of a doublet of a doublet, dq = doublet of a quartet, dt = doublet of a triplet, qq = quartet of a quartet, and tt = triplet of a triplet. All quoted optical rotation values are corrected for 100 % ee samples. IR spectra were recorded as thin films or neat on NaCl plates on an ATI Mattson Genesis Series FT-IR spectrometer. Low and high resolution mass spectra were obtained on a Micromass Inc., Autospec with an E-B-E geometry. Analytical chiral HPLC analysis was conducted using a *S,S*-Whelk-O 1 column (Pirkle) and a Waters model 440 UV detector at wavelength 254 nm. Gas chromatograms (GC) were run on an Agilent 19091Z-413E gas chromatograph equipped with an enhanced HPCHEM integrator. An HP-1 capillary methyl siloxane column of 30 m in length and 0.32 mm in diameter was used for all runs. The initial temperature of the program was 50 °C with a temperature ramp of 10 °C/min up to 315 °C, where

after the same temperature is maintained for 10 min further. Thin layer chromatography (TLC) was performed on silica gel 60 F₂₅₄ glass-backed plates with a layer thickness of 0.25 mm manufactured by E. Merck. TLC visualization was achieved by illumination with a 254 nm UV lamp or by staining with iodine impregnated silica gel. Flash chromatography was performed on silica gel (230–400 mesh ASTM) purchased from Bodman or Sorbtech. Optical rotations were measured on a Perkin-Elmer 241 polarimeter at the Na D-line ($\lambda = 589$ nm) using a 1 dm cell.

6.2. General Procedures

6.2.1. General procedure for acylation of anilines (I)

To a CH₂Cl₂ solution of aniline (1.0 equiv) was added triethyl amine (1.1 equiv). The reaction mixture was cooled to 0 °C and the respective acid chloride (1.1 equiv) was added dropwise. The solution was warmed to room temperature. The reaction mixture was monitored by TLC and quenched accordingly with water upon completion. After separation of the layers, the aqueous layer was extracted with CH₂Cl₂ (3 x). The combined organic layers were washed with brine (1x) and dried with MgSO₄. Filtration and solvent evaporation *in vacuo* followed by purification by using flash chromatography on silica gel eluting with hexanes/ethyl acetate or recrystallization provided the corresponding *o*-iodoanilide.

6.2.2. General procedure for N-allylation of anilides (II)

To a THF slurry of NaH (1.1 equiv) at 0 °C was added the respective *o*-iodoanilide **60** (1.0 equiv) dissolved in THF (2 mL/mmol iodoanilide). The reaction mixture was stirred until the solution became clear and then the appropriate allyl bromide or iodide (1.3 equiv) was added dropwise. The solution was warmed to room temperature. The reaction mixture was monitored

by TLC and quenched accordingly with water upon completion. The resulting mixture was extracted with diethyl ether (3 x 25 mL/mmol of anilide). The combined organic layers were washed with brine (1 x) and dried with MgSO₄. Filtration and solvent evaporation *in vacuo* followed by purification by flash chromatography on silica gel eluting with hexanes/ethyl acetate provided the respective racemic anilide.

6.2.3. General procedure for thermally initiated radical cyclization of anilides (III)

To a benzene solution of the respective *o*-iodoanilide (1.0 equiv) was added Bu₃SnH (1.5 equiv) and AIBN (0.2 equiv). The reaction mixture was refluxed until the starting material was deemed consumed by TLC. The solvents were removed *in vacuo* and the crude was submitted to the DBU workup.⁷⁶ Purification of the remaining crude by flash column chromatography on silica gel eluting with hexanes/diethyl ether (9/1) provided the respective dihydroindole.

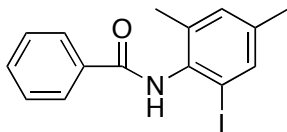
6.2.4. General procedure for Et₃B initiated radical cyclization of N-allyl anilides (IV)

To an aerated benzene solution of the respective *o*-iodoanilide (1.0 equiv) and Bu₃SnH (1.5 equiv, 0.01 M) was added a hexane solution of Et₃B (1.0 M, 1.0 equiv). The reaction mixture was sealed and stirred at room temperature (23 °C) until the starting material was deemed consumed by TLC (typically less than 5 min). The solvents were removed *in vacuo* and the crude was submitted the DBU workup.⁷⁶ Purification of the remaining crude by flash column chromatography on silica gel eluting with hexanes/diethyl ether provided the respective dihydroindole.

6.2.5. General procedure for Et₃B initiated radical cyclizations of acrylanilides (V)

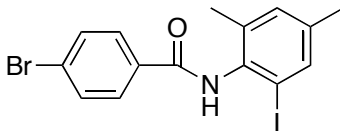
To an aerated benzene solution of the respective *o*-iodoanilide (1.0 equiv) and Bu₃SnH (1.5 equiv, 0.01 M) was added a hexane solution of Et₃B (1.0 M, 1.0 equiv). The reaction mixture was sealed and stirred at room temperature (23 °C) until the starting material was deemed consumed by TLC (typically less than 5 min). The solvent was removed under reduced pressure and the crude product was purified by flash column chromatography on silica gel eluting with hexanes/diethyl ether provided the respective oxindole.

6.3. Compound Data for Chapter 3



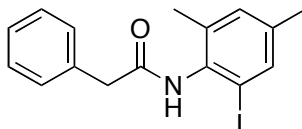
6.3.1. *N*-(2-Iodo-4,6-dimethylphenyl)benzamide (not shown in text):

This compound was prepared according to general procedure I. A white, crystalline solid (mp 175–176 °C) was obtained in quantitative yield: IR (thin film, CH₂Cl₂, NaCl, cm⁻¹) 1679, 1500, 1480, 1265, 1257; ¹H NMR (300 MHz, CDCl₃) δ 2.25 (s, 6 H), 7.06 (s, 1 H), 7.45–7.60 (m, 3 H), 7.55 (s, 1 H), 7.65 (s, 1 H), 7.97 (d, *J* = 7.1 Hz, 2 H); ¹³C NMR (75 MHz, CDCl₃) δ 19.6, 20.5, 99.3, 127.4, 128.7, 131.8, 131.9, 134.2, 134.4, 137.2, 137.3, 139.1, 165.6; HRMS (EI) calcd for C₁₅H₁₄INO 351.0120, found 351.0107; LRMS (EI) *m/z* 351 (M⁺, 50), 259 (29), 246 (51), 224 (49), 105 (100), 77 (50).



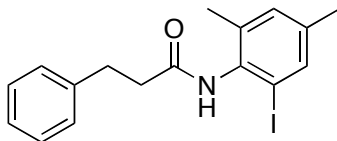
6.3.2. N-(2-Iodo-4,6-dimethylphenyl)-4-bromobenzamide (not shown in text):

This compound was prepared according to general procedure I. A white, crystalline solid (mp 242–244 °C) was obtained in 82 % yield: IR (thin film, CH₂Cl₂, NaCl, cm⁻¹) 1681, 1477, 1421, 1271, 896; ¹H NMR (300 MHz, CDCl₃) δ 2.30 (s, 6 H), 7.09 (s, 1 H), 7.45 (bs, 1 H), 7.57 (s, 1 H), 7.65 (d, *J* = 6.8 Hz, 2 H), 7.68 (d, *J* = 6.8 Hz, 2 H); ¹³C NMR (75 MHz, CDCl₃) δ 19.6, 20.5, 99.1, 126.8, 129.0, 132.0, 132.1, 133.0, 134.1, 137.1, 137.3, 139.4; HRMS (EI) calcd for C₁₅H₁₃NOBrI 428.9225, found 428.9225; LRMS (EI) *m/z* 429 (M⁺, 23), 302 (87), 183 (100).



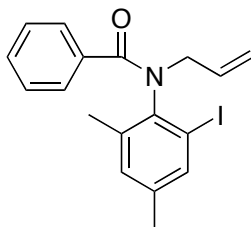
6.3.3. N-(2-Iodo-4,6-dimethylphenyl)-2-phenylacetamide (not shown in text):

This compound was prepared according to general procedure I. A white, crystalline solid (mp 161–162 °C) was obtained in 47 % yield: IR (thin film, CHCl₃, NaCl, cm⁻¹) 3388, 3015, 2923, 1680, 1601, 1558, 1490, 1283, 1236, 852; ¹H NMR (300 MHz, CDCl₃) δ 2.18 (s, 3 H), 2.24 (s, 3 H), 3.80 (s, 2 H), 6.70 (s, 1 H), 6.99 (s, 1 H), 7.45 (m, 5 H), 7.47 (s, 1 H); ¹³C NMR (75 MHz, CDCl₃) δ 19.4, 20.4, 44.1, 99.0, 127.6, 129.2, 129.9, 131.7, 134.2, 134.6, 136.9, 137.0, 139.1, 169.1; HRMS (EI) calcd for C₁₆H₁₆INO 365.0277, found 365.0289; LRMS (EI) *m/z* 365 (M⁺, 3), 274 (3), 273 (4), 247 (66), 238 (100), 91 (71).



6.3.4. *N*-(2-Iodo-4,6-dimethylphenyl)-3-phenylpropionamide (not shown in text):

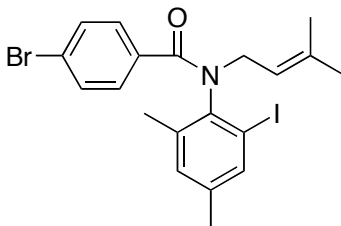
This compound was prepared according to general procedure I. A white, crystalline solid (mp 156–157 °C) was obtained in 76 % yield: IR (thin film, CH₂Cl₂, NaCl, cm⁻¹) 1689, 1482, 1421, 1265; ¹H NMR (300 MHz, CDCl₃) δ 2.13 (s, 3 H), 2.25 (s, 3 H), 2.74 (t, *J* = 8.1 Hz, 2 H), 3.10 (t, *J* = 8.1 Hz, 2 H), 6.93 (s, 1 H), 6.98 (s, 1 H), 7.15–7.45 (m, 5 H), 7.49 (s, 1 H); ¹³C NMR (75 MHz, CDCl₃) δ 19.5, 20.4, 31.5, 38.3, 99.4, 126.3, 128.5, 128.6, 131.7, 134.4, 137.0, 137.1, 139.0, 140.7, 170.5; HRMS (EI) calcd for C₁₇H₁₈INO 379.0433, found 379.0439; LRMS (EI) *m/z* 379 (M⁺, 37), 351 (88), 252 (68), 247 (53), 224 (99), 111 (80), 105 (100).



6.3.5. *rac*-*N*-Allyl-*N*-(2-iodo-4,6-dimethylphenyl)benzamide (56a):

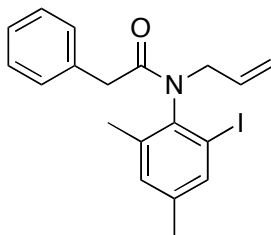
This compound was prepared according to general procedure II. A clear, colorless oil was obtained in 35 % yield: IR (thin film, CH₂Cl₂, NaCl, cm⁻¹) 2927, 1641, 1380, 1258; ¹H NMR (300 MHz, CDCl₃) δ 2.10 (s, 3 H), 2.18 (s, 3 H), 4.04 (dd, *J* = 14.2, 7.9 Hz, 1 H), 4.80 (dd, *J* = 14.2, 6.1 Hz, 1 H), 5.05–5.20 (m, 2 H), 6.08 (dddd, *J* = 14.0, 9.9, 7.8, 6.2 Hz, 1 H), 6.82 (s, 1 H), 7.13 (t, *J* = 7.6 Hz, 2 H), 7.21 (d, *J* = 7.6 Hz, 1 H), 7.39 (d, *J* = 7.0 Hz, 2 H); ¹³C NMR (75 MHz, CDCl₃) δ 19.8, 20.3, 53.1, 101.4, 119.0, 127.3, 127.9, 129.8, 132.0, 132.5, 135.8, 137.6, 138.3, 139.3, 140.7; HRMS (EI) calcd for C₁₈H₁₈INO 391.0433, found 391.0432; LRMS (EI) *m/z* 391 (M⁺, 27), 264 (70), 223 (31), 144 (32), 105 (100), 77 (58); The racemate was submitted to

preparative chiral HPLC separation (Regis Technologies (*S,S*)-Whelk-O 1; 25 cm x 10.0 mm I.D.; 10 mL/min Hexanes/iPrOH; first eluting enantiomer (*P*) α_D^{23} +140, 87 % ee (*c* 5.4 mg/mL, CHCl₃); second eluting enantiomer (*M*) α_D^{23} -191, 97 % ee (*c* 2.4 mg/mL, CHCl₃).



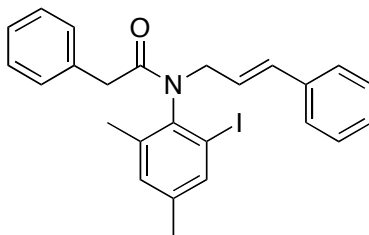
6.3.6. *rac*-N-(2-Iodo-4,6-dimethylphenyl)-N-(3-methylbut-2-enyl)-4-bromobenzamide (56b):

This compound was prepared according to general procedure II. A white, crystalline solid (mp 101 °C) was obtained in 91 % yield: IR (thin film, CH₂Cl₂, NaCl, cm⁻¹) 2927, 1642, 1442, 1399, 1264, 1012; ¹H NMR (300 MHz, CDCl₃) δ 1.44 (s, 3 H), 1.66 (s, 3 H), 2.08 (s, 3 H), 2.23 (s, 3 H), 4.11 (dd, *J* = 14.5, 8.6 Hz, 1 H), 4.71 (dd, *J* = 14.5, 6.8 Hz, 1 H), 5.42 (app t, *J* = 7.0 Hz, 1 H), 6.85 (s, 1 H), 7.20–7.35 (m, 4 H), 7.52 (s, 1 H); ¹³C NMR (75 MHz, CDCl₃) δ 17.6, 19.6, 20.3, 25.7, 47.5, 101.2, 118.4, 124.3, 129.7, 130.6, 132.1, 134.9, 136.9, 137.7, 138.5, 139.5, 140.6, 168.8; HRMS (EI) calcd for C₂₀H₂₃IBrNO 496.9851, found 496.9859; LRMS (EI) *m/z* 497 (M⁺, 37), 454 (13), 429 (28), 302 (32), 191 (100); The racemate was submitted to preparative chiral HPLC separation (Regis Technologies (*S,S*)-Whelk-O 1; 25 cm x 10.0 mm I.D.; 10 mL/min Hexanes/iPrOH; first eluting enantiomer (*P*) α_D^{23} +156, 99 % ee (*c* 1.4 mg/mL, CHCl₃); second eluting enantiomer (*M*) α_D^{23} -146, 98 % ee (*c* 1.5 mg/mL, CHCl₃).



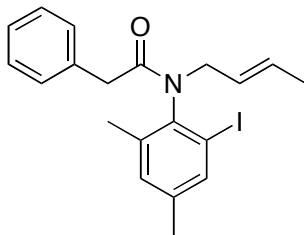
6.3.7. rac-N-Allyl-N-(2-iodo-4,6-dimethylphenyl)-2-phenylacetamide (56c):

This compound was prepared according to general procedure II. A clear, colorless oil was obtained in 93 % yield: IR (thin film, CHCl₃, NaCl, cm⁻¹) 3066, 3024, 3013, 2961, 2926, 2858, 1652, 1466, 1456, 1389, 1261, 990; ¹H NMR (300 MHz, CDCl₃) δ 2.05 (s, 3 H), 2.33 (s, 3 H), 3.22 (d, *J* = 15.0 Hz, 1 H), 3.40 (d, *J* = 15.0 Hz, 1 H), 4.00 (dd, *J* = 14.3, 7.5 Hz, 1 H), 4.45 (dd, *J* = 14.3, 6.3 Hz, 1 H), 5.05 (dd, *J* = 10.0, 1.4 Hz, 1 H), 5.09 (dd, *J* = 17.3, 1.4 Hz, 1 H), 5.96 (dddd, *J* = 17.3, 10.0, 7.5, 6.3 Hz, 1 H), 7.04 (s, 1 H), 7.09 (d, *J* = 6.2 Hz, 2 H), 7.20–7.29 (m, 3 H), 7.64 (s, 1 H); ¹³C NMR (75 MHz, CDCl₃) δ 19.8, 20.8, 41.8, 52.3, 102.3, 119.1, 119.2, 127.0, 128.5, 130.0, 132.5, 133.2, 134.9, 138.7, 140.4, 140.7, 171.0; HRMS (EI) calcd for C₁₉H₂₀INO 405.0590, found 405.0601; LRMS (EI) *m/z* 405 (M⁺, 43), 314 (19), 287 (26), 278 (100), 187 (58), 158 (52), 91 (97); The racemate was submitted to preparative chiral HPLC separation (Regis Technologies (*S,S*)-Whelk-O 1; 25 cm x 10.0 mm I.D.; 10 mL/min Hexanes/*i*PrOH; first eluting enantiomer (*P*) α_D²³ -55, 97 % ee (*c* 3.5 mg/mL, CHCl₃); second eluting enantiomer (*M*) α_D²³ +59, 99 % ee (*c* 1.4 mg/mL, CHCl₃).



6.3.8. *rac*-N-(2-Iodo-4,6-dimethylphenyl)-N-(3-phenylallyl)-2-phenylacetamide (56d):

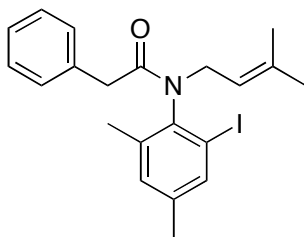
This compound was prepared according to general procedure II. A clear, yellow oil was obtained in 100 % yield: IR (thin film, CHCl₃, NaCl, cm⁻¹) 3008, 2925, 1652, 1495, 1465, 1455, 1393, 1351, 1310, 1247, 968; ¹H NMR (300 MHz, CDCl₃) δ 2.05 (s, 3 H), 2.32 (s, 3 H), 3.23 (d, *J* = 15.0 Hz, 1 H), 3.43 (d, *J* = 15.0 Hz, 1 H), 4.10–4.21 (m, 1 H), 4.50–4.61 (m, 1 H), 6.37–6.40 (m, 2 H), 7.02 (s, 1 H), 7.07–7.12 (m, 2 H), 7.18–7.30 (m, 8H), 7.64 (s, 1 H); ¹³C NMR (75 MHz, CDCl₃) δ 19.3, 20.4, 41.3, 51.3, 101.3, 124.1, 126.3, 126.6, 127.5, 128.1, 128.4, 129.5, 132.2, 133.4, 134.4, 136.5, 138.1, 138.3, 140.0, 140.1, 170.6; HRMS (EI) calcd for C₂₅H₂₄INO 481.0903, found 481.0927; LRMS (EI) *m/z* 481 (M⁺, 58), 390 (44), 363 (8), 236 (27), 158 (21), 117 (100), 91 (84); The racemate was submitted to preparative chiral HPLC separation (Regis Technologies (*S,S*)-Whelk-O 1; 25 cm x 10.0 mm I.D.; 10 mL/min hexanes/*i*PrOH; first eluting enantiomer (*P*) α_D²³ -17, 94 % ee (*c* 6.3 mg/mL, CHCl₃); second eluting enantiomer (*M*) α_D²³ +11, 98 % ee (*c* 9.9 mg/mL, CHCl₃).



6.3.9. *rac*-N-But-2*E*-enyl-N-(2-iodo-4,6-dimethylphenyl)-2-phenylacetamide (56e):

This compound was prepared according to general procedure II. A clear, yellow oil was obtained in 41 % yield: IR (thin film, CHCl₃, NaCl, cm⁻¹) 3012, 2921, 2856, 1650, 1496, 1465,

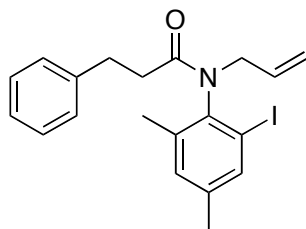
1455, 1393, 1313, 1262, 1247, 1165, 970; ^1H NMR (300 MHz, CDCl_3) δ 1.59 (d, $J = 5.9$ Hz, 3 H), 2.04 (s, 3 H), 2.33 (s, 3 H), 3.20 (d, $J = 15.0$ Hz, 1 H), 3.39 (d, $J = 15.0$ Hz, 1 H), 3.94 (dd, $J = 14.0, 7.1$ Hz, 1 H), 4.38 (dd, $J = 14.0, 6.3$ Hz, 1 H), 5.50–5.79 (m, 2 H), 7.03 (s, 1 H), 7.05–7.14 (m, 2 H), 7.20–7.34 (m, 3 H), 7.63 (s, 1 H); ^{13}C NMR (75 MHz, CDCl_3) δ 17.5, 19.2, 20.3, 41.4, 50.9, 101.9, 125.5, 126.5, 128.0, 129.1, 129.5, 129.9, 132.0, 134.6, 138.2, 139.8, 140.3, 170.4; HRMS (EI) calcd for $\text{C}_{20}\text{H}_{22}\text{INO}$ 419.0746, found 419.0737; LRMS (EI) m/z 419 (M^+ , 55), 292 (44), 238 (37), 174 (30), 158 (33), 91 (98), 55(100); The racemate was submitted to preparative chiral HPLC separation (Regis Technologies (*S,S*)-Whelk-O 1; 25 cm x 10.0 mm I.D.; 10 mL/min Hexanes/*i*PrOH; first eluting enantiomer (*P*) α_D^{23} -46, 99 % ee (*c* 4.7 mg/mL, CHCl_3); second eluting enantiomer (*M*) α_D^{23} +41, 99 % ee (*c* 11.4 mg/mL, CHCl_3).



6.3.10. *rac*-N-(2-Iodo-4,6-dimethylphenyl)-N-(3-methylbut-2-enyl)-2-phenylacetamide (56f):

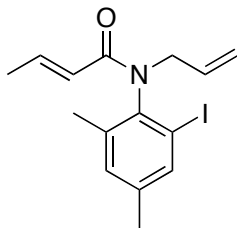
This compound was prepared according to general procedure II. A clear, yellow oil was obtained in 79 % yield: IR (thin film, CHCl_3 , NaCl , cm^{-1}) 3026, 3014, 2925, 2861, 1650, 1495, 1455, 1383, 1236, 1186, 1162, 1032; ^1H NMR (300 MHz, CDCl_3) δ 1.43 (s, 3 H), 1.62 (s, 3 H), 2.03 (s, 3 H), 2.43 (s, 3 H), 3.21 (d, $J = 15.0$ Hz, 1 H), 3.39 (d, $J = 15.0$ Hz, 1 H), 4.04 (dd, $J = 14.3, 8.0$ Hz, 1 H), 4.45 (dd, $J = 14.3, 7.1$ Hz, 1 H), 5.03 (dd, $J = 7.0, 7.0$ Hz, 1 H), 7.03 (s, 1 H), 7.05–7.13 (m, 2 H), 7.17–7.28 (m, 3 H), 7.62 (s, 1 H); ^{13}C NMR (75 MHz, CDCl_3) δ 17.4, 19.0, 20.3, 25.5, 41.1, 45.9, 53.8, 101.7, 118.7, 126.4, 127.9, 129.4, 131.9, 134.5, 136.2, 138.1, 139.7, 140.0, 170.4; HRMS (EI) calcd for $\text{C}_{21}\text{H}_{24}\text{INO}$ 433.0903, found 433.0901; LRMS (EI) m/z 433

(M^+ , 100), 390 (9), 365 (27), 300 (21), 273 (14), 247 (17), 238 (41), 91 (93), 69 (66); The racemate was submitted to preparative chiral HPLC separation (Regis Technologies (*S,S*)-Whelk-O 1; 25 cm x 10.0 mm I.D.; 10 mL/min Hexanes/*i*PrOH; first eluting enantiomer (*P*) α_D^{23} -49, 99 % ee (*c* 2.2 mg/mL, CHCl_3); second eluting enantiomer (*M*) α_D^{23} +43, 99 % ee (*c* 4.5 mg/mL, CHCl_3).



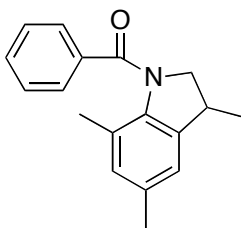
6.3.11. *rac-N-Allyl-N-(2-iodo-4,6-dimethylphenyl)-3-phenylpropionamide (56g)*:

This compound was prepared according to general procedure II. A clear, yellow oil was obtained in 97 % yield: IR (thin film, CHCl_3 , NaCl, cm^{-1}) 2926, 1649, 1395; ^1H NMR (300 MHz, CDCl_3) δ 2.12 (s, 3 H), 2.28 (s, 3 H), 2.95–3.05 (m, 2 H), 3.96 (dd, $J = 14.3, 7.6$ Hz, 1 H), 4.54 (dd, $J = 14.3, 6.5$ Hz, 1 H), 5.04–5.15 (m, 2 H), 5.97 (dddd, $J = 6.5, 7.5, 9.8, 13.7$ Hz, 1 H), 7.02 (s, 1 H), 7.10–7.20 (m, 3 H), 7.23 (d, $J = 6.7$ Hz, 2 H), 7.58 (s, 1 H); ^{13}C NMR (75 MHz, CDCl_3) δ 19.4, 20.4, 31.2, 36.3, 51.6, 101.4, 118.7, 125.9, 128.3, 128.5, 132.1, 132.9, 137.7, 138.3, 139.9, 140.1, 141.4, 171.8; HRMS (EI) calcd for $\text{C}_{20}\text{H}_{22}\text{INO}$ 419.0746, found 419.0743; LRMS (EI) m/z 419 (M^+ , 32), 292 (100), 160 (37), 158 (32), 155 (25), 131 (34), 105 (59); The racemate was submitted to preparative chiral HPLC separation (Regis Technologies (*S,S*)-Whelk-O 1; 25 cm x 10.0 mm I.D.; 10 mL/min Hexanes/*i*PrOH; first eluting enantiomer (*P*) α_D^{23} -60, 99 % ee (*c* 3.8 mg/mL, CHCl_3); second eluting enantiomer (*M*) α_D^{23} +58, 99 % ee (*c* 4.3 mg/mL, CHCl_3).



6.3.12. *rac*-N-Allyl-N-(2-iodo-4,6-dimethylphenyl)-*trans*-crotonamide (56h):

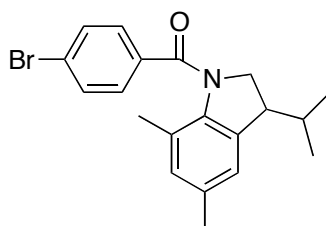
This compound was prepared according to general procedure I. A white, crystalline solid (mp 56–58 °C) was obtained in 64 % yield: IR (thin film, CH₂Cl₂, NaCl, cm⁻¹) 2984, 2854, 1666, 1629, 1445, 1384, 1273; ¹H NMR (300 MHz, CDCl₃) δ 1.73 (dd, *J* = 6.9, 1.5 Hz, 3 H), 2.18 (s, 3 H), 2.31 (s, 3 H), 3.94 (ddd, *J* = 14.3, 7.1, 0.6 Hz, 1 H), 4.58 (dd, *J* = 14.3, 6.4 Hz, 1 H), 5.02–5.11 (m, 2 H), 5.48 (dd, *J* = 15.0, 1.7 Hz, 1 H), 5.97 (dddd, *J* = 17.0, 10.0, 7.7, 6.5 Hz, 1 H), 7.00 (dq, *J* = 15.0, 6.9 Hz, 1 H), 7.04 (s, 1 H), 7.60 (s, 1 H); ¹³C NMR (75 MHz, CDCl₃) δ 18.0, 19.7, 20.5, 51.6, 101.6, 118.7, 121.9, 125.4, 132.0, 133.1, 138.2, 138.8, 139.9, 140.0, 142.4, 165.8; HRMS (EI) calcd for C₁₅H₁₈INO 355.0433, found 355.0445; LRMS (EI) *m/z* 355 (M⁺, 25), 340 (20), 313 (13), 287 (16), 228 (100), 18 (39), 158 (32), 69 (68).



6.3.13. Phenyl-(3,5,7-trimethyl-2,3-dihydroindol-1-yl)methanone (57a):

This compound was prepared according to general procedure IV. The atropisomer (*P*)-**56a** (99.5/0.5 er, first eluting enantiomer) yielded a white, crystalline solid in 95 % yield (93/7 er, +3, *c* 6.2 mg/mL, first eluting enantiomer). The atropisomer (*M*)-**56a** (>99.5/0.5 er, second eluting enantiomer) yielded a white, crystalline solid in 92 % yield (93.5/6.5 er, -3, *c* 6.8 mg/mL, second eluting enantiomer): IR (thin film, CH₂Cl₂, NaCl, cm⁻¹) 2966, 1649, 1371, 1264; ¹H NMR (300

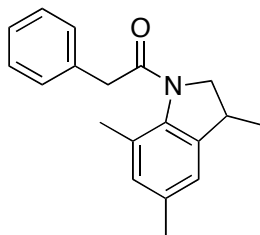
MHz, CDCl₃) δ 1.24 (d, *J* = 7.0 Hz, 3 H), 2.20 (s, 3 H), 2.34 (s, 3 H), 3.33 (sex, *J* = 7.3 Hz, 1 H), 3.65 (dd, *J* = 10.4, 7.6 Hz, 1 H), 4.22 (dd, *J* = 10.4, 7.7 Hz, 1 H), 6.88 (s, 1 H), 6.91 (s, 1 H), 7.40–7.55 (m, 3 H), 7.74 (d, *J* = 6.7 Hz, 2 H); ¹³C NMR (75 MHz, CDCl₃) δ 17.8, 19.9, 21.1, 36.9, 61.6, 121.2, 128.4, 128.5, 128.6, 130.3, 131.1, 135.2, 136.2, 139.2, 139.5, 169.6; HRMS (EI) calcd for C₁₈H₁₉NO 265.1467, found 265.1462; LRMS (EI) *m/z* 265 (M⁺, 39), 105 (100), 77 (35).



6.3.14. (4-Bromophenyl)-(3-isopropyl-5,7-dimethyl-2,3-dihydroindol-1-yl)methanone

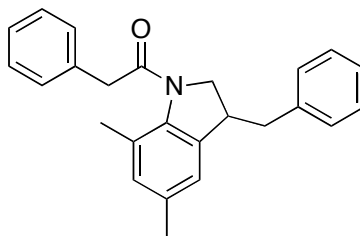
(57b):

This compound was prepared according to general procedure IV. The atropisomer (*P*)-**56b** (99.5/0.5 er, first eluting enantiomer) yielded a white, crystalline solid in 72 % yield (74/26 er, +16, *c* 4.4 mg/mL, second eluting enantiomer). The atropisomer (*M*)-**56b** (99/1 er, second eluting enantiomer) yielded a white, crystalline solid in 95 % yield (73.5/26.5 er, -15, *c* 9.5 mg/mL, first eluting enantiomer): IR (thin film, CH₂Cl₂, NaCl, cm⁻¹) 1649, 1421, 1267, 896; ¹H NMR (300 MHz, CDCl₃) δ 0.79 (d, *J* = 6.8 Hz, 3 H), 0.88 (d, *J* = 7.2 Hz, 3 H), 1.92 (sex, *J* = 6.7 Hz, 1 H), 2.16 (s, 3 H), 2.33 (s, 3 H), 2.99 (p, *J* = 4.1 Hz, 1 H), 3.86 (dd, *J* = 10.8, 3.3 Hz, 1 H), 4.08 (dd, *J* = 10.8, 8.1 Hz, 1 H), 6.89 (s, 1 H), 6.91 (s, 1 H), 7.60 (s, 4 H); ¹³C NMR (75 MHz, CDCl₃) δ 18.3, 20.0, 20.3, 21.1, 30.8, 48.2, 56.2, 122.8, 125.7, 128.4, 130.2, 130.6, 131.7, 135.1, 134.2, 136.8, 139.6, 168.6; HRMS (EI) calcd for C₂₀H₂₂NOBr 371.0885, found 371.0870; LRMS (EI) *m/z* 371 (M⁺, 33), 183 (87), 91 (100).



6.3.15. 1-(3-5,7-Trimethyl-2,3-dihydroindol-1-yl)-2-phenylethanone (57c):

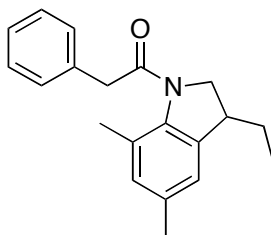
This compound was prepared according to general procedure IV. The atropisomer (*P*)-**56c** (>99.5/0.5 er, second eluting enantiomer) yielded a clear oil in 54 % yield (96.5/3.5 er, +27, *c* 2.5 mg/mL, first eluting enantiomer). The atropisomer (*M*)-**56c** (98.5/1.5 er, first eluting enantiomer) yielded a clear oil in 53 % yield (93.5/6.5 er, -32, *c* 3.7 mg/mL, second eluting enantiomer): IR (thin film, CHCl₃, NaCl, cm⁻¹) 2965, 2928, 1649, 1388; ¹H NMR (300 MHz, CDCl₃) δ 1.15 (d, *J* = 6.8 Hz, 3 H), 2.26 (s, 3 H), 2.30 (s, 3 H), 3.21 (sex, *J* = 6.9 Hz, 1 H), 3.52 (dd, *J* = 10.3, 7.3 Hz, 1 H), 3.88 (s, 2 H), 4.17 (app t, *J* = 8.5 Hz, 1 H), 6.81 (s, 1 H), 6.87 (s, 1 H), 7.23–7.36 (m, 5 H); ¹³C NMR (75 MHz, CDCl₃) δ 19.4, 20.5, 20.9, 36.5, 43.4, 58.4, 121.0, 126.8, 127.1, 128.6, 128.7, 129.6, 130.4, 135.0, 135.1, 136.0, no carbonyl signal observed; IR (thin film, CH₂Cl₂, NaCl, cm⁻¹) 1679, 1500, 1480, 1265, 1257; HRMS (EI) calcd for C₁₉H₂₁NO 279.1623, found 279.1627; LRMS (EI) *m/z* 279 (M⁺, 64), 188 (7), 161 (100), 146 (69), 91 (52).



6.3.16. 1-(3-Benzyl-5,7-dimethyl-2,3-dihydroindol-1-yl)-2-phenylethanone (57d):

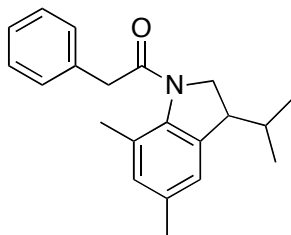
This compound was prepared according to general procedure IV. The atropisomer (*P*)-**56d** (>99.5/0.5 er, second eluting enantiomer) yielded a clear oil in 95 % yield (87/13 er, +24, *c* 4.7 mg/mL, first eluting enantiomer). The atropisomer (*M*)-**56d** (99/1 er, first eluting enantiomer)

yielded a clear oil in 72 % yield (88/12 er, -29, *c* 4.3 mg/mL, second eluting enantiomer): IR (thin film, CH₂Cl₂, NaCl, cm⁻¹) 2927, 1660, 1377, 1268; ¹H NMR (300 MHz, CDCl₃) δ 2.27 (s, 3 H), 2.29 (s, 3 H), 2.53 (dd, *J* = 13.9, 9.9 Hz, 1 H), 2.96 (dd, *J* = 13.9, 5.3 Hz, 1 H), 3.23 – 3.42 (m, 1 H), 3.76 (m, 1 H), 3.82 (d, *J* = 3.2 Hz, 2 H), 3.94 (dd, *J* = 10.6, 7.4 Hz, 1 H), 6.75 (s, 1 H), 6.91 (s, 1 H), 7.30 (m, 10H); ¹³C NMR (75 MHz, CDCl₃) δ 20.6, 21.0, 29.7, 39.6, 43.6, 55.9, 121.8, 126.4, 126.9, 128.6 (2 C), 128.8 (6 C), 130.9, 135.0, 135.1, 127.7, 137.7, 139.2; HRMS (EI) calcd for C₂₅H₂₅NO 355.1936, found 355.1938; LRMS (EI) *m/z* 355 (M⁺, 37), 146 (100), 131 (20), 105 (18), 91 (62).



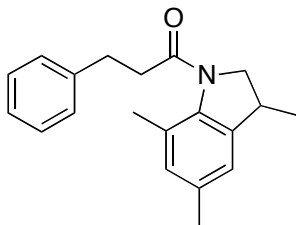
6.3.17. 1-(3-Ethyl-5,7-dimethyl-2,3-dihydroindol-1-yl)-2-phenylethanone (57e):

This compound was prepared according to general procedure IV. The atropisomer (*P*)-**56e** (>99.5/0.5 er, second eluting enantiomer) yielded a clear oil in 77 % yield (89.5/10.5 er, +34, *c* 6.7 mg/mL, first eluting enantiomer). The atropisomer (*M*)-**56e** (>99.5/0.5 er, first eluting enantiomer) yielded a clear oil in 71 % yield (91.5/8.5 er, -38, *c* 1.8 mg/mL, second eluting enantiomer): IR (thin film, CH₂Cl₂, NaCl, cm⁻¹) 2927, 2876, 1656, 1598, 1379, 1268; ¹H NMR (300 MHz, CDCl₃) δ 0.84 (t, *J* = 7.4 Hz, 3 H), 1.25–1.35 (m, 1 H), 1.61–1.70 (m, 1 H), 2.26 (s, 3 H), 2.30 (s, 3 H), 2.95 (m, 1 H), 3.69 (dd, *J* = 10.3, 5.4 Hz, 1 H), 3.88 (s, 2 H), 4.09 (app t, *J* = 8.8 Hz, 1 H), 6.82 (s, 1 H), 6.87 (s, 1 H), 7.20–7.34 (m, 5 H); ¹³C NMR (75 MHz, CDCl₃) δ 11.5, 20.5, 20.9, 26.2, 56.2, 64.7, 121.7, 126.8, 128.7, 128.8, 130.0, 130.6, 134.9, 135.2, 138.4, 139.1; HRMS (EI) calcd for C₂₀H₂₃NO 293.1780, found 293.1779; LRMS (EI) *m/z* 293 (M⁺, 64), 175 (86), 146 (100), 91 (56).



6.3.18. 1-(3-Isopropyl-5,7-dimethyl-2,3-dihydroindol-1-yl)-2-phenylethanone (57f):

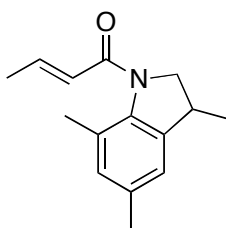
This compound was prepared according to general procedure IV. The atropisomer (*P*)-**56f** (>99.5/0.5 er, first eluting enantiomer) yielded a white, waxy solid in 79 % yield (80/20 er, +12, *c* 1.9 mg/mL, second eluting enantiomer). The atropisomer (*M*)-**56f** (>99.5/0.5 er, second eluting enantiomer) yielded a white, waxy solid in 81 % yield (79/21 er, -11, *c* 2.3 mg/mL, first eluting enantiomer): IR (thin film, CH₂Cl₂, NaCl, cm⁻¹) 1656, 1602, 1378; ¹H NMR (300 MHz, CDCl₃) δ 0.68 (d, *J* = 6.7 Hz, 3 H), 0.88 (d, *J* = 6.8 Hz, 3 H), 1.77 (o, *J* = 6.7 Hz, 1 H), 2.24 (s, 3 H), 2.29 (s, 3 H), 2.83 (q, *J* = 5.9 Hz, 1 H), 3.83–3.90 (m, 2 H), 3.90–4.01 (m, 2 H), 6.81 (s, 1 H), 6.87 (s, 1 H), 7.25–7.35 (m, 2 H), 7.38–7.56 (m, 3 H); ¹³C NMR (75 MHz, CDCl₃) δ 18.5, 20.3, 20.7, 21.0, 30.5, 43.7, 48.1, 54.5, 122.8, 126.9, 128.7, 128.9, 130.7, 134.6, 135.0, 136.9, 136.9, 139.4, 168.9; LRMS (EI) *m/z* 307 (M⁺, 22), 189 (19), 146 (100), 91 (47), 69 (16); HRMS (EI) calcd for C₁₉H₂₀INO 307.1936, found 307.1931; LRMS (EI) *m/z* 307 (M⁺, 27), 189 (22), 146 (100), 91 (37).



6.3.19. 1-(3-Methyl-5,7-dimethyl-2,3-dihydroindol-1-yl)-3-phenylpropanone (57g):

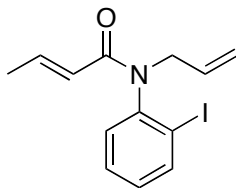
This compound was prepared according to general procedure IV. The atropisomer (*P*)-**56g** (98/2 er, second eluting enantiomer) yielded a clear oil in 67 % yield (92.5/7.5 er, +24, *c* 5.2 mg/mL,

first eluting enantiomer). The atropisomer (*M*)-**56g** (>99.5/0.5 er, first eluting enantiomer) yielded a clear oil in 74 % yield (95/5 er, -25, *c* 4.1 mg/mL, second eluting enantiomer): IR (thin film, CH₂Cl₂, NaCl, cm⁻¹) 1641, 1421, 1264; ¹H NMR (300 MHz, CDCl₃) δ 1.18 (d, *J* = 6.8 Hz, 3 H), 2.20 (s, 3 H), 2.30 (s, 3 H), 2.8 (t, *J* = 7.5 Hz, 2 H), 3.09 (t, *J* = 7.5 Hz, 2 H), 3.08–3.20 (m, 1 H), 3.46 (dd, *J* = 10.1, 7.7 Hz, 1 H), 4.04–4.24 (m, 1 H), 6.81 (s, 1 H), 6.86 (s, 1 H), 7.15–7.35 (m, 5 H); ¹³C NMR (75 MHz, CDCl₃) δ 17.8, 21.0, 29.7, 31.8, 35.9, 41.4, 58.4, 118.1, 121.1, 126.0, 126.2, 127.6, 128.5, 129.0, 130.4, 132.0, 133.0, 134.9, 138.2, 138.9, 141.1, 172.1; HRMS (EI) calcd for C₂₀H₂₃NO 293.1780, found 279.1792; LRMS (EI) *m/z* 293 (M⁺, 34), 205 (9), 161 (100), 146 (38), 105 (25), 91 (44).



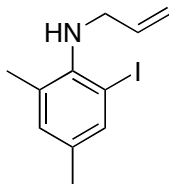
6.3.20. 1-(3-Methyl-5,7-dimethyl-2,3-dihydroindol-1-yl)but-2-enone (**57h**):

This compound was prepared from **56h** according to general procedure I. A brown oil was obtained in 72 % yield: IR (thin film, CH₂Cl₂, NaCl, cm⁻¹) 1666, 1630, 1470, 1423; ¹H NMR (300 MHz, CDCl₃) δ 1.26 (d, *J* = 6.7 Hz, 3 H), 1.92 (dd, *J* = 6.9, 1.5 Hz, 3 H), 2.22 (s, 3 H), 2.31 (s, 3 H), 3.32 (sex, *J* = 7.1 Hz, 1 H), 3.61 (dd, *J* = 10.2, 7.6 Hz, 1 H), 4.33 (app t, *J* = 8.2 Hz, 1 H), 6.17 (d, *J* = 15.0 Hz, 1 H), 6.85 (s, 1 H), 6.87 (s, 1 H), 7.00 (dt, *J* = 15.0, 6.8 Hz, 1 H); ¹³C NMR (75 MHz, CDCl₃) δ 18.1, 18.2, 20.2, 21.0, 21.1, 36.5, 58.9, 121.3, 124.6, 130.4, 134.9, 138.9, 140.2, 141.7, 165.4; HRMS (EI) calcd for C₁₁H₁₅N 161.1204, found 161.1211; LRMS (EI) *m/z* 161 (M⁺, 67), 146 (100), 131 (67).



6.3.21. *rac*-N-Allyl-N-(2-iodophenyl)-*trans*-crotonamide (71b-I):

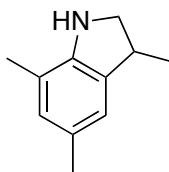
This compound was prepared according to general procedure I from *N*-allyl-2-iodoaniline. A clear, yellow oil was obtained in 59 % yield: IR (thin film, CH₂Cl₂, NaCl, cm⁻¹) 1666, 1630, 1470, 1422, 1386, 1271; ¹H NMR (300 MHz, CDCl₃) δ 1.67 (d, *J* = 7.0 Hz, 3 H), 3.62 (dd, *J* = 14.6, 7.6 Hz, 1 H), 4.83 (dd, *J* = 14.6, 5.2 Hz, 1 H), 4.98–5.11 (m, 2 H), 5.44 (d, *J* = 15.0 Hz, 1 H), 5.80–5.98 (m, 1 H), 6.94 (dq, *J* = 14.6, 7.0 Hz, 1 H), 7.06 (t, *J* = 7.6 Hz, 1 H), 7.13 (d, *J* = 7.6 Hz, 1 H), 7.36 (t, *J* = 7.6 Hz, 1 H), 7.91 (d, *J* = 7.6 Hz, 1 H); ¹³C NMR (75 MHz, CDCl₃) δ 17.9, 51.1, 100.7, 118.4, 122.3, 129.1, 129.6, 130.9, 132.6, 139.6, 142.1, 143.8, 165.2; HRMS (EI) calcd for C₁₃H₁₄INO 327.0120, found 327.0123; LRMS (EI) *m/z* 327 (M⁺, 3), 259 (21), 200 (99), 130 (33), 69 (100).



6.3.22. *N*-Allyl-2-iodo-4,6-dimethylaniline (75):

A dry flask was charged with a stir bar and aniline **59** (1.0 g, 4.0 mmol) before capping with a septum and back filling with argon. Anhydrous THF (15 mL) was introduced via syringe and the flask was cooled to 0 °C. A solution of LDA (2.0 M, 1.8 mL, 3.7 mmol) was added via syringe and the reaction mixture was stirred for 5 min. Finally, allyl iodide (343 mL, 3.7 mmol) was added and reaction mixture was allowed to warm to room temperature over an hour. After warming, water (50 mL) was added and the biphasic solution extracted with diethyl ether (3 x 15

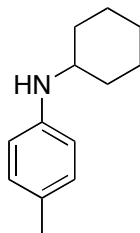
mL). The combined organic fractions were washed with brine, dried with MgSO₄, filtered and concentrated *in vacuo*. The resulting crude oil was purified by silica gel flash chromatography (hexanes/diethyl ether, 9/1) to give the *title compound* as a reddish oil in 83 % yield: ¹H NMR (300 MHz, CDCl₃) δ 1.77 (s, 3H), 1.84 (s, 3H), 2.27 (s, 3H), 2.42 (s, 3H), 3.29 (s, 1H), 3.58 (d, *J* = 6.9 Hz, 2 H), 5.51 (m, 1H), 6.97 (s, 1H), 7.50 (s, 1H); ¹³C NMR (75 MHz, CDCl₃) δ 17.8, 19.4, 19.6, 22.5, 25.6, 31.5, 46.3, 96.1, 122.1, 130.9, 132.2, 133.5, 134.8, 136.8, 145.6; HRMS (EI) calcd for C₁₁H₁₄IN 287.0171, found 287.0173; LRMS (EI) *m/z* 287 (M⁺, 100), 246 (80), 160 (84) 145 (58), 119 (57), 91 (50), 77 (32), 65 (29).



6.3.23. 3,5,7-Trimethyl-2,3-dihydroindole (76):

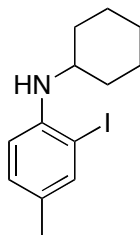
This compound was prepared according to general procedure III using **75**. A clear, orange oil was obtained in 72 % yield: IR (thin film, CHCl₃, NaCl, cm⁻¹) 2964, 2927, 2872, 2857, 1660, 1605, 1486, 1463; ¹H NMR (300 MHz, CDCl₃) δ 1.42 (d, *J* = 6.8 Hz, 3 H), 2.22 (s, 3 H), 2.37 (s, 3 H), 3.19 (t, *J* = 8.6 Hz, 1 H), 3.38–3.50 (m, 1 H), 3.78 (t, *J* = 8.6 Hz, 1 H), 6.82 (s, 1 H), 6.89 (s, 1 H); ¹³C NMR (75 MHz, CDCl₃) δ 16.5, 18.6, 20.7, 36.9, 55.4, 118.8, 121.4, 128.1, 128.7, 133.9, 147.2; HRMS (EI) calcd for C₁₁H₁₅N 161.1204, found 161.1211; LRMS (EI) *m/z* 161 (M⁺, 67), 146 (100), 131 (67).

6.4. Compound Data for Chapter 4



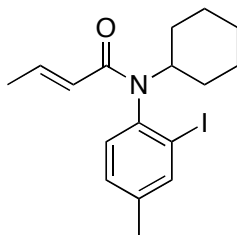
6.4.1. *N*-Cyclohexyl-*p*-toluidine (108):

To a dry septum-capped tube was added K_2CO_3 (8.08 g, 58.5 mmol), L-proline (2.0 g, 17.5 mmol), and cyclohexylamine (5.0 mL, 43.8 mmol). A solution of *p*-bromotoluene (5.0 g, 29.2 mmol) in anhydrous DMSO (19.5 mL) was introduced by syringe. Cu(I) iodide (1.67 g, 87.7 mmol) was added and the tube was capped. The reaction mixture was heated at 100 °C for 24 hours.⁴⁹ After cooling, the reaction mixture was diluted with CH_2Cl_2 (20 mL) and filtered twice through a pad of silica gel/celite (1/1) to remove insolubles. The remaining solution was concentrated *in vacuo*. Water (20 mL) was added to the crude and the mixture was extracted with diethyl ether (4 x 20 mL). The organic fractions were dried over MgSO_4 , filtered, and concentrated *in vacuo*. The crude oil was purified via silica gel flash chromatography (hexanes/ Et_2O , 95/5) to give the title compound as a tan, crystalline solid (mp 40–41 °C) in 55 % yield: ^1H NMR (300 MHz, CDCl_3) δ 1.09–1.50 (m, 5H), 1.64–1.74 (m, 1 H), 1.74–1.87 (m, 2 H), 2.05–2.16 (m, 2 H), 2.26 (s, 3 H), 3.26 (tt, $J = 10.1, 3.7$ Hz, 1 H), 3.31 (bs, 1 H), 6.54 (d, $J = 7.9$ Hz, 2 H), 7.01 (d, $J = 7.9$ Hz, 2 H); ^{13}C NMR (75 MHz, CDCl_3) δ 20.3, 25.0, 26.0, 33.5, 52.0, 113.4, 126.0, 129.7, 145.1.



6.4.2. *N*-Cyclohexyl-2-iodo-4-methylaniline (not shown in text):

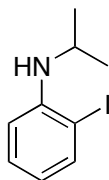
To a solution of aniline **108** (500 mg, 2.64 mmol) in CH₂Cl₂ (6.6 mL) was added (pyridine)₂I•BF₄ (982 mg, 2.64 mmol).^{77a} After 15 min, water (5 mL) was added and the mixture was extracted with CH₂Cl₂ (3 x 10 mL). The combined organic fractions were washed with sat. Na₂S₂O₃ and dried over MgSO₄. The solids were removed by filtration and the volatiles were removed *in vacuo*. Purification by silica gel flash chromatography (hexanes/diethyl ether, 95/5) gave the title compound as a clear, yellow oil in 68 % yield: IR (thin film, CH₂Cl₂, NaCl, cm⁻¹) 3020, 2931, 2856, 1604, 1510, 1313; ¹H NMR (300 MHz, CDCl₃) δ 1.25–1.55 (m, 5H), 1.65–1.75 (m, 1 H), 1.78–1.90 (m, 2 H), 2.30–2.15 (m, 2 H), 2.55 (s, 3 H), 3.35 (bs, 1 H), 4.00 (m, 1 H), 6.56 (d, *J* = 8.2 Hz, 1 H), 7.04 (d, *J* = 8.2 Hz, 1 H), 7.56 (s, 1 H); ¹³C NMR (75 MHz, CDCl₃) δ 19.7, 24.7, 25.9, 33.0, 52.0, 86.0, 111.2, 127.4, 129.9, 139.3, 144.2; HRMS (EI) calcd for C₁₃H₁₈IN 315.0484, found 315.0484; LRMS (EI) *m/z* 315 (M⁺, 100), 272 (82), 259 (23), 144 (36), 106 (27).



6.4.3. *N*-Cyclohexyl-*N*-(2-iodo-4-methylphenyl)-but-2*E*-enamide (*rac*-109):

To a dry sealable tube was added DMAP (78 mg, 0.64 mmol), *N*-Cyclohexyl-2-iodo-4-methylaniline (100 mg, 0.32 mmol), pyridine (77 μL, 0.95 mmol) to CH₂Cl₂ (1 mL). *Trans*-

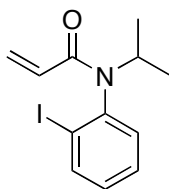
crotonyl chloride (91 μL , 0.95 mmol) was introduced via syringe and the tube was sealed. The reaction mixture was heated at 35 $^{\circ}\text{C}$ for 4 h, cooled, and then quenched with sat. NaHCO_3 (5 mL). The resulting heterogeneous mixture was extracted with CH_2Cl_2 (3 x 10 mL). The organic fractions were washed with brine (5 mL), dried over MgSO_4 , filtered of solids and concentrated *in vacuo*. The resulting crude oil was purified by silica gel flash chromatography (hexanes/diethyl ether, 7/3) to give the title compound as a white, crystalline solid (mp 134–135 $^{\circ}\text{C}$) in 74 % yield: IR (thin film, CH_2Cl_2 , NaCl , cm^{-1}) 3024, 2935, 1664, 1616, 1483; ^1H NMR (300 MHz, CDCl_3) δ 0.79–1.08 (m, 2 H), 1.22–1.51 (m, 4 H), 1.58–1.85 (m, 2 H), 1.71 (d, $J = 7.0$ Hz, 3 H), 1.92–2.02 (m, 1 H), 2.11–2.23 (m, 1 H), 2.37 (s, 3 H), 4.47 (tt, $J = 11.8, 3.4$ Hz, 1 H), 5.42 (dd, $J = 14.9, 1.4$ Hz, 1 H), 6.93 (dq, $J = 14.9, 7.0$ Hz, 1 H), 7.08 (d, $J = 8.0$ Hz, 1 H), 7.20 (d, $J = 8.0$ Hz, 1 H), 7.77 (s, 1 H); ^{13}C NMR (75 MHz, CDCl_3) δ 17.9, 20.5, 25.7, 25.8, 25.9, 30.3, 32.4, 56.4, 103.9, 123.8, 129.8, 130.3, 139.8, 139.9, 140.6, 141.1, 165.4; HRMS (EI) calcd for $\text{C}_{16}\text{H}_{19}\text{INO}$ 368.0511, found 368.0515; LRMS (EI) m/z 368 (M^+ , 8), 301 (48), 256 (88), 174 (83), 149 (64), 57 (100).



6.4.4. (2-Iodophenyl)-isopropylamine (111):

A round bottom flask was charged with a stir bar and of sodium triacetoxymethylborohydride (6.1 g, 28.8 mmol) and capped with a septum. Acetone (532 μL , 7.2 mmol) was added via syringe to the flask followed by 2-iodoaniline (1.58 g, 7.2 mmol) dissolved in 1/1 THF/dichloromethane (18 mL). Two drops of glacial acetic acid was introduced and the heterogeneous mixture was stirred for 7 d.⁷⁸ The reaction was quenched with water (25 mL) and the resulting biphasic

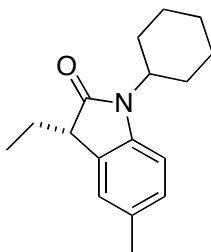
solution was extracted with dichloromethane (3 x 20 mL). The combined organic fractions were washed with brine, dried with MgSO₄, filtered and concentrated *in vacuo*. The crude oil was purified by silica gel flash chromatography (hexanes/diethyl ether, 98/2) to give 1.46 g of the title compound as a clear oil (78 % yield): IR (thin film, CH₂Cl₂, NaCl, cm⁻¹) 2965, 1586, 1500, 1458, 1316, 1169; ¹H NMR⁷⁹ (300 MHz, CDCl₃) δ 1.29 (d, *J* = 6.3 Hz, 6 H), 3.69 (sept, *J* = 6.2 Hz, 1 H), 4.04 (bs, 1 H), 6.43 (td, *J* = 7.7, 1.4 Hz, 1 H), 6.60 (dd, *J* = 8.2, 1.1 Hz, 1 H), 7.21 (td, *J* = 7.3, 1.5 Hz, 1 H), 7.68 (dd, *J* = 7.8, 1.5 Hz, 1 H); ¹³C NMR (75 MHz, CDCl₃) δ 22.9 (2 C), 44.77, 85.8, 111.1, 118.1, 129.3, 139.2, 146.6; HRMS (EI) calcd for C₉H₁₂IN 261.0015, found 261.0008; LRMS (EI) *m/z* 261 (M⁺, 44), 246 (100).



6.4.5. *N*-(2-Iodophenyl)-*N*-isopropylacrylamide (*rac*-112):

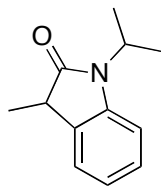
A dry flask was charged with a stir bar and aniline **111** (2.61 g, 10 mmol) before capping with a septum and back filling with argon. Diisopropylethylamine (2.67 mL, 15 mmol) and anhydrous dichloromethane (33 mL) was introduced via syringe. Acryloyl chloride (1.21 mL, 15 mmol) was added and the reaction mixture was heated at reflux for 4 h. After cooling, water (50 mL) was added and the biphasic solution extracted with dichloromethane (3 x 25 mL). The combined organic fractions were washed with sat. NaHCO₃, dried with MgSO₄, filtered and concentrated *in vacuo*. The resulting crude oil was purified by silica gel flash chromatography (hexanes/diethyl ether, 8/2) to give the *title compound* as a white, crystalline solid (mp 77–79 °C) in 84 % yield: IR (thin film, CH₂Cl₂, NaCl, cm⁻¹) 2976, 1655, 1616, 1463, 1410, 1331; ¹H NMR (300 MHz, CDCl₃) δ 1.05 (d, *J* = 6.9 Hz, 3 H), 1.35 (d, *J* = 6.6 Hz, 3 H), 4.83 (sept, *J* = 6.8 Hz, 1 H), 5.49

(dd, $J = 10.3, 2.0$ Hz, 1 H), 5.76 (dd, $J = 16.7, 10.3$ Hz, 1 H), 6.40 (dd, $J = 16.7, 2.0$ Hz, 1 H), 7.11 (td, $J = 7.7, 1.5$ Hz, 1 H), 7.24 (dd, $J = 7.8, 1.5$ Hz, 1 H), 7.43 (td, $J = 7.6, 1.2$ Hz, 1 H), 7.97 (dd, $J = 7.8, 1.2$ Hz, 1 H); ^{13}C NMR (75 MHz, CDCl_3) δ 19.6, 22.2, 48.7, 104.0, 127.8, 129.2, 129.4, 129.8, 130.6, 140.3, 142.0; HRMS (EI) calcd for $\text{C}_{12}\text{H}_{14}\text{INO}$ 315.0120, found 315.0124; LRMS (EI) m/z 315 (M^+ , <1), 246 (44), 188 (84), 146 (85), 55 (100).



6.4.6. 3-Ethyl-1-cyclohexyl-5-methyl-1,3-dihydroindol-2-one (114):

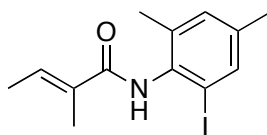
Enantioenriched samples of **109** were cyclized according to the general asymmetric radical cyclization procedure in benzene. The atropisomer (*M*)-**109** (91/9 er, first eluting enantiomer) yielded a clear, colorless oil (*R*)-**114** in 81 % yield (71/29 er, +3 (CHCl_3 , c 4.2 mg/mL), second eluting enantiomer). The atropisomer (*P*)-**109** (86/14 er, second eluting enantiomer) yielded a clear, colorless oil (*S*)-**114** in 85 % yield (75/25 er, -3 (CHCl_3 , c 4.3 mg/mL), first eluting enantiomer). IR (thin film, CH_2Cl_2 , NaCl, cm^{-1}) 2932, 2857, 1706, 1622, 1597, 1490; ^1H NMR (300 MHz, CDCl_3) δ 0.83 (t, $J = 7.4$ Hz, 3 H), 1.27 (tt, $J = 12.6, 2.9$ Hz, 1 H), 1.34–1.52 (m, 2 H), 1.62 (app s, 1 H), 1.65–1.83 (m, 2 H), 1.85–1.94 (m, 2 H), 1.96–2.07 (m, 2 H), 2.07–2.23 (m, 2 H), 2.34 (s, 3 H), 3.35 (t, $J = 5.5$ Hz, 1 H), 4.19 (tt, $J = 12.4, 3.9$ Hz, 1 H), 6.94 (d, $J = 8.0$ Hz, 1 H), 7.04 (d, $J = 8.0$ Hz, 1 H), 7.07 (s, 1 H); ^{13}C NMR (75 MHz, CDCl_3) δ 9.6, 21.0, 23.9, 25.5, 26.0, 29.1, 29.3, 46.5, 51.9, 109.5, 124.8, 127.6, 129.5, 131.0, 141.2, 177.6; HRMS (EI) calcd for $\text{C}_{17}\text{H}_{23}\text{NO}$ 257.1780, found 257.1786; LRMS (EI) m/z 257 (M^+ , 68), 175 (100), 147 (44).



6.4.7. 3-Methyl-1-isopropyl-1,3-dihydroindolin-2-one (115):

Enantioenriched samples of **112** were cyclized according to the general asymmetric radical cyclization procedure in benzene. The atropisomer (*M*)-**112** (83/17 er, second eluting enantiomer) yielded a clear, colorless oil (*R*)-**115** in 85 % yield (76/24 er, +5 (CHCl₃, *c* 10.0 mg/mL), second eluting enantiomer). The atropisomer (*P*)-**112** (86/14 er, first eluting enantiomer) yielded a clear, colorless oil (*S*)-**115** in 78 % yield (75/25 er, -4 (CHCl₃, *c* 10.4 mg/mL), first eluting enantiomer). IR (thin film, CH₂Cl₂, NaCl, cm⁻¹) 2930, 2857, 1704, 1622, 1596, 1490; ¹H NMR (300 MHz, CDCl₃) δ 1.46 (d, *J* = 7.6 Hz, 3 H), 1.48 (d, *J* = 7.0 Hz, 6 H), 3.38 (q, *J* = 7.6 Hz, 1 H), 4.67 (sept, *J* = 7.0 Hz, 1 H), 6.98–7.08 (m, 2 H), 7.20–7.28 (m, 2 H); ¹³C NMR (75 MHz, CDCl₃) δ 15.5, 19.3, 40.5, 43.4, 109.7, 121.7, 123.7, 127.5, 131.2, 142.5, 178.3; HRMS (EI) calcd for C₁₂H₁₅NO 189.1154, found 189.1148; LRMS (EI) *m/z* 189 (M⁺, 93), 174 (62), 146 (100) 119 (43).

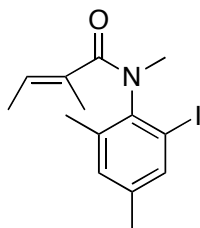
6.5. Compound Data for Chapter 5



6.5.1. *N*-(2-Iodo-4,6-dimethylphenyl)-2-methyl-2*E*-butenamide (153a):

In a round bottom flask equipped with a stir bar aniline **59** (700 mg, 2.83 mmol) and pyridine (344 μL, 4.24 mmol) were dissolved in dichloromethane (5 mL). The flask was capped and backfilled with argon. The contents were cooled of the flask were cooled to 0 °C and tigloyl

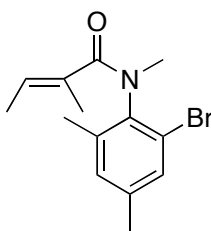
chloride (508 μL , 4.24 mmol) was added via syringe. The reaction mixture was allowed to warm to room temperature over 1 hr. After quenching with water (5 mL), the biphasic mixture was extracted with dichloromethane (3 x 5 mL). The combined organic fractions were washed with brine, dried over MgSO_4 , and concentrated *in vacuo*. The resulting crude was purified by silica gel chromatography (hexanes/diethyl ether, 6/4) to give the title compound as a white, crystalline solid (mp 108–110 $^\circ\text{C}$) n 81 % yield: IR (neat, KBr, cm^{-1}) 2918, 2856, 1666, 1631, 1495, 1381, 1286; ^1H NMR (300 MHz, CDCl_3) δ 1.83 (d, $J = 6.8$ Hz, 3 H), 1.98 (s, 3 H), 2.24 (s, 3 H), 2.27 (s, 3 H), 6.67 (q, $J = 6.8$ Hz, 1 H), 7.02 (s, 1 H), 7.15 (bs, 1 H), 7.51 (s, 1 H); ^{13}C NMR (75 MHz, CDCl_3) δ 12.6, 14.0, 19.5, 20.4, 99.2, 131.7, 134.6, 136.9, 137.2, 38.7, 167.4; HRMS (EI) calcd for $\text{C}_{13}\text{H}_{16}\text{INO}$ 329.0277, found 329.0278; LRMS (EI) m/z 329 (M^+ , 23), 247 (9), 202 (100), 83 (92).



6.5.2. *N*-(2-Iodo-4,6-dimethylphenyl)-*N*,2-dimethyl-2*E*-butenamide (154a):

To a round bottom flask equipped with a stir bar a slurry of NaH (95 %, 55 mg, 2.19 mmol) and THF (1 mL) was created. The flask was capped, backfilled with argon, and its contents cooled to 0 $^\circ\text{C}$. Amide **153a** (600 mg, 1.82 mmol) was dissolved in THF (5 mL) and added dropwise via syringe to the slurry. After stirring for 15 min methyl iodide (127 μL , 2.19 mmol) was added via syringe. After a further 15 min water was carefully added to quench remaining hydride. The resulting biphasic mixture was extracted with diethyl ether (3 x 5 mL). The combined organic fractions were washed with brine, dried over MgSO_4 , and concentrated *in vacuo*. The resulting crude material was purified by silica gel chromatography (hexanes/diethyl ether, 7/3) to give a

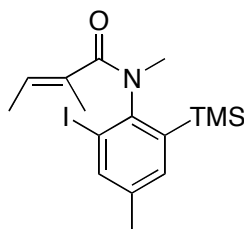
white, crystalline solid (mp 80–82 °C) in 77 % yield: IR (thin film, CH₂Cl₂, NaCl, cm⁻¹) 2921, 1634, 1472, 1354; Note: Compound exists as a 3.2:1 mixture of *E/Z* amide rotamers in CDCl₃. ¹H NMR (300 MHz, CDCl₃) δ 1.48 (d, *J* = 6.8 Hz, 3 H), 1.65 (s, 3 H), 2.22 (s, 3 H), 2.27 (s, 3 H), 3.15 (s, 3 H), 5.79 (qd, *J* = 6.8, 1.1 Hz, 1 H), 7.00 (s, 1 H), 7.52 (s, 1 H); ¹³C NMR (75 MHz, CDCl₃) δ 13.5, 13.8, 19.1, 20.3, 35.9, 100.5, 130.0, 132.0, 132.0, 136.9, 137.9, 138.2, 139.1, 172.7; HRMS (EI) calcd for C₁₄H₁₈INO 344.0511, found 344.0503; LRMS (EI) *m/z* 344 (M+H⁺, 52), 216 (100), 83 (78). The racemate was submitted to preparative chiral HPLC separation (Regis Technologies (*S,S*)-Whelk-O 1; 25 cm x 10.0 mm I.D.; 10 mL/min Hexanes/*i*PrOH, 95/5; first eluting enantiomer (*M*) α_D²³ -51, 93/7 er (*c* 4.4 mg/mL, CHCl₃); second eluting enantiomer (*P*) α_D²³ 52, 96/4 er (*c* 6.9 mg/mL, CHCl₃).



6.5.3. *N*-(2-Bromo-4,6-dimethylphenyl)-*N*,2-dimethyl-2*E*-butenamide (**154b**):

To a round bottom flask equipped with a stir bar a slurry of NaH (95 %, 11 mg, 0.45 mmol) and THF (600 μL) was created. The flask was capped, backfilled with argon, and its contents cooled to 0 °C. Amide **153b** (106 mg, 0.38 mmol) was dissolved in THF (600 μL) and added dropwise via syringe to the slurry. After stirring for 15 min methyl iodide (28 μL, 0.45 mmol) was added via syringe. After a further 15 min water was carefully added to quench remaining hydride. The resulting biphasic mixture was extracted with diethyl ether (3 x 5 mL). The combined organic fractions were washed with brine, dried over MgSO₄, and concentrated *in vacuo*. The resulting crude material was purified by silica gel chromatography (hexanes/diethyl ether, 1/1) to give a

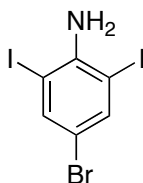
white, crystalline solid (mp 50–52 °C) in 69 % yield: Note: Compound exists as a 4.2:1 mixture of *E/Z* amide rotamers in CDCl₃; signals assigned to the major isomer are in **bold** and those of a mixture *italicized*. ¹H NMR (300 MHz, CDCl₃) δ **1.46** (dd, *J* = 6.8, 1.1 Hz, 3 H), 1.64 (s, 3 H), **1.64** (t, *J* = 1.4 Hz, 3 H), 1.76 (dd, *J* = 6.8, 1.1 Hz, 3 H), 1.96 (t, *J* = 1.4 Hz, 3 H), 2.21 (s, 3 H), 2.29 (s, 3 H), **3.14** (s, 3 H), 3.19 (s, 3 H), **5.34** (qq, *J* = 6.8, 1.4 Hz, 1 H), 5.89 (qq, *J* = 6.8, 1.4 Hz, 1 H), **6.96** (s, 1 H), 7.03 (s, 1 H), **7.25** (s, 1 H), 7.27 (s, 1 H); ¹³C NMR (75 MHz, CDCl₃) δ 13.5, 18.6, 20.7, 35.6, 123.7, 129.3, 131.0, 131.6, 132.0, 137.4, 138.9, 139.6.



6.5.4. N-(2-Iodo-4-methyl-6-trimethylsilylphenyl)-N,2-dimethyl-2*E*-butenamide (rac-156a):

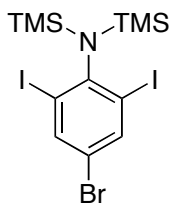
To a round bottom flask equipped with a stir bar was dissolved 2-iodo-*N*,4-bismethyl-*N*,6-bis(trimethylsilyl)aniline (657 mg, 1.68 mmol) in dichloromethane (6 mL). Tigloyl chloride (219 mg, 1.85 mmol) was added and the reaction mixture stirred for 24 hr.⁹ⁱ The reaction was quenched with sat. NaHCO₃ (10 mL) and the resulting biphasic mixture was extracted with dichloromethane (3 x 10 mL). The combined organic fractions were washed with brine (10 mL), dried with MgSO₄, filtered, and concentrated *in vacuo*. The crude material was purified by silica gel flash chromatography (hexanes/diethyl ether, 8/4 → 6/2) to give a clear, yellow oil in 97 % yield: Note: Compound exists as a 1.2:1 mixture of *E/Z* amide rotamers in CDCl₃; signals assigned to the major isomer are in **bold** and those of a mixture *italicized*. ¹H NMR (300 MHz, CDCl₃) δ 0.27 (s, 9 H), **1.47** (dd, *J* = 6.9, 1.1 Hz, 3 H), **1.65** (s, 3 H), 1.76 (dd, *J* = 6.9, 1.1 Hz, 3 H), 1.98 (s, 3 H), 2.29 (s, 3 H), **2.30** (s, 3 H), **3.16** (s, 3 H), 3.19 (s, 3 H), **5.69** (qq, *J* = 6.7, 1.1

Hz, 1 H), 5.98 (qq, $J = 6.7, 1.1$ Hz, 1 H), **7.28** (d, $J = 0.6$ Hz, 1 H), 7.32 (d, $J = 0.6$ Hz, 1 H), **7.68** (d, $J = 0.6$ Hz, 1 H), 7.46 (d, $J = 0.6$ Hz, 1 H).



6.5.5. 4-Bromo-2,6-diiodoaniline (not shown in text):

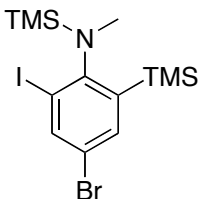
In a round bottom flask equipped with a stir bar was dissolved 4-bromoaniline (1.70 g, 10.0 mmol) in ethanol (30 mL). In succession, iodine (5.08 g, 20.0 mmol) and Ag₂SO₄ (6.22 g, 20.0 mmol) were added to the reaction mixture.⁸⁰ After stirring for 2.5 h the solids were removed by filtration and the resulting solution was concentrated *in vacuo*. The crude material was redissolved in dichloromethane (30 mL) and washed with 5 % NaOH (25 mL) and water (25 mL). The organic fraction was dried over MgSO₄ and concentrated *in vacuo*. The resulting crude was purified by silica gel chromatography (hexanes/diethyl ether, 8/2) to give a white, crystalline solid (mp 132–133 °C) in 67 % yield: ¹H NMR^{77b} (300 MHz, CDCl₃) δ 4.63 (bs, 2 H), 7.81 (s, 2 H).



6.5.6. 4-Bromo-2,6-diiodo-N,N-bis(trimethylsilyl)aniline (158):

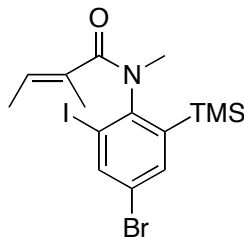
In a round bottom flask equipped with a stir bar was dissolved 4-bromo-2,6-diiodoaniline (1.00 g, 2.36 mmol) in THF (10 mL). The flask was capped with a septum, backfilled with Ar, and cooled to -78 °C. In succession a 2.0 M solution of LDA (2.83 mL, 5.66 mmol) and TMSCl (657 μL, 5.19 mmol) were added via syringe. After 5 min, another round of reagents were added

and the entire reaction mixture allowed to stir for 30 min.⁹ⁱ The reaction was quenched at -78 °C with water and allowed to warm to room temperature. The resulting biphasic mixture was extracted with diethyl ether (3 x 10 mL), dried over MgSO₄, filtered, and dried *in vacuo*. The crude material was purified by silica gel flash chromatography (hexanes/diethyl ether, 99/1) to give an orange oil in 83 % yield: ¹H NMR (300 MHz, CDCl₃) δ 0.26 (s, 18 H), 8.00 (s, 2 H).



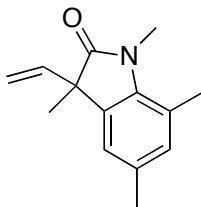
6.5.7. 4-Bromo-2-iodo-N-methyl-N,6-bis-(trimethylsilyl)aniline (not shown in text):

In a round bottom flask equipped with a stir bar was dissolved aniline **158** (1.20 g, 2.11 mmol) in THF (6 mL). The flask was capped with a septum, backfilled with Ar, and cooled to -78 °C. A 1.4 M solution of *sec*-BuLi (3.02 mL, 4.22 mmol) was via syringe. After 10 min, methyl iodide (144 μL, 2.32 mmol) was added via syringe and the reaction mixture was allowed to warm to room temperature over 30 min.⁹ⁱ Water (5 mL) was added and the resulting biphasic mixture was extracted with diethyl ether (3 x 5 mL). The combined organic fractions were washed with brine (5 mL), dried over MgSO₄, filtered, and concentrated *in vacuo*. The resulting crude material was purified by silica gel flash chromatography (hexanes/diethyl ether, 98/2) to give the title compound as a clear, yellow oil in 50 % yield: ¹H NMR (300 MHz, CDCl₃) δ 0.19 (s, 9 H), 0.31 (s, 9 H), 2.71 (s, 3 H), 7.54 (d, *J* = 2.4 Hz, 1 H), 8.02 (s, *J* = 2.4 Hz, 1 H).



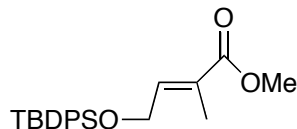
6.5.8. *N*-(4-Bromo-2-iodo-6-trimethylsilylphenyl)-*N*,2-dimethyl-2*E*-butenamide (rac-156b):

In a round bottom flask equipped with a stir bar was dissolved 4-bromo-2-iodo-*N*-methyl-*N*,6-bis-(trimethylsilyl)aniline (45.6 mg, 0.100 mmol) in dichloromethane (400 μ L). The flask was capped with a septum, backfilled with Ar. Tigloyl chloride (13.0 μ L, 0.110 mmol) was added via syringe and the reaction mixture was stirred at room temperature for 24 h. The reaction was quenched with sat. NaHCO₃ (10 mL) and the resulting biphasic mixture was extracted with dichloromethane (3 x 3 mL). The combined organic fractions were washed with brine (1 mL), dried with MgSO₄, filtered, and concentrated *in vacuo*. The crude material was purified by silica gel flash chromatography (hexanes/diethyl ether, 8/4) to give a clear, yellow oil in 53 % yield: Note: Compound exists as a 1:1 mixture of *E/Z* amide rotamers in CDCl₃; signals assigned as a mixture *italicized*. ¹H NMR (300 MHz, CDCl₃) δ 0.30 (s, 9 H), 1.50 (d, *J* = 6.7 Hz, 3 H), 1.69 (s, 3 H), 1.78 (d, *J* = 6.7 Hz, 3 H), 1.98 (s, 3 H), 3.17 (s, 3 H), 3.21 (s, 3 H), 5.67 (qq, *J* = 6.1, 1.1 Hz, 1 H), 5.99 (qq, *J* = 6.1, 1.1 Hz, 1 H), 7.61 (d, *J* = 0.7 Hz, 1 H), 7.64 (d, *J* = 0.7 Hz, 1 H), 8.00 (d, *J* = 0.7 Hz, 1 H), 8.07 (d, *J* = 0.7 Hz, 1 H).



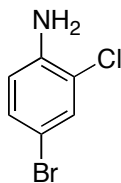
6.5.9. 1,3,5,7-Tetramethyl-1-vinyl-1,3-dihydroindol-2-one (*rac*-**159**):

To a dry flask equipped with a stir bar was charged Pd₂(dba)₃ (18 mg, 20 μmol) and (*tert*-Bu)₃PH•BF₄ (23 mg, 80 μmol). The flask was capped with a septum and backfilled with Ar. A solution of enantioenriched anilide **154a** (34 mg, 99 μmol) in degassed toluene (500 μL) was added by syringe, followed by triethyl amine (19 μL, 14 μmol). The reaction mixture was stirred at room temperature for 48 h. The reaction mixture was diluted with CH₂Cl₂ (5 mL) and filtered through a pad of celite. The resulting solution was concentrated *in vacuo* to generate a dark brown crude solid. The crude material was purified by silica gel flash chromatography (hexanes/ethyl ether, 6/4) to give **159** as a yellow oil. The atropisomer (-)-(*M*)-**154a** (92/7 er, first eluting enantiomer) yielded a yellow oil (+)-**159** in 85 % yield (79/21, +30, *c* 13.4 mg/mL, second eluting enantiomer). The atropisomer (+)-(*P*)-**154a** (96/4 er, second eluting enantiomer) yielded a yellow oil (-)-**159** in 88 % yield (85/15 er, -34, *c* 11.2 mg/mL, first eluting enantiomer): IR (neat, KBr, cm⁻¹) 2972, 2925, 1711, 1635, 1601, 1481, 1342, 1088; ¹H NMR (300 MHz, CDCl₃) δ 1.56 (s, 3 H), 2.23 (s, 3 H), 2.55 (s, 3 H), 3.48 (s, 3 H), 5.13 (d, *J* = 17.0 Hz, 1 H), 5.15 (d, *J* = 10.6 Hz, 1 H), 5.91 (dd, *J* = 17.0, 10.6 Hz, 1 H), 6.83 (s, 2 H); ¹³C NMR (75 MHz, CDCl₃) δ 18.9, 20.8, 22.7, 29.6, 50.6, 115.0, 119.5, 122.5, 131.9, 132.2, 133.6, 138.3, 138.5, 179.3; HRMS (EI) calcd for C₁₄H₁₇NO 215.1310, found 215.1308; LRMS (EI) *m/z* 215 (M⁺, 100), 200 (58), 173 (46).



6.5.10. Methyl 4-(*tert*-butyldiphenylsilyloxy)-2-methylbut-2*E*-enoate (not shown in text):

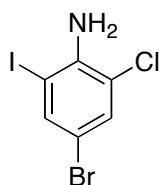
A round bottom flask equipped a stir bar was charged with alcohol **168** (1.13 g, 8.7 mmol), imidazole (887 mg, 13.0 mmol), DMAP (53 mg, 0.43 mmol), and dichloromethane (9 mL). The flask was capped and backfilled with argon. To the reaction mixture was added *tert*-butyldiphenylchlorosilane (2.5 mL, 9.6 mmol) *via syringe*. Over time a white precipitate was observed. After 3 h, water was added and the resulting biphasic mixture was extracted with dichloromethane (3 x 5 mL). The combined organic fractions were washed with brine, dried over MgSO₄, and concentrated *in vacuo*. The resulting crude oil was purified with silica gel chromatography (hexanes/diethyl ether, 8/2) to give a clear oil in 99 % yield: IR (neat, KBr, cm⁻¹) 3070, 3049, 2950, 2933, 2895, 2858, 1714, 1655, 1429, 1244; ¹H NMR (300 MHz, CDCl₃) δ 1.06 (s, 9 H), 1.66 (s, 3 H), 3.76 (s, 3 H), 4.36 (dd, *J* = 5.8, 0.8 Hz, 2 H), 6.90 (qd, *J* = 5.8, 1.4 Hz, 1 H), 7.37–7.48 (m, 6 H), 7.68 (dd, *J* = 7.7, 1.8 Hz, 4 H); ¹³C NMR (75 MHz, CDCl₃) δ 12.6, 19.1, 26.7, 51.8, 61.3, 127.2, 127.8, 129.8, 133.3, 135.5, 141.2, 167.2; HRMS (EI) calcd for C₂₂H₂₈O₃Si 368.1808, found 368.1813; LRMS (EI) *m/z* 368 (M⁺, 2), 311 (34), 213 (100), 199 (32), 183 (19), 84 (34).



6.5.11. 4-Bromo-2-chloroaniline (166):

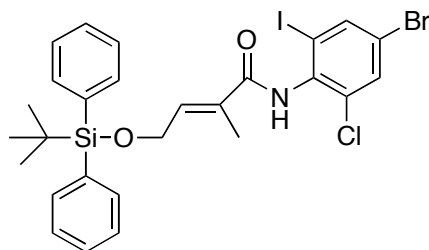
A round bottom flask equipped with a stir bar was charged with 2-chloroaniline (2.54 g, 20.0 mmol), NaBO₃•(H₂O)₄ (3.40 g, 22.0 mmol), KBr (2.86 g, 24.0 mmol), (NH₃)₆Mo₇O₂₄•(H₂O)₄

(248 mg, 0.68 mmol).⁸¹ Acetic acid (24 mL) was added and the reaction mixture was stirred for 2 hr at room temperature. The reaction was quenched with ice and the resulting precipitate was filtered and washed with water. The resulting crude solid was flushed through plug of silica (hexanes/diethyl ether, 7/3) to remove any residual inorganics. After concentration *in vacuo* brownish crystals (mp 156–157 °C) were obtained in 76 % yield: ¹H NMR (300 MHz, CDCl₃) δ 4.05 (s, 2 H), 6.65 (d, *J* = 8.5 Hz, 1 H), 7.17 (dd, *J* = 8.5, 2.2 Hz, 1 H), 7.39 (d, *J* = 2.2 Hz, 1 H); ¹³C NMR (75 MHz, CDCl₃) δ 109.3, 116.8, 119.9, 130.5, 131.6, 142.1.



6.5.12. 4-Bromo-2-chloro-6-iodoaniline (167):

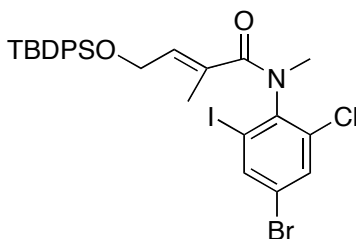
To a round bottom flask equipped with a stir bar aniline **166** (900 mg, 4.36 mmol) was dissolved in ethanol (14.5 mL). In succession, iodine (1.11 g, 4.36 mmol) and Ag₂SO₄ (1.35 g, 4.36 mmol) were added to the reaction mixture.⁸⁰ After stirring for 2 h the solids were removed by filtration and the resulting solution was concentrated *in vacuo*. The crude was redissolved in dichloromethane (30 mL) and washed with 5 % NaOH (25 mL) and water (25 mL). The organic fraction was dried over MgSO₄ and concentrated *in vacuo*. The resulting crude was purified by silica gel chromatography (hexanes, 100 %) to give a white, crystalline solid (mp 92–94 °C) in 79 % yield: ¹H NMR^{77b} (300 MHz, CDCl₃) δ 4.55 (bs, 2 H), 7.39 (d, *J* = 2.0 Hz, 1 H), 7.67 (d, *J* = 2.0 Hz, 1 H); ¹³C NMR (75 MHz, CDCl₃) δ 83.1, 109.1, 118.0, 131.8, 139.1, 142.7.



6.5.13. N-(4-Bromo-2-chloro-6-iodophenyl)-4-(tert-butyldiphenylsilyloxy)-N,2-methylbut-2E-enamide (169):

A dry tube equipped with a stir bar, sealed, and backfilled with Ar. Benzene (7 mL) was added and the flask cooled to 0 °C. A 2.0 M solution of AlMe₃ (4.9 mL, 9.8 mmol) was slowly added,⁸² followed by 4-bromo-6-chloro-2-iodoaniline (1.6 g, 4.9 mmol) dissolved in benzene (15 mL). The mixture was allowed to warm to room temperature over 1 hr before methyl 4-(tert-butyldiphenylsilyloxy)-2-methylbut-2E-enoate (1.8 g, 4.9 mmol) was added as a solution in benzene (7 mL). The tube was then sealed and then refluxed at 80 °C for 24 hr. When the mixture had cooled to room temperature 1 M HCl (15 mL) was added, followed by stirring for 1 hr. The organic layer was separated and the remaining aqueous layer was extracted with ethyl acetate (2 x 15 mL). The combined organic layers were washed with brine (15 mL), dried with MgSO₄, filtered, and concentrated *in vacuo*. The crude was purified by silica gel flash chromatography (hexanes/diethyl ether, 8/2) to give yellow, viscous oil in 75 % yield: IR (thin neat, KBr, cm⁻¹) 326, 3070, 2952, 2931, 2856, 1670, 1641, 1560, 1493, 1371, 1265, 1113, 1061; ¹H NMR (300 MHz, CDCl₃) δ 1.09 (s, 9 H), 1.76 (d, *J* = 0.9 Hz, 3 H), 4.45 (d, *J* = 4.9 Hz, 2 H), 6.58 (t, *J* = 4.9 Hz, 1 H), 7.01 (s, 1 H), 7.38–7.52 (m, 6 H), 7.61 (d, *J* = 2.0 Hz, 1 H), 7.68–7.80 (m, 4 H), 7.93 (d, *J* = 2.0 Hz, 1 H); ¹³C NMR (75 MHz, CDCl₃) δ 13.1, 19.1, 26.8 (3 C), 61.1, 100.4, 121.6, 127.8 (4 C), 129.9 (2 C), 131.0, 132.7, 133.2, 133.3 (2 C), 135.6 (4 C), 135.7,

136.4, 139.9, 166.9; HRMS (EI) calcd for C₂₇H₂₈I¹²⁷BrClSiNO₂Na²³ 689.9704, found 689.9687; LRMS (EI) *m/z* 692 (M+Na⁺ (Br⁸¹), 100), 592 (37).

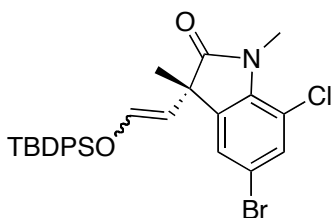


6.5.14. N-(4-Bromo-2-chloro-6-iodophenyl)-4-(*tert*-butyldiphenylsilyloxy)-N,2-dimethylbut-2*E*-enamide (164**):**

In a dry flask equipped with a stir bar, a slurry of 95 % NaH (118 mg, 4.7 mmol) in anhydrous THF (12 mL) was prepared. The flask was capped with a septa, backfilled with Ar, and cooled to 0 °C. Amide **169** (2.4 g, 3.6 mmol) was dissolved in THF (24 mL) and added dropwise to the flask. After stirring for 10 min, methyl iodide (2.2 mL, 36.0 mmol) was added dropwise. The reaction mixture was allowed to warm to room temperature over 3 h. The remaining base was carefully quenched with water. The biphasic mixture was extracted with diethyl ether (3 x 25 mL). The combined organic fractions were washed with brine (25 mL), dried with MgSO₄, filtered, and concentrated *in vacuo*. The crude mixture was purified by silica gel flash chromatography (hexanes/diethyl ether, 8/2) to give anilide **164** as a colorless oil in 99 % yield: IR (neat, KBr, cm⁻¹) 3066, 3051, 2952, 2856, 1668, 1645, 1558, 1441, 1348, 1111; Note: Compound exists as a 6.3/1 mixture of *E/Z* amide rotamers in CDCl₃. ¹H NMR (300 MHz, CDCl₃) δ 0.99 (s, 9 H), 1.68 (s, 3 H), 3.19 (s, 3 H), 4.09 (d, *J* = 5.7 Hz, 2 H), 5.88 (td, *J* = 5.7, 1.1 Hz, 1 H), 7.34–7.48 (m, 6 H), 7.51–7.60 (m, 4 H), 7.73 (dd, *J* = 7.1, 1.6 Hz, 1 H), 7.92 (d, *J* = 2.1 Hz, 1 H); ¹³C NMR (75 MHz, CDCl₃) δ 14.6, 19.2, 26.7 (3 C), 35.3, 60.5, 101.6, 122.2, 127.8 (4 C), 129.8 (2 C), 130.6, 133.3, 133.4, 134.1, 134.2, 135.4 (4 C), 135.6, 140.8, 144.0,

172.0; HRMS (EI) calcd for C₂₄H₂₁NOSiClBrI 623.9258, found 623.9261; LRMS (EI) *m/z* 668 (M+Na⁺, <1), 626 (100), 199 (84), 135 (41).

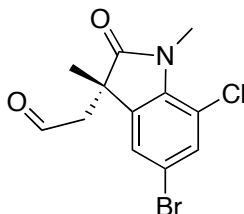
Enantiomers of **164** were separated by injection (36, 40 mg ea) onto a preparative (*S,S*)-Whelk-O 1 chiral column (25 cm x 10.0 mm I.D.) eluting with hexanes/*i*PrOH 98/2. The first eluting enantiomer was recovered in 31 %; second eluting enantiomer, 19 %. Second eluting enantiomer α_D^{23} 16, 98 % ee (*c* 3.2 mg/mL, CHCl₃).



6.5.15. (*S*)-5-Bromo-3-(2-(*tert*-butyldiphenylsilyloxy)vinyl)-7-chloro-1,3-dimethylindolin-2-one (170**):**

To a dry flask equipped with a stir bar was charged Pd₂(dba)₃ (59 mg, 64 μmol) and (*tert*-Bu)₃PH•BF₄ (37 mg, 0.13 mmol). The flask was capped with a septum and backfilled with Ar. A solution of anilide (+)-**164** (220 mg, 0.32 mmol, 99/1 er) in degassed toluene (3.2 mL) was added by syringe, followed by triethyl amine (63 μL, 0.45 mmol). The reaction mixture was stirred at room temperature for 48 h. The reaction mixture was diluted with CH₂Cl₂ (5 mL) and filtered through a pad of celite. The resulting solution was concentrated *in vacuo* to generate a dark brown crude solid. The crude material was purified by silica gel flash chromatography (hexanes/ethyl ether, 9/1) to remove the majority of the dibenzylideneacetone. The mixture of alkene isomers was determined to be 1.2/1 by ¹H NMR, the first eluting isomer being the major component. The er of each geometrical isomer was determined to be 83/17 by injection of a sample onto a (*S,S*)-Whelk O 1 chiral HPLC column. For each geometrical isomer, the first

eluting enantiomer was the major component. ^1H NMR (300 MHz, CDCl_3 , peaks assigned to the major isomer are in **bold** and those of a mixture *italicized*) δ 0.83 (s, 9 H), **1.03** (s, 9 H), **1.29** (s, 3 H), 1.99 (s, 3 H), **3.47** (s, 3 H), 3.54 (s, 3 H), 4.64 (d, $J = 5.6$ Hz, 1 H), **5.11** (d, $J = 12.1$ Hz, 1 H), 6.01 (d, $J = 5.6$ Hz, 1 H), **6.22** (d, $J = 12.1$ Hz, 1 H), **6.87** (d, $J = 2.0$ Hz, 1 H), 7.26 (d, $J = 2.1$ Hz, 1 H), 7.30–7.57 (m, 14 H), 7.58–7.70 (m, 8 H).

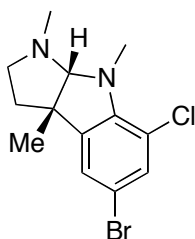


6.5.16. (S)-5-Bromo-7-chloro-1,2-dihydro-3-(2-oxoethyl)-1,3-dimethyl-2-oxo-[3H]indole

(163):

In a glass vial equipped with a stir bar, silyl enol ethers (*E/Z*)-**170** (150 mg, 27.0 mmol) was dissolved in pyridine (3.75 mL). The flask was cooled to 0 °C and HF-pyridine (375 μL) was added dropwise. The reaction mixture was warmed to room temperature over 90 min. The reaction mixture was then diluted with diethyl ether (10 mL) and carefully quenched with sat. NaHCO_3 . The organic layer was removed and the aqueous fraction was extracted further with diethyl ether (2 x 10 mL). The combined organic fractions were dried with MgSO_4 , filtered, and concentrated *in vacuo*. The crude mixture was purified by silica gel flash chromatography (hexanes/diethyl ether, 8/2 \rightarrow 1/1) to give **163** as a white, crystalline solid (mp 158–160 °C) in 70 % yield over two steps from **164** (+18, c 2.0 mg/mL): IR (thin film, CH_2Cl_2 , NaCl , cm^{-1}) 1708, 1454; ^1H NMR (300 MHz, CDCl_3) δ 1.37 (s, 3 H), 3.07 (qd, $J = 18.2, 1.1$ Hz, 2 H), 3.61 (s, 3 H), 7.14 (d, $J = 1.9$ Hz, 1 H), 7.37 (d, $J = 1.9$ Hz, 1 H), 9.51 (d, $J = 1.1$ Hz, 1 H); ^{13}C NMR (75 MHz, CDCl_3) δ 24.4, 29.7, 44.5, 50.8, 114.8, 116.4, 123.9, 132.6, 137.3, 138.7, 179.3, 197.6;

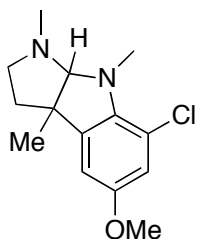
HRMS (EI) calcd for C₁₂H₁₁NO₂ClBr 314.9668, found 314.9661; LRMS (EI) *m/z* 317 (M⁺[Br⁸¹], 4), 315 (4), 253 (30), 186 (28), 57 (100).



6.5.17. (3a*S*-cis)-5-Bromo-7-chloro-1,3a,8-trimethyl-1,2,3,3a,8,8a-hexahydro-pyrrolo[2,3-b]indole (*S*-cis-171):

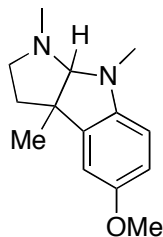
A dry flask equipped with a stir bar was charged with MgSO₄ (26 mg), capped with a septum, and backfilled with Ar.^{61a} Enriched aldehyde (12 mg, 38 μmol) dissolved in THF (925 μL) and methylamine (23 μL, 2.0 M in THF) were added to the flask via syringe. After triethylamine (5.3 μL, 38 μmol) was added the reaction mixture was stirred at room temperature for 20 h. The flask was uncapped and lithium aluminum hydride (2 mg, 57 μmol) was added slowly. A water-cooled reflux condenser was attached to the flask and the reaction mixture was refluxed for 3 h. When the reaction mixture had cooled to room temperature a 1/1 mixture of ethyl acetate/sat. NaHCO₃ was carefully added to quench remaining reagent. The biphasic mixture was extracted with ethyl acetate (3 X, 5 mL). The combined organic fractions were dried with MgSO₄, filtered, and concentrated *in vacuo*. The crude material was purified by silica gel flash chromatography (hexanes/ethyl acetate, 1/1 → 1/4) to give 5.1 mg of a ~1/1 mixture (as determined by GC) of the title compound and debromo by-product. The mixture was dissolved in acetonitrile (500 μL) and *N*-bromosuccinimide (1.9 mg, 10.8 μmol) was added. After 1 h the solvents were removed *in vacuo*. The reddish crude material was purified by semi-preparative HPLC (Nova-Pak silica, 7.8 x 300 mm, hexanes/ethyl acetate 8/2) to give **171** as a white solid in 43 % yield (-16, *c* 5.0

mg/mL): ^1H NMR (300 MHz, CDCl_3) δ 1.43 (s, 3 H), 1.92–1.97 (m, 3 H), 2.53 (s, 3 H), 2.54–2.62 (m, 1 H), 2.65–2.74 (m, 1 H), 2.78 (s, 3 H), 3.19 (s, 3 H), 4.01 (s, 1 H), 6.97 (d, $J = 1.9$ Hz, 1 H), 7.17 (d, $J = 1.9$ Hz, 1 H).



6.5.18. (*rac-cis*)-7-Chloro-5-methoxy-1,3a,8-trimethyl-1,2,3,3a,8,8a-hexahydro-pyrrolo[2,3-b]indole (not shown in text):

In a dry tube equipped with a stir bar was added absolute MeOH (150 μL). Na metal (12 mg, 0.53 mmol) was carefully added. When the metal was consumed, *rac*-**171** (16.7 mg, 52.9 μmol) that was dissolved in DMF (600 μL) was added to the methoxide solution. Cu(I)I (40.2 mg, 0.21 mmol) was introduced, the flask was sealed and heated to 120 $^\circ\text{C}$ for 3 h. After cooling to room temperature, the reaction mixture was passed through a celite plug to remove insoluble salts. Brine (1 mL) was added to the filtrate and the resulting solution was extracted with diethyl ether (3 x 3 mL). The combined organic fractions were concentrated *in vacuo*. The resulting crude oil was purified by silica gel flash chromatography (hexanes/ethyl acetate, 2/8) to give a yellow oil in 65 % yield: ^1H NMR (300 MHz, CDCl_3) δ 1.44 (s, 3 H), 1.88–1.96 (m, 2 H), 2.52 (s, 3 H), 2.50–2.68 (m, 2 H), 3.11 (s, 3 H), 3.74 (s, 3 H), 3.99 (s, 1 H), 6.54 (d, $J = 2.4$ Hz, 1 H), 6.68 (d, $J = 2.4$ Hz, 1 H).



6.5.19. *rac*-esermethole (*rac*-162):

A flask equipped with a stir bar was charged with sodium formate (22.8 mg, 0.34 mmol), 10 % Pd/C (60 mg), and (*rac-cis*)-7-chloro-5-methoxy-1,3a,8-trimethyl-1,2,3,3a,8,8a-hexahydro-pyrrolo[2,3-b]indole (4.5 mg, 17 μ mol). Water (1.5 mL) was added and the reaction stirred for 24 h. After filtration through a plug of cotton, the filtrate was extracted with diethyl ether (3 x 3 mL). The combined organic fractions were concentrated *in vacuo* to give a yellow crude solid: ^1H NMR (300 MHz, CDCl_3) δ 1.44 (s, 3 H), 1.94 (dd, $J = 7.1, 5.5$ Hz, 2 H), 2.54 (s, 3 H), 2.61–2.75 (m, 2 H), 2.96 (s, 3 H), 3.76 (s, 3 H), 4.06 (s, 1 H), 6.36 (d, $J = 8.0$ Hz, 1 H), 6.62–6.69 (m, 2 H).

6.6. Resolution of Compounds by Chiral HPLC

Listed below are typical sets of conditions for analytical and semi-preparative methods.

6.6.1. Analytical method

Column: Regis Technologies, Inc. (*S,S*)-Whelk-O 1; 25 cm x 4.6 mm I.D.

Solvent: 10 % isopropanol in hexanes

Flow: 1 ml/min (uncyclized substrates), 2 mL/min (cyclized products)

Sample concentration: 3–5 mg/mL

Injection volume: 10 μ L

6.6.2. Semi-preparative method

Column: Regis Technologies, Inc. (*S,S*)-Whelk-O 1; 25 cm x 10.0 mm I.D.

Solvent: 10–40 % isopropanol in hexanes

Flow: 8–10 mL/min

Sample concentration: 40–80 mg/mL

Injection volume: 1 μ L

6.7. Measurement of N-Aryl Bond Rotation Barriers

6.7.1. General Procedure for N-Aryl Bond Rotation Barrier Measurement

Enantiomerically enriched anilide is dissolved in a 10 % solution of iPrOH in hexanes (10 mg/mL) in a sealable tube. The tube is sealed and equilibrated to the given temperature. At given interval of time an aliquot of 100 μ L is removed via syringe and injected into the HPLC to measure the ee. The ratio of enantiomers is plotted against time and the barrier to rotation is calculated according to the method described in Eliel.⁸³ As an example, a full treatment of data is shown for anilide **56b**.

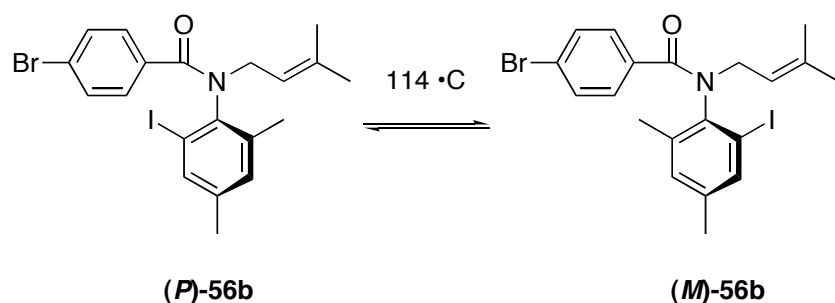


Figure 6.1 – Thermal Equilibration of 56b

56b		T = 387 K
Time (mins)	% ee	
0	96	
7	96	
36	92	
68	70	
104	61	
131	55	
161	49	
196	41	
267	32	

Table 6-1 – Thermal Equilibration Data for 56b

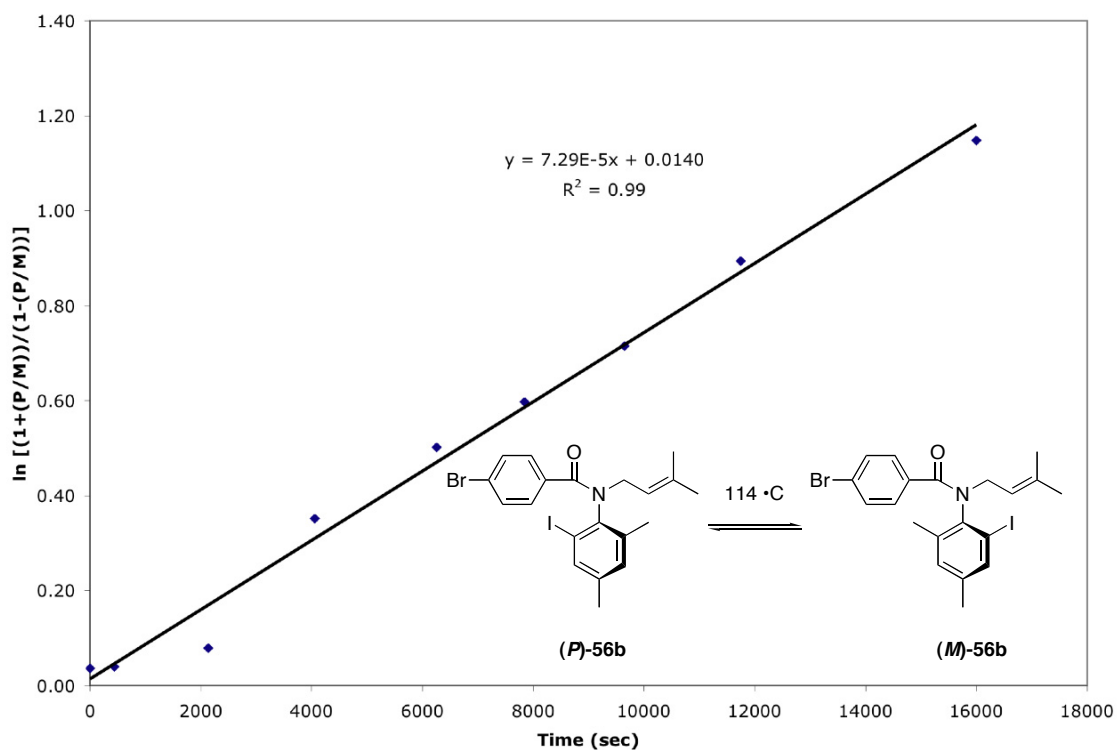


Figure 6.2 – Thermal Equilibration Plot for 56b

(M)-56b		T = 387 K
Time (min)	% ee	
0	96	
36	92	
68	70	
104	61	
131	55	
161	49	
196	41	
267	32	

Table 6-2 – Thermal Equilibration Data for (M)-56b

Equation		Plot
$\ln \left[\frac{1 + [P-56b]/[M-56b]}{1 - [P-56b]/[M-56b]} \right] = 2kt + c$		$\ln \left[\frac{1 + [P-56b]/[M-56b]}{1 - [P-56b]/[M-56b]} \right] \text{ vs Time (seconds)}$
		<p>where slope = k_{rac} or $2k_{rot}$</p>

$$2k_{rac} = 7.29 \times 10^{-5} \text{ s}^{-1}$$

$$k_{rot} = \text{slope}/2 = (7.29 \times 10^{-5} \text{ s}^{-1})/2 = 3.65 \times 10^{-5} \text{ s}^{-1}$$

$$K_{rot}^{\ddagger} = k_{rac}h / kT = \frac{(3.65 \times 10^{-5} \text{ s}^{-1}) (6.626 \times 10^{-34} \text{ Js})}{(1.381 \times 10^{-23} \text{ J/K}) (387 \text{ K})}$$

$$K_{rot}^{\ddagger} = 4.52 \times 10^{-18} \text{ substitute into } \Delta G^{\ddagger} = -RT \ln K^{\ddagger}$$

$$\Delta G_{rot}^{\ddagger} = 128.314 \text{ kJ/mol or } 30.7 \text{ kcal/mol}$$

Equation 6-1 - Calculation of N-Aryl Bond Rotation Barrier of (M)-56b

(M)-56a		T = 387 K
Time (min)	% ee	
0	99	
17	86	
37	66	
68	48	
120	26	

Table 6-3 – Thermal Equilibration Data for (M)-56a

$$\Delta G_{rot} = 124.3 \text{ kJ/mol or } 29.7 \text{ kcal/mol}$$

(M)-56c		T = 413 K
Time (min)	% ee	
0	100	
15	98	
30	93	
46	87	
113	59	
200	32	

Table 6-4 – Thermal Equilibration Data for (M)-56c

$\Delta G_{\text{rot}} = 136.0 \text{ kJ/mol}$ or 32.5 kcal/mol

(M)-56g		T = 413 K
Time (min)	% ee	
0	93	
19	84	
34	80	
57	70	
128	47	

Table 6-5 – Thermal Equilibration Data for (M)-56g

$\Delta G_{\text{rot}} = 136.9 \text{ kJ/mol}$ or 32.7 kcal/mol

(M)-109		T = 296 K
Time (sec)	% ee	
0	91.7	
5820	47.9	
8400	36.7	
11280	26.6	
14100	20.3	

Table 6-6 – Thermal Equilibration Data for (M)-109

$\Delta G_{\text{rot}} = 96.7 \text{ kJ/mol}$ or 23.1 kcal/mol

<i>(P)</i> -112		T = 296 K
Time (sec)	% ee	
0	83.0	
1740	59.7	
3540	46.6	
4680	38.0	
6240	27.8	

Table 6-7 – Thermal Equilibration Data for *(P)*-112

$\Delta G_{\text{rot}} = 95.5 \text{ kJ/mol}$ or 22.8 kcal/mol

<i>(P)</i> -154a		T = 363 K
Time (sec)	% ee	
0	85.0	
900	49.0	
1380	43.0	
2340	34.0	
3600	18.0	

Table 6-8 – Thermal Equilibration Data for *(P)*-154a

$\Delta G_{\text{rot}} = 115.1 \text{ kJ/mol}$ or 27.5 kcal/mol

FEE-164		T = 353 K
Time (sec)	% ee	
0	92.0	
1020	54.0	
2040	32.0	
3060	26.0	
6360	24.0	

Table 6-9 – Thermal Equilibration Data for FEE-164

$\Delta G_{\text{rot}} = 111.8 \text{ kJ/mol}$ or 26.7 kcal/mol

6.8. Rate Constant Studies

The rate constant of radical cyclization was measured by cyclization of the respective substrates at variable Bu_3SnH concentrations and analyzing aliquots of the finished reaction by analytical

GC, using an internal standard (dibutyl phthalate) to quantify the ratio of cyclized to reduced product. Calculations were performed according to the indirect competition method.⁴⁰

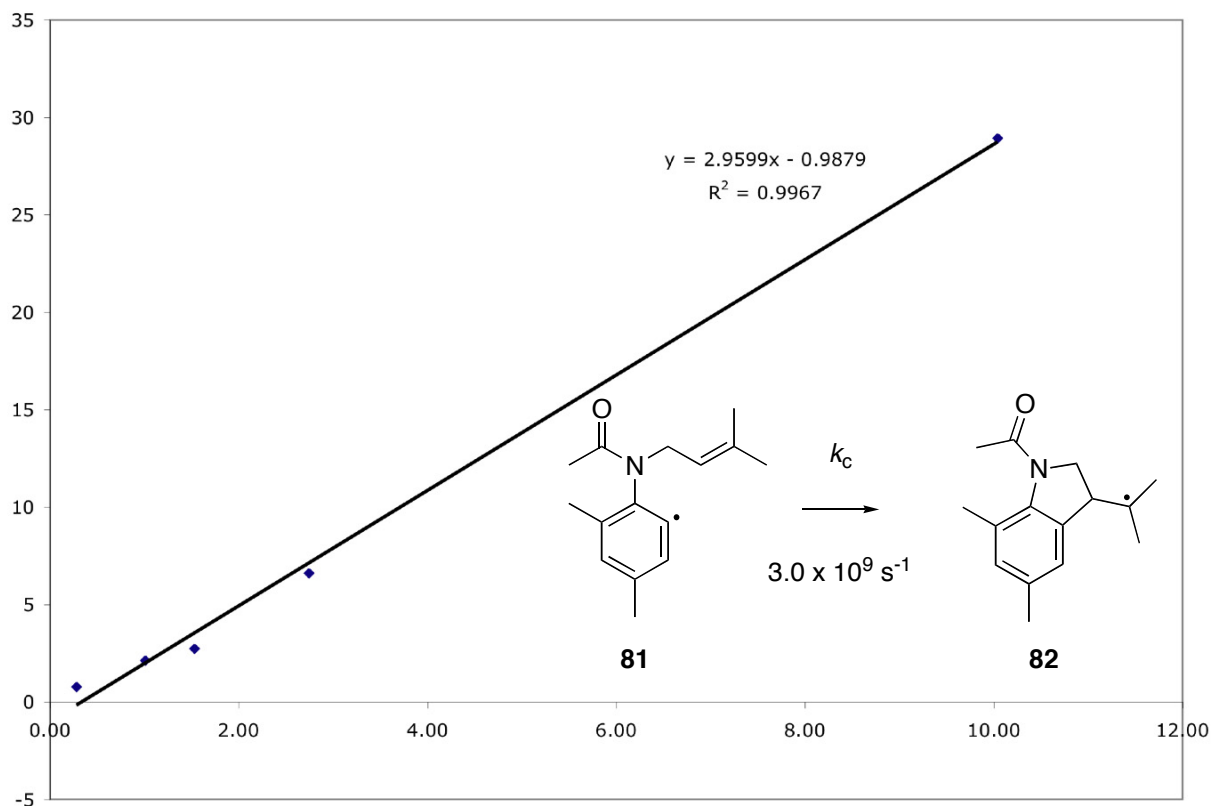


Figure 6.3 - Rate Constant Plot for 81

[Tin] corr (mol / L)	1/[Tin]corr (L / mol)	Area Integration (GC)		C / R
		Cyclized	Reduced	
0.100	10.00	28.95	1.00	28.9
0.364	2.74	6.62	1.00	6.6
0.655	1.53	2.74	1.00	2.7
0.990	1.01	2.04	0.95	2.2
3.565	0.28	0.78	1.00	0.8

Table 6-10 - Rate Constant Data for 81

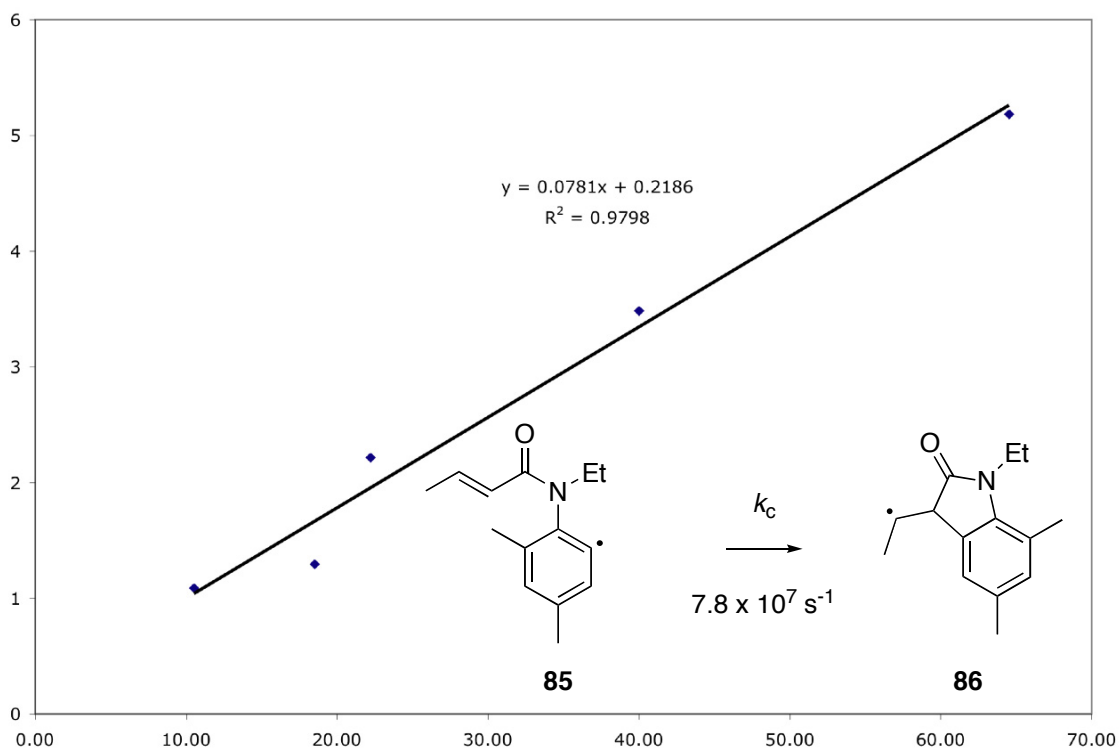


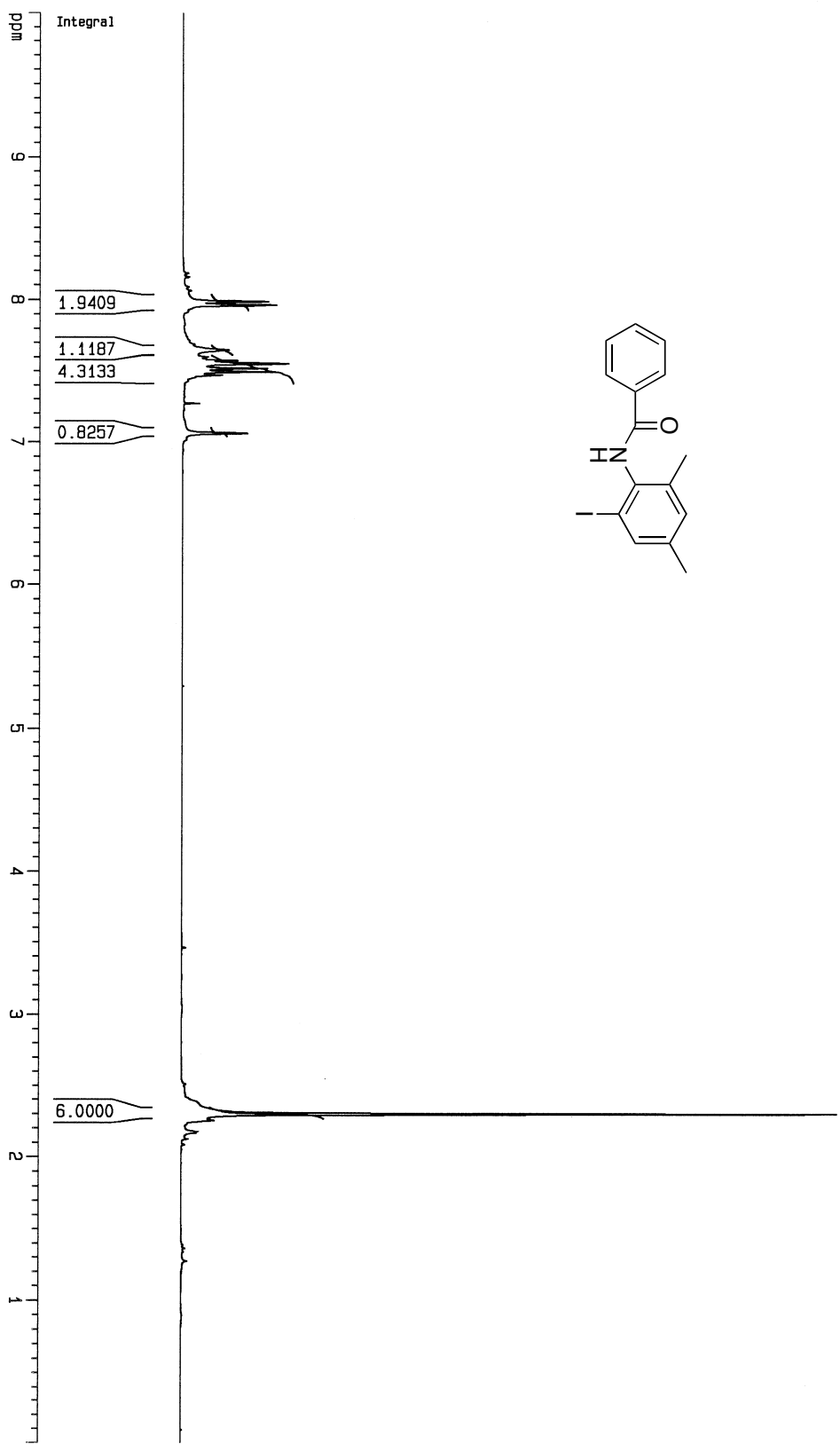
Figure 6.4 - Rate Constant Plot for 85

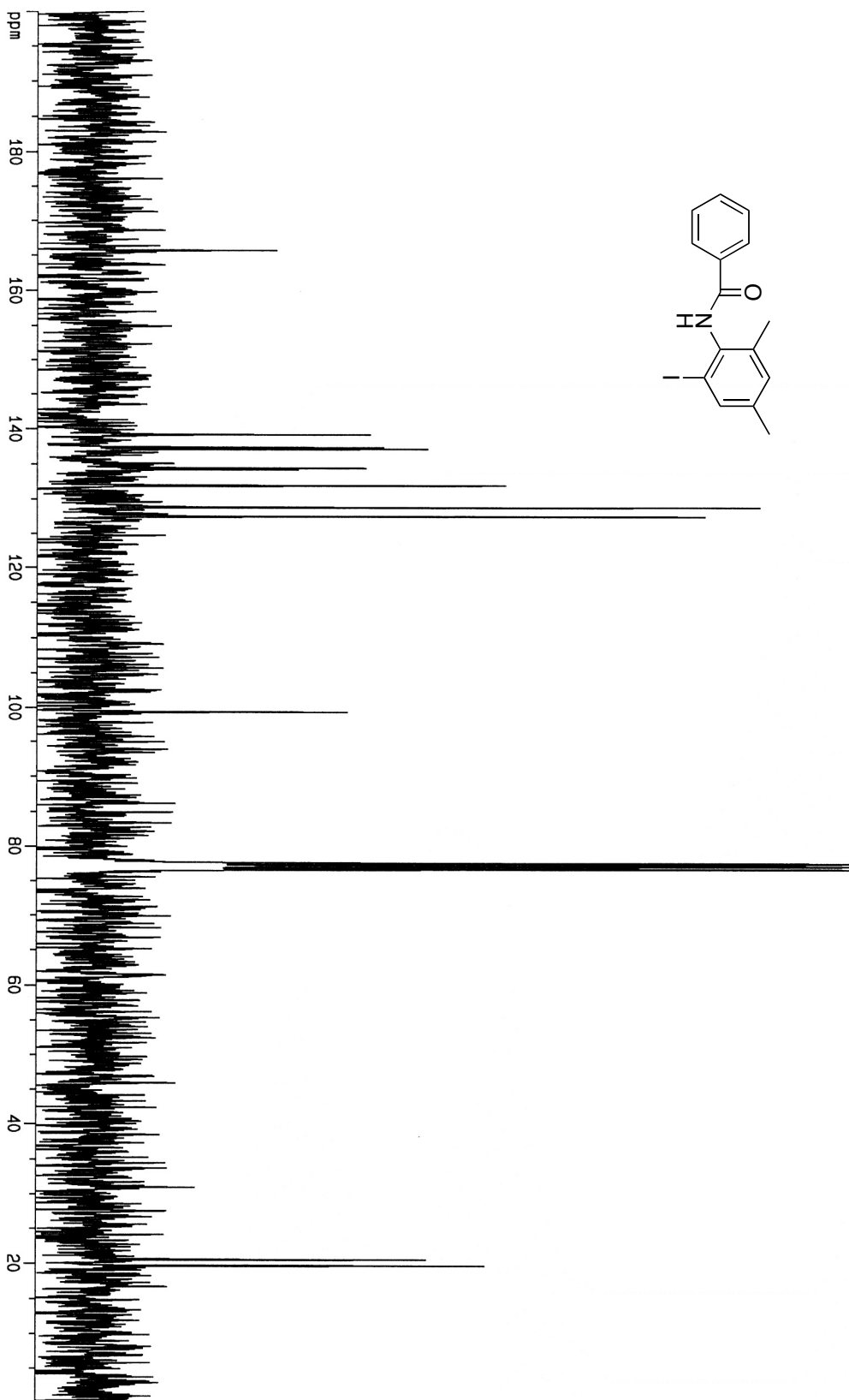
<i>(X-axis)</i>		<i>(Y-axis)</i>		
[Tin] corr (mol / L)	1/[Tin]corr (L / mol)	Area Integration (GC)		C / R
		Cyclized	Reduced	
0.016	64.52	3.00	0.58	5.2
0.025	40.00	3.00	0.86	3.5
0.045	22.22	3.00	1.35	2.2
0.054	18.52	3.00	2.32	1.3
0.095	10.53	3.00	2.75	1.1

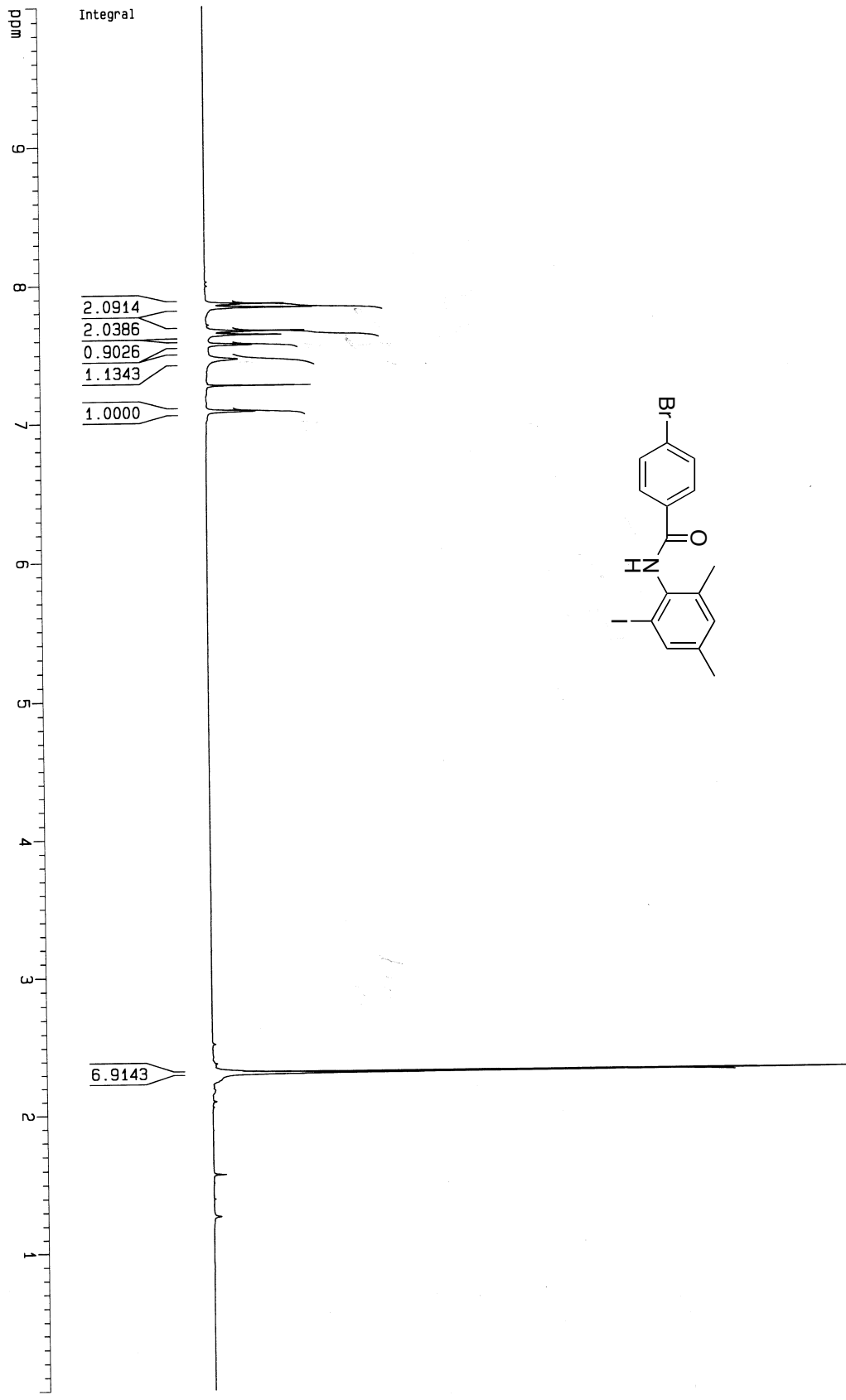
Table 6-11 - Rate Constant Data for 85

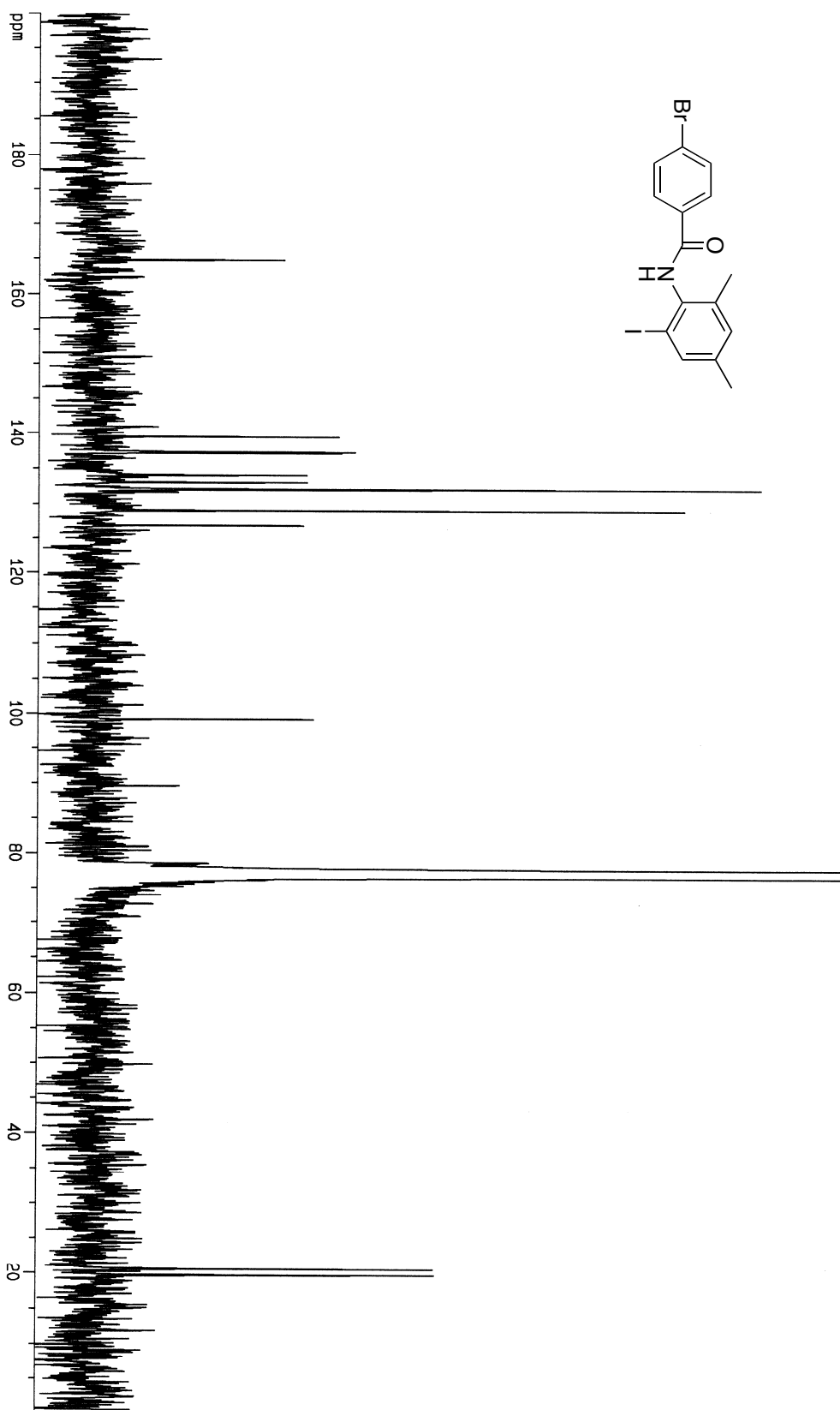
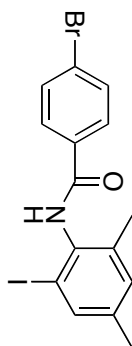
7. SUPPLEMENTARY DATA

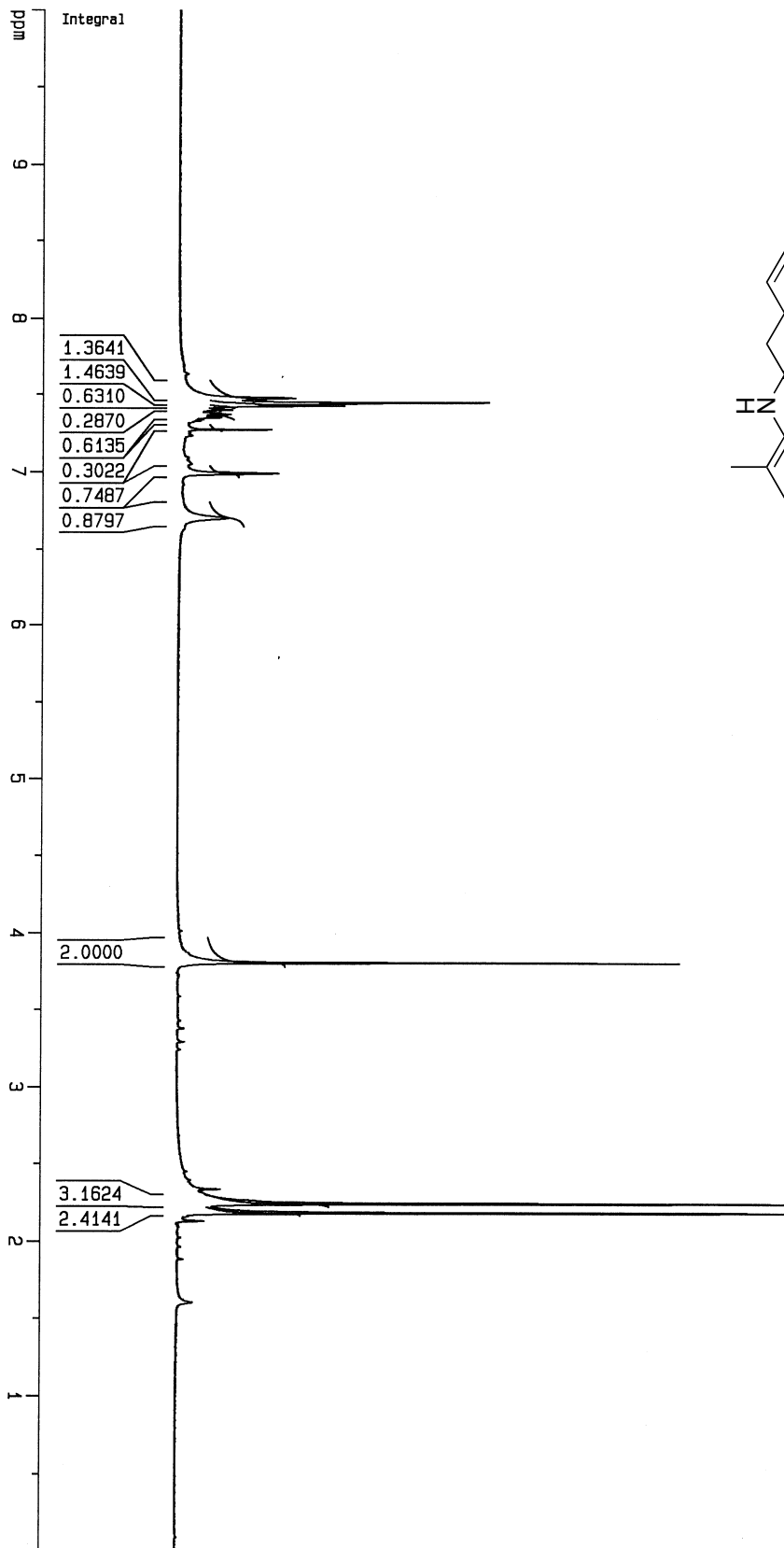
7.1. Select ^1H and ^{13}C NMR

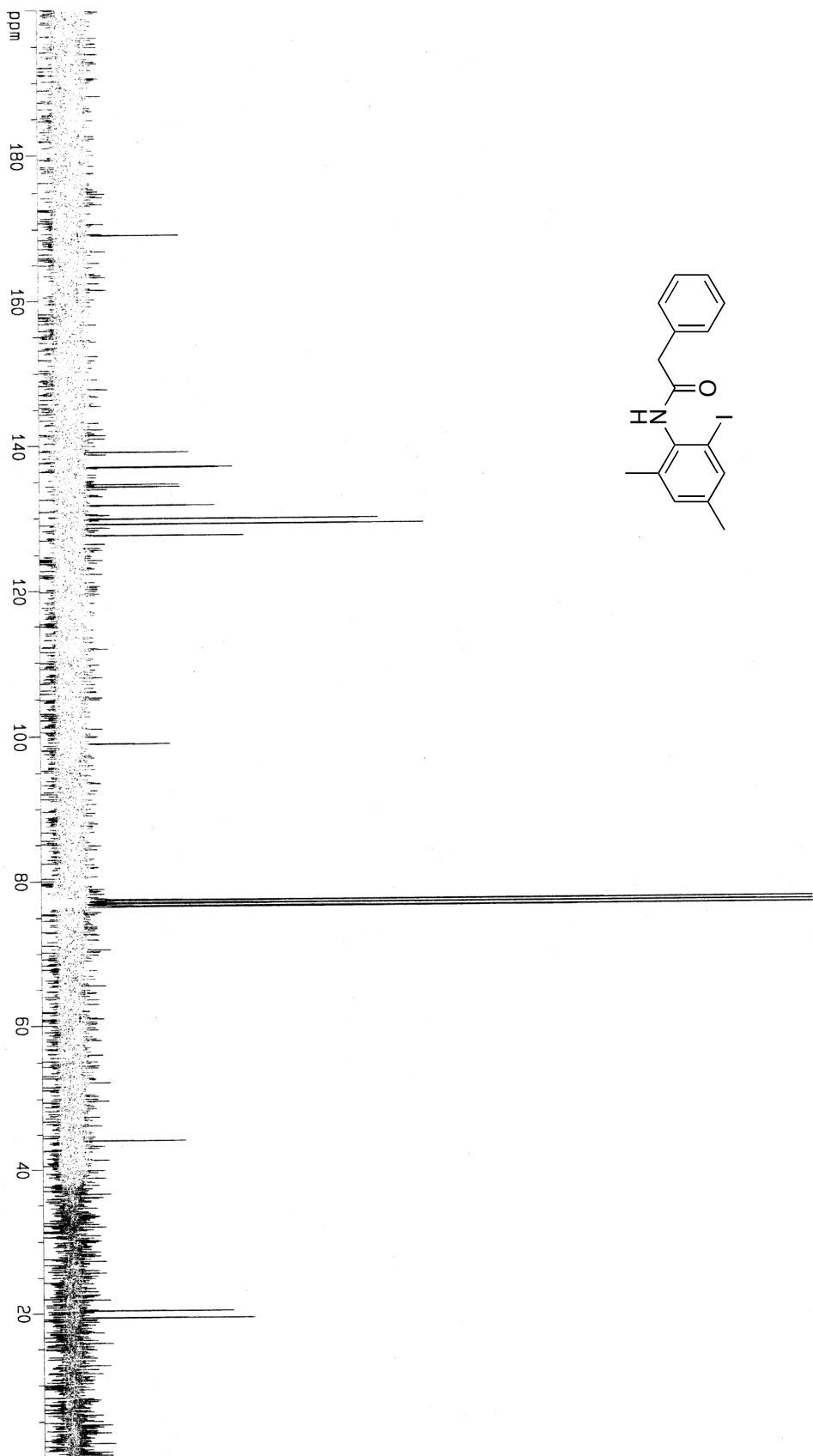
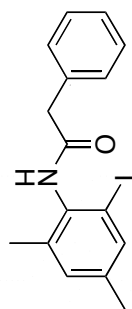


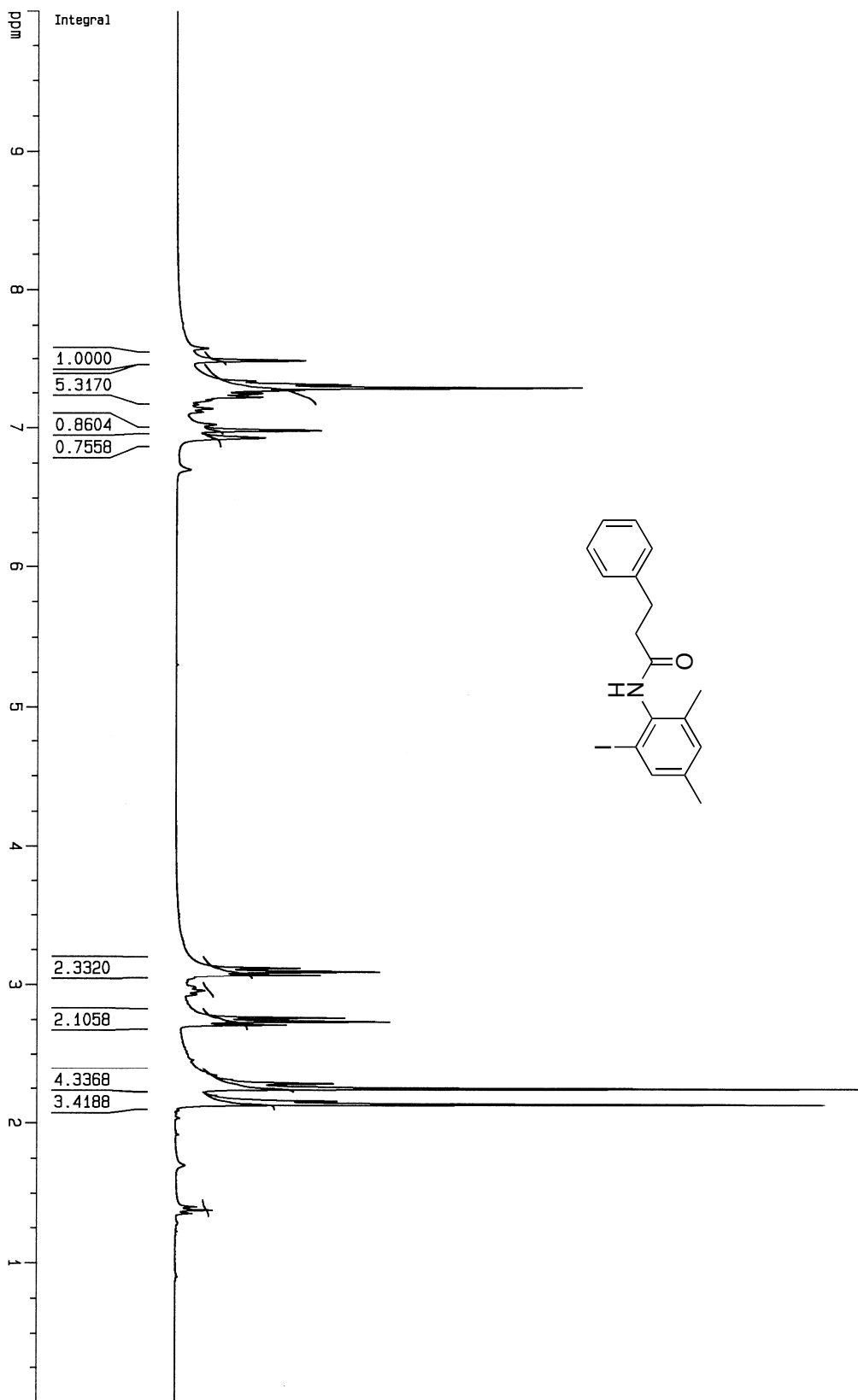


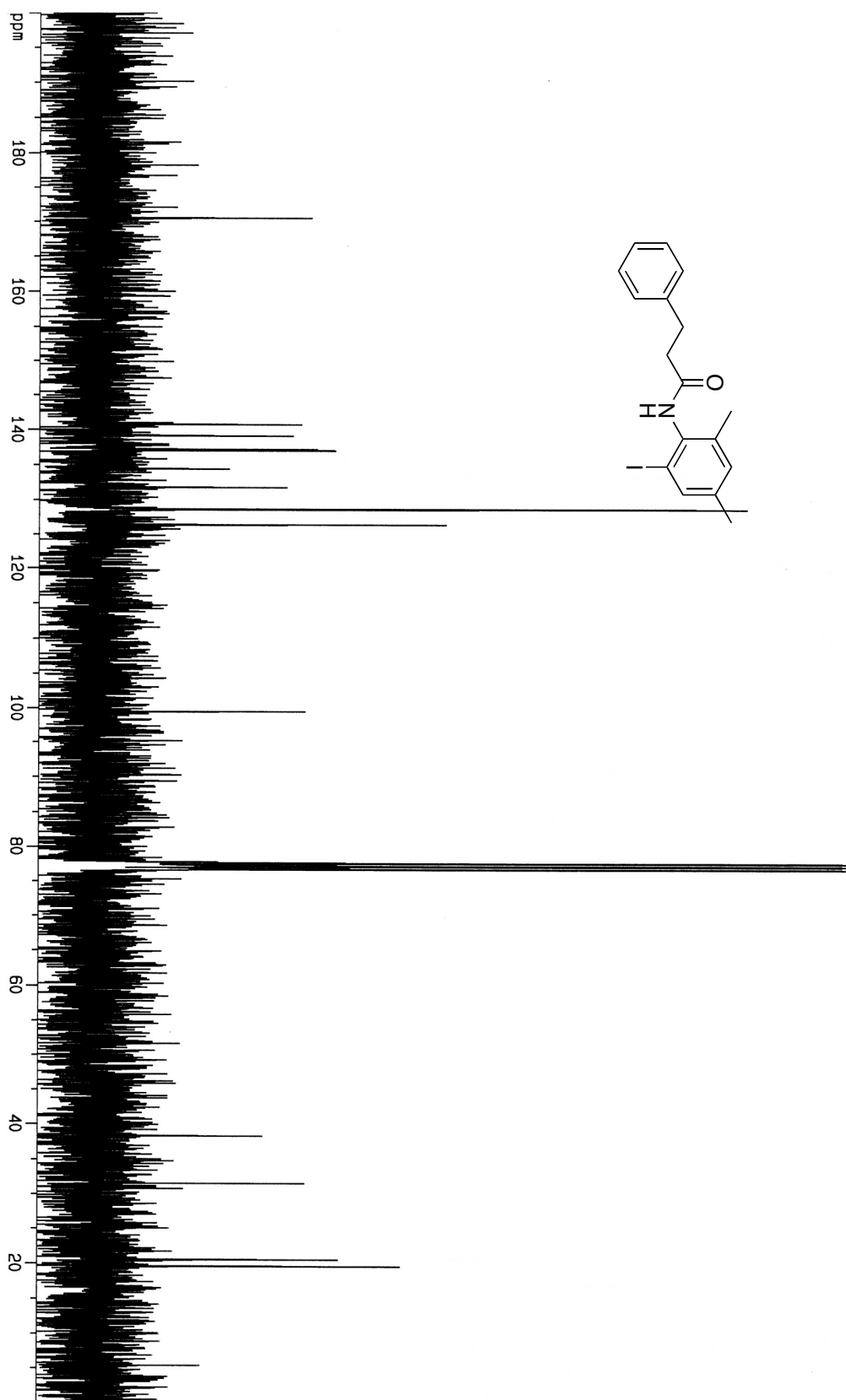


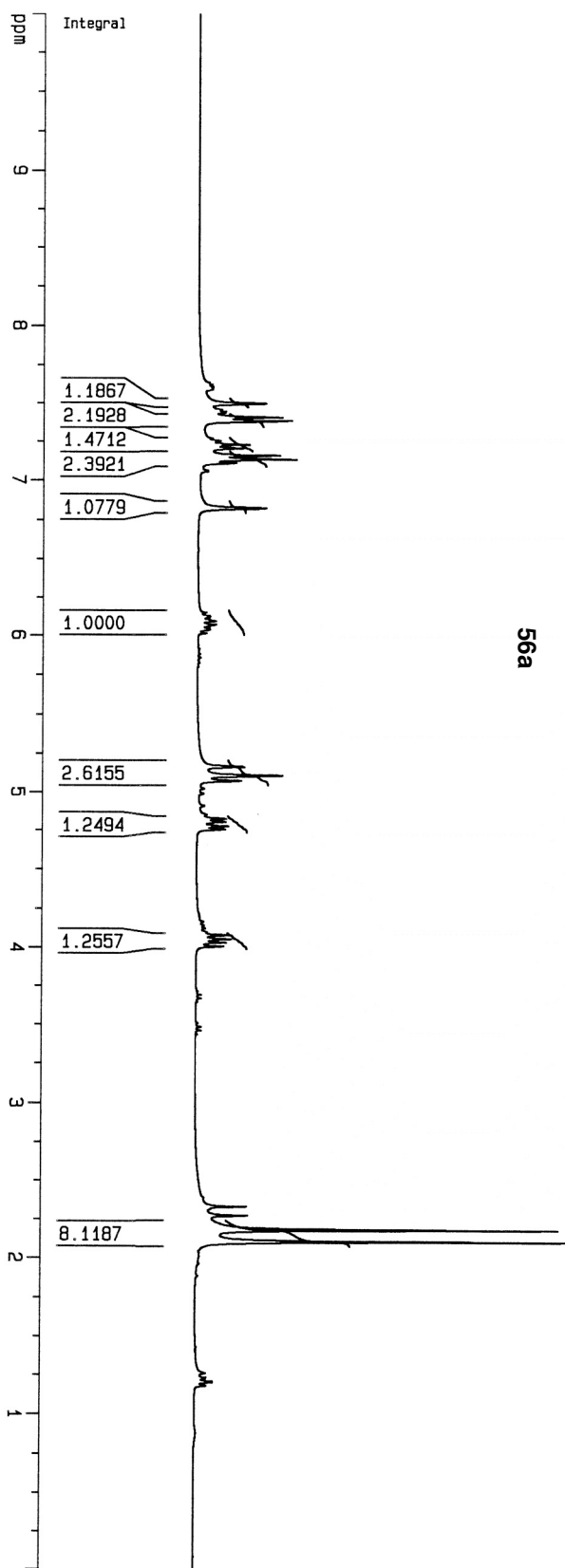




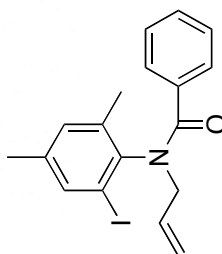


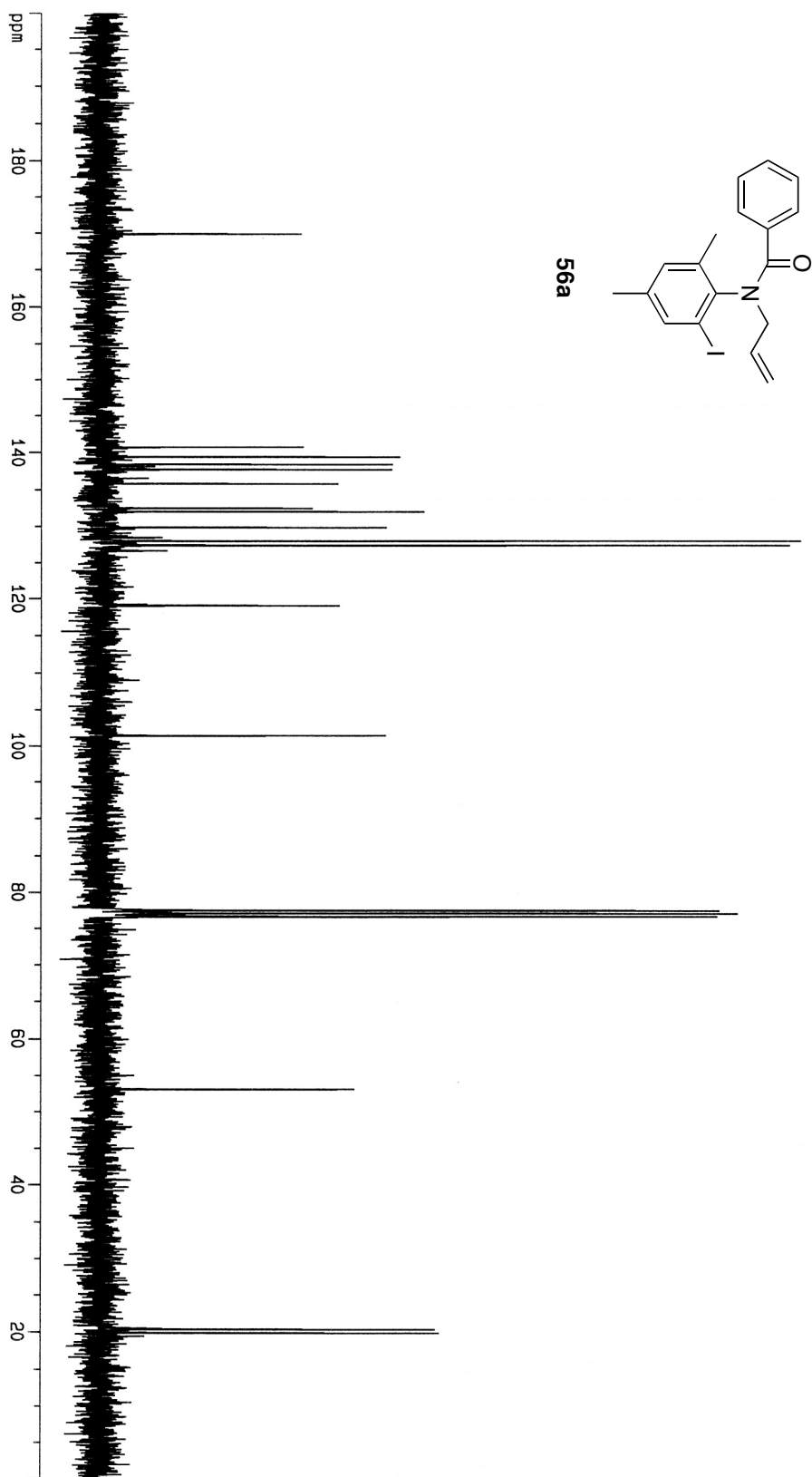


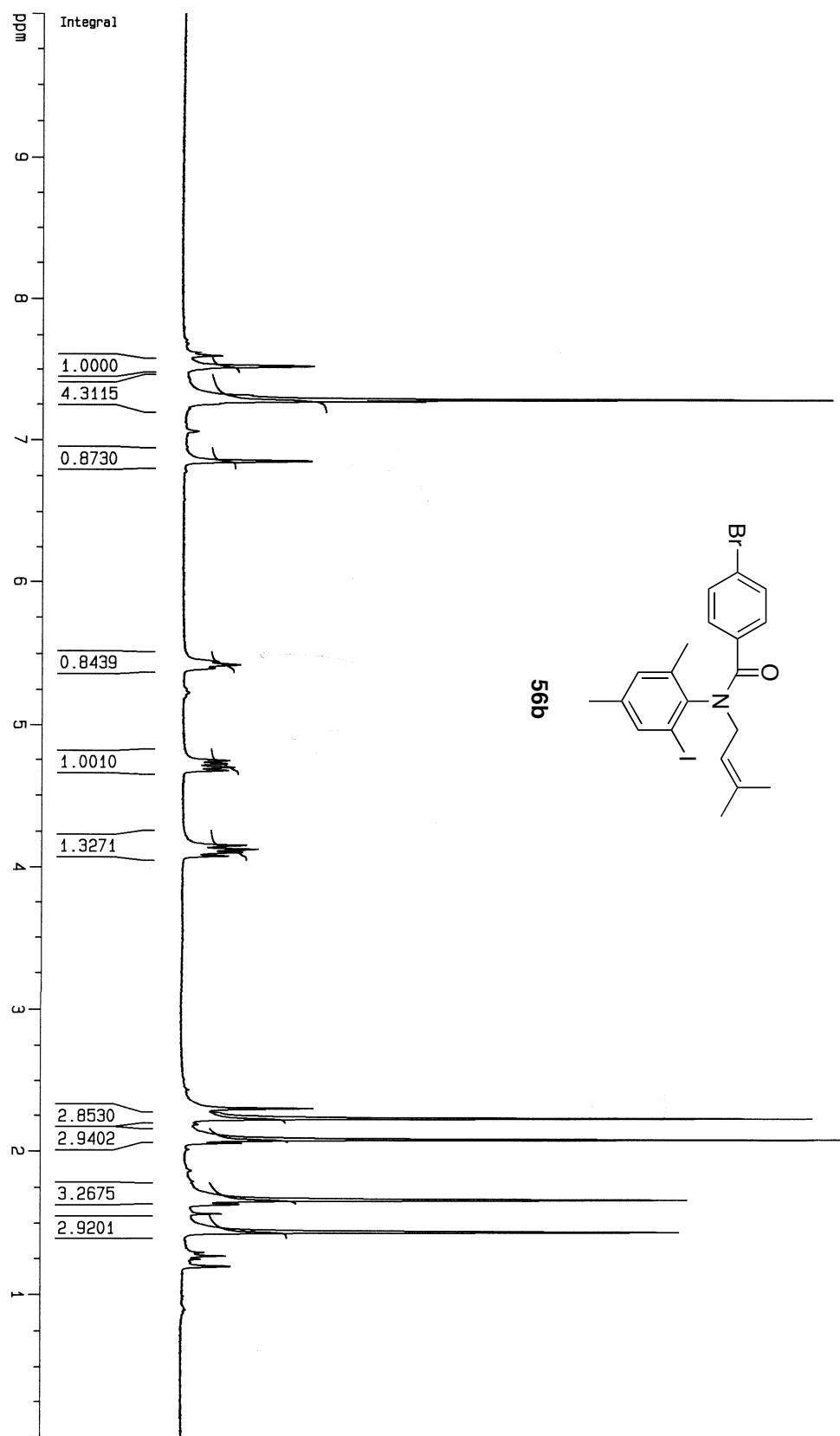


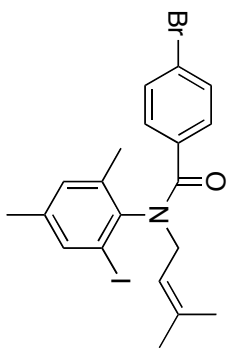


56a

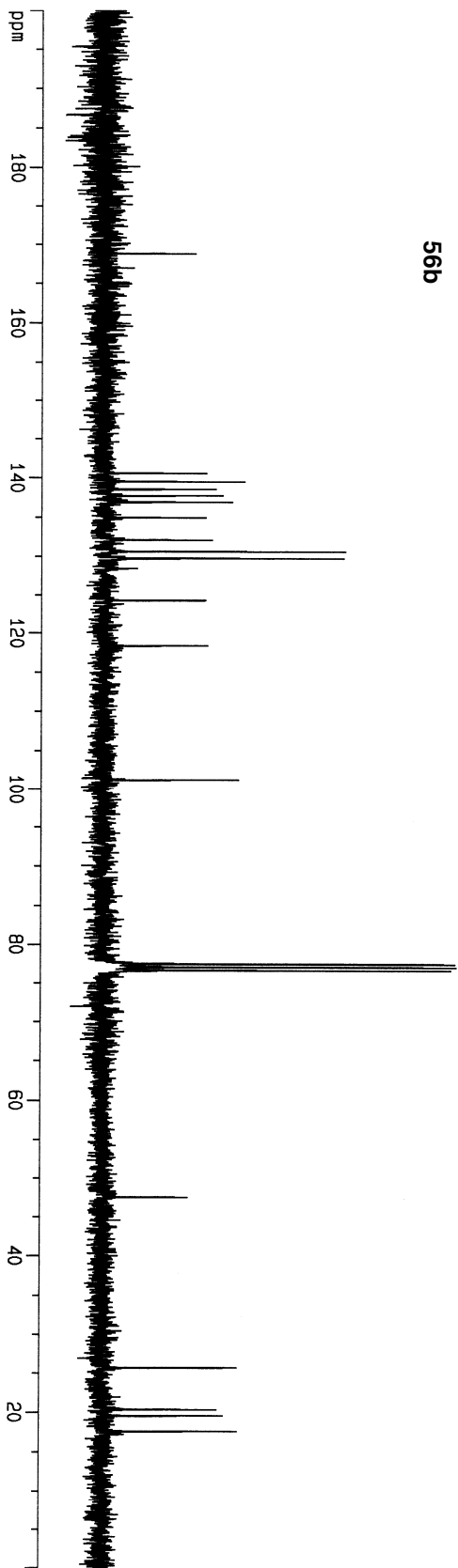


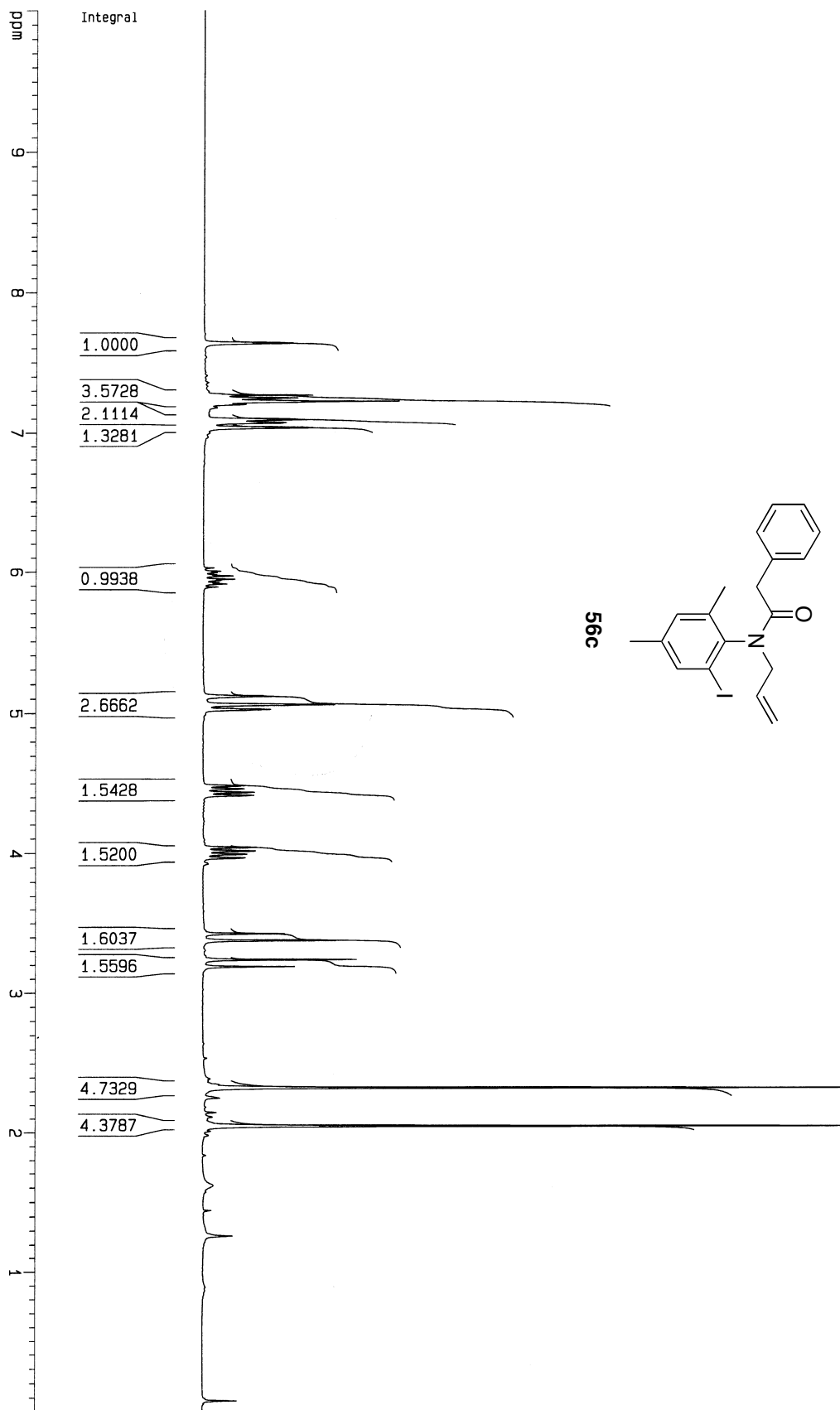


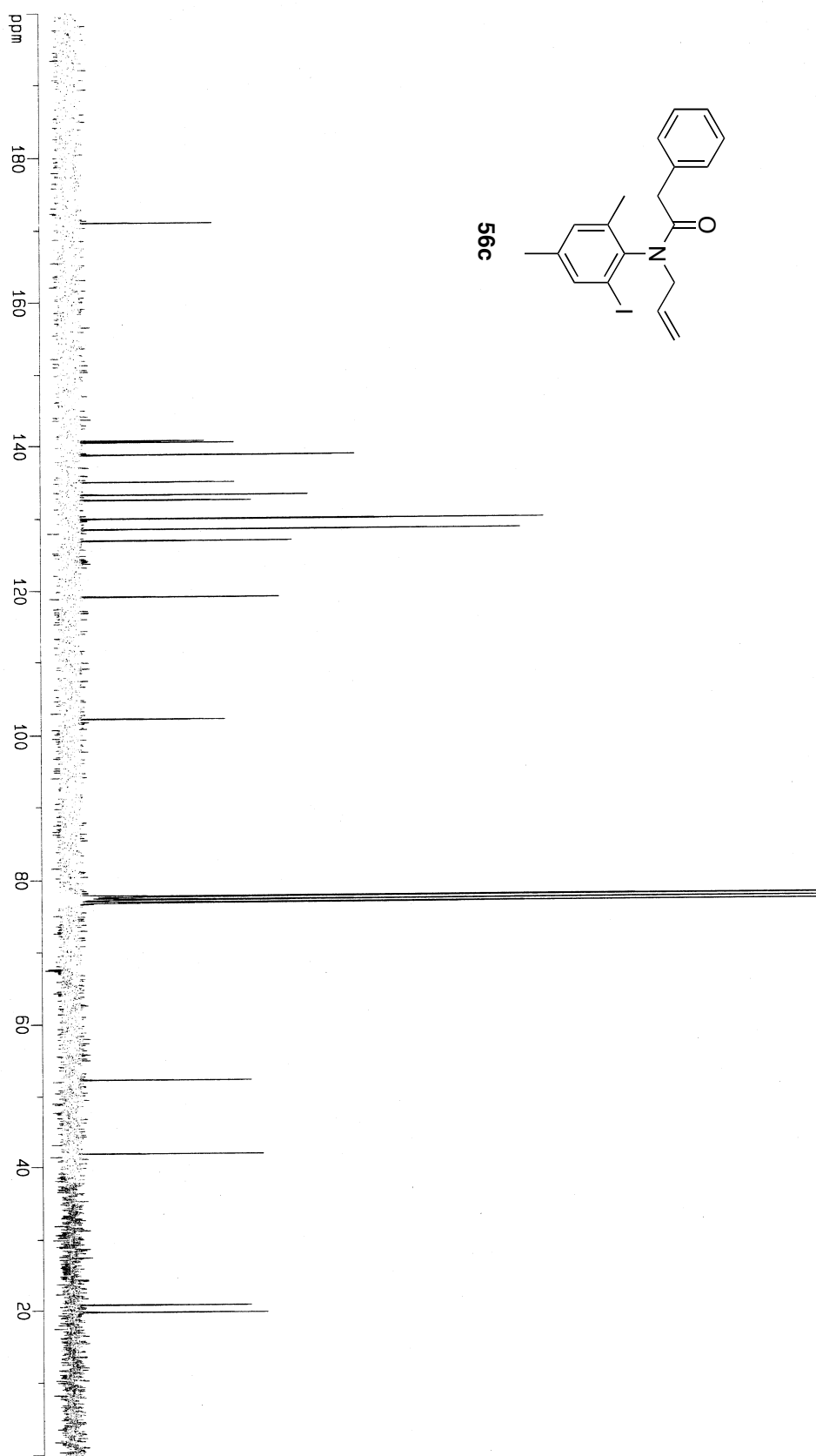




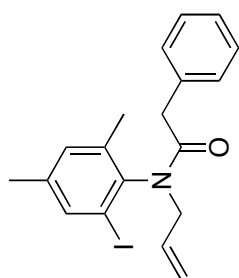
56b

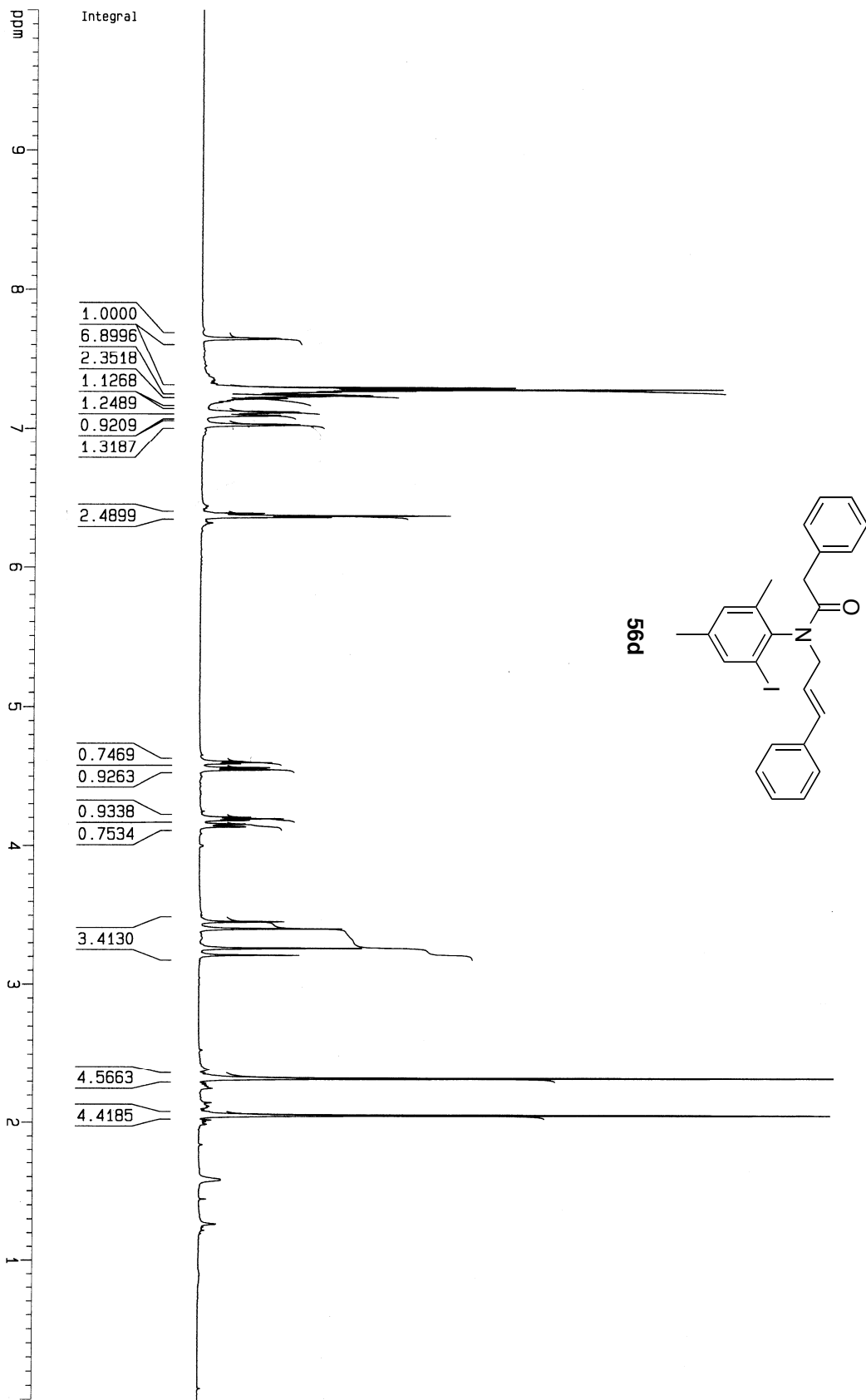


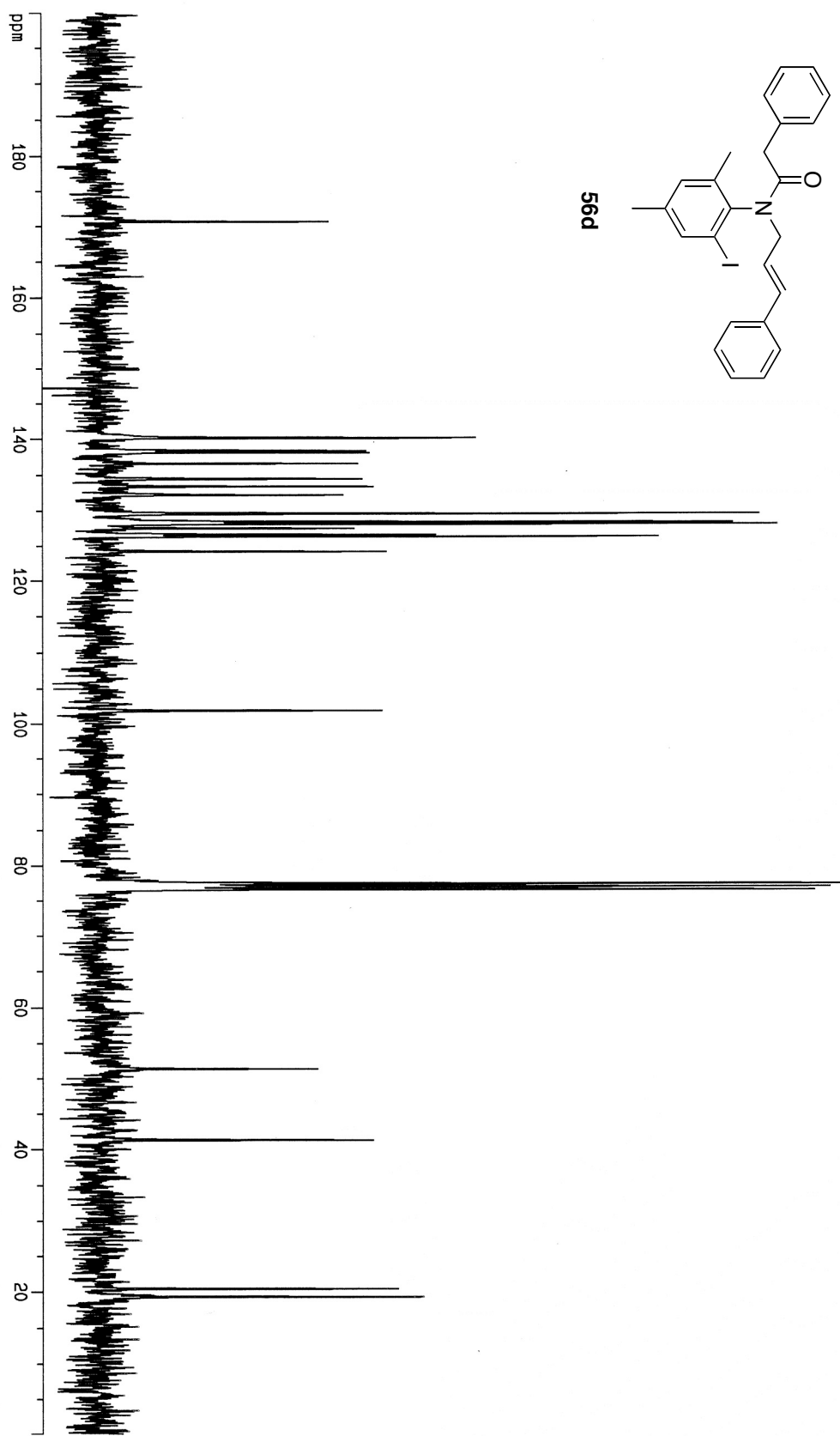


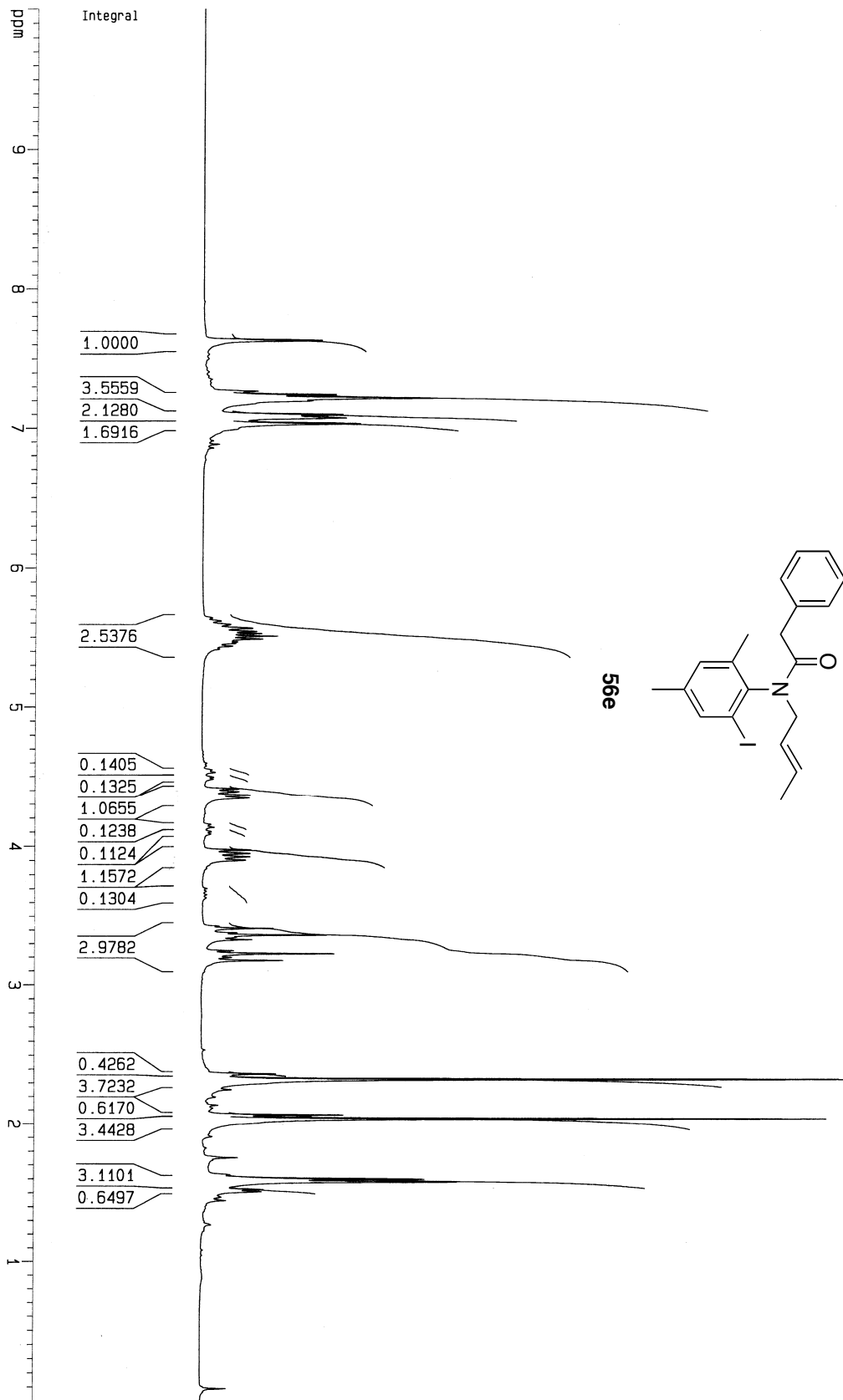


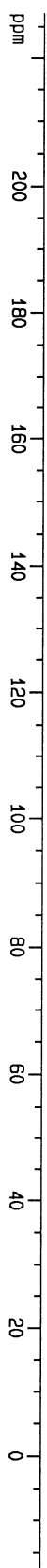
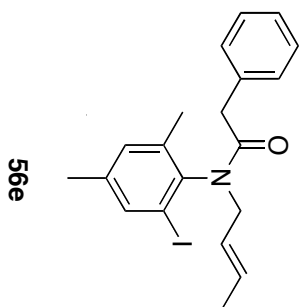
56c



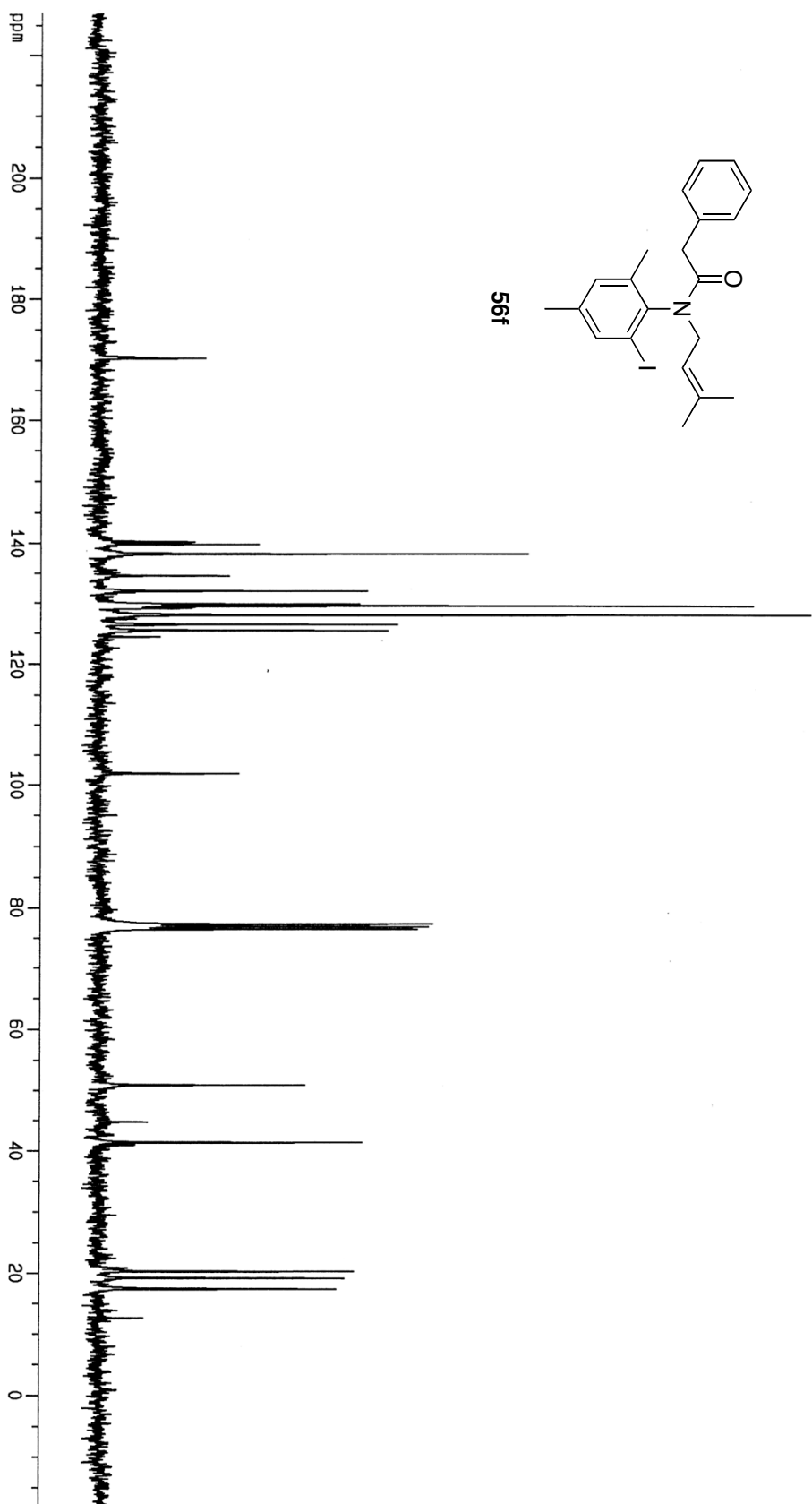


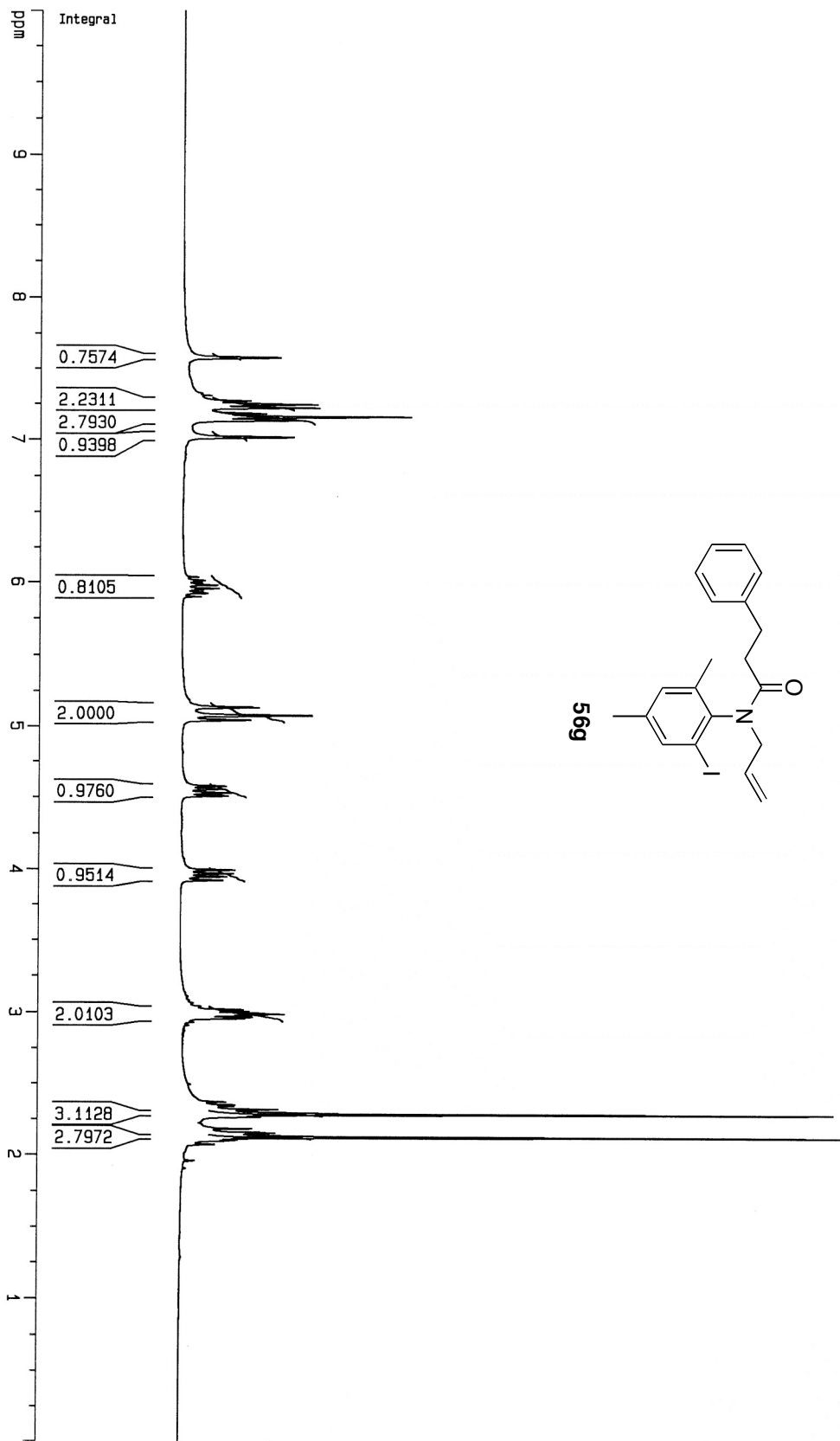


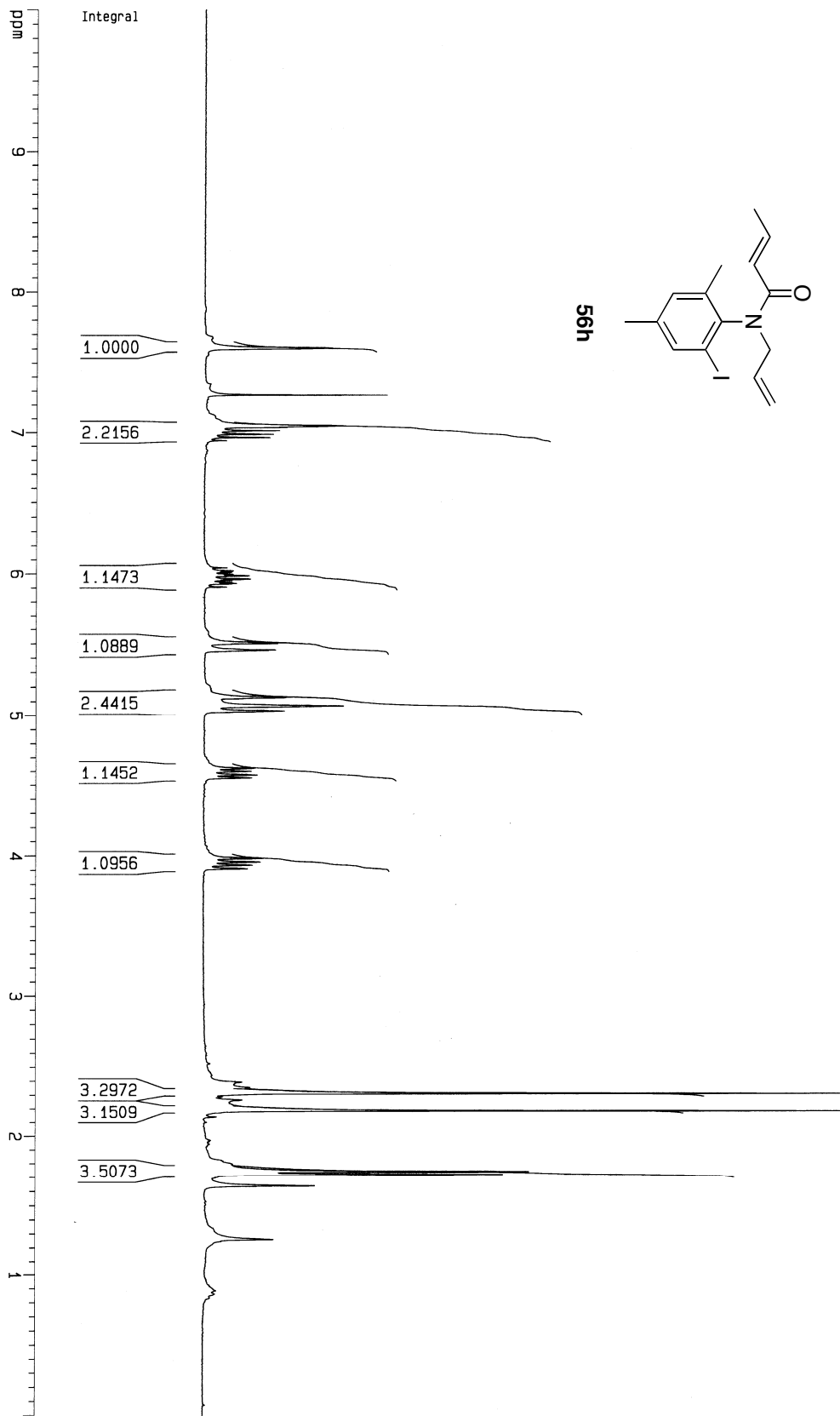


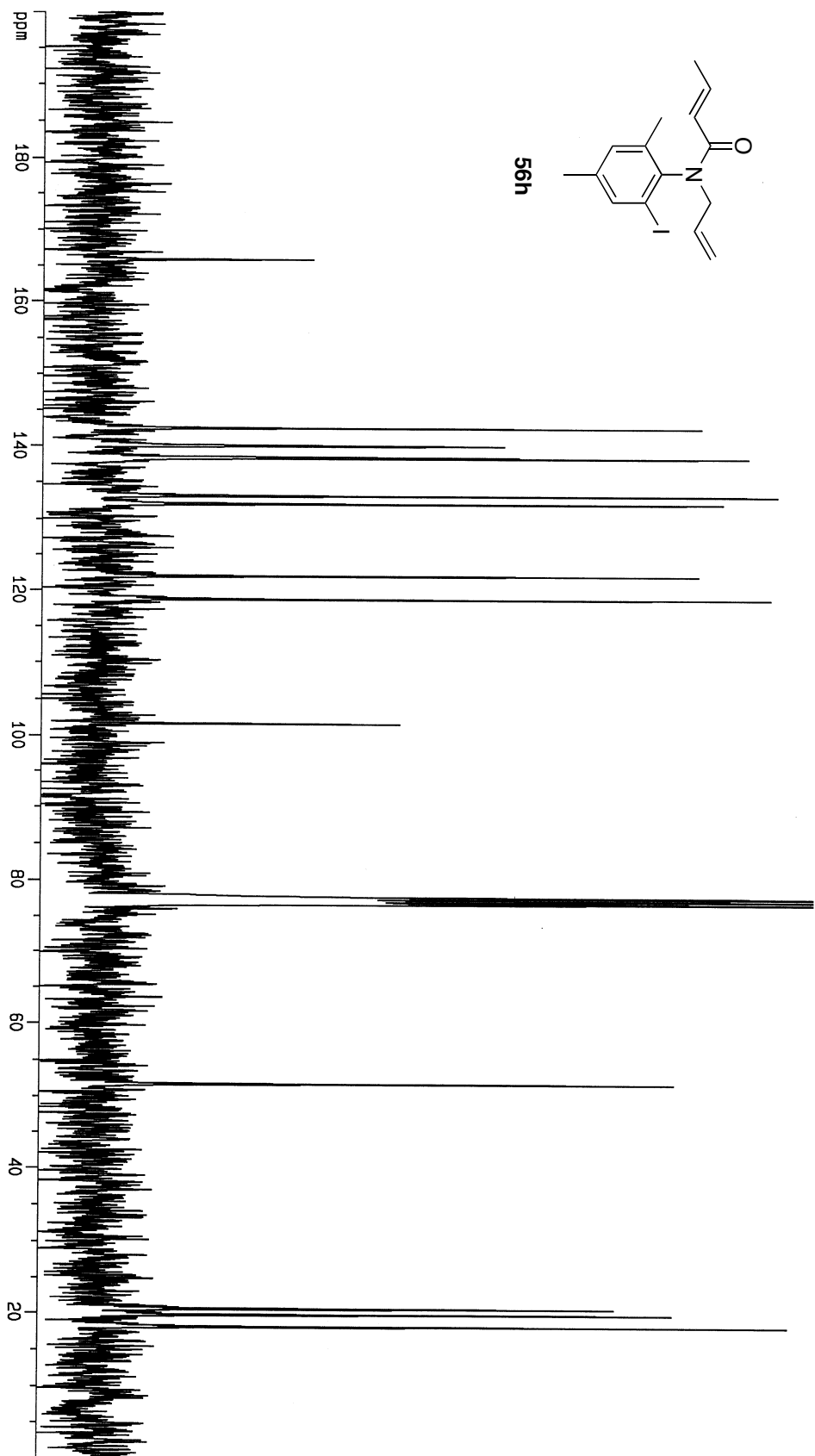


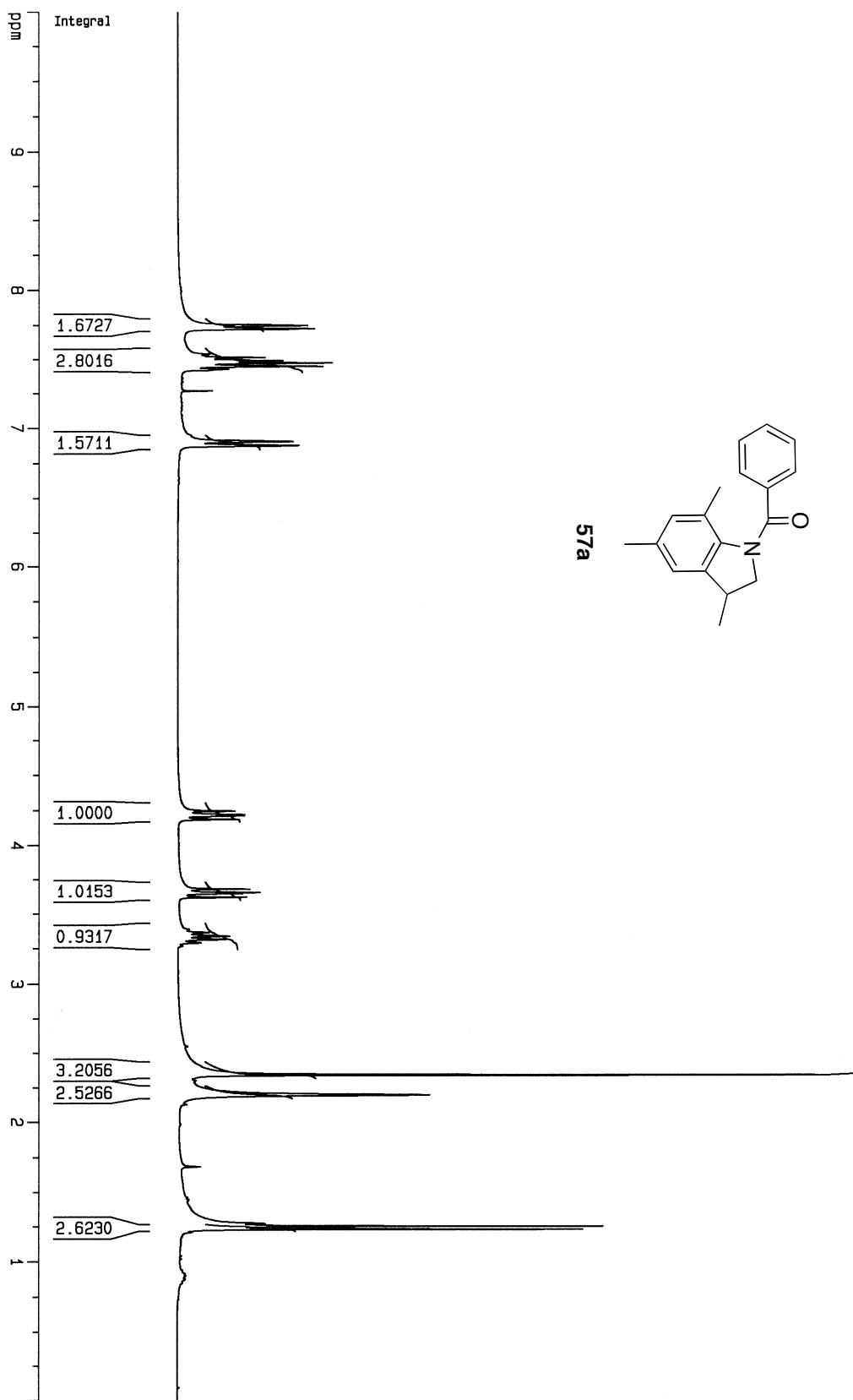


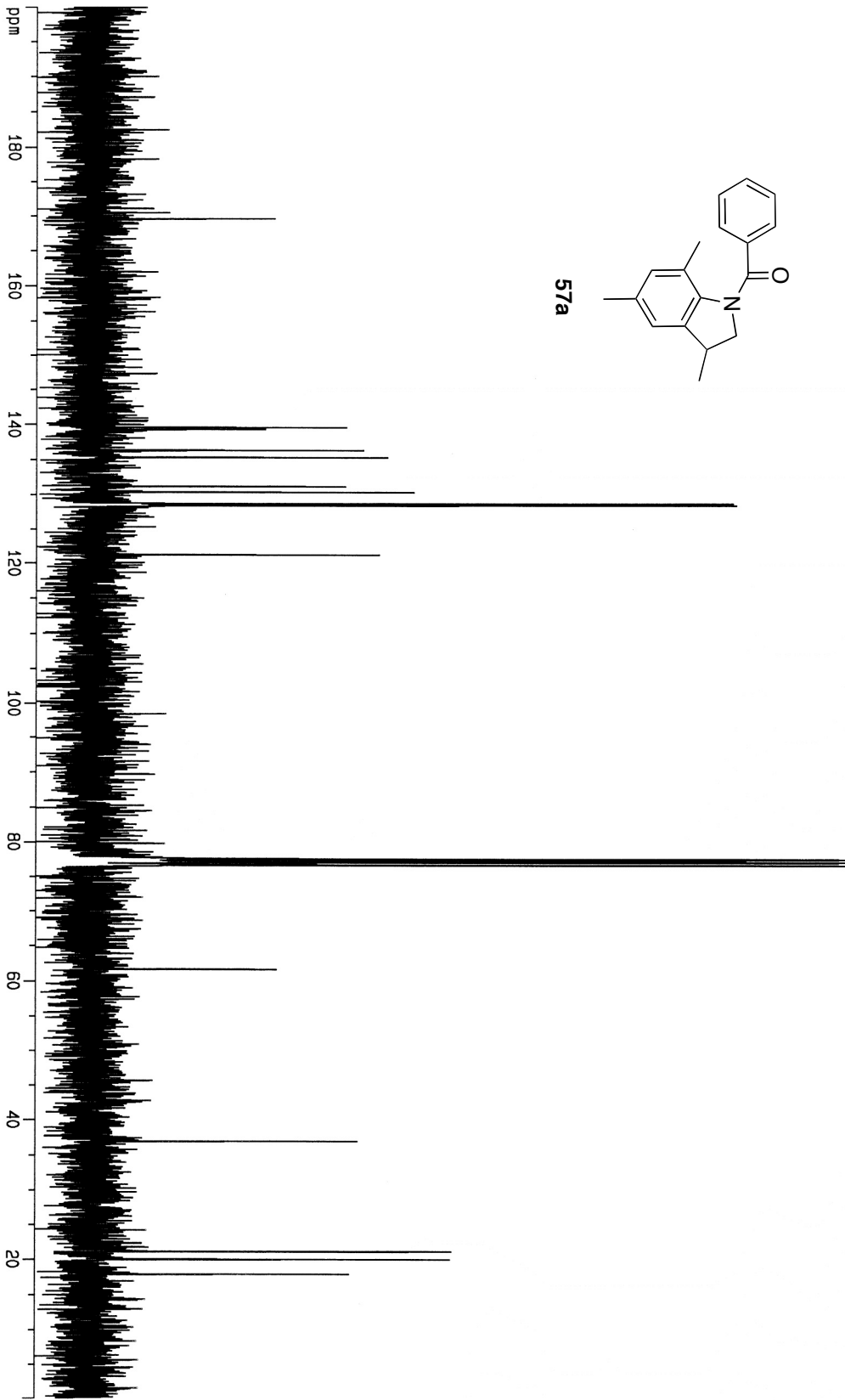


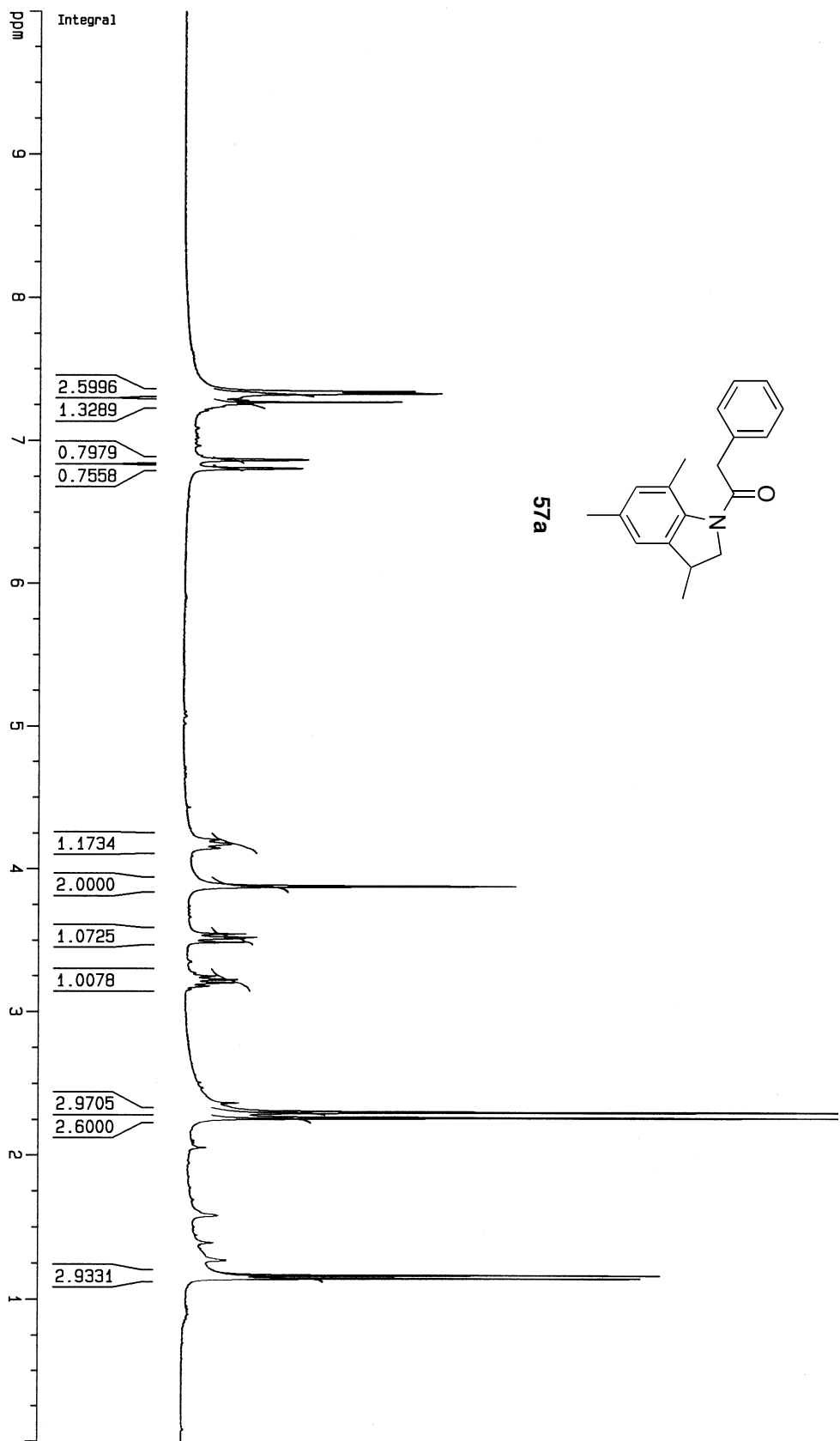


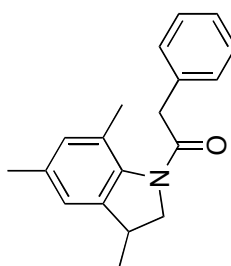




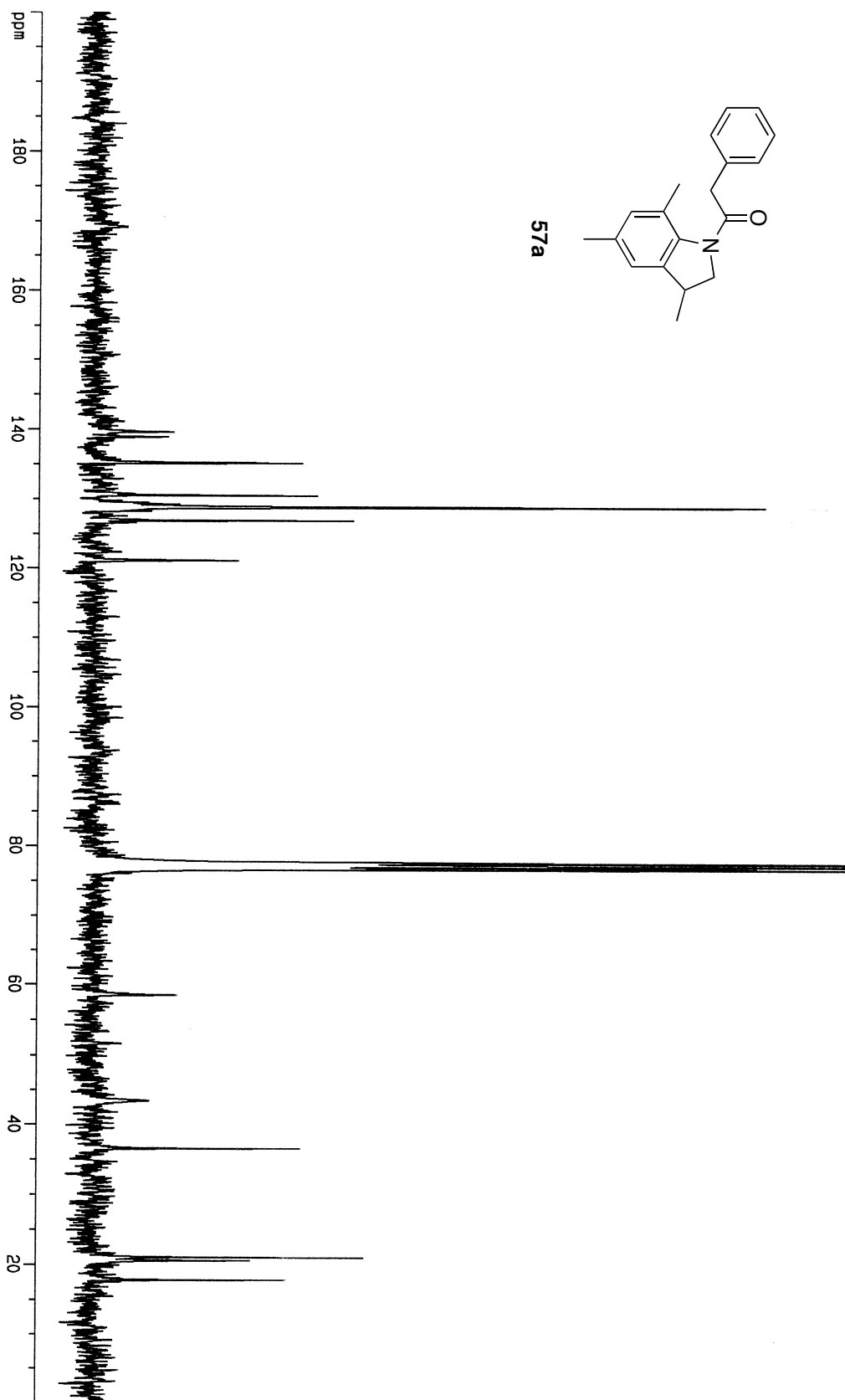


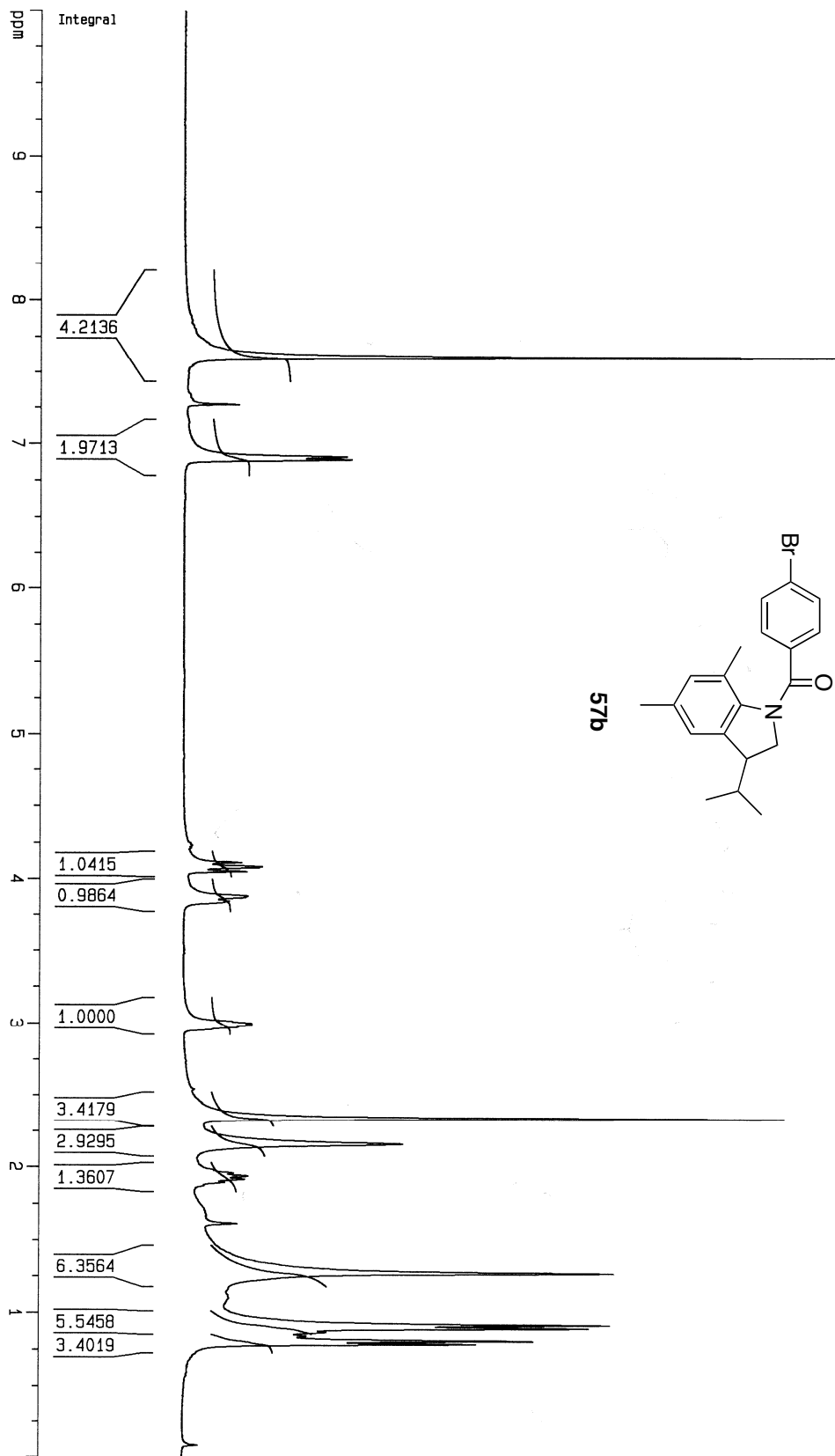


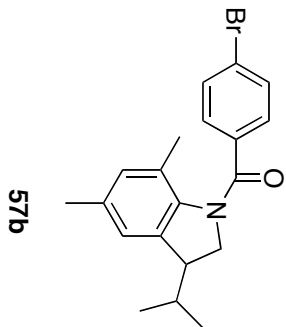
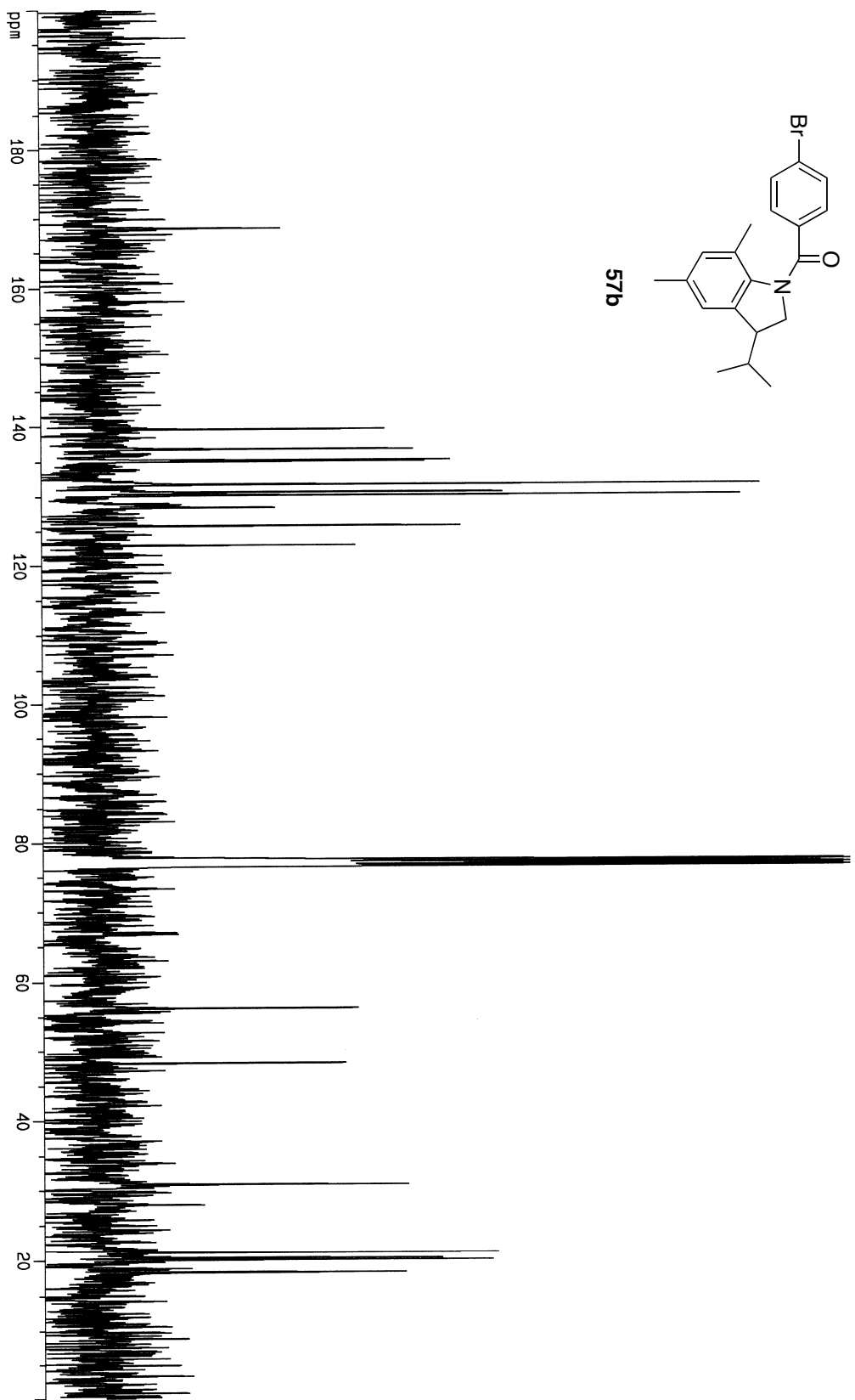


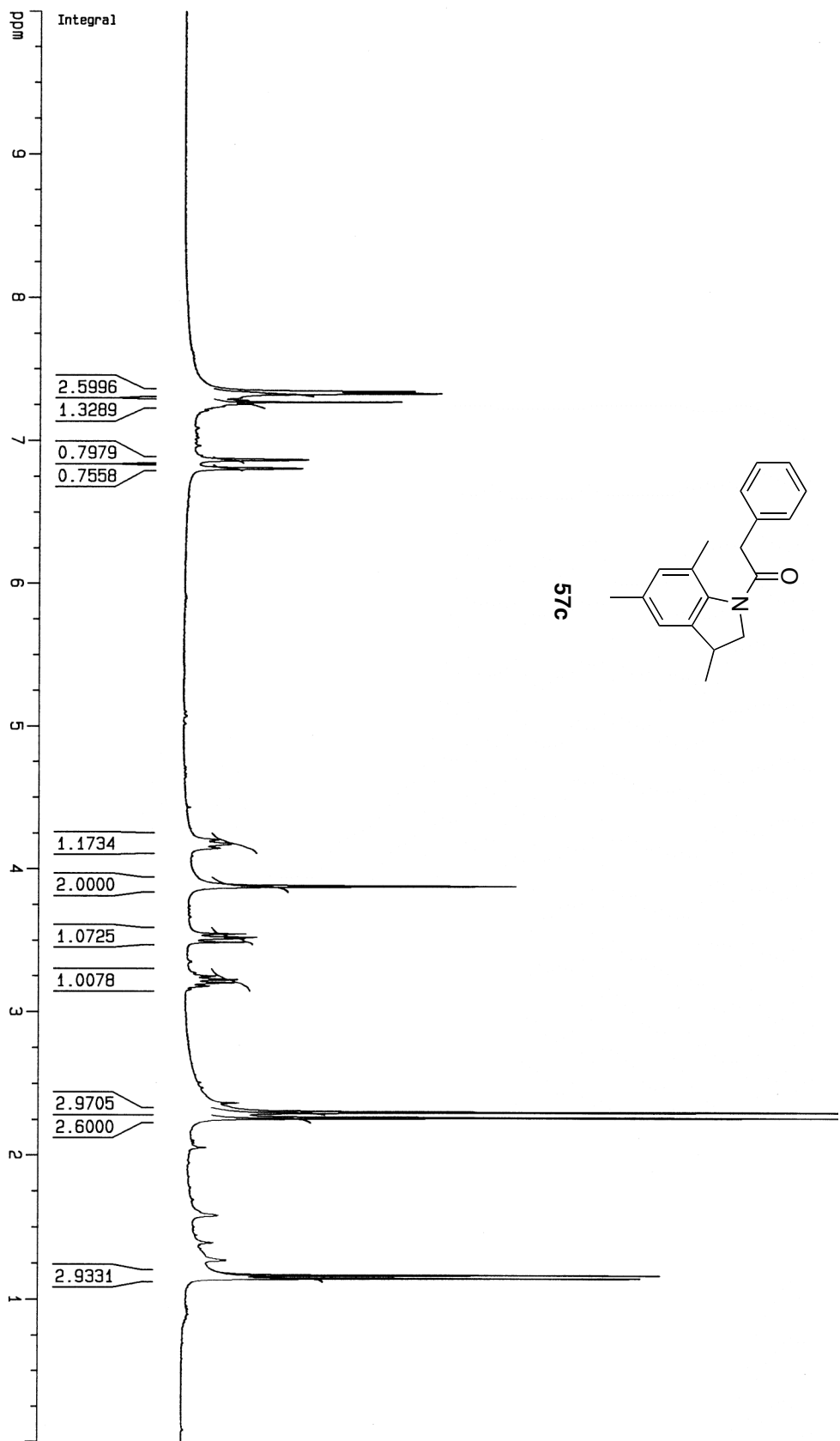


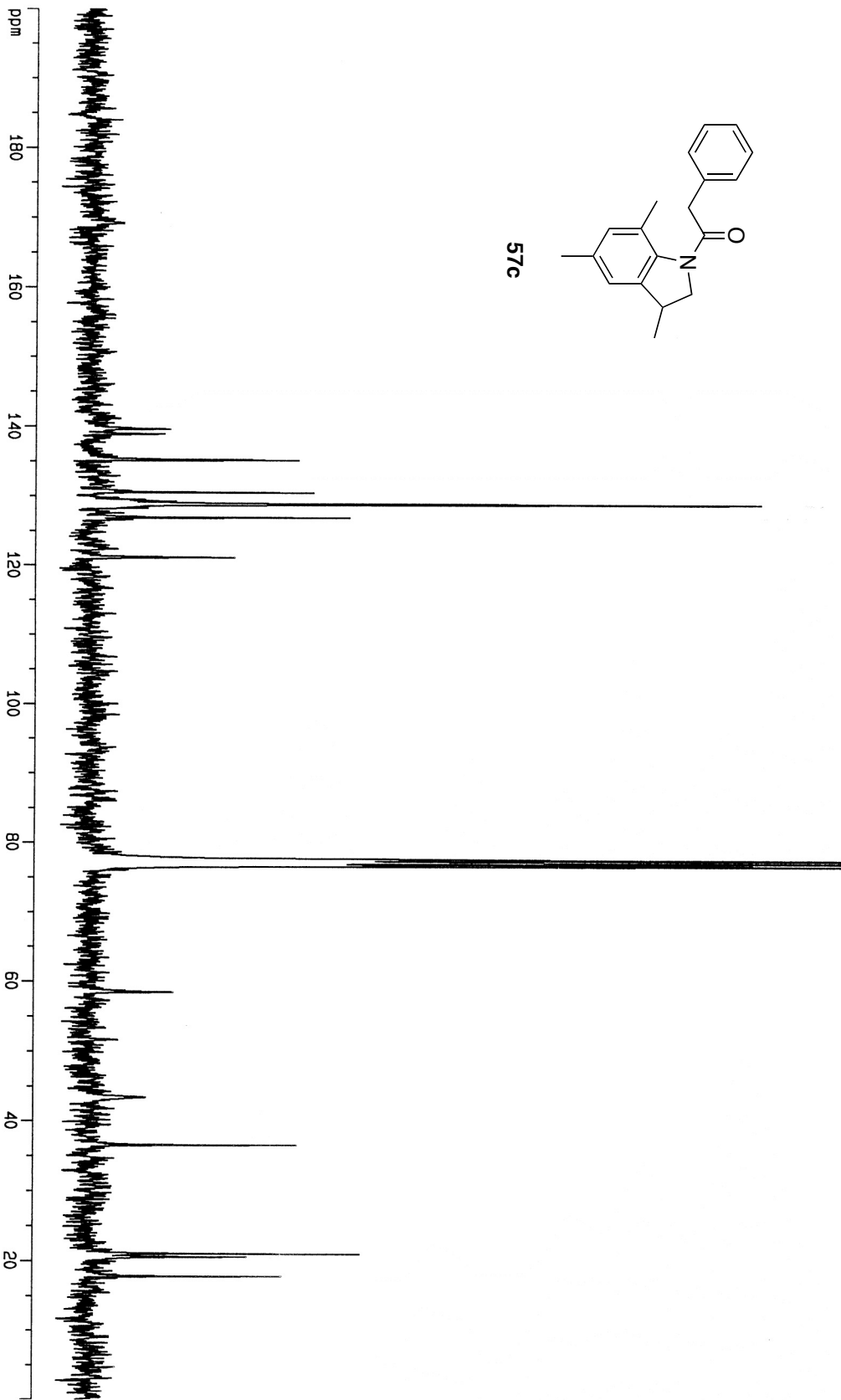
57a

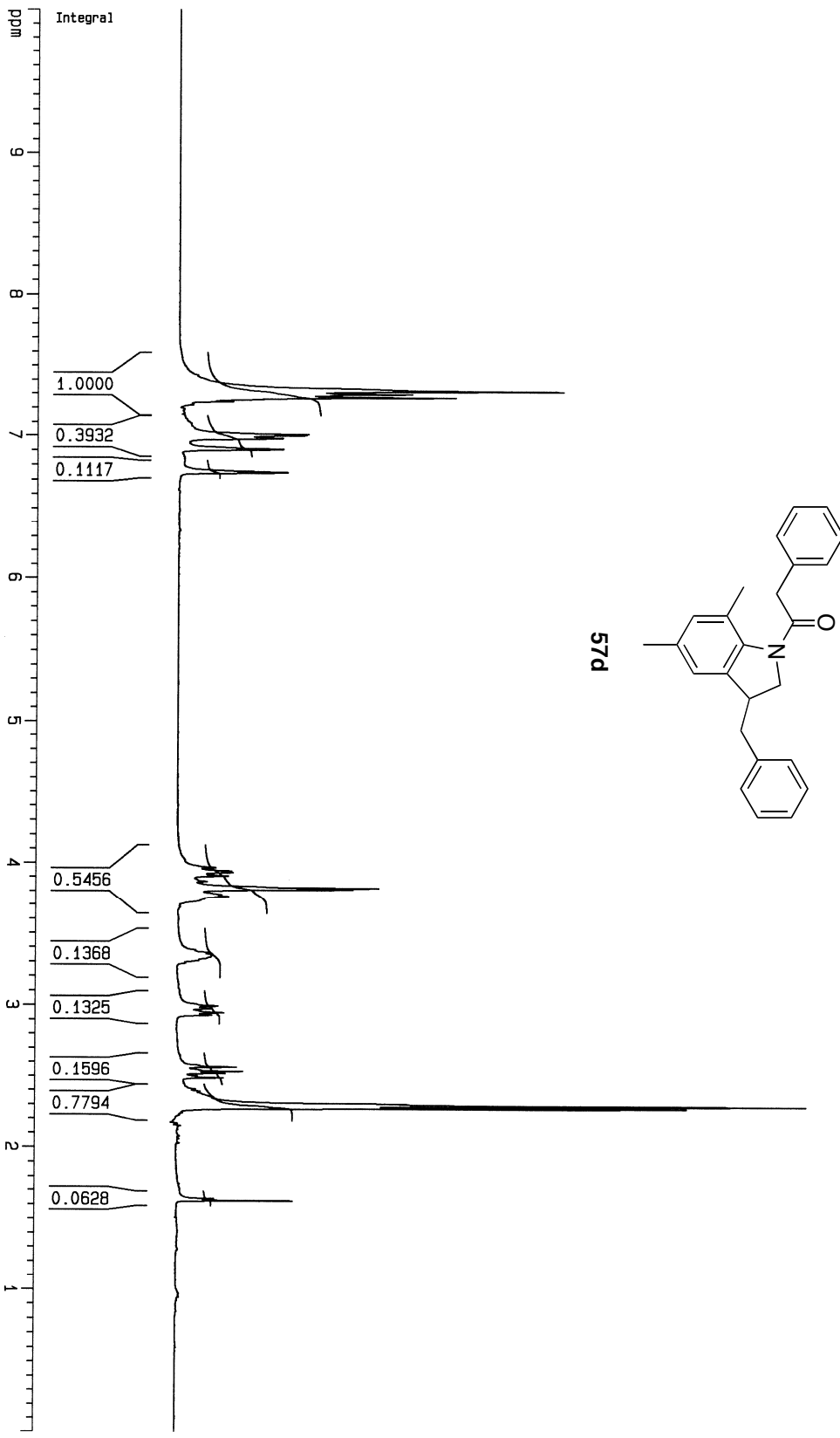




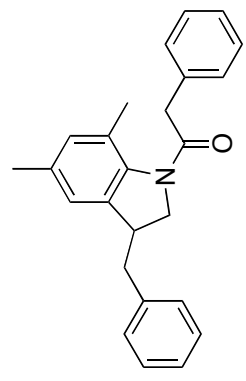


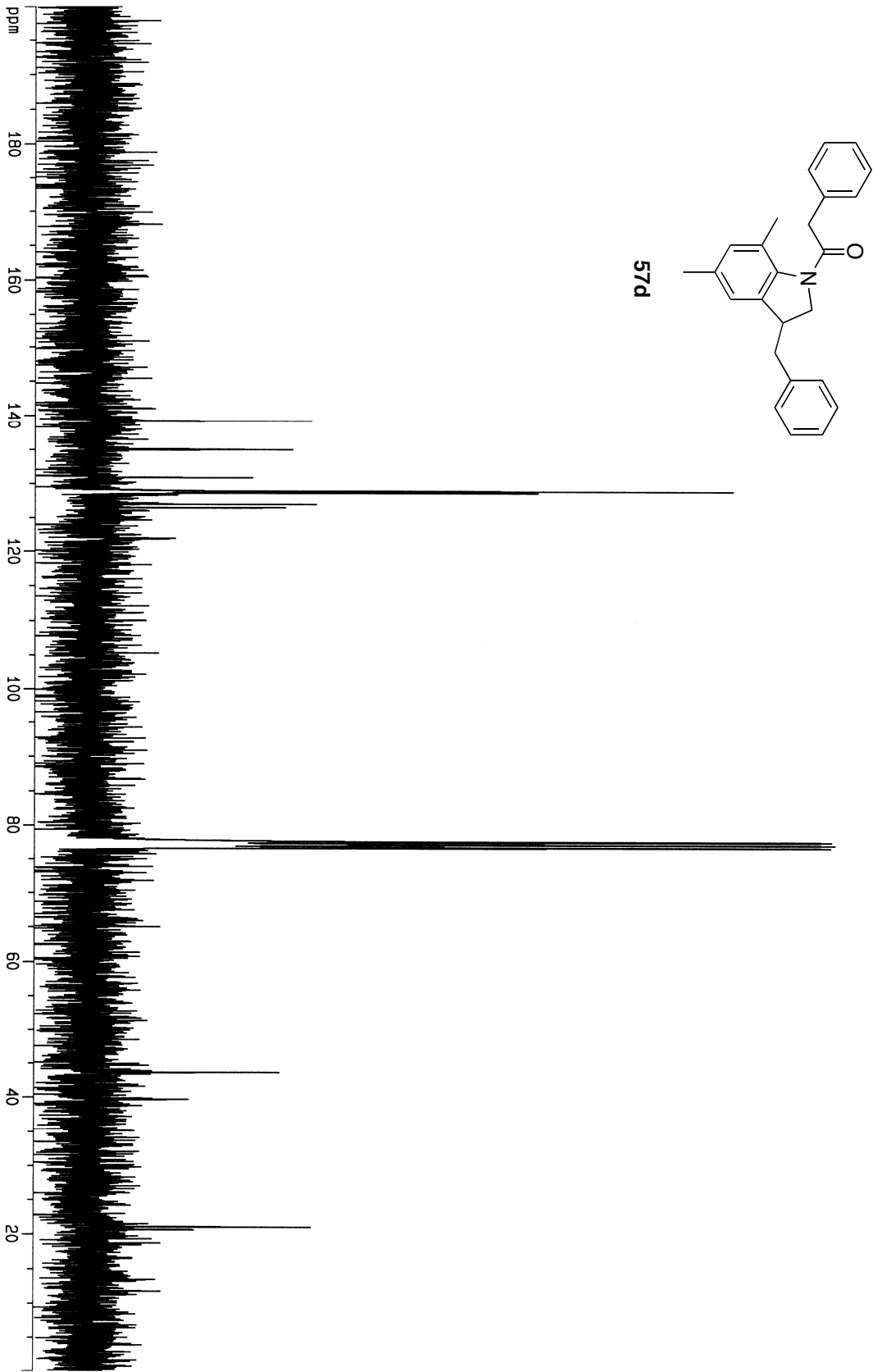


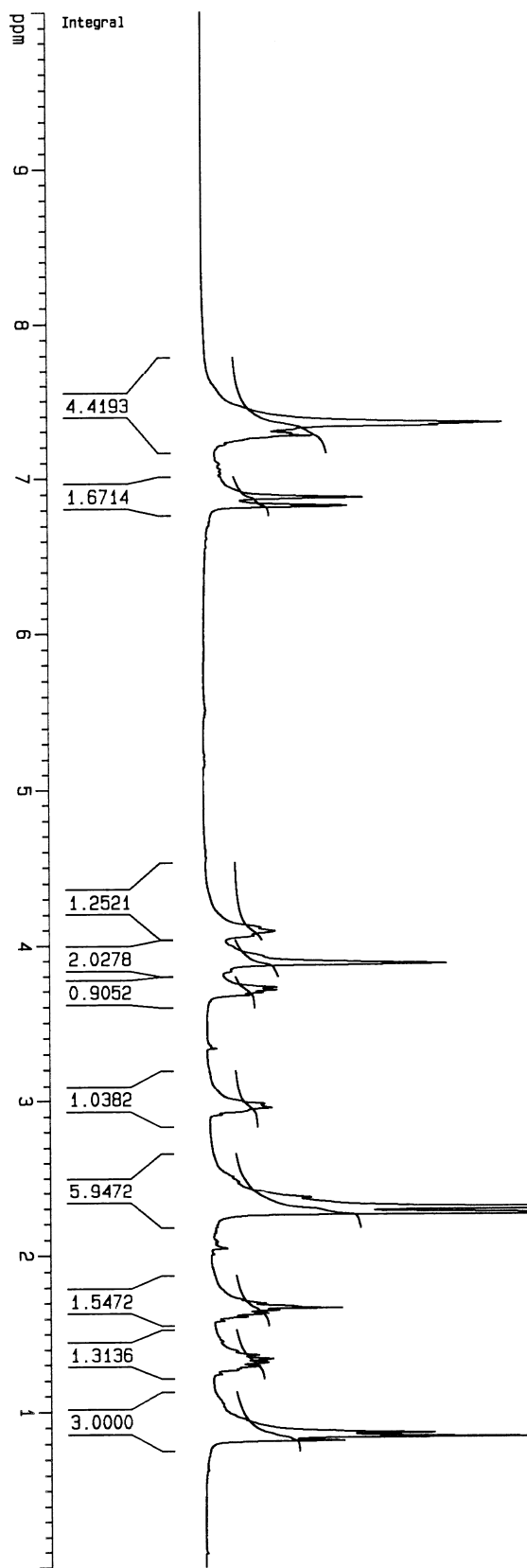




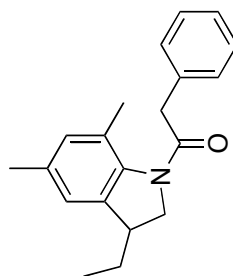
57d

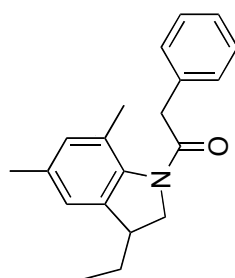




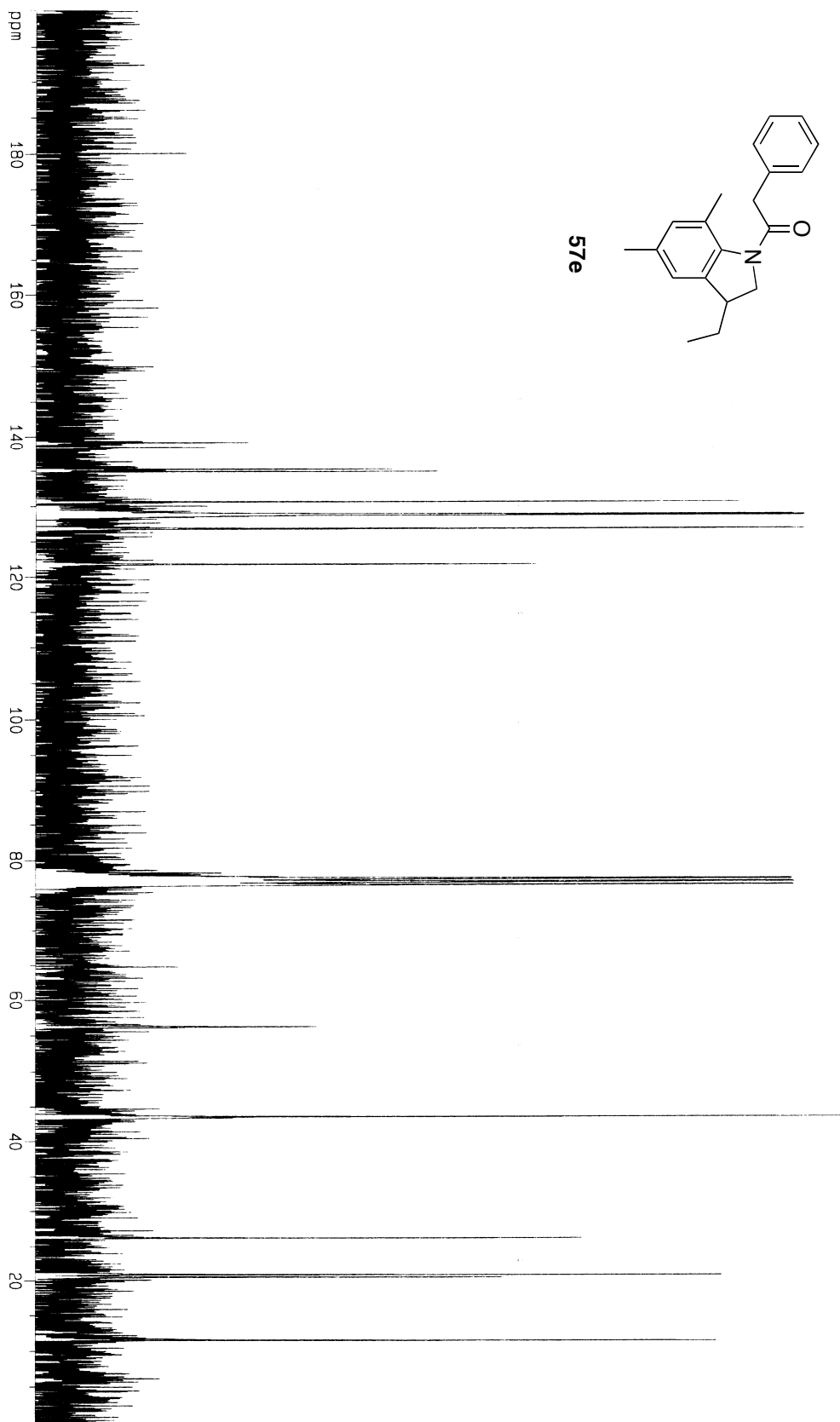


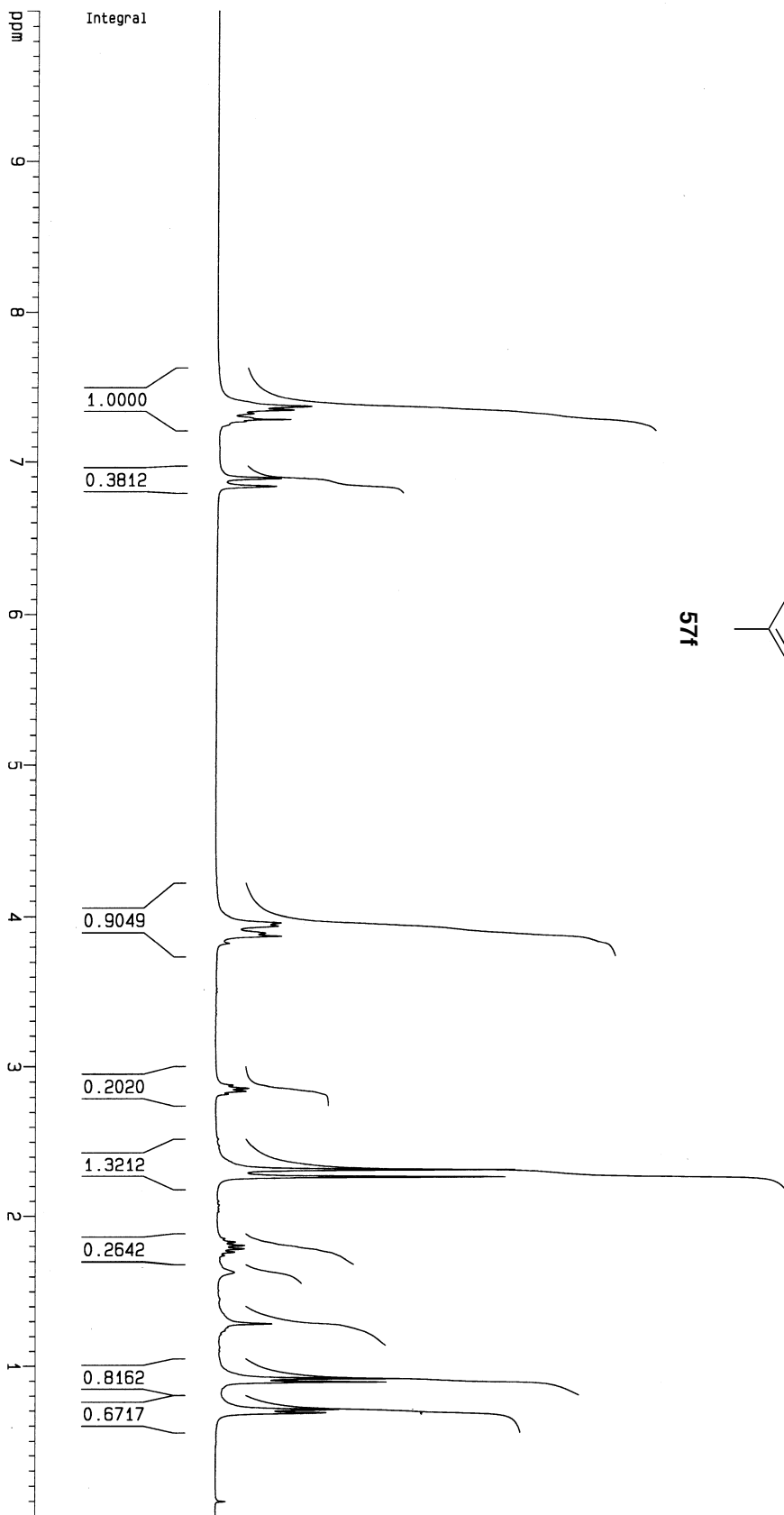
57e



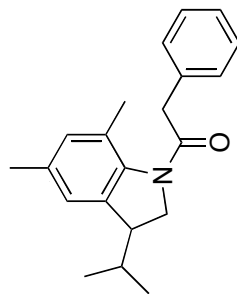


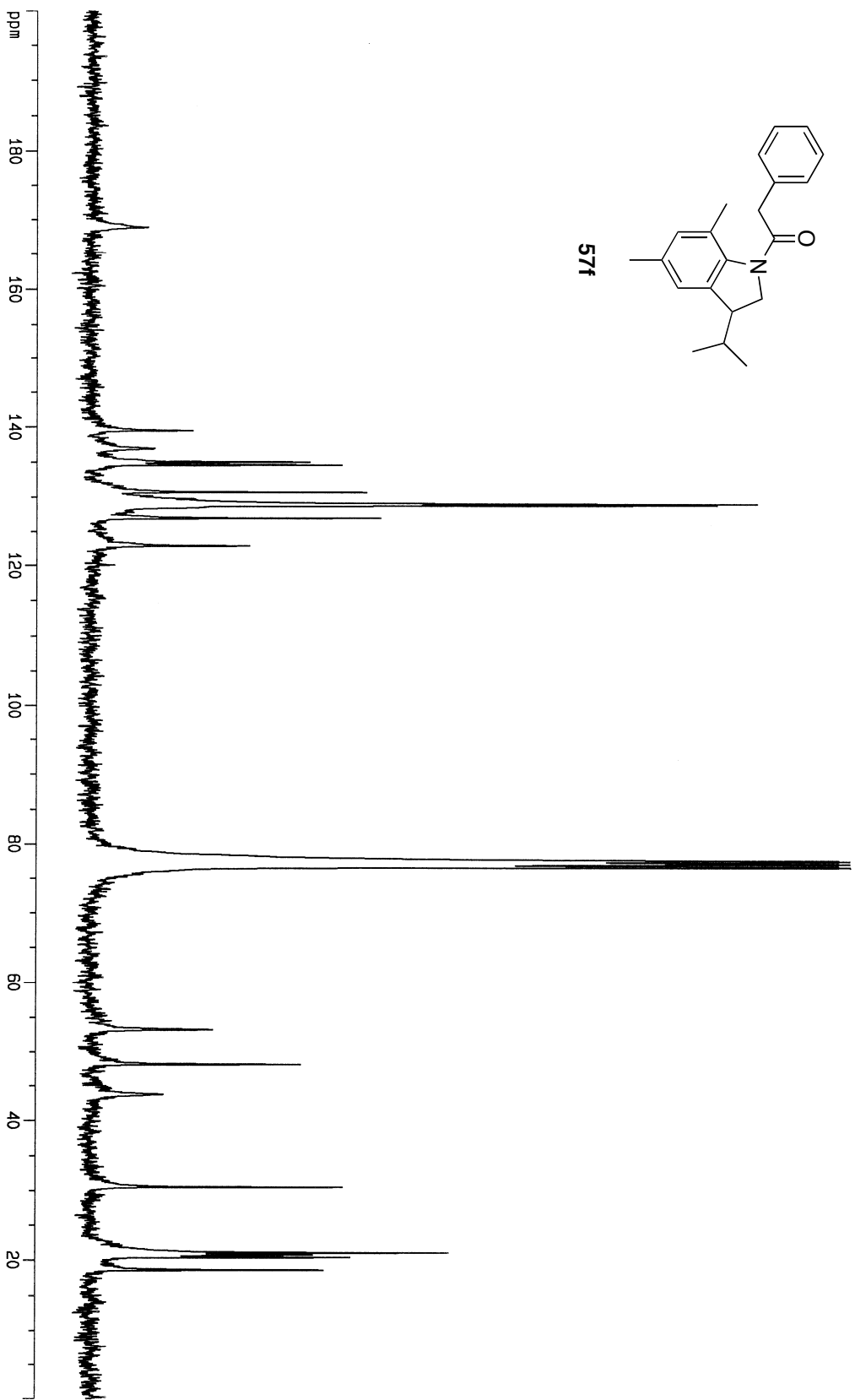
57e



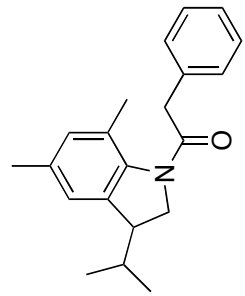


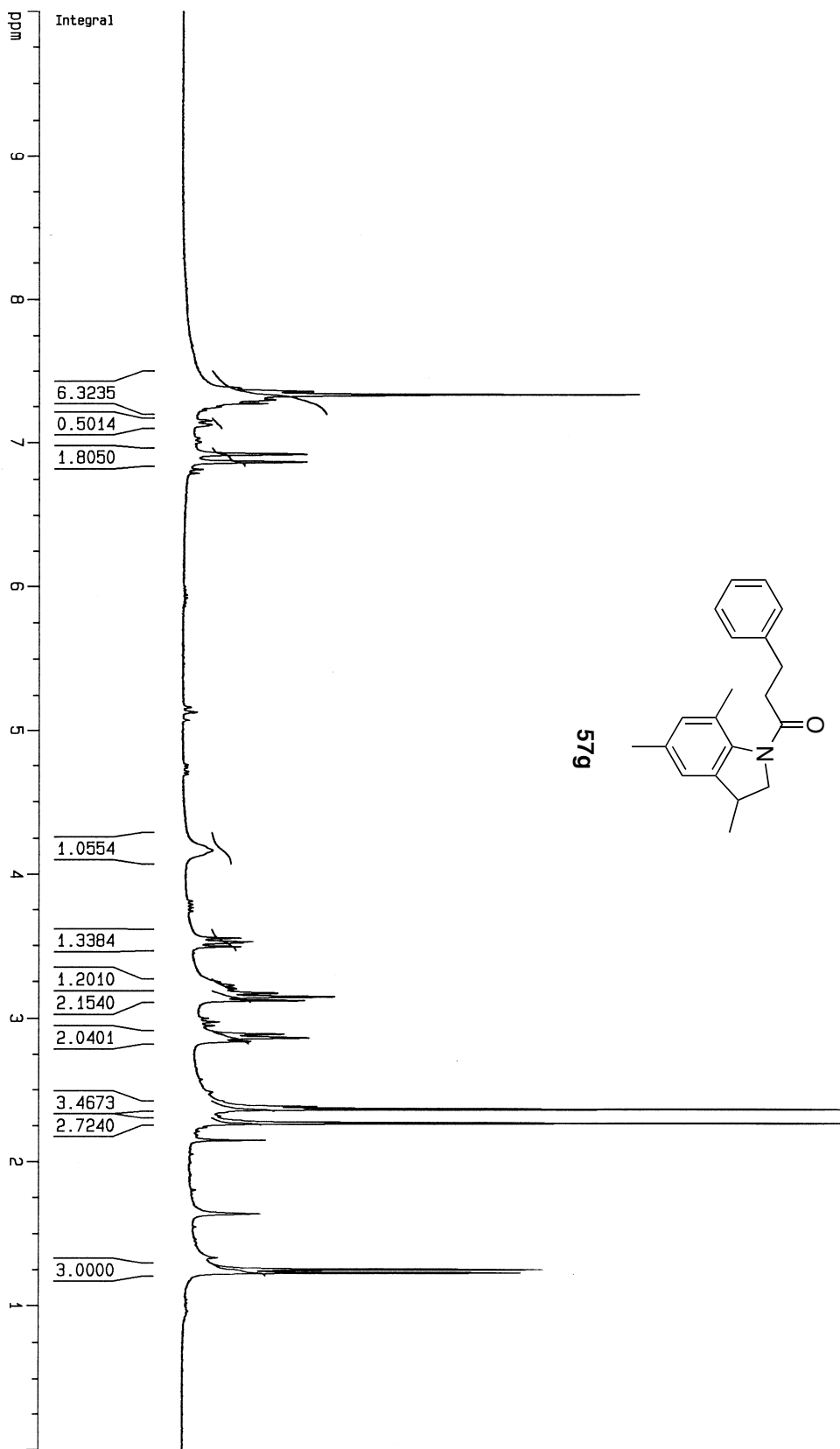
574

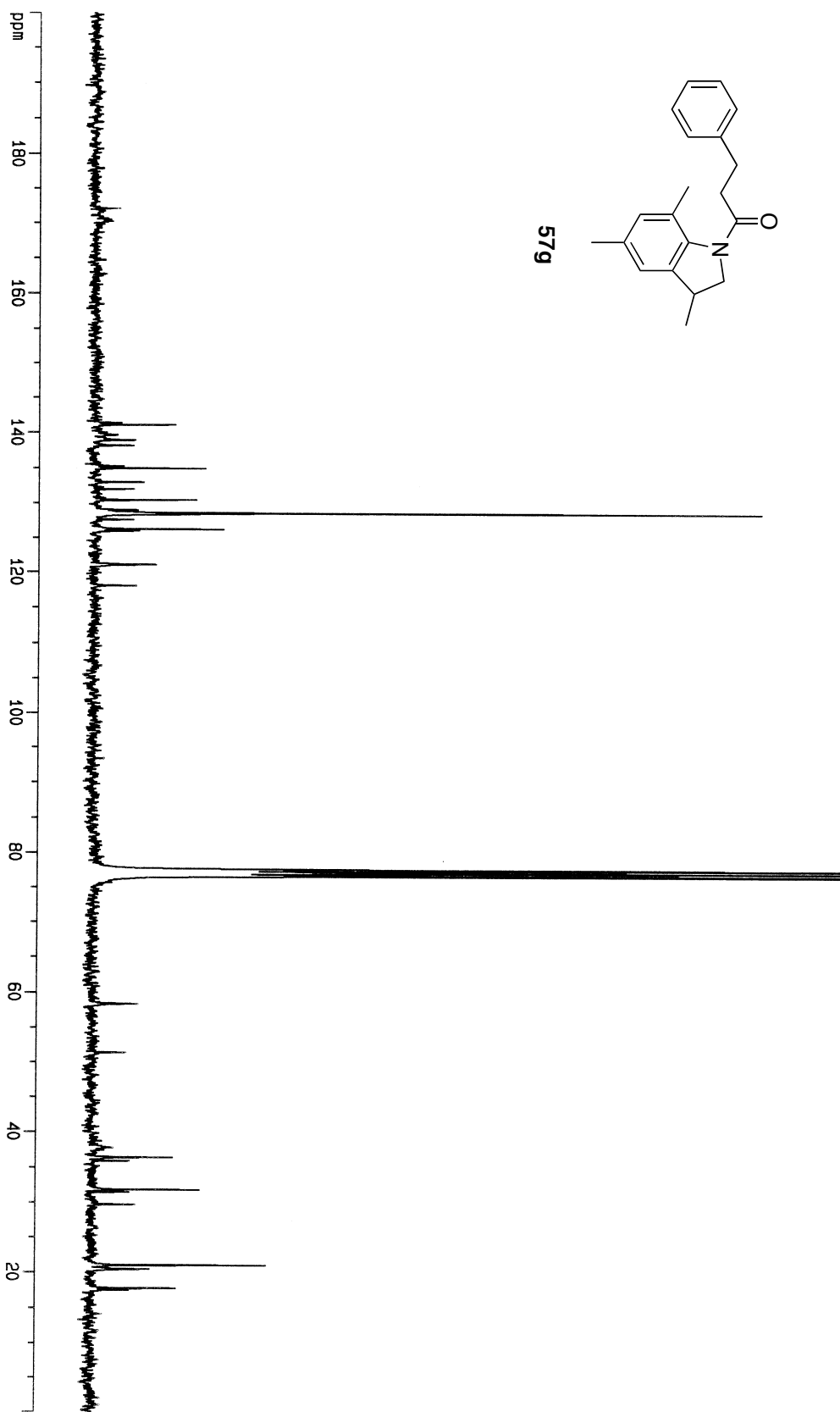
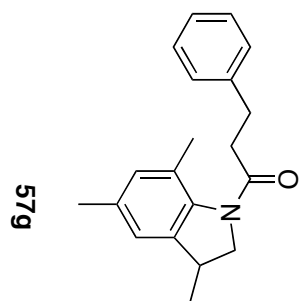


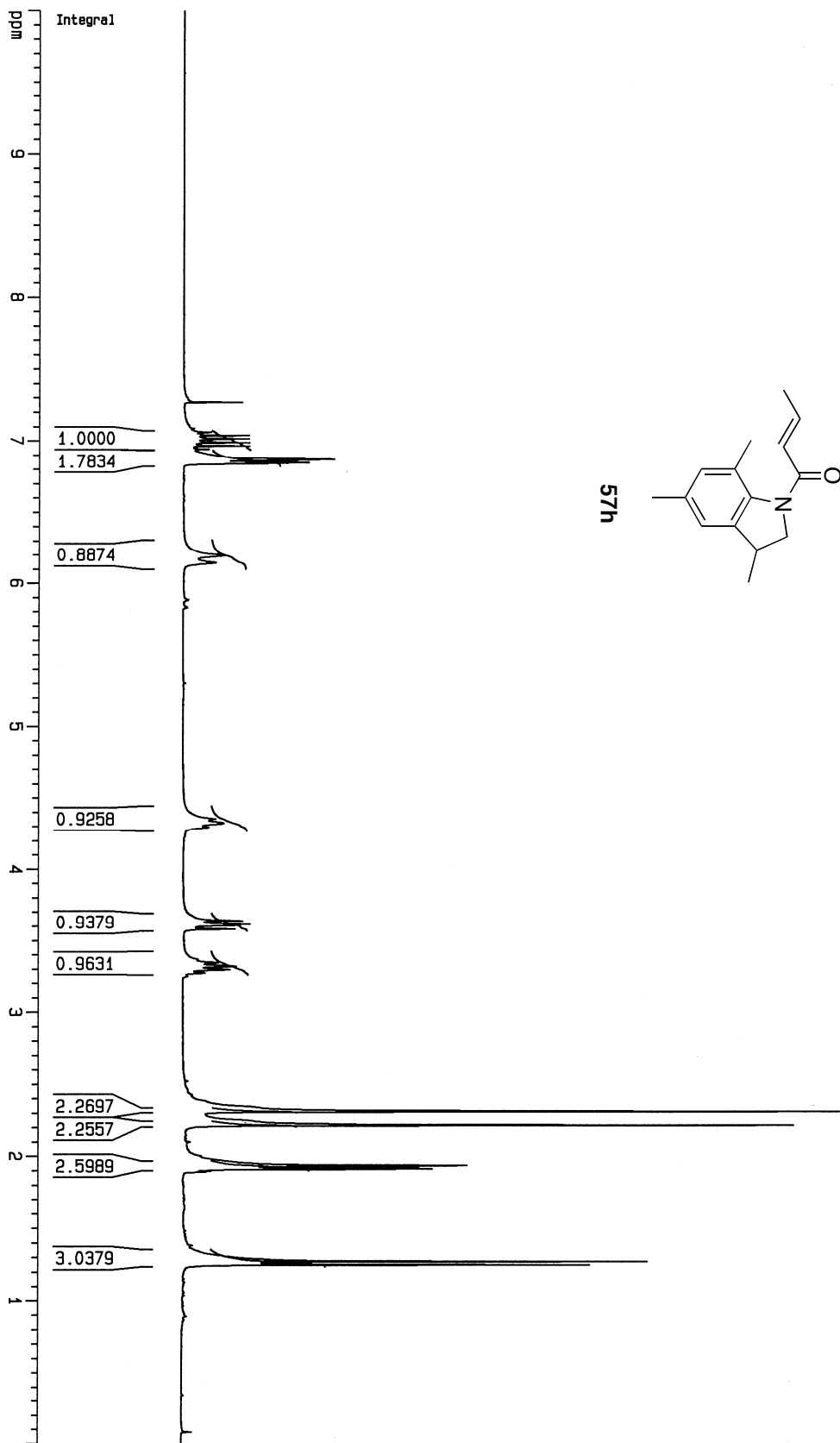


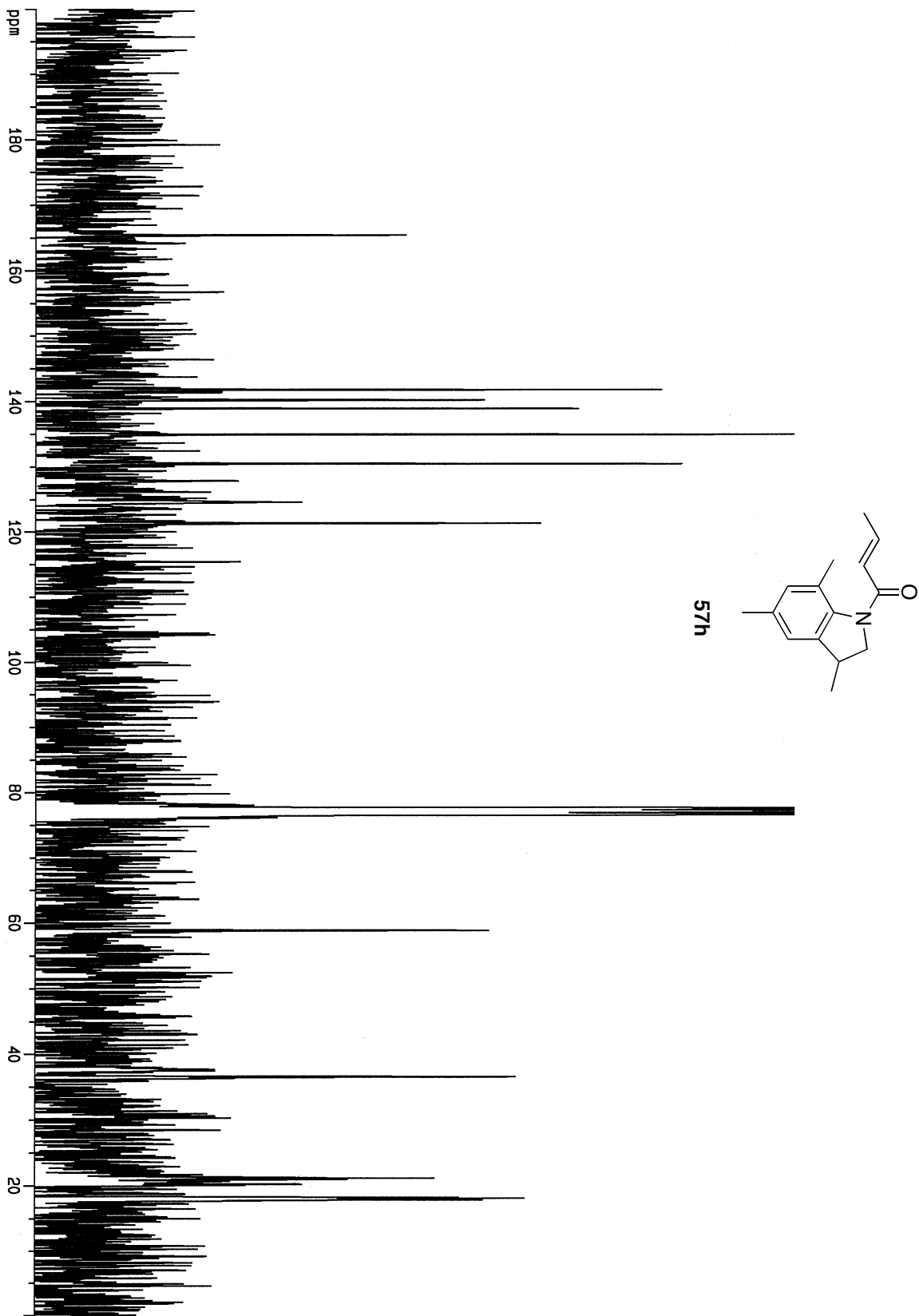
571

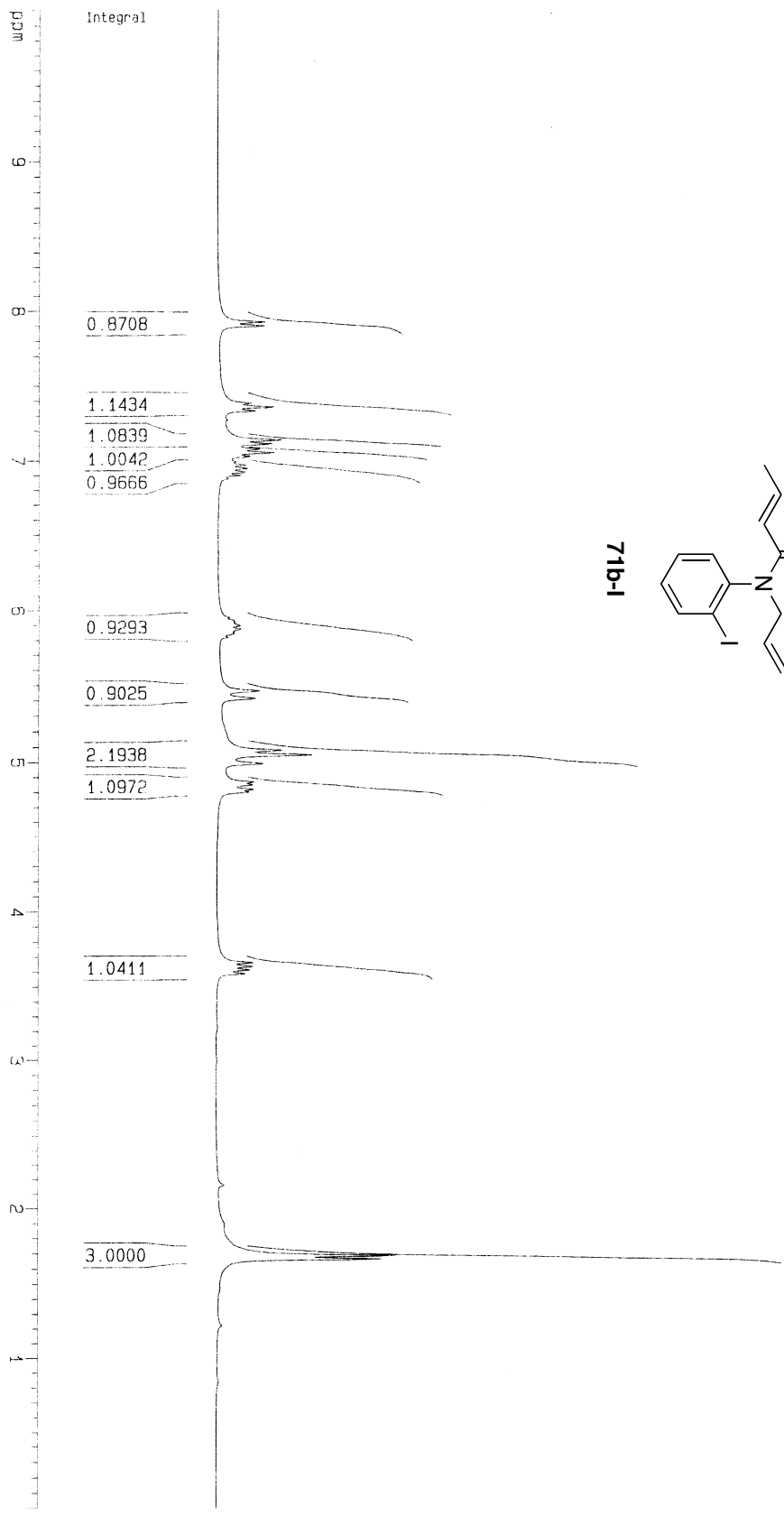




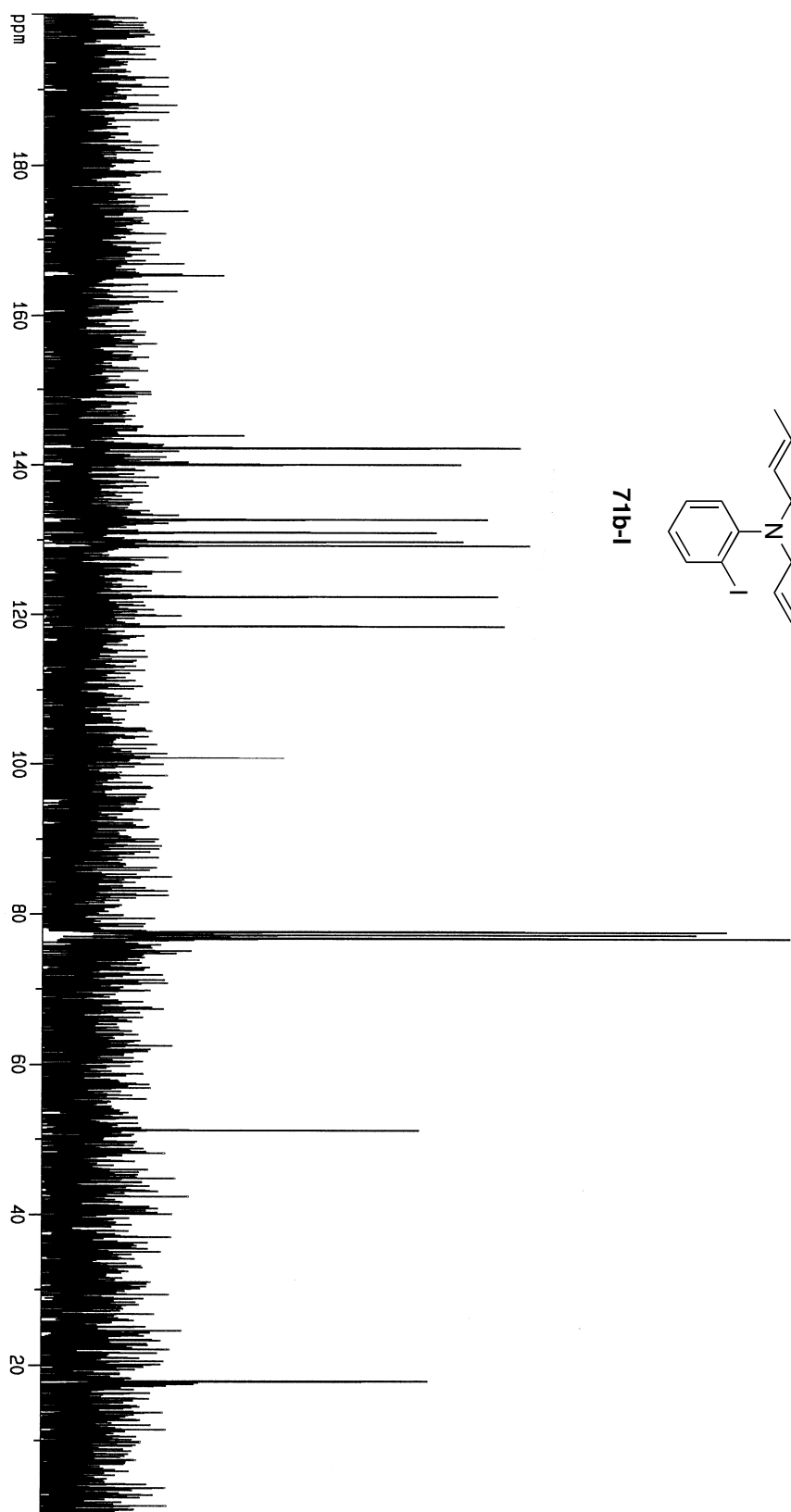
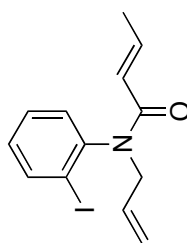


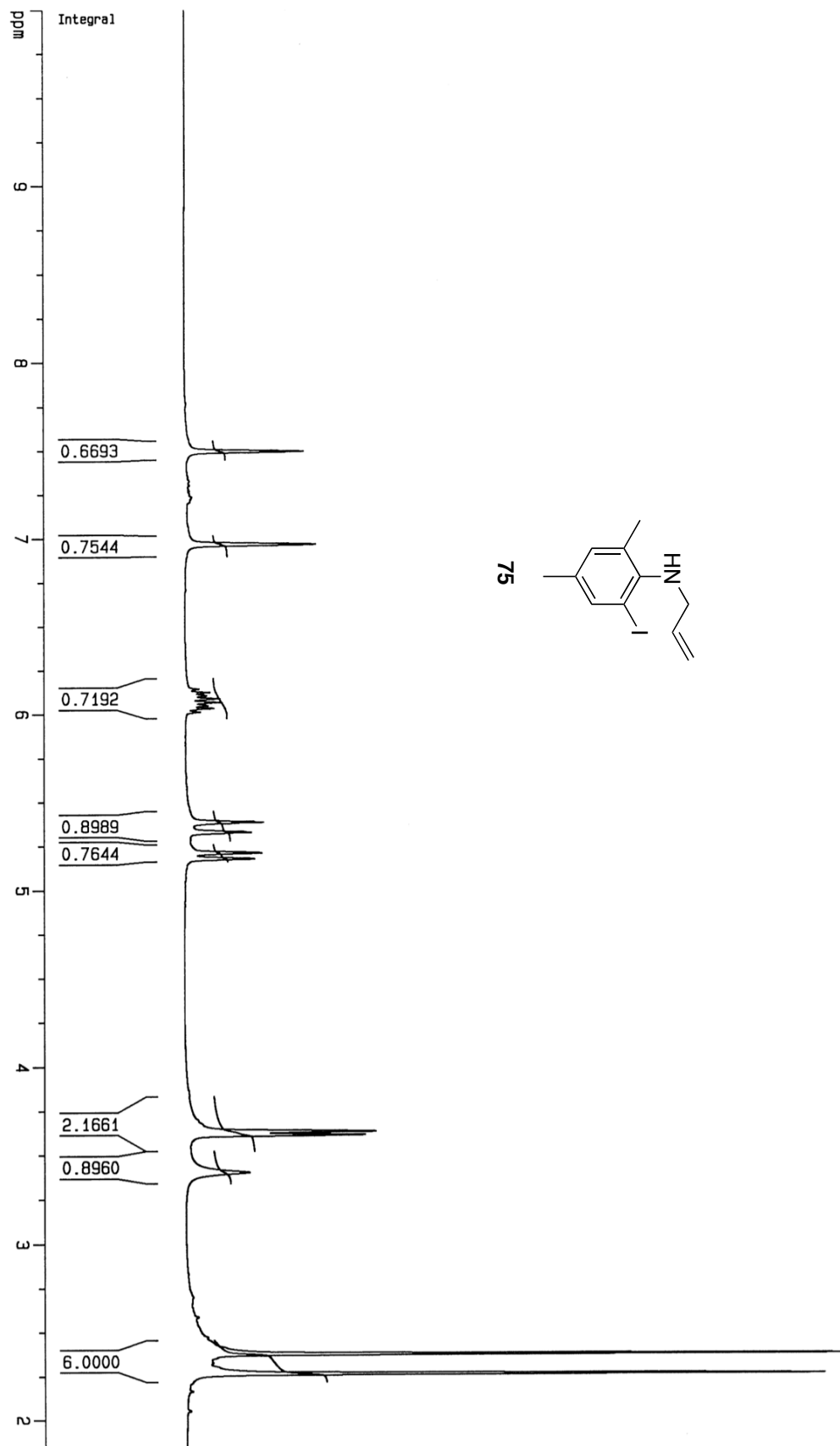


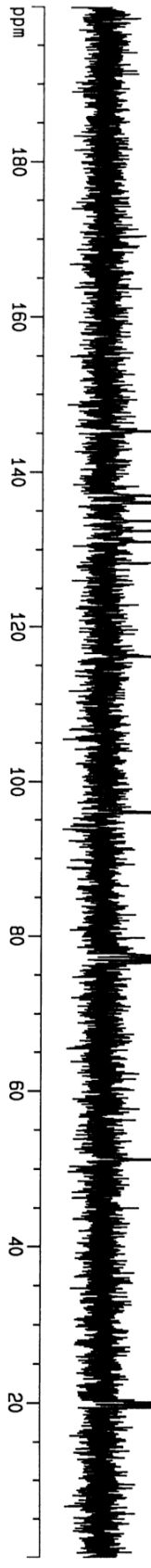
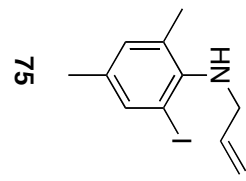


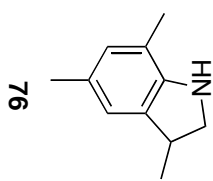
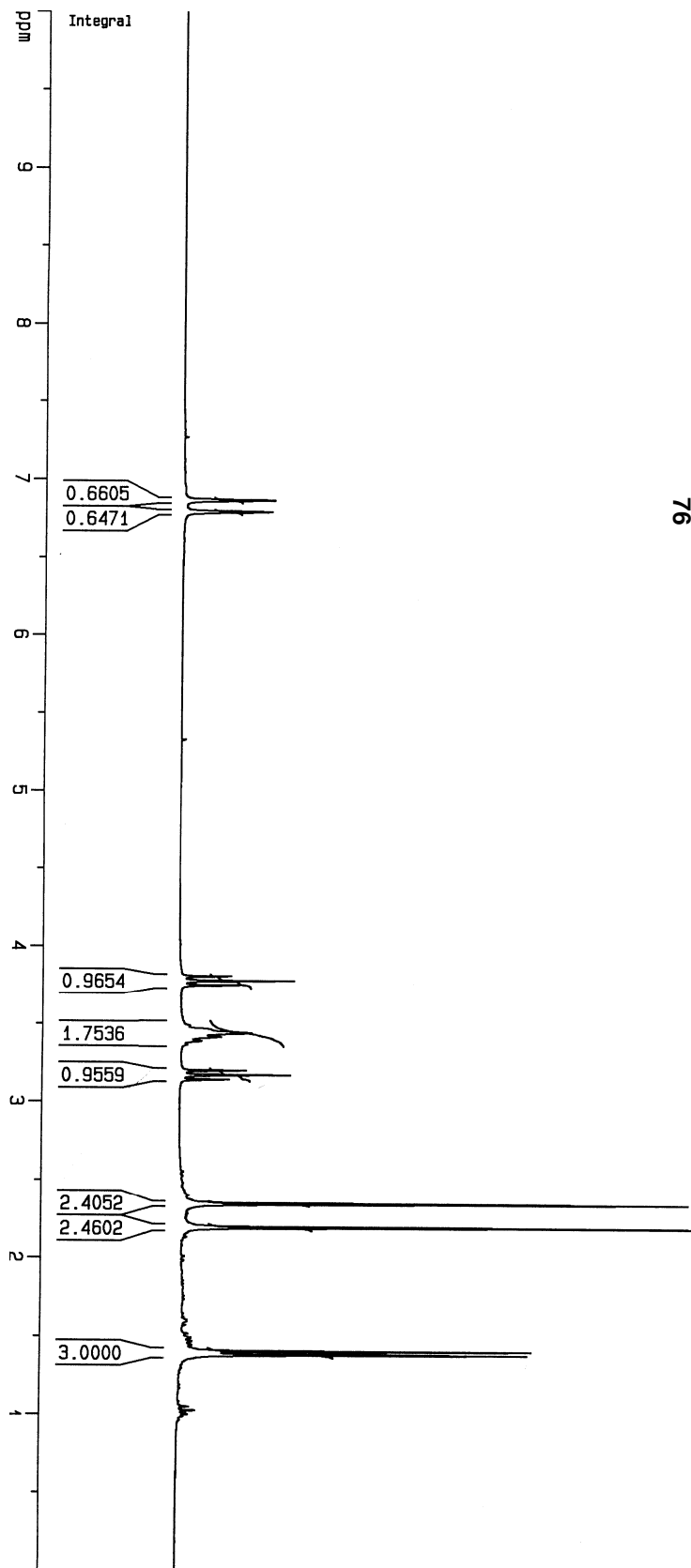


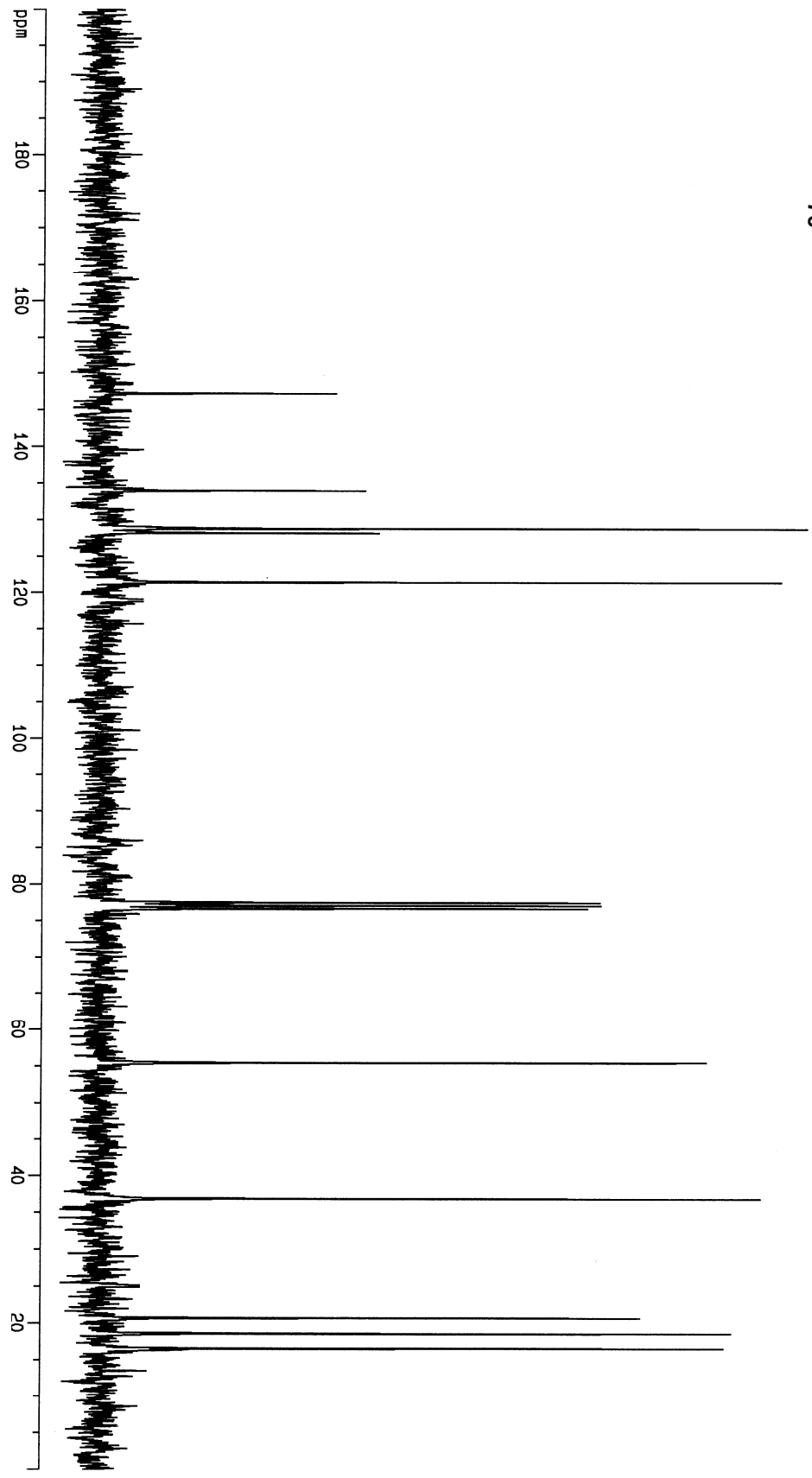
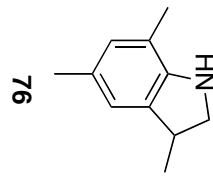
71b-1

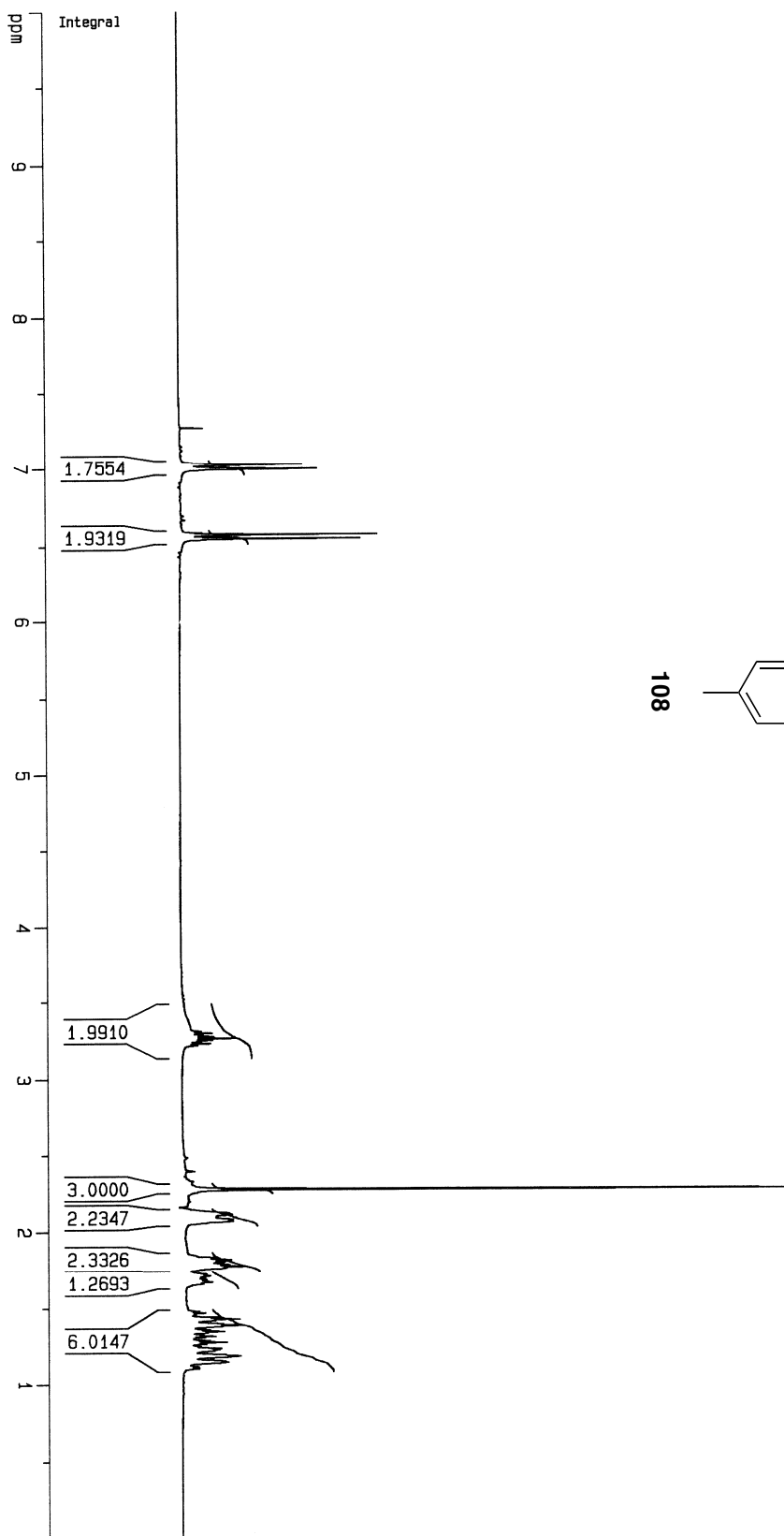




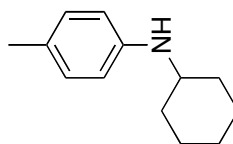


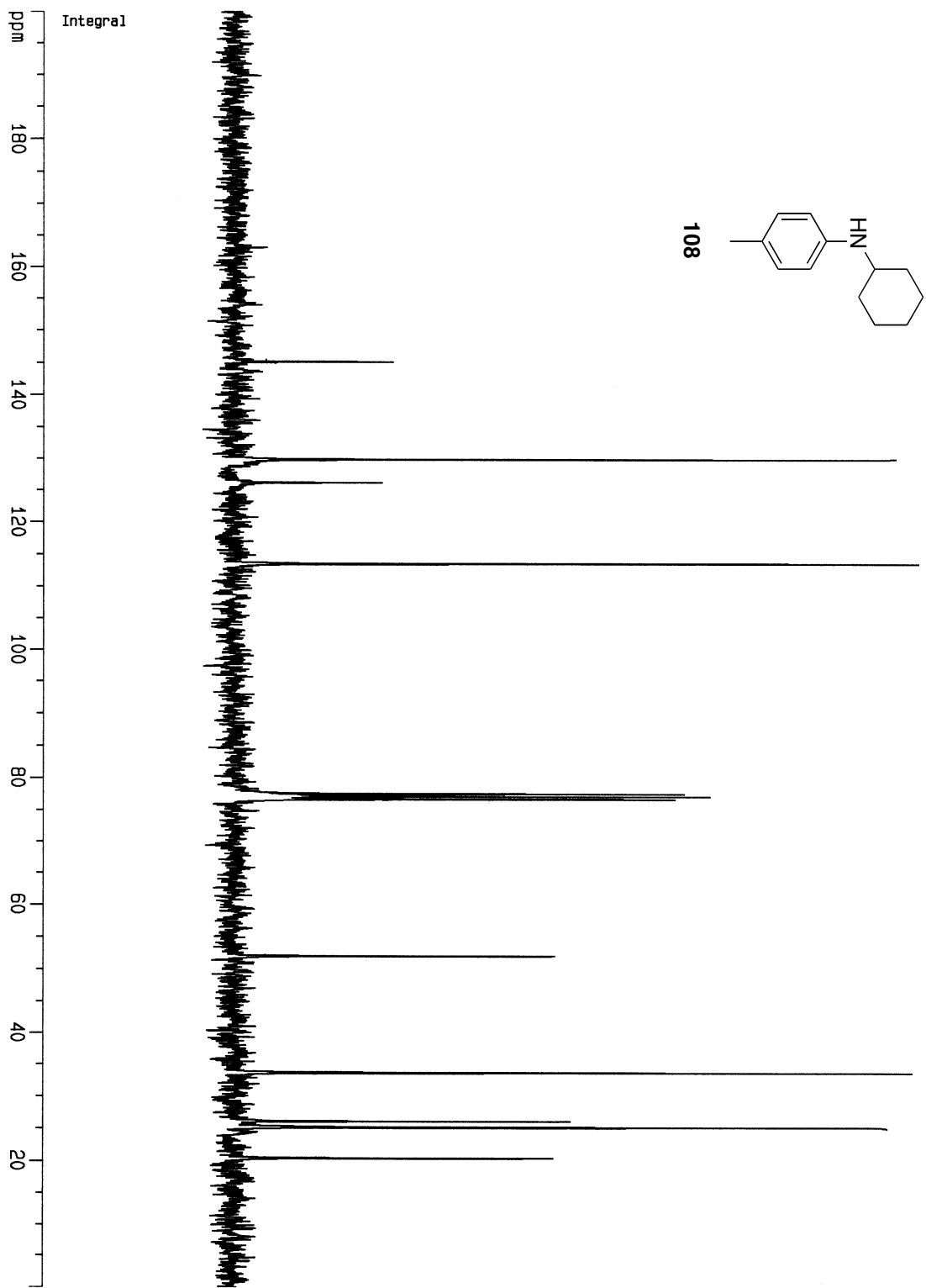


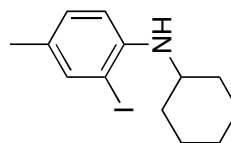
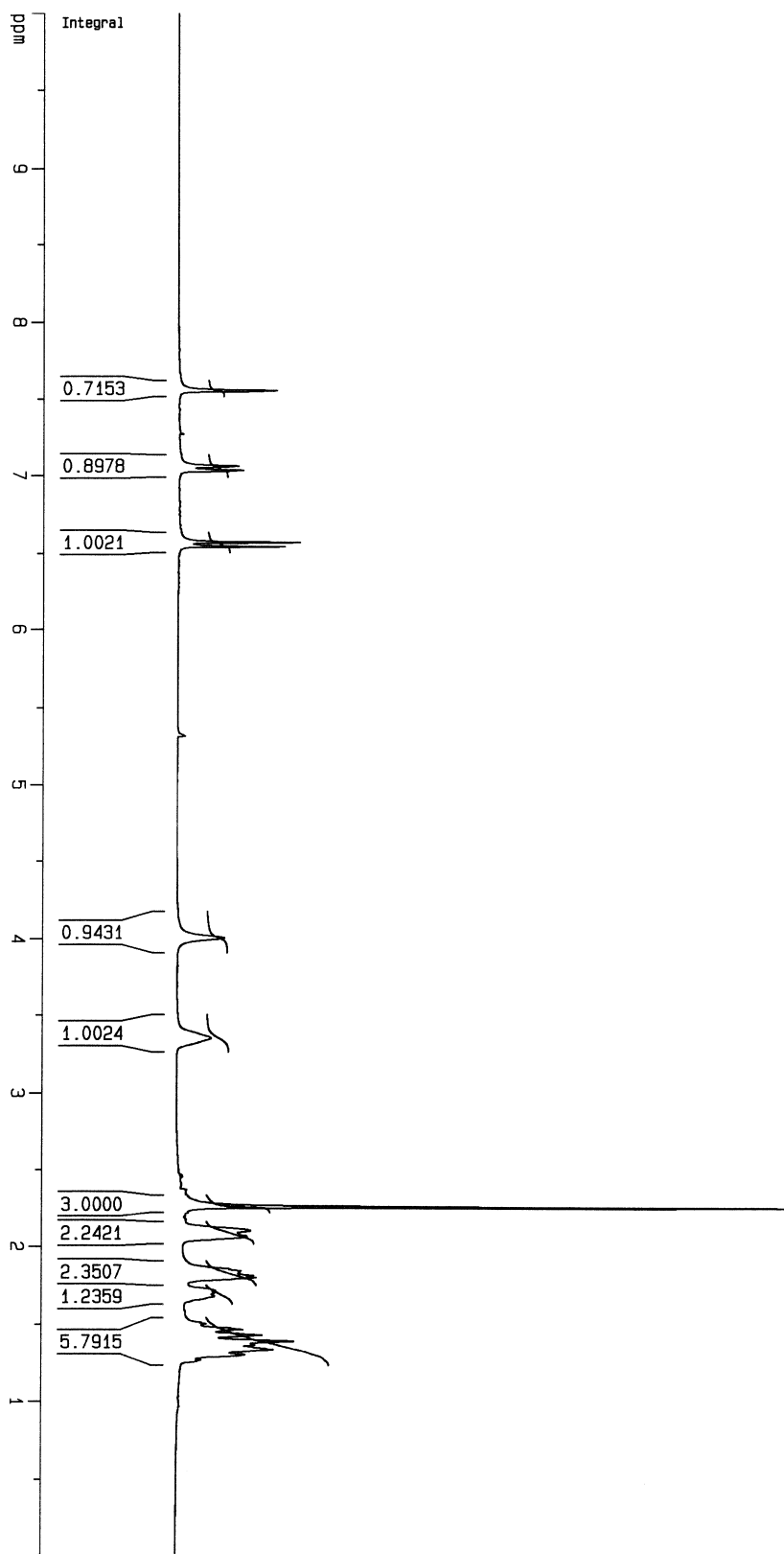


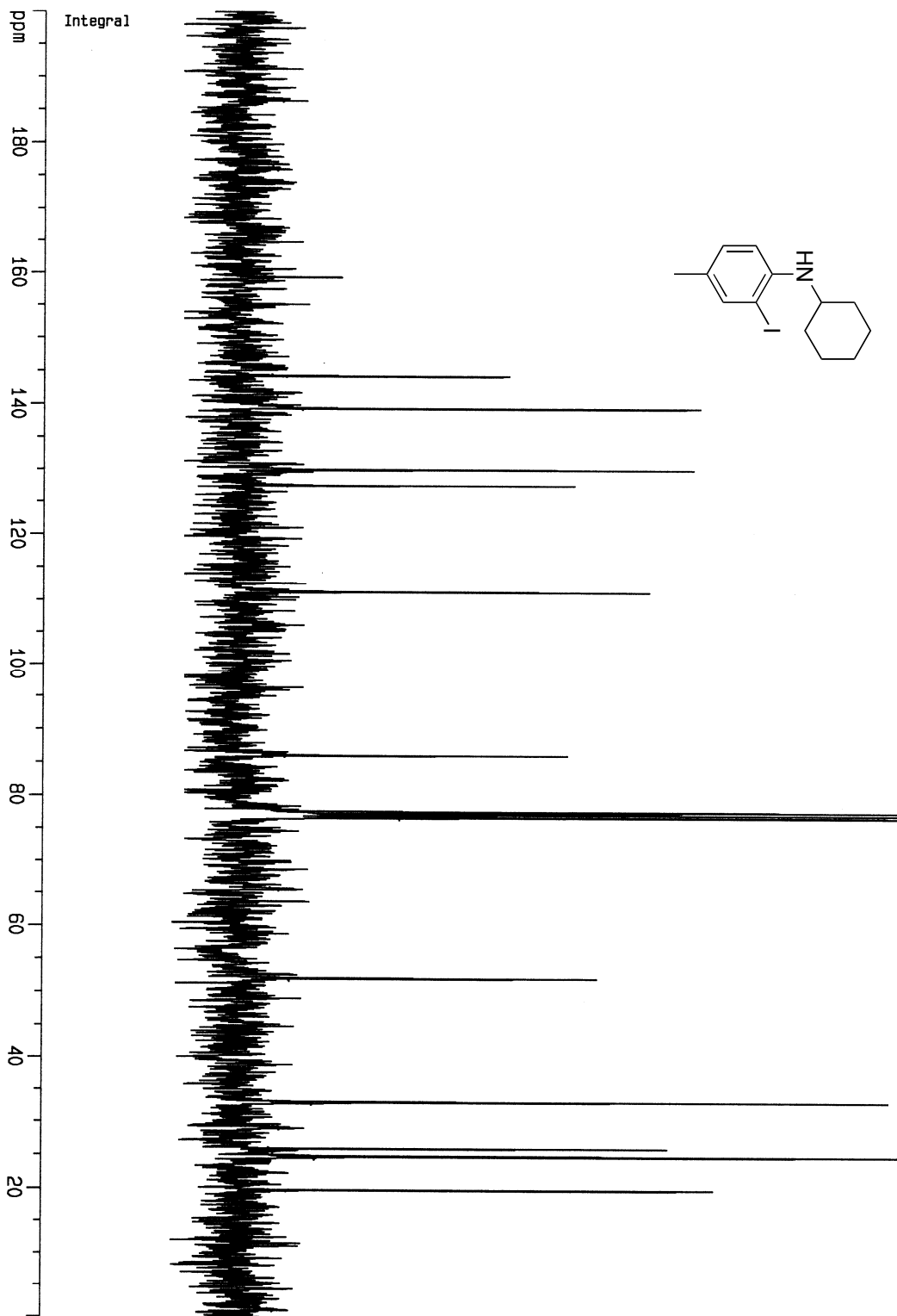


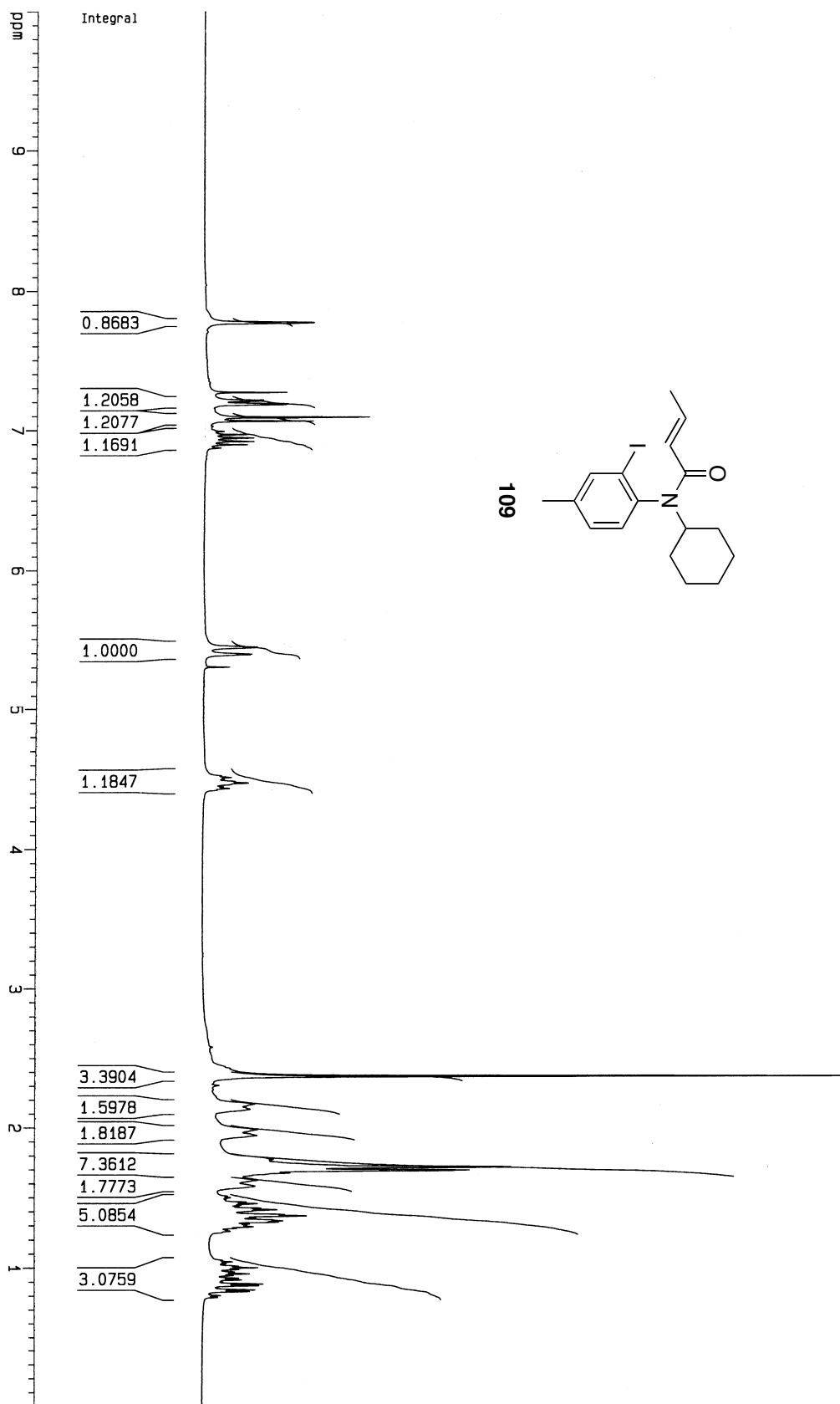
108

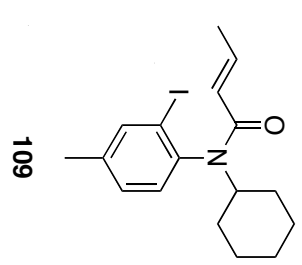
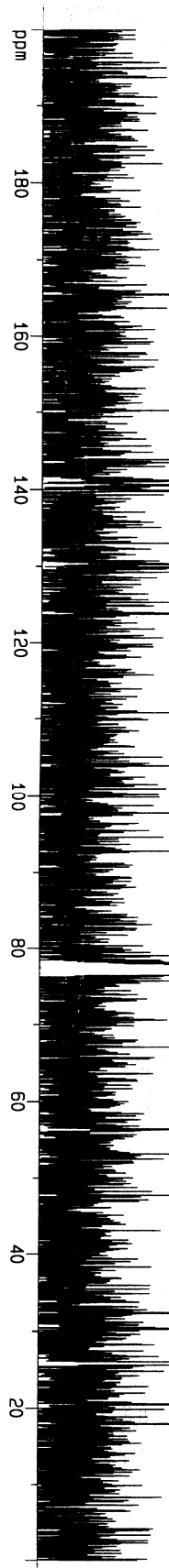


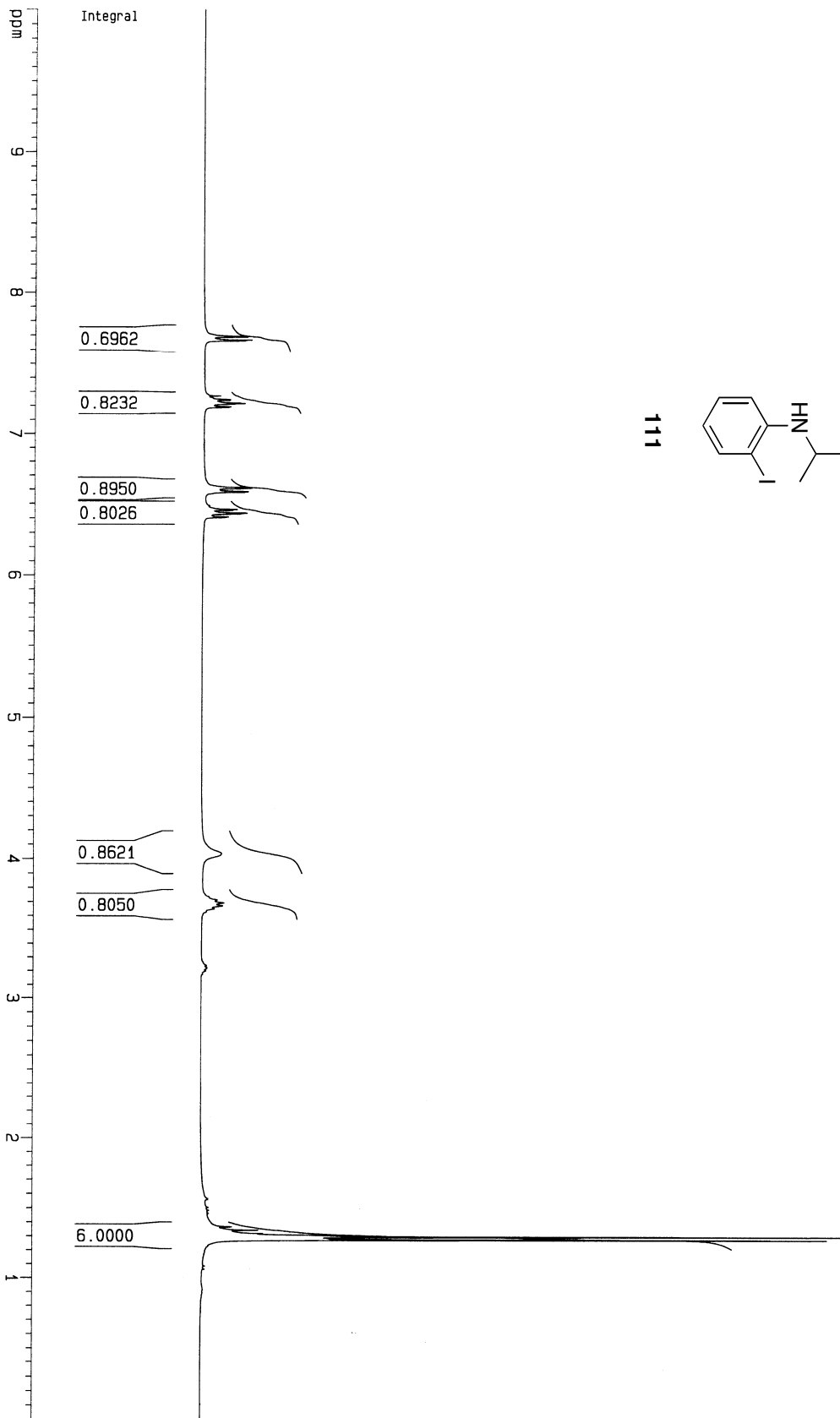


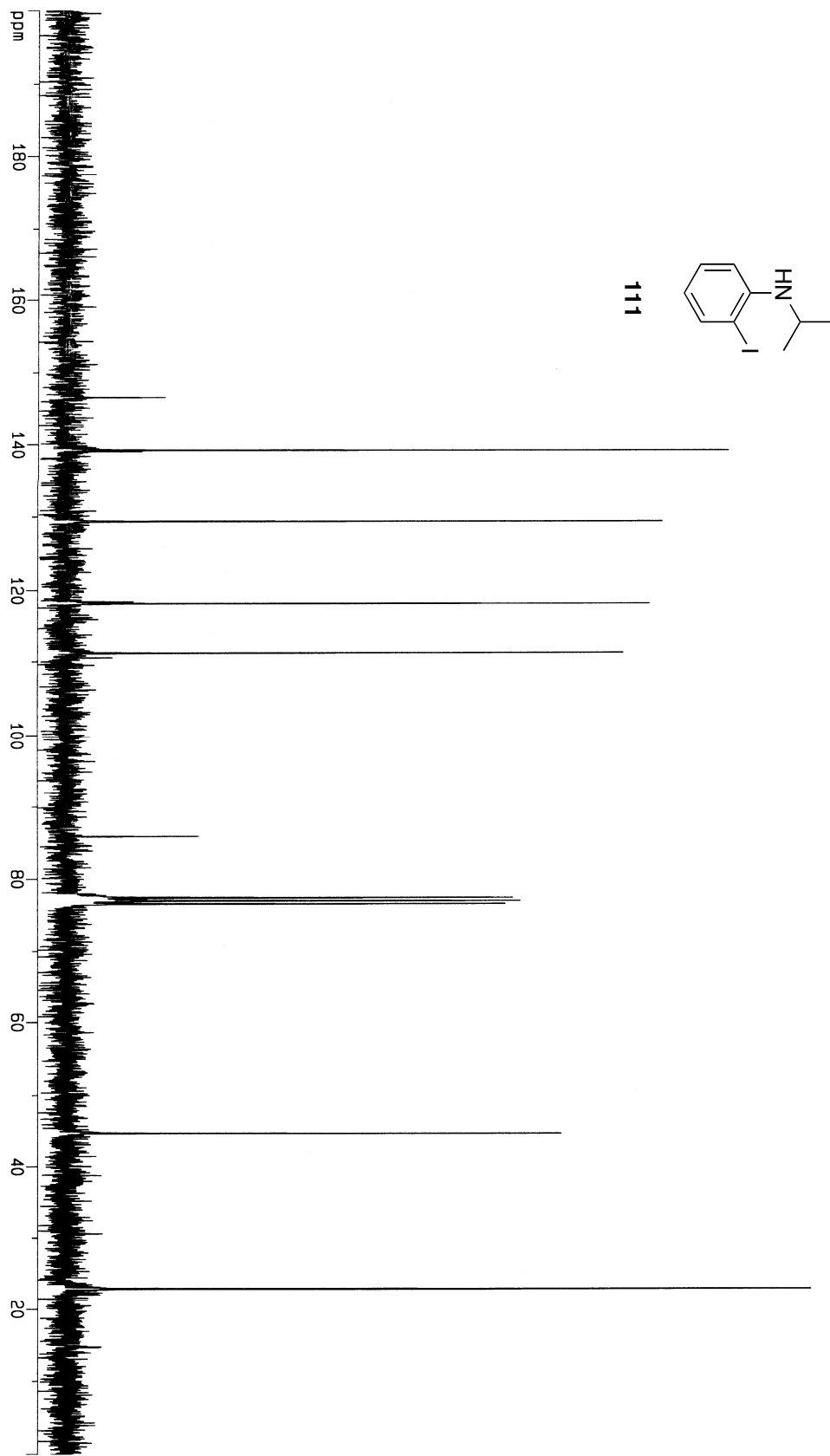


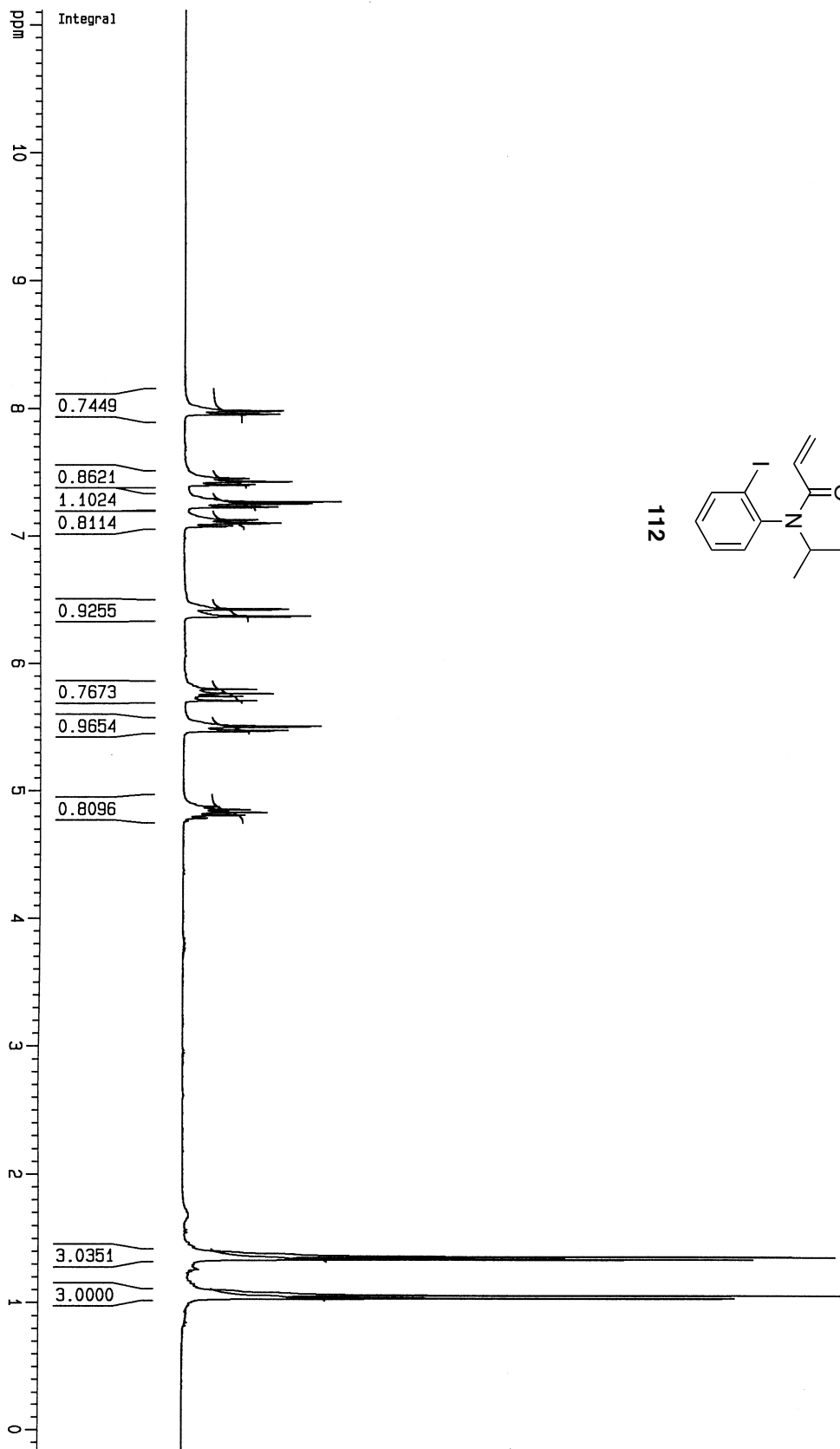




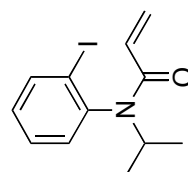


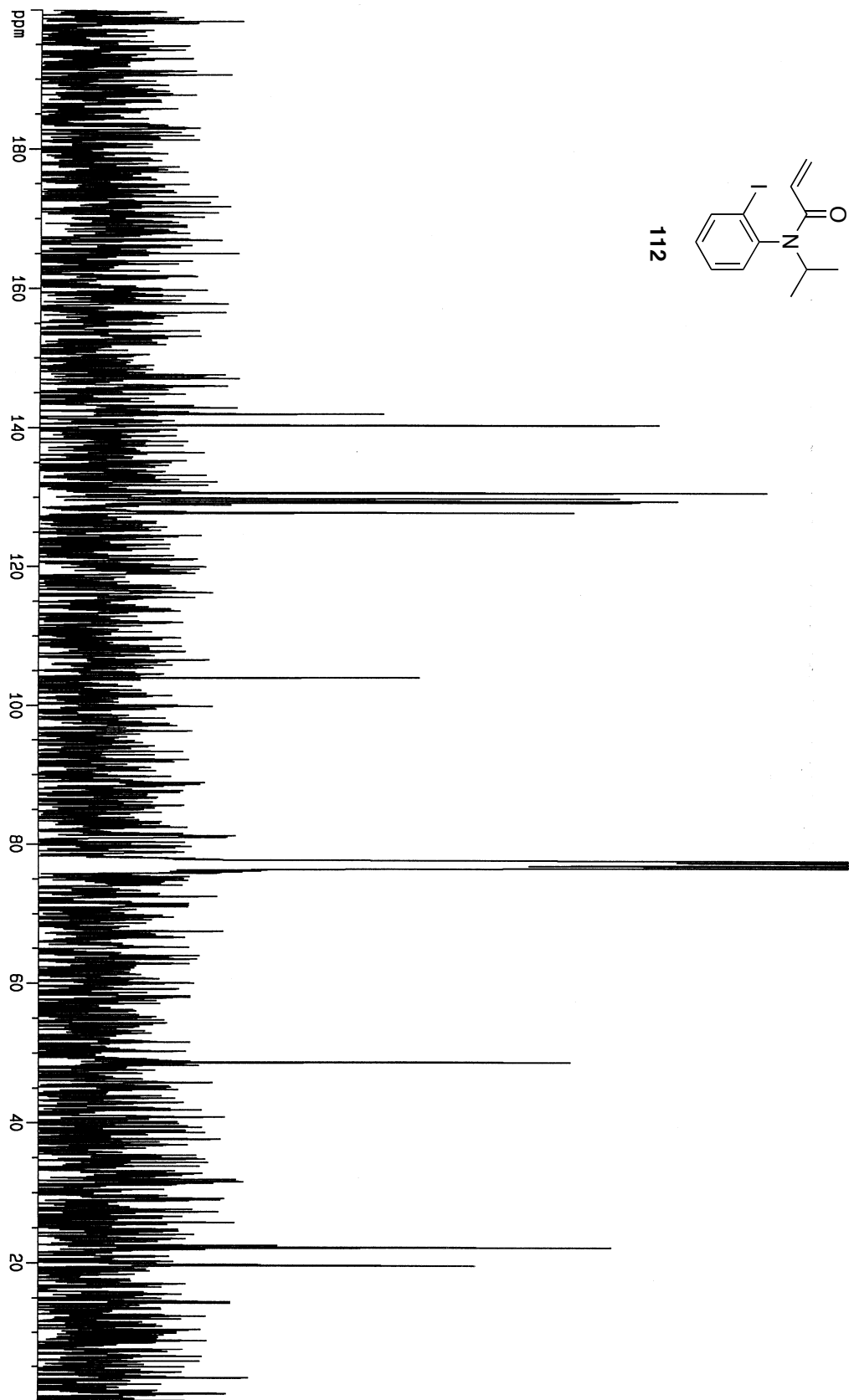
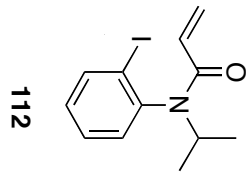


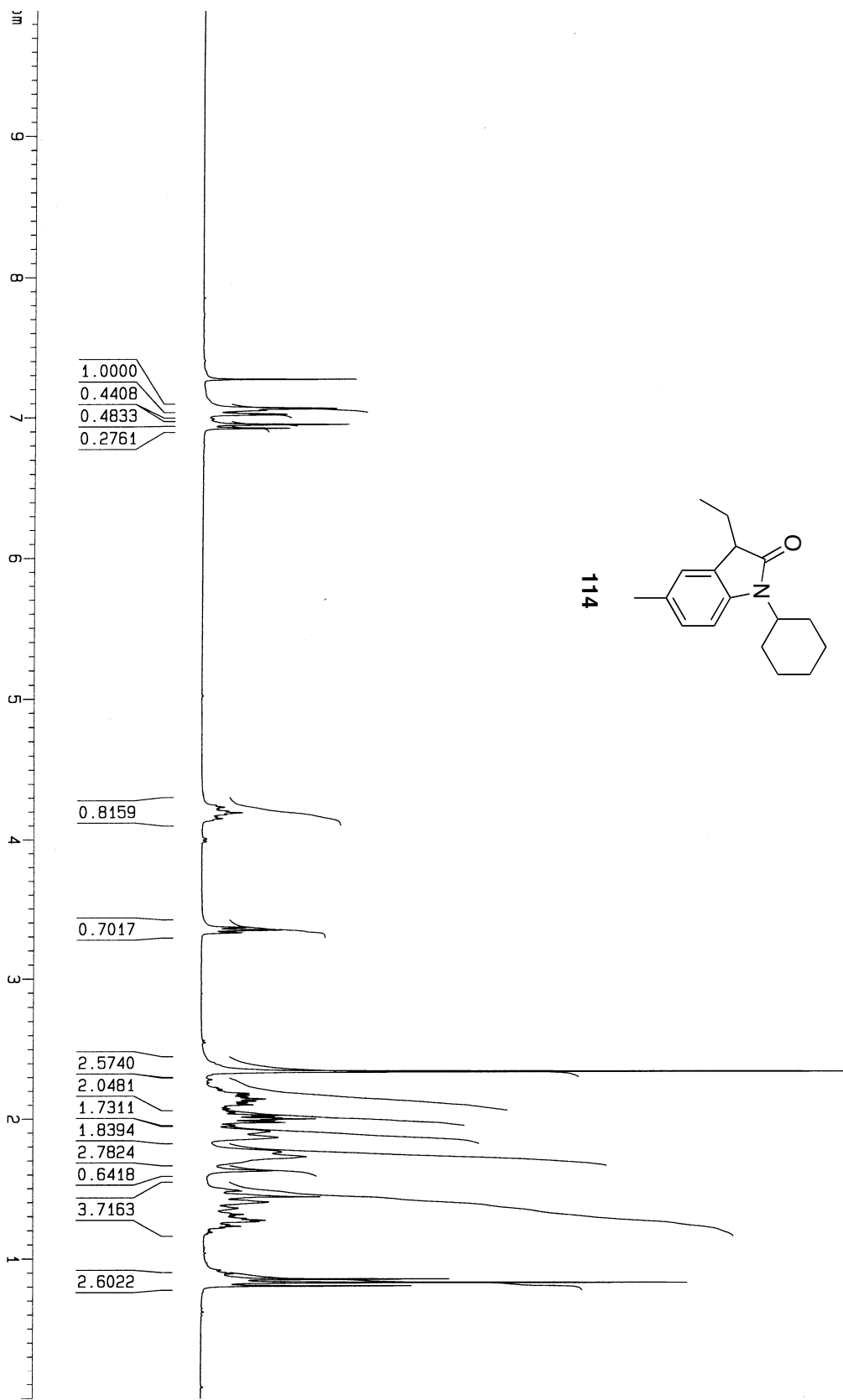


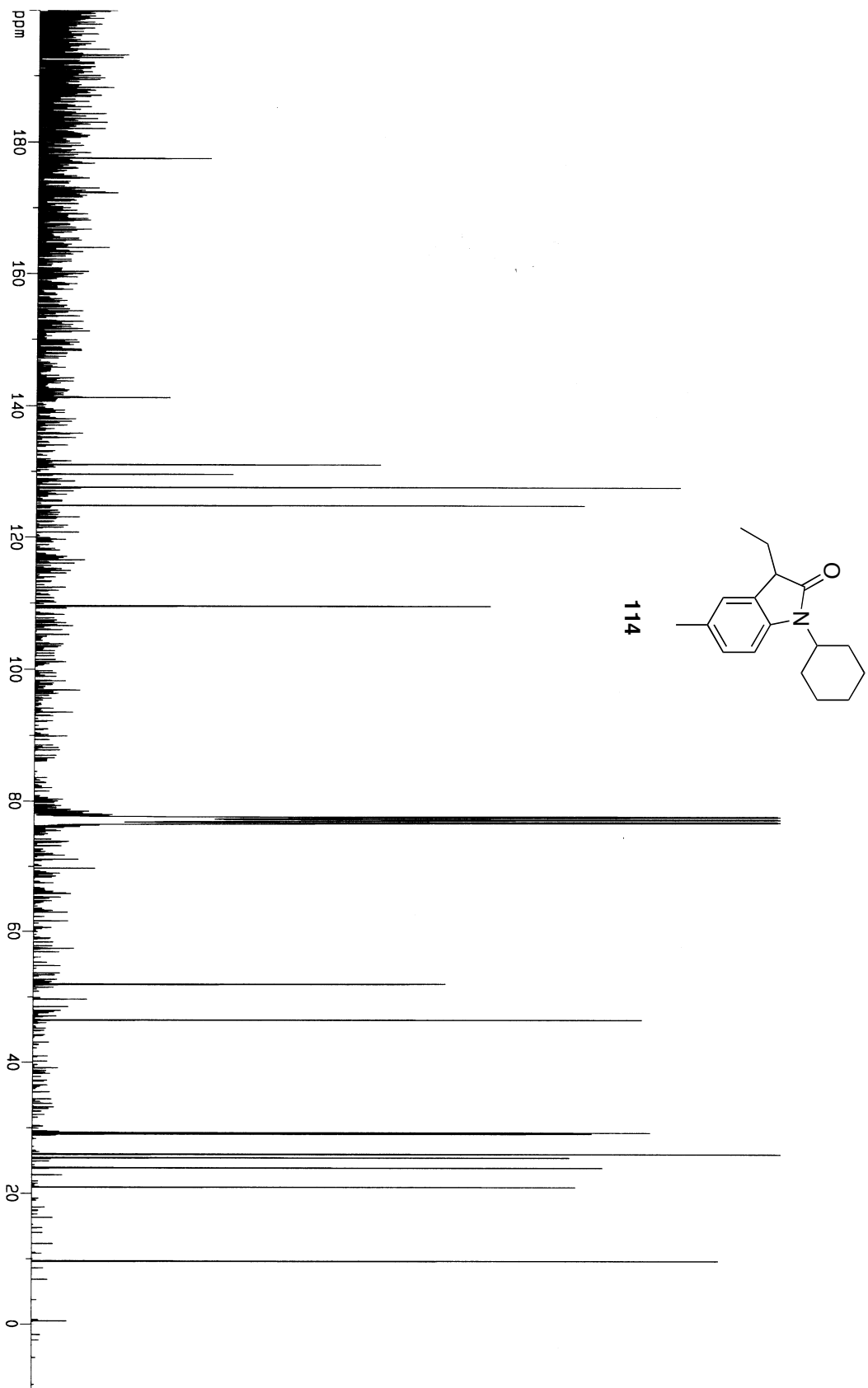


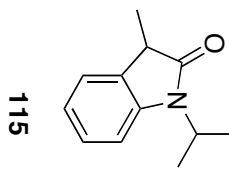
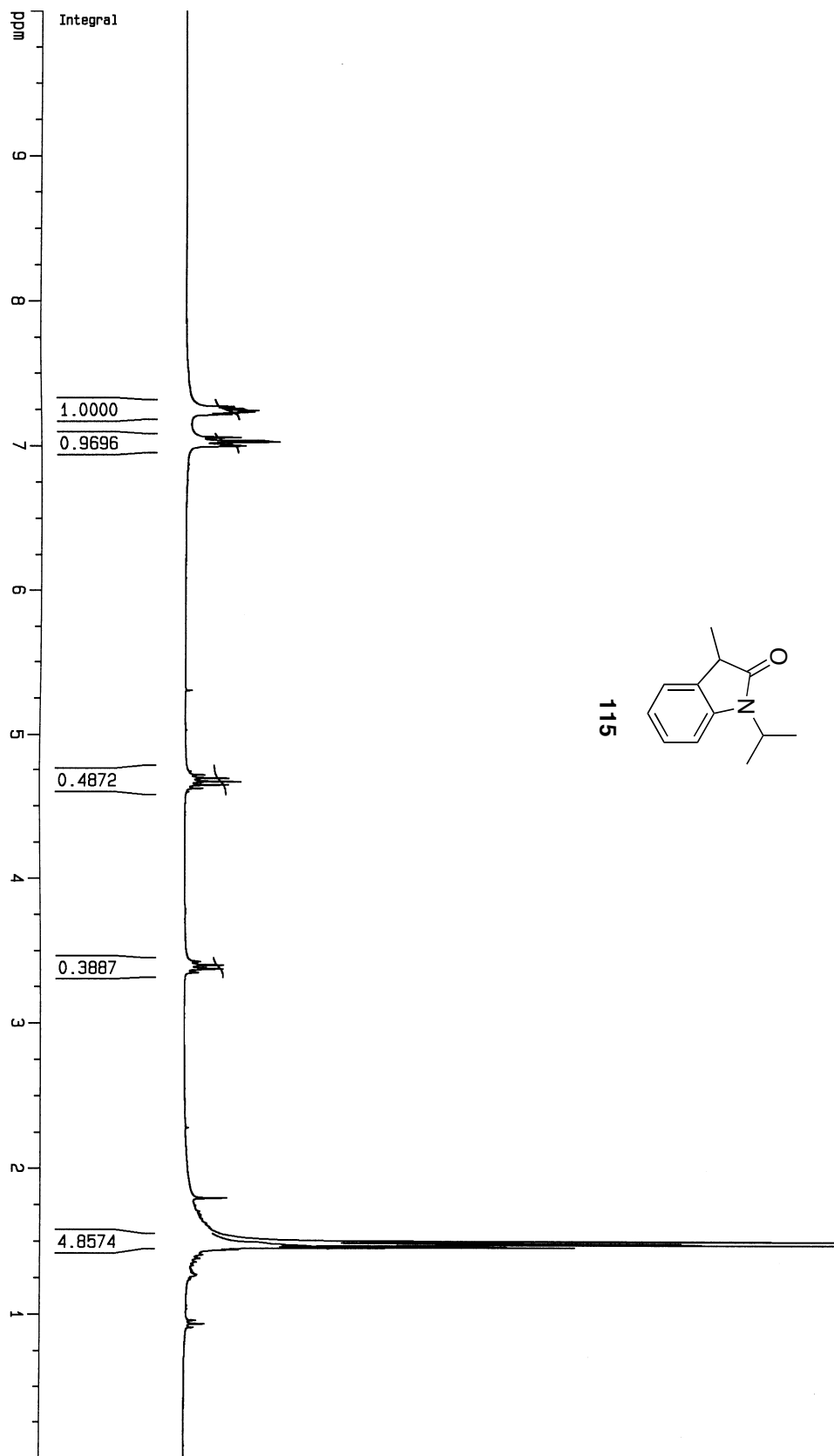
112

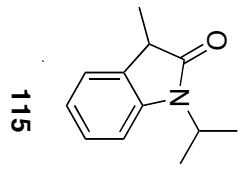
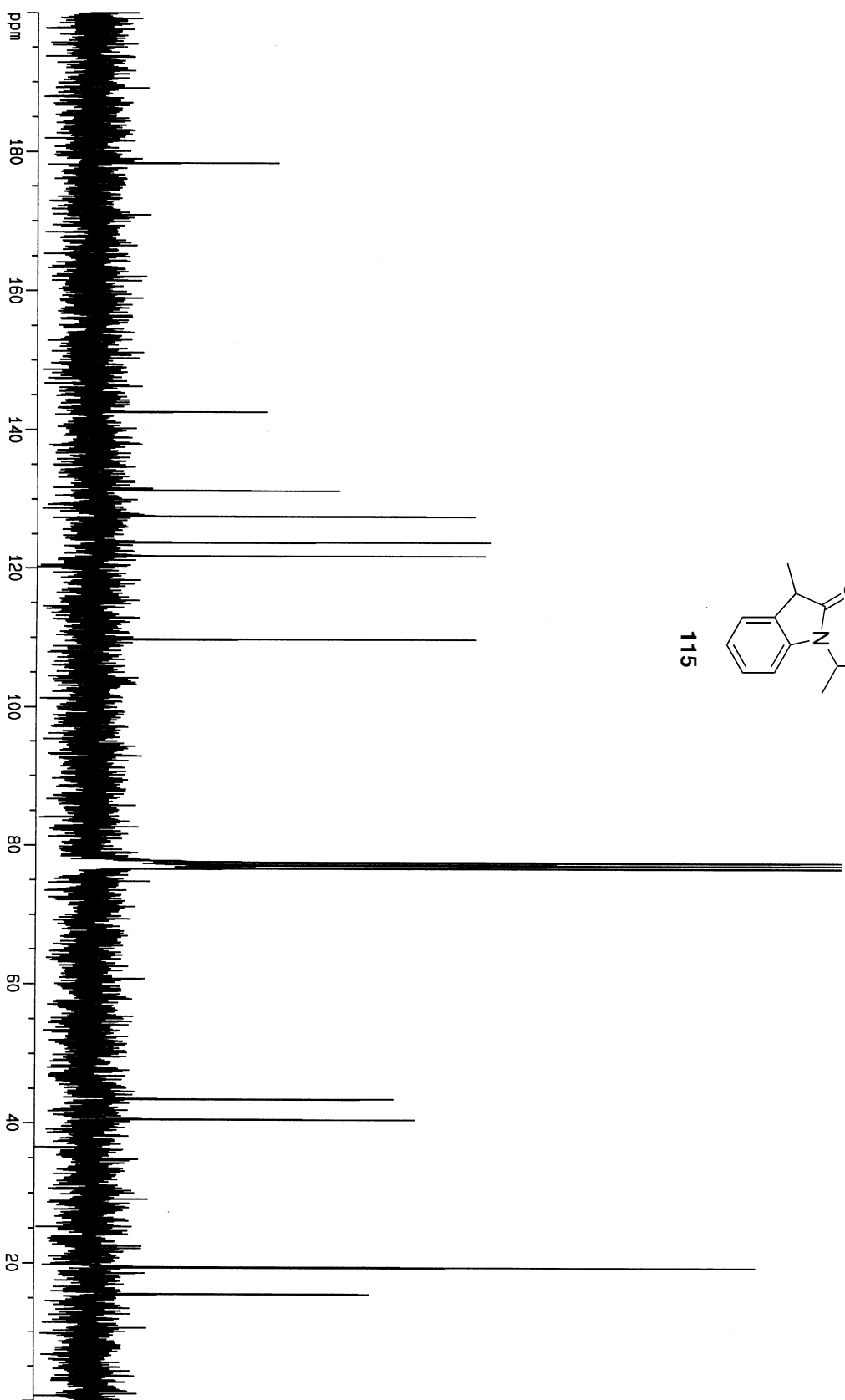


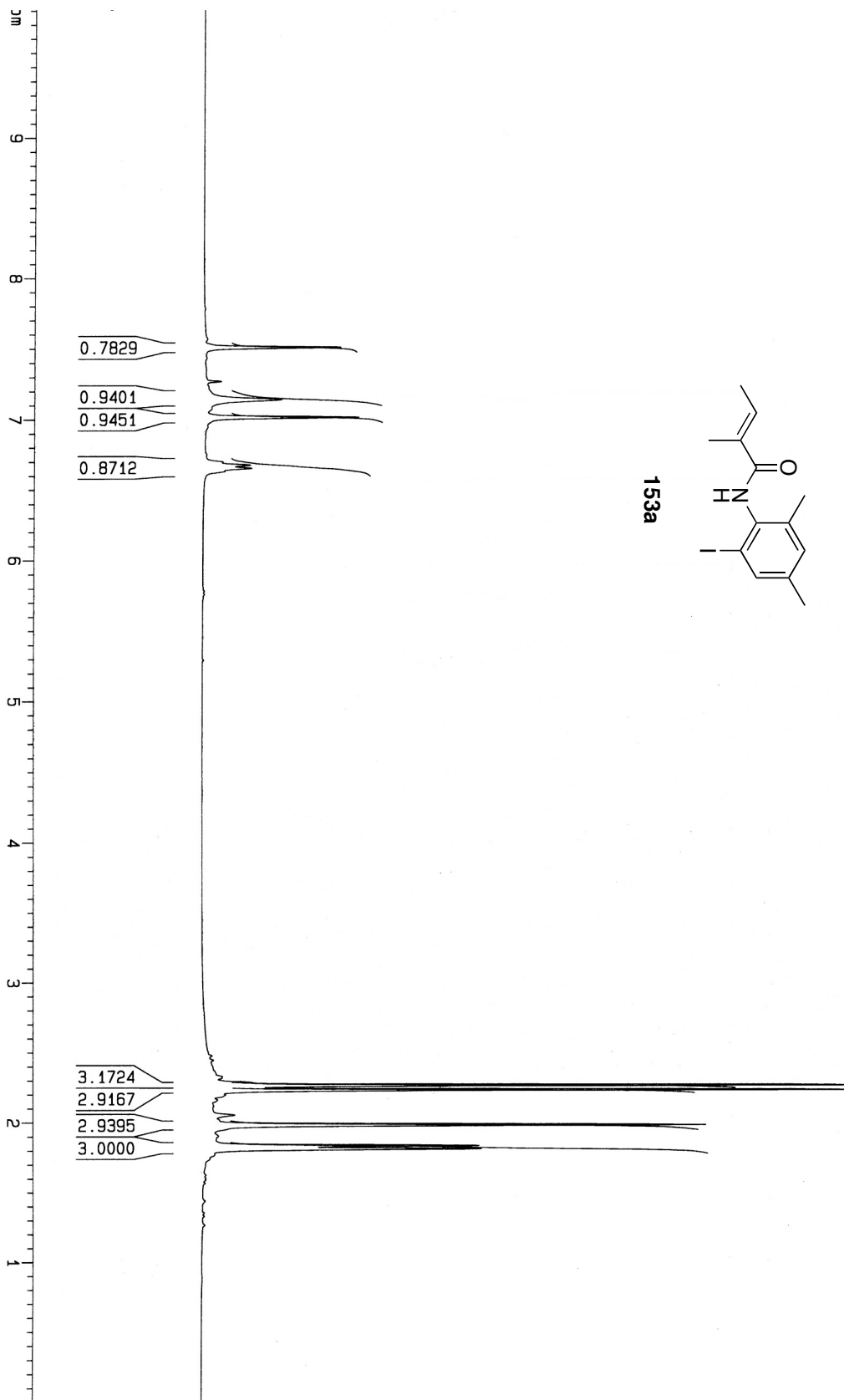


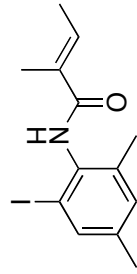






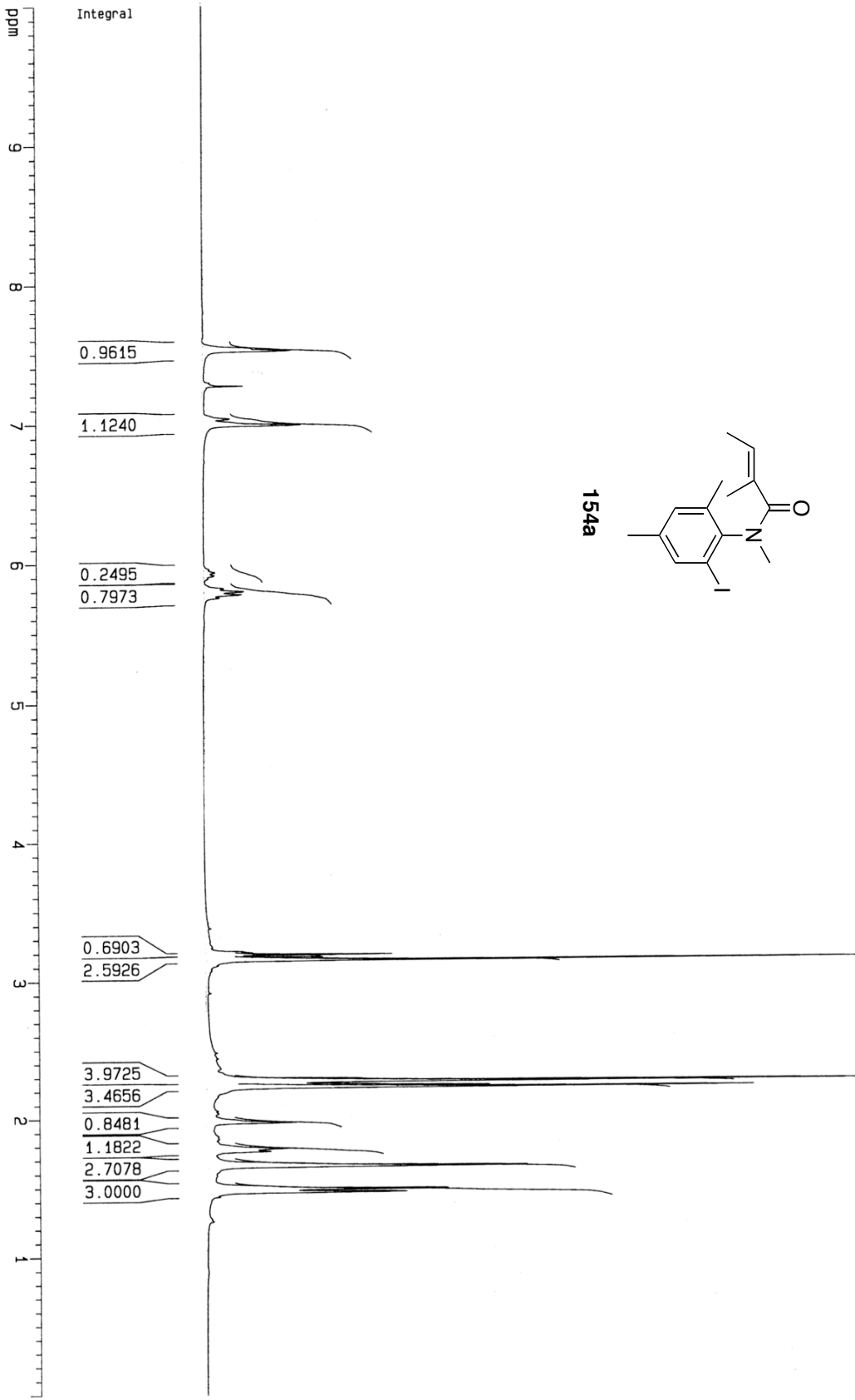


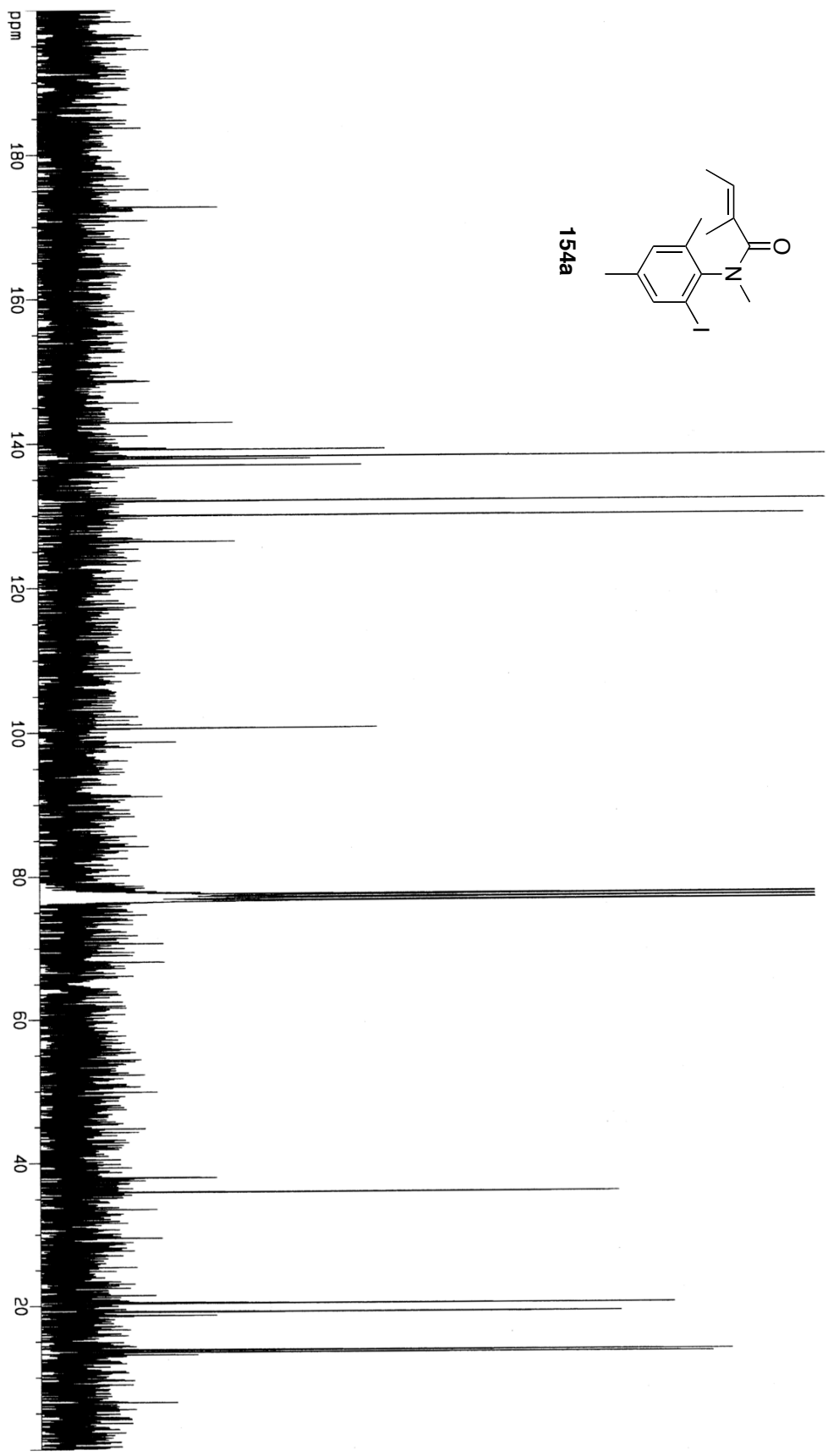


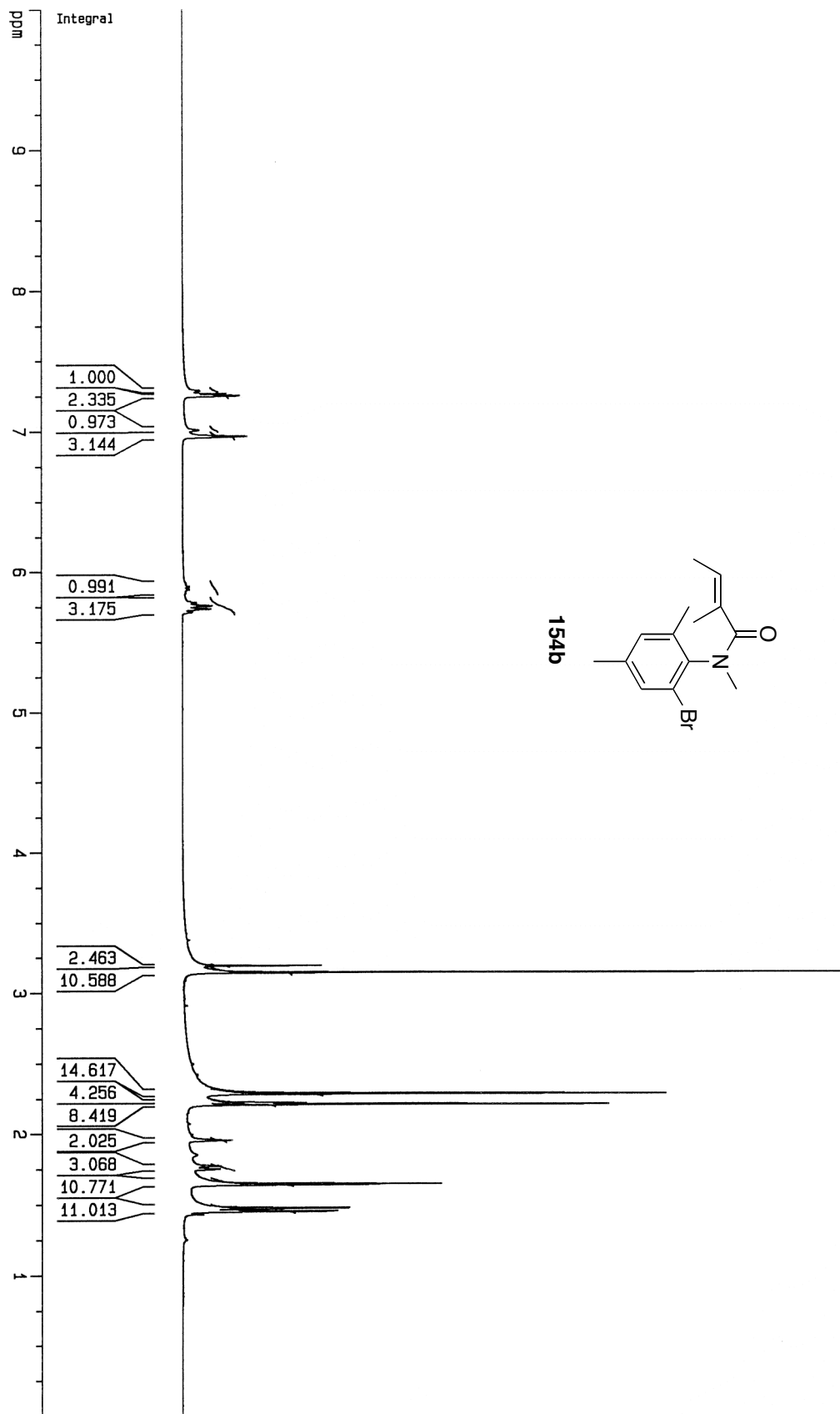


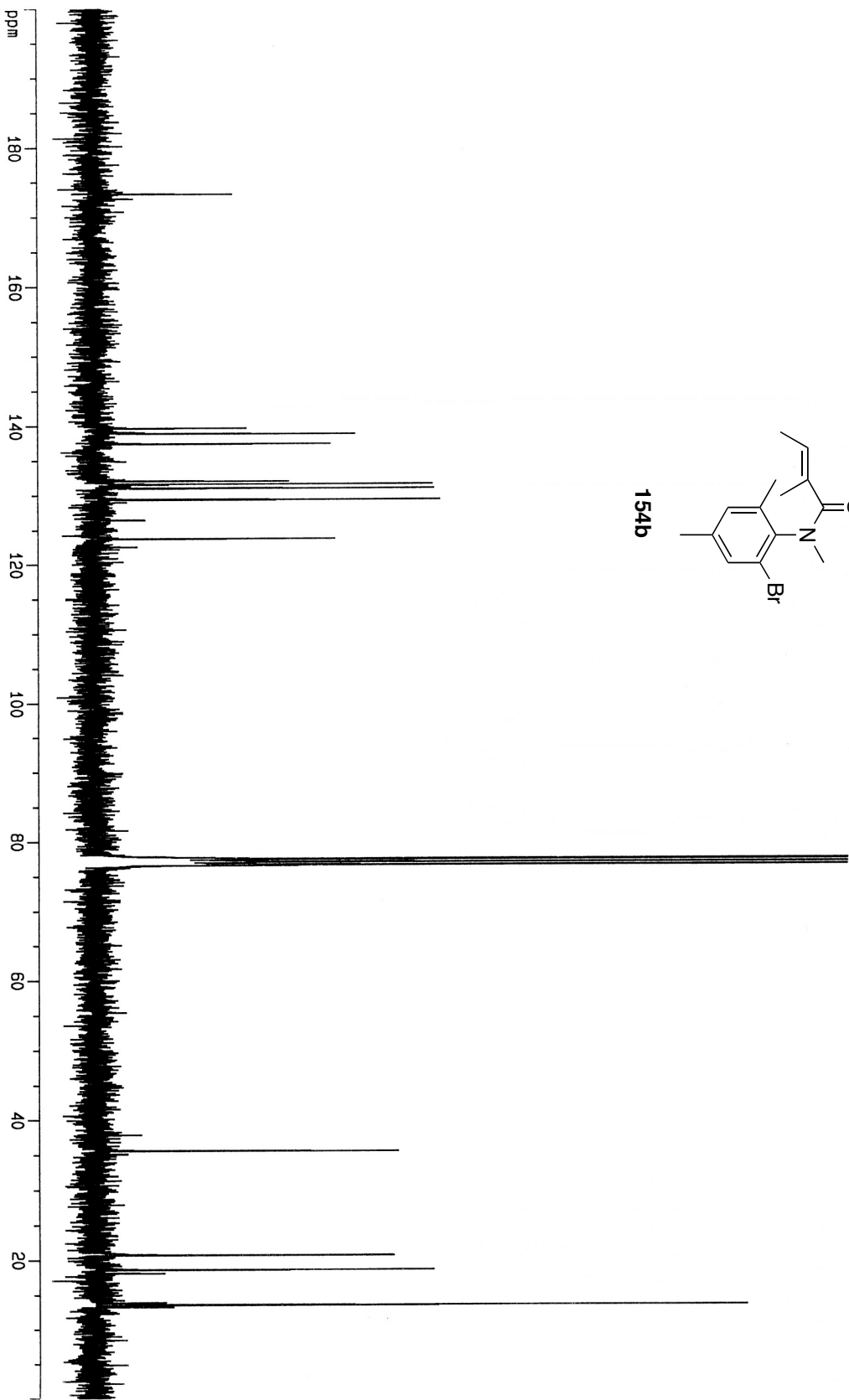
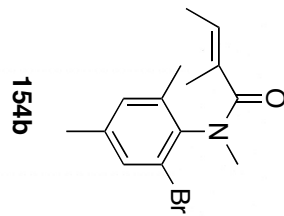
153a

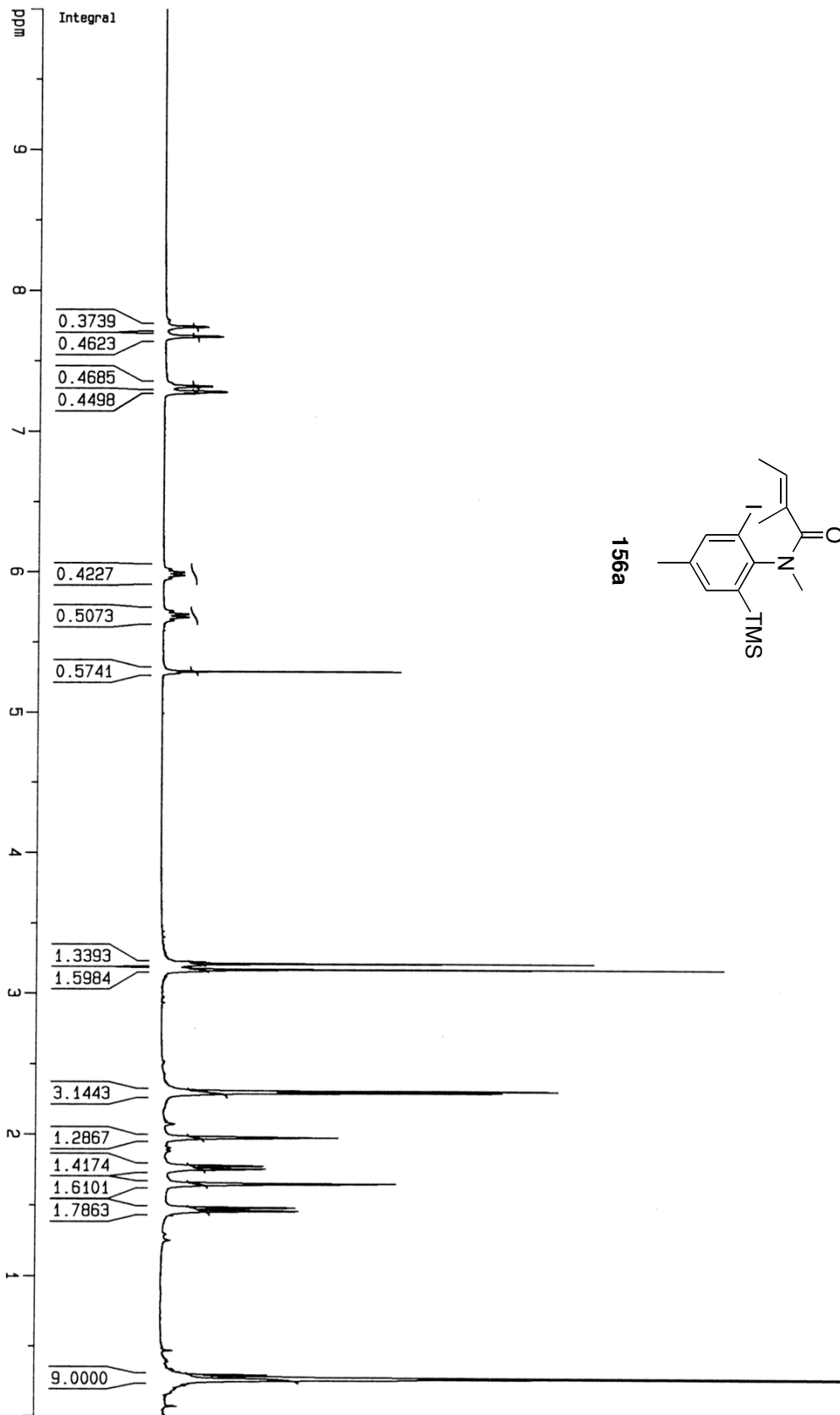


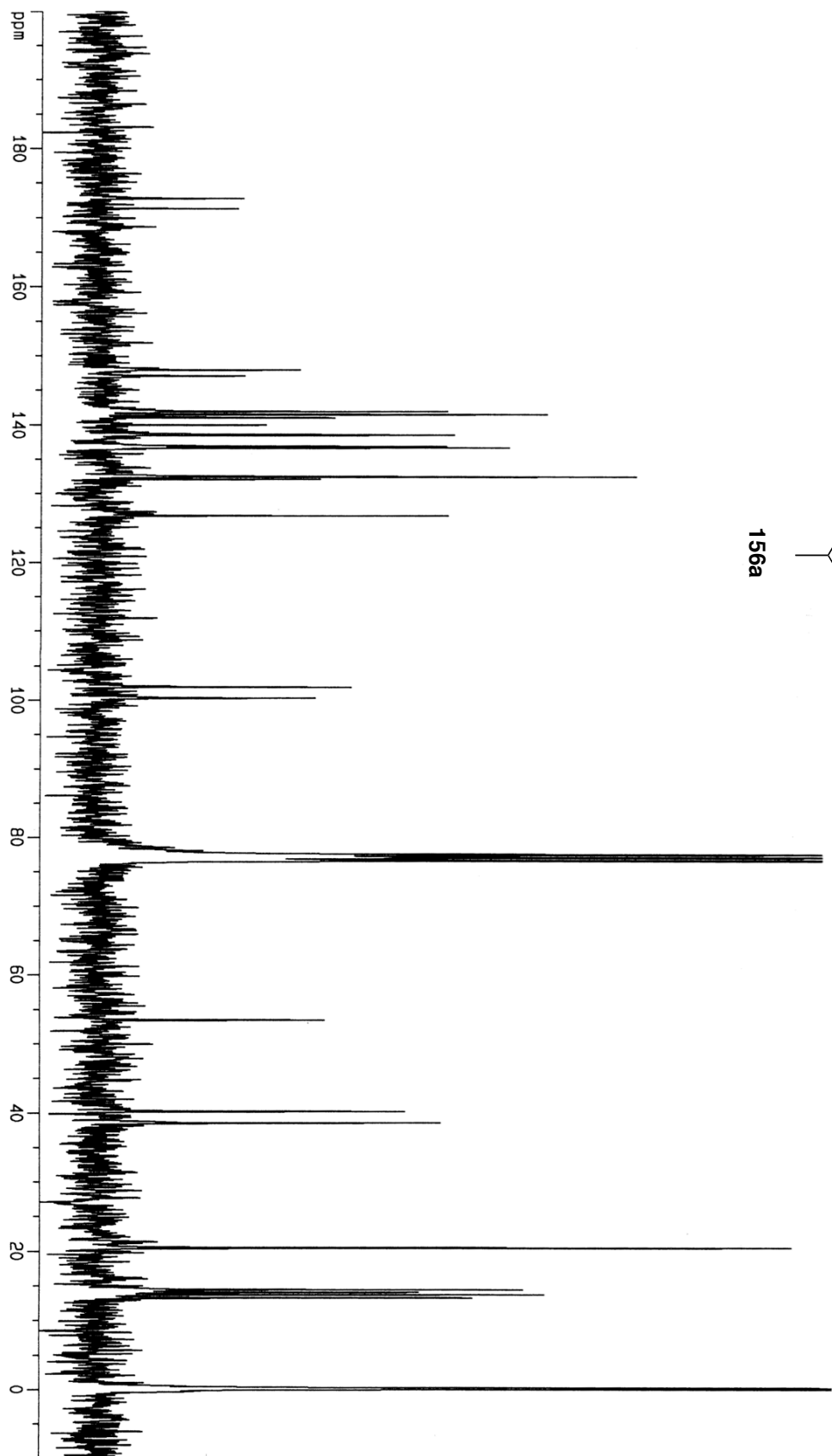
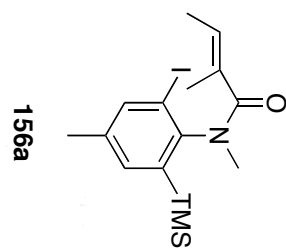


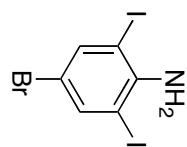
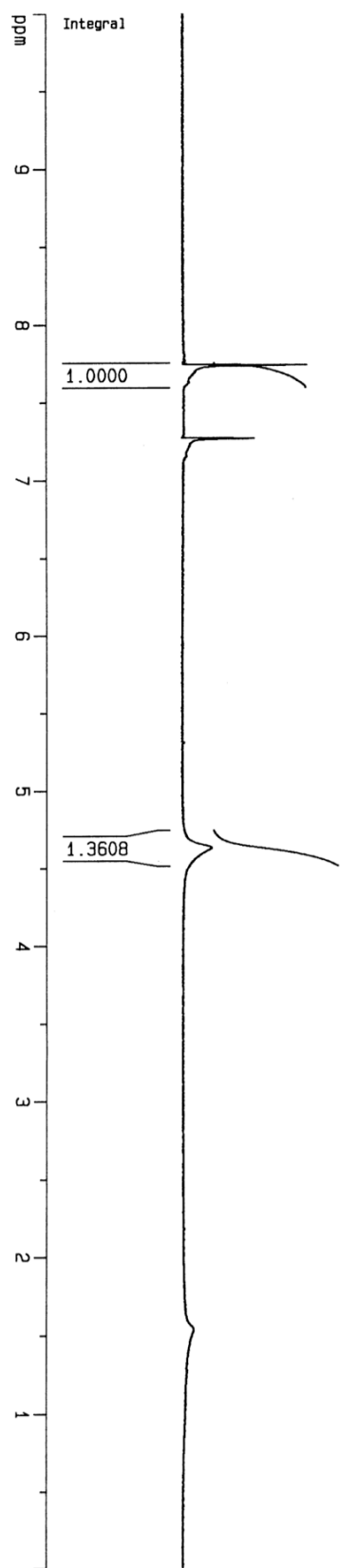


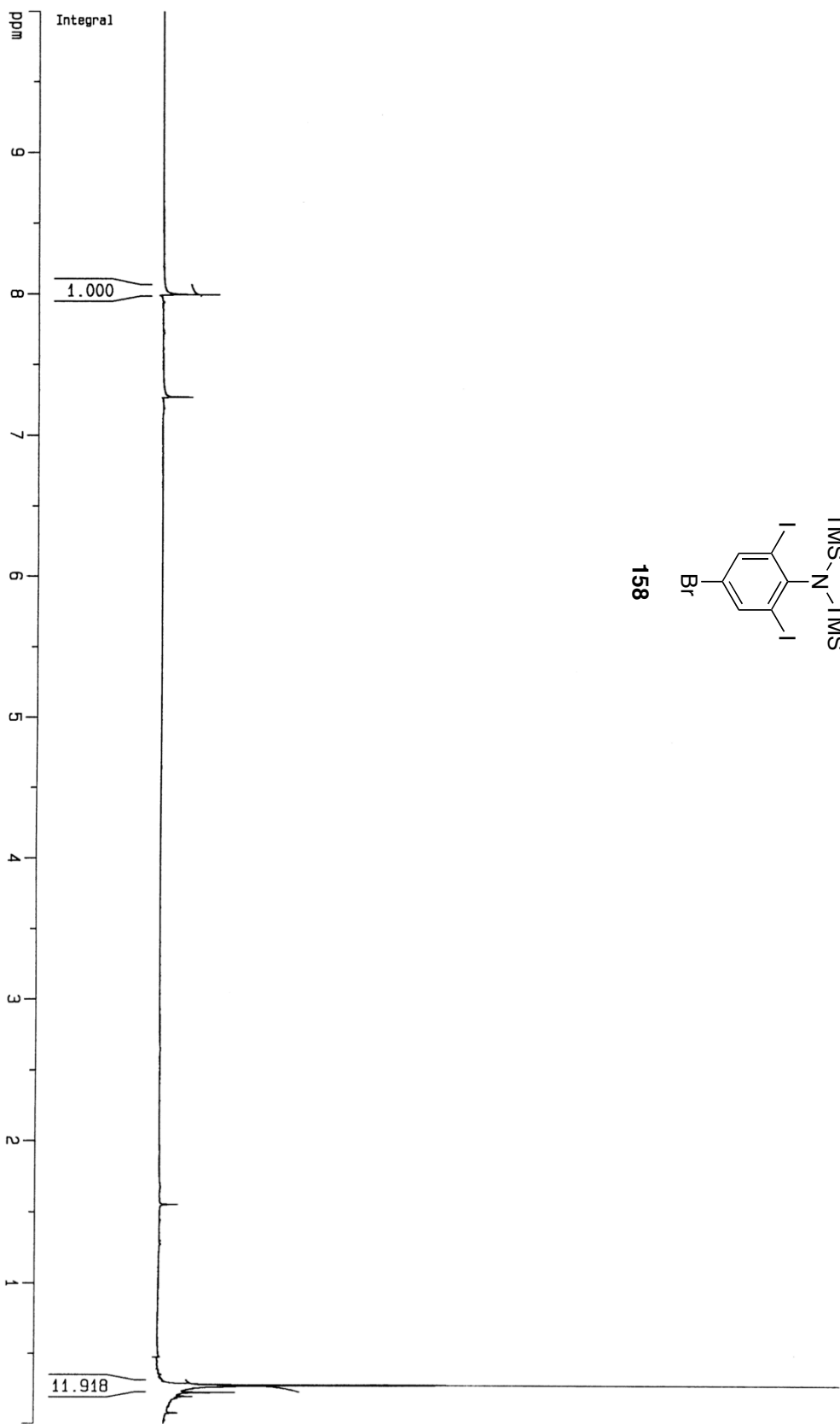


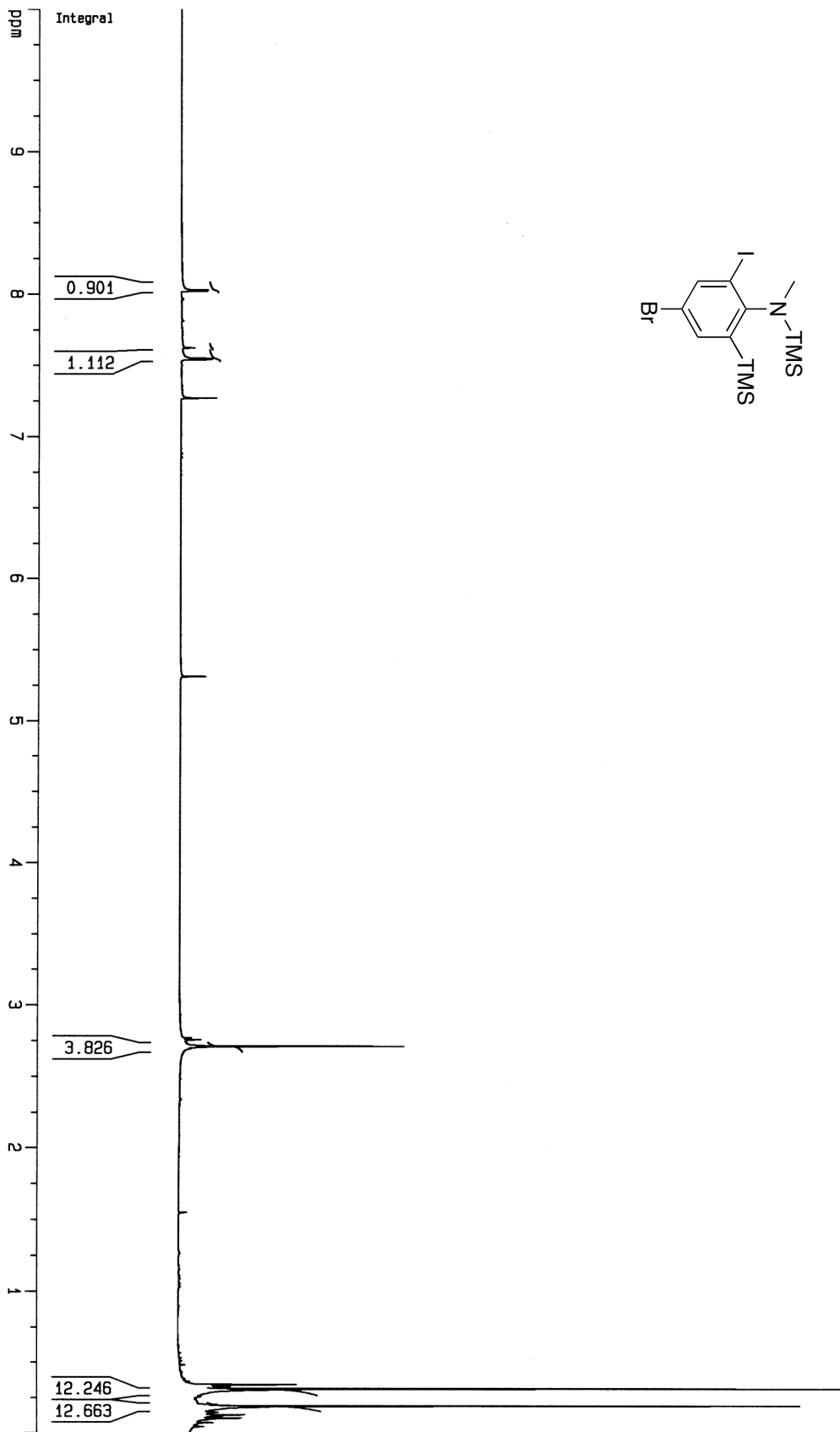


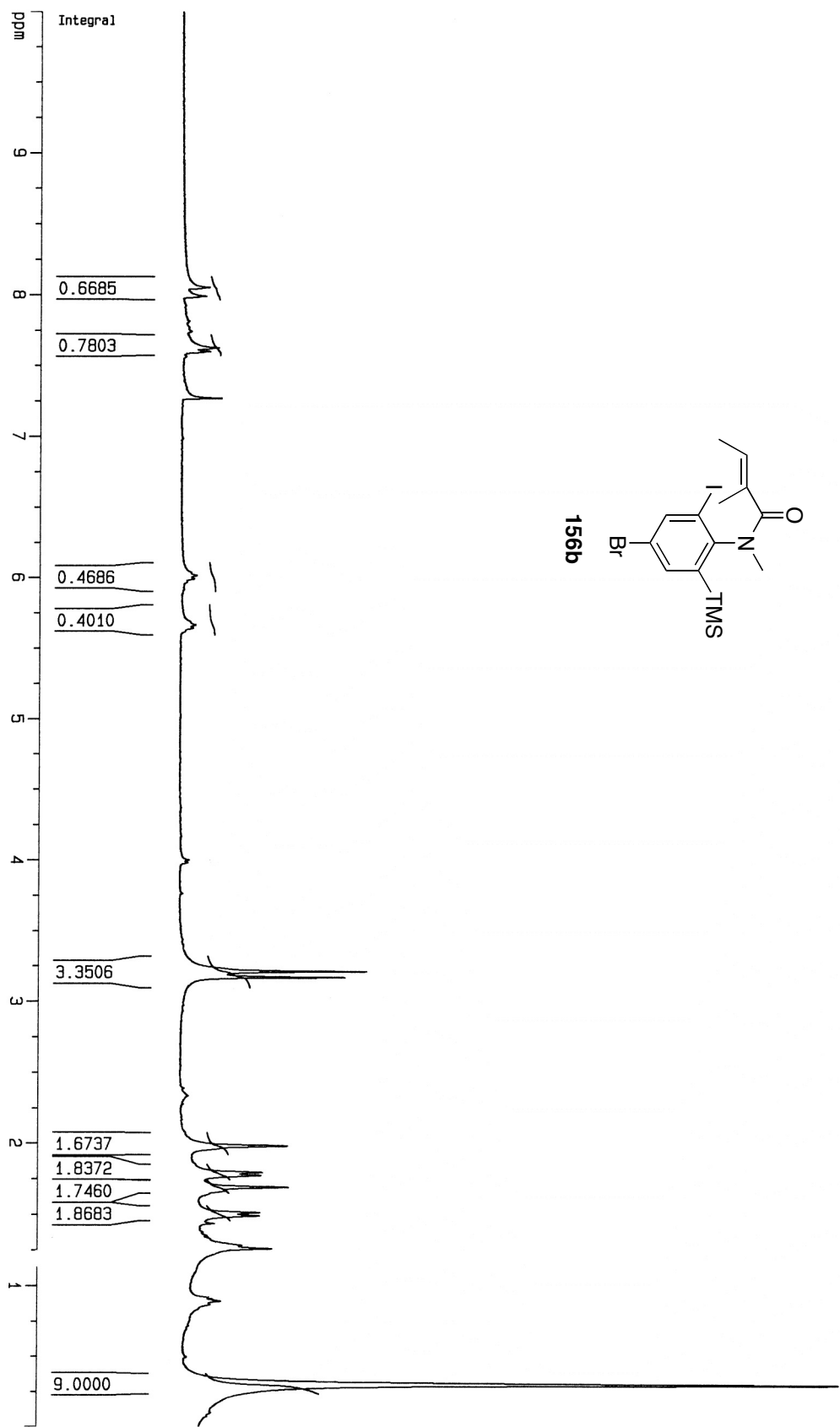


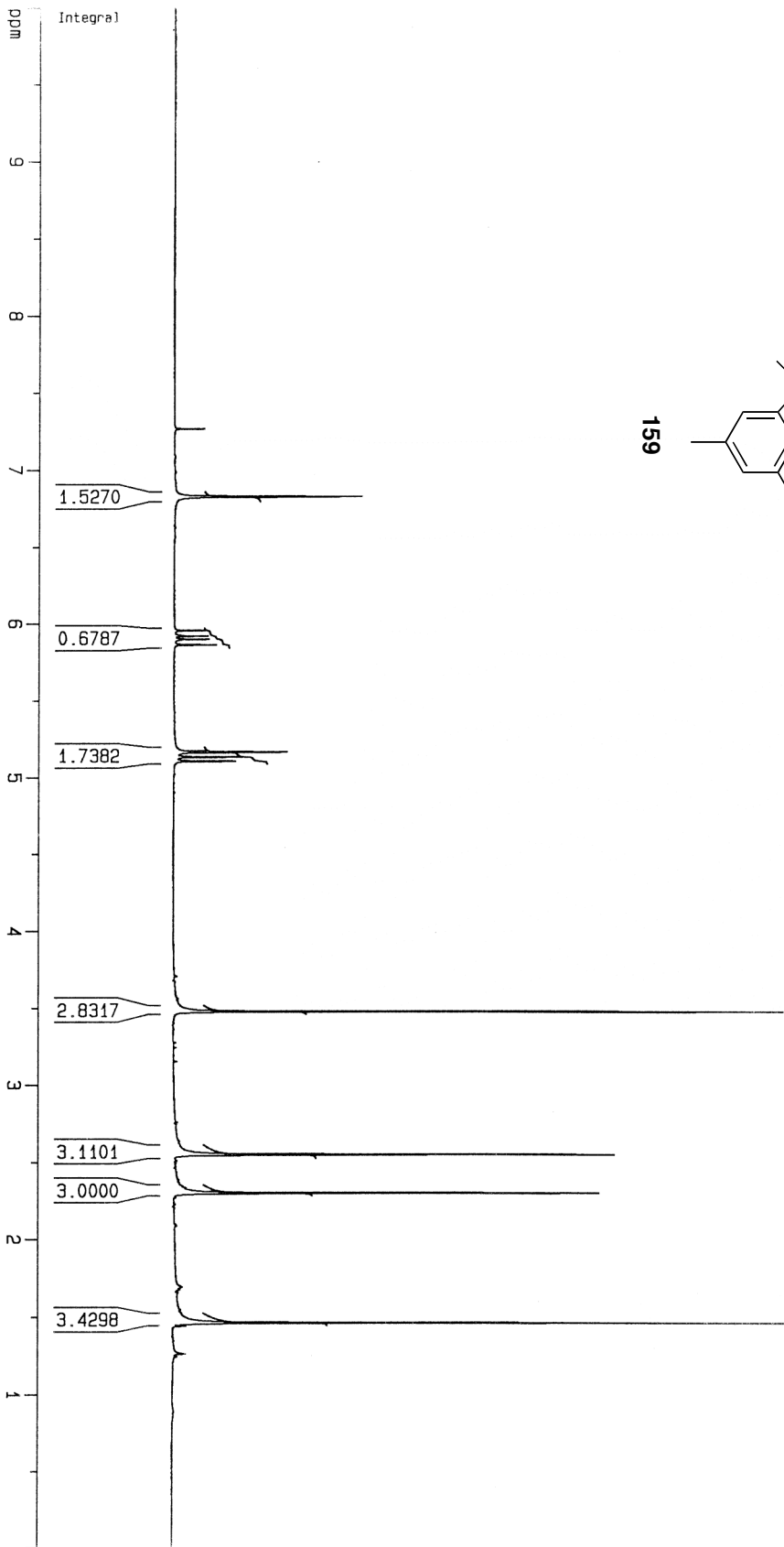




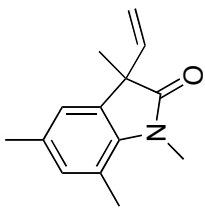


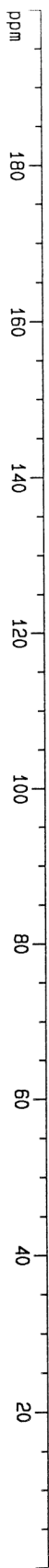
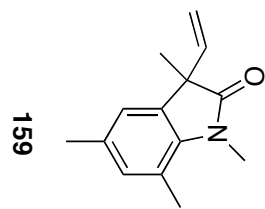


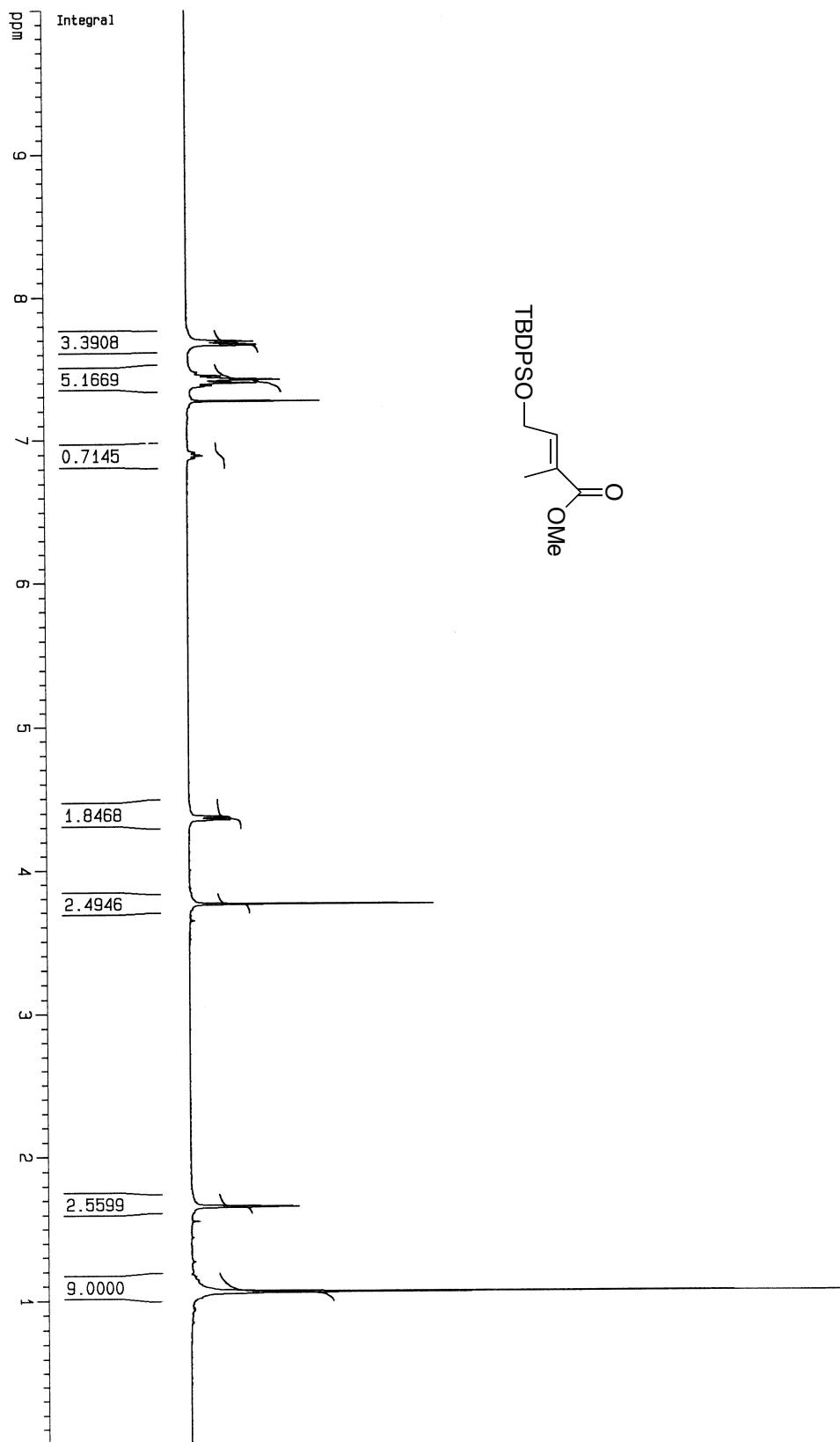


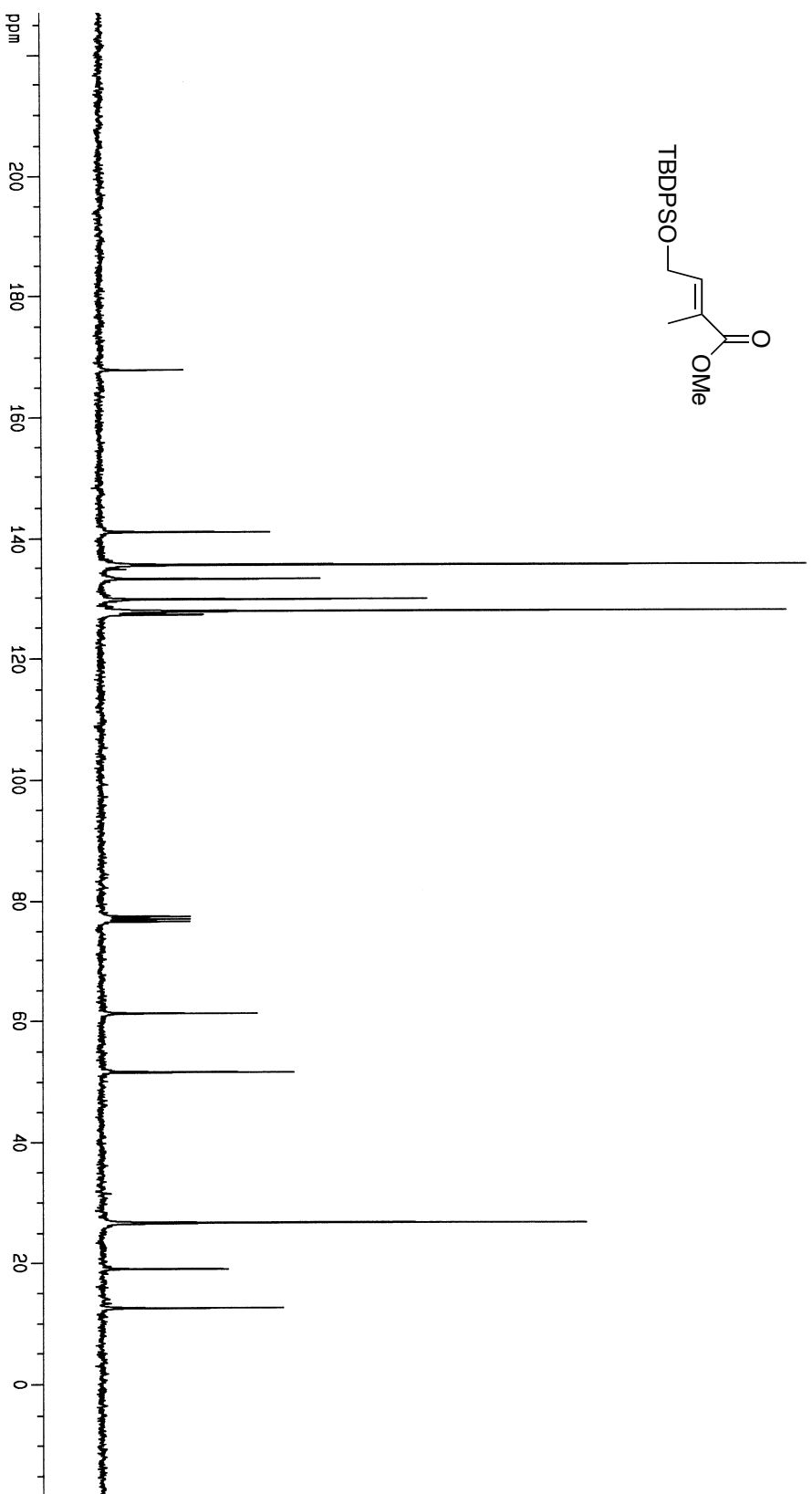
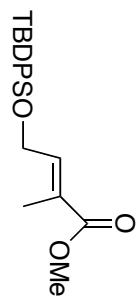


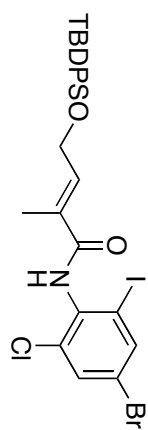
159





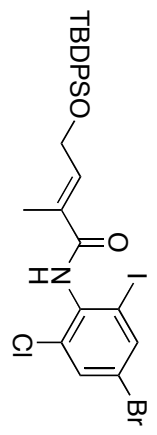




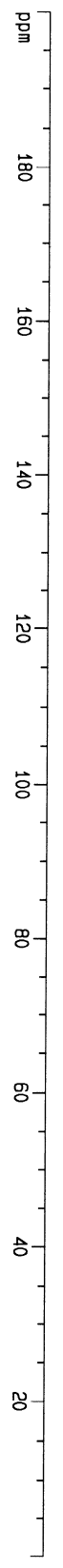


169



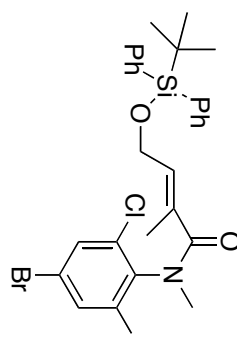


169

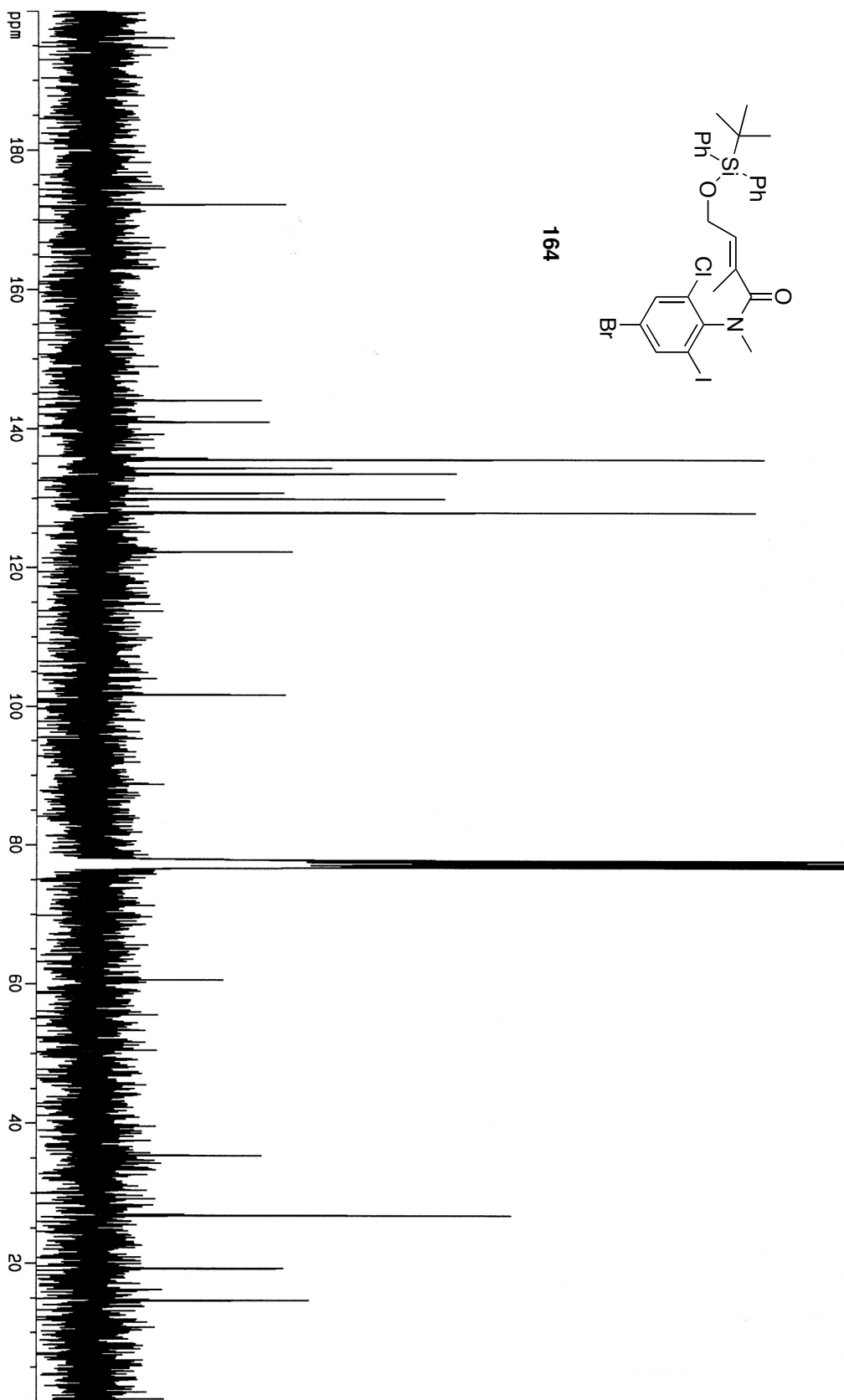


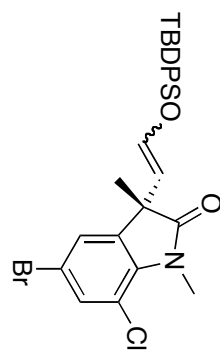


164

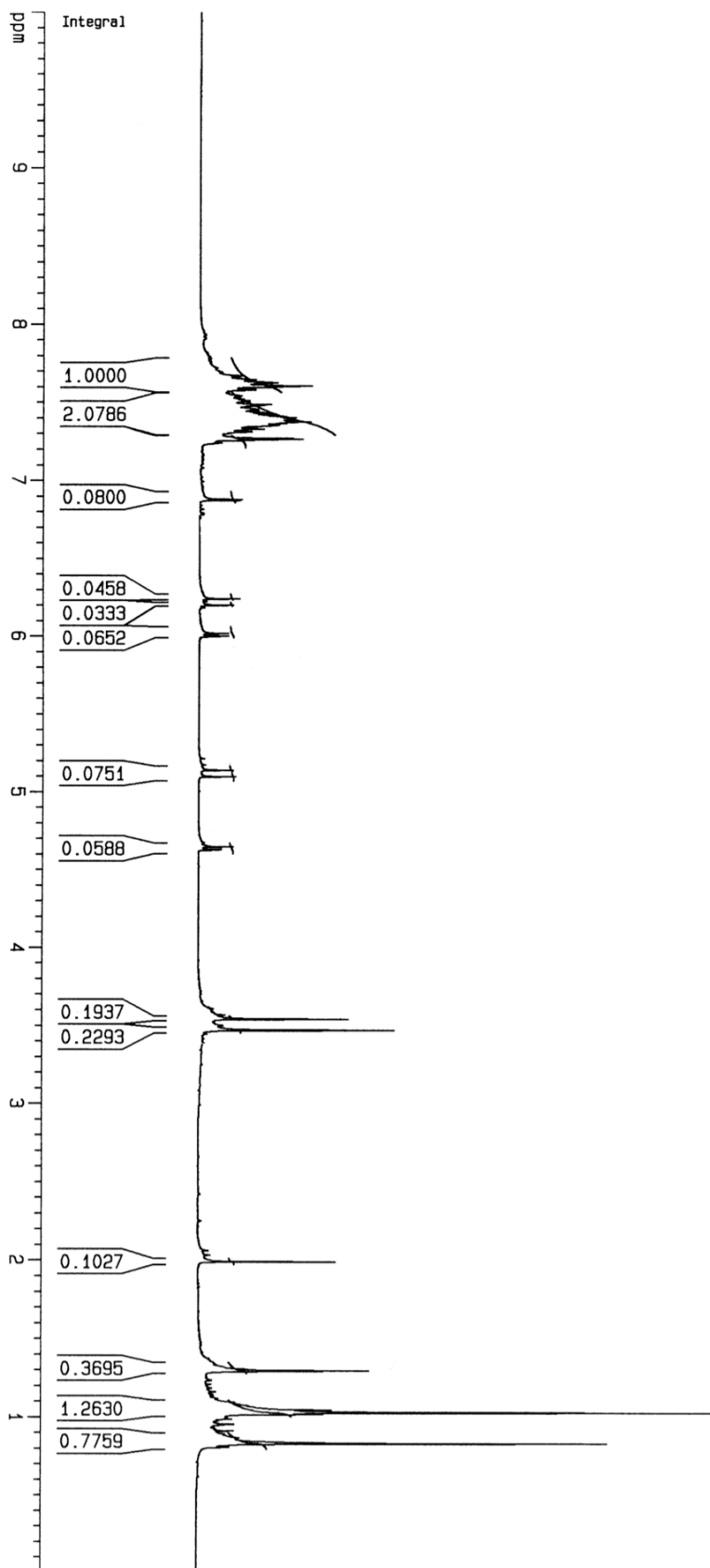


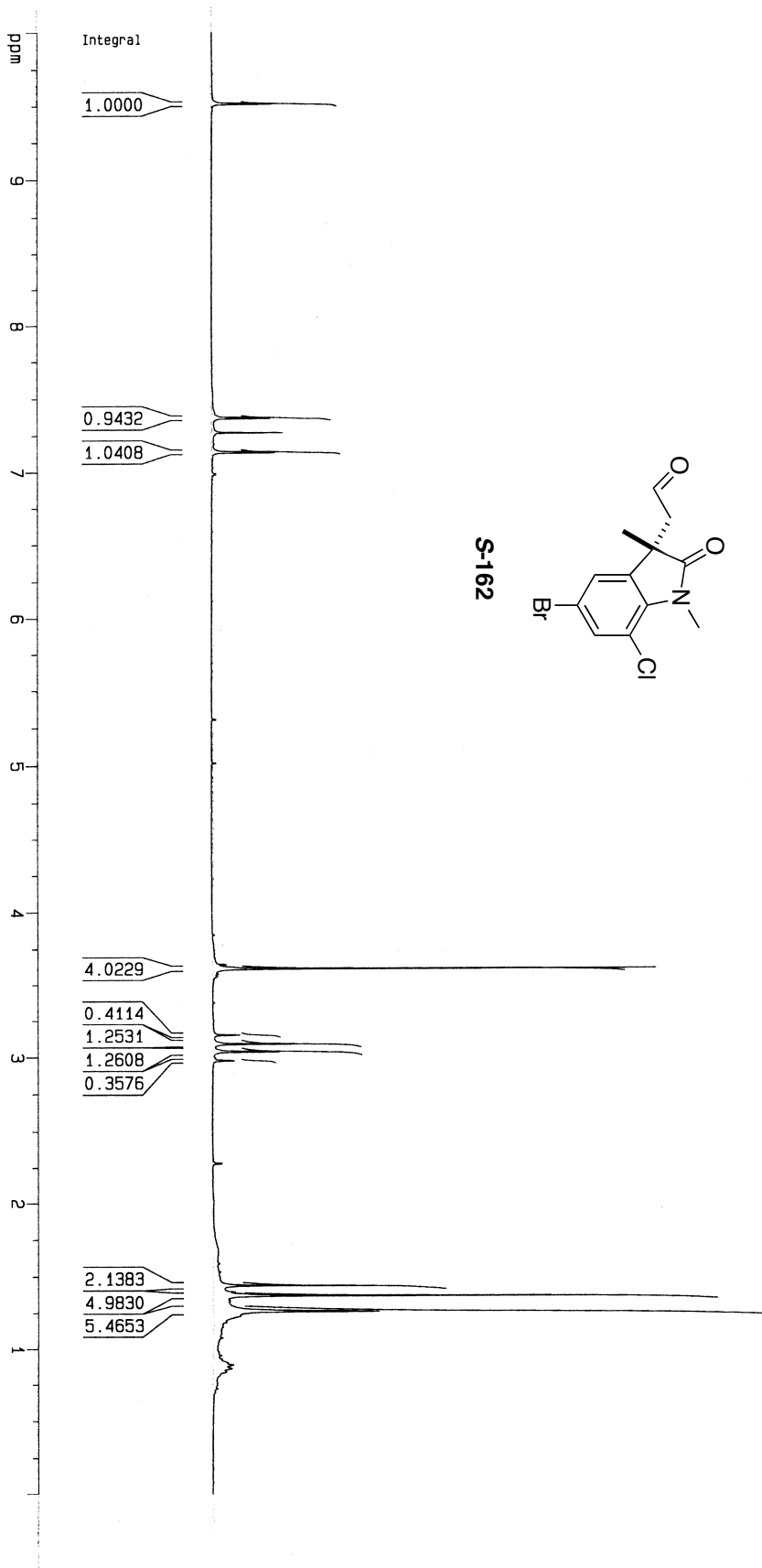
164

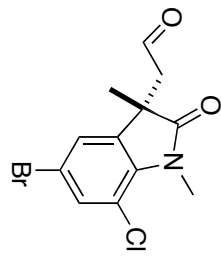




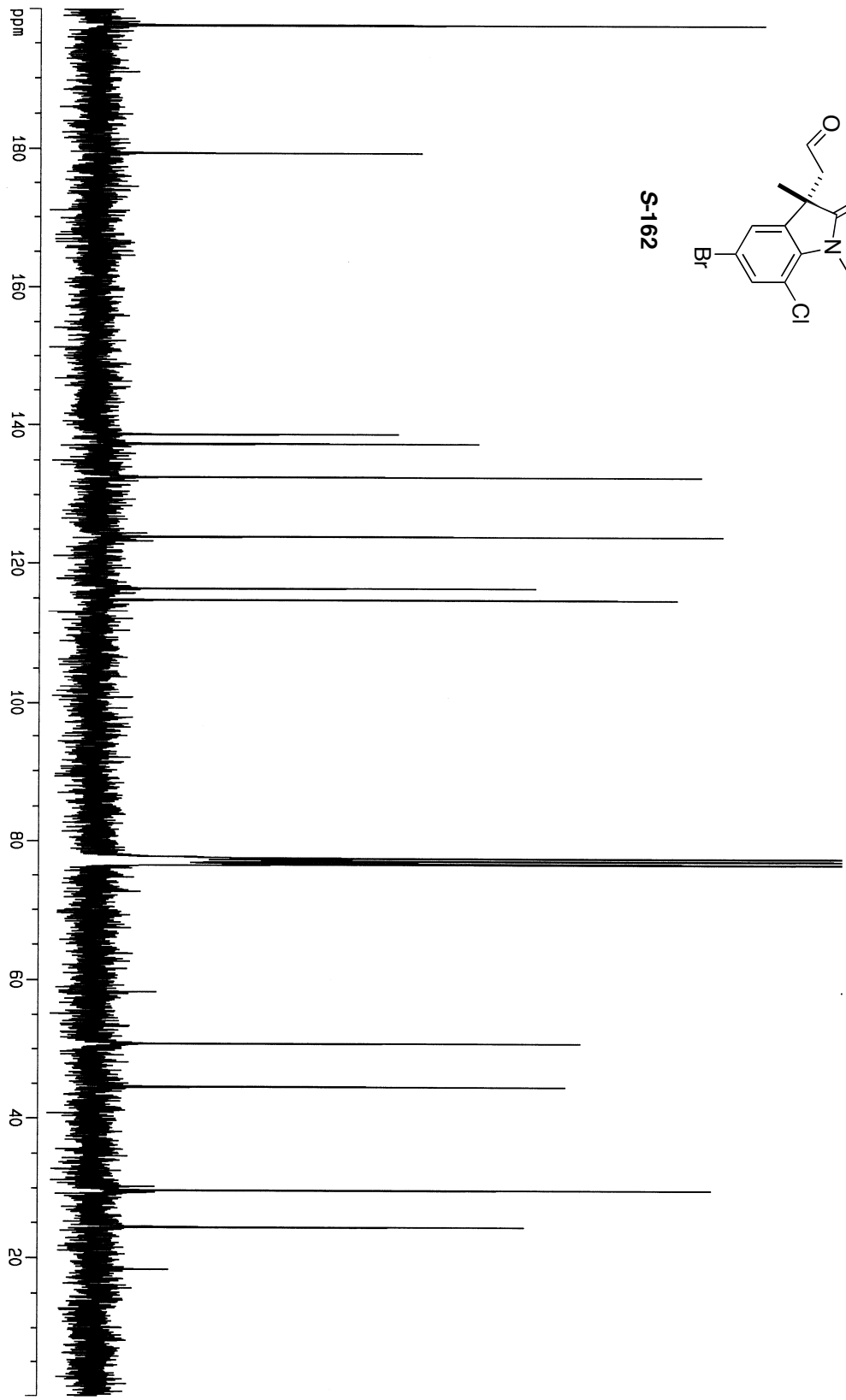
S-170

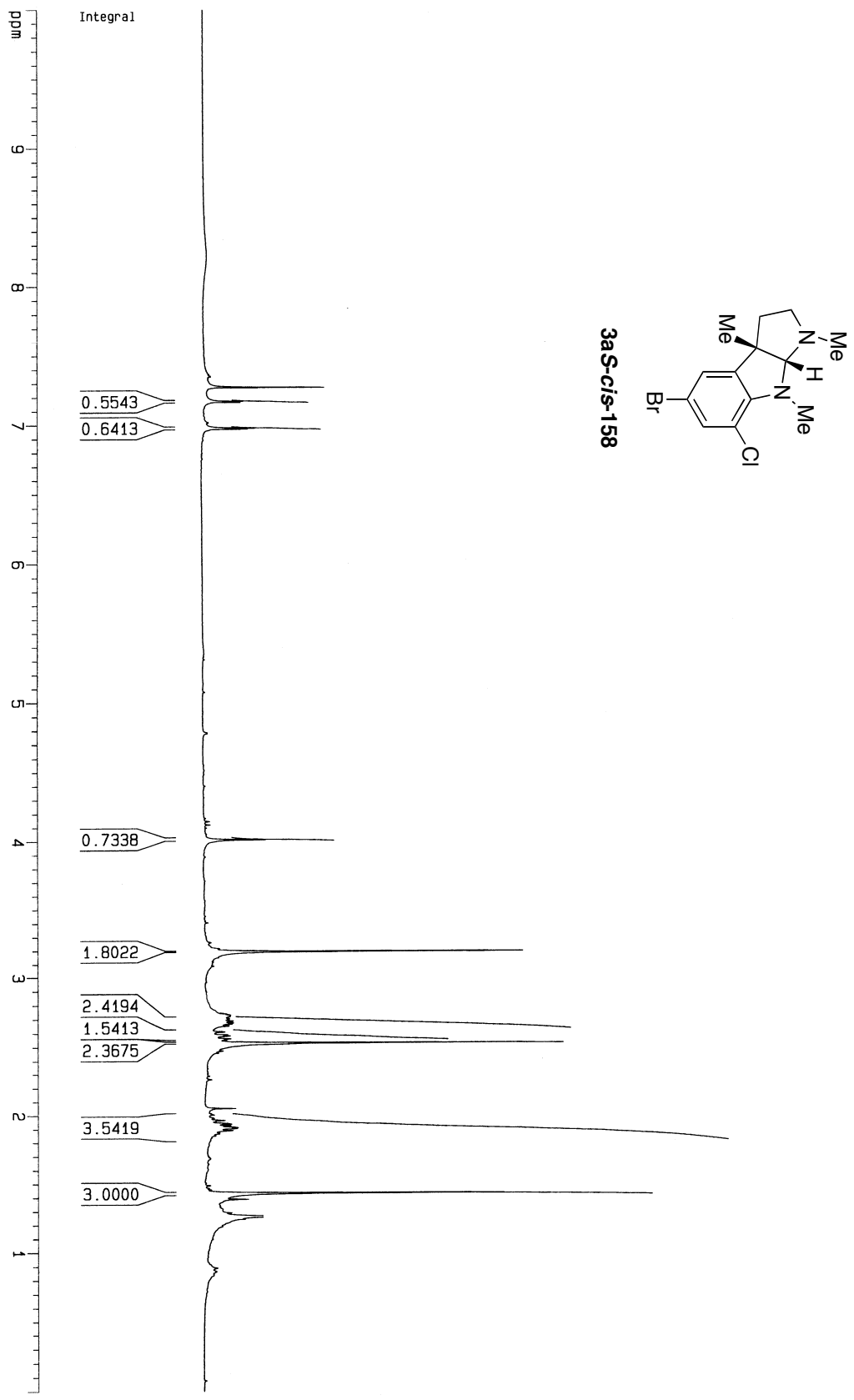


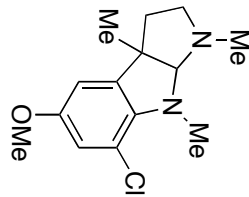
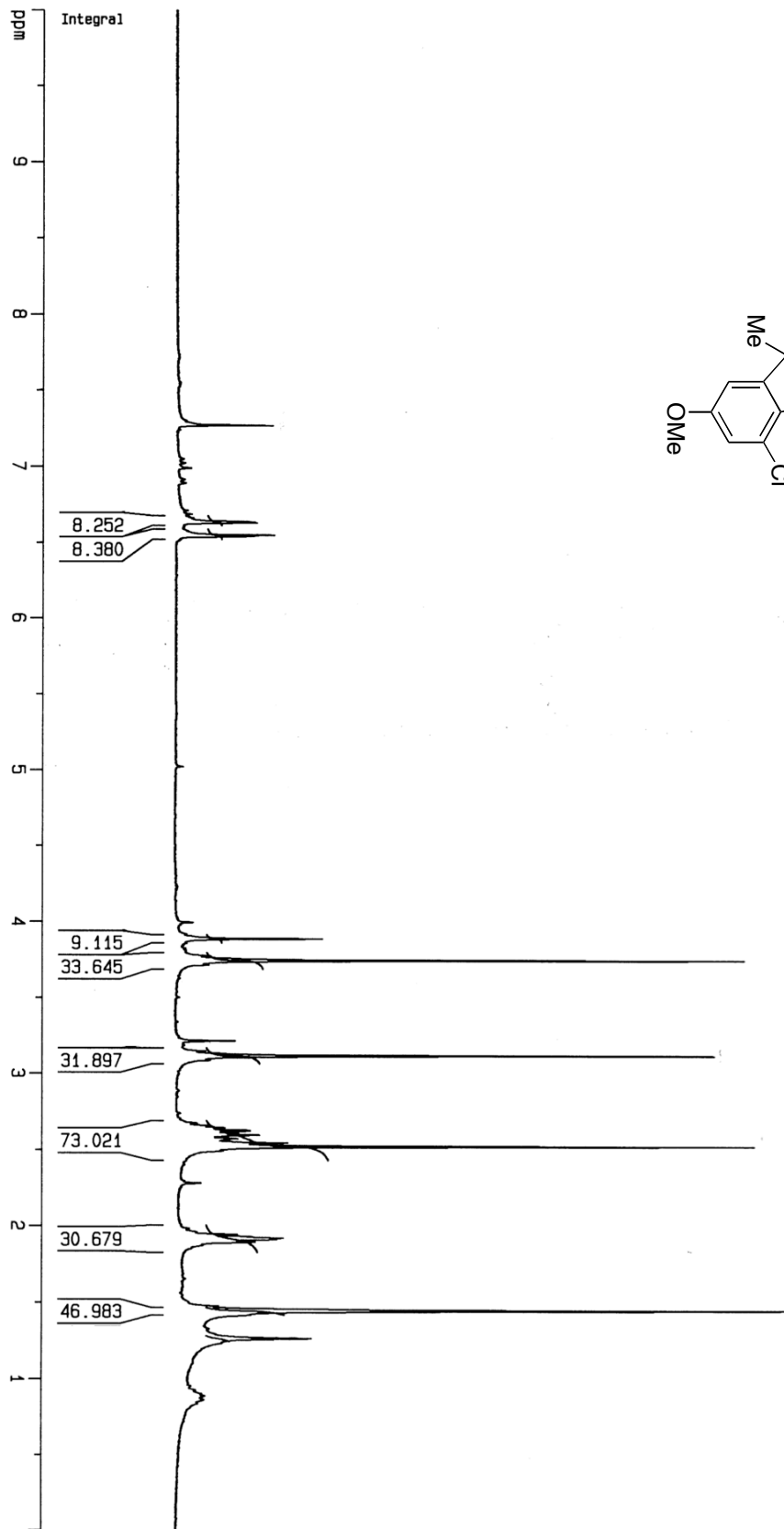


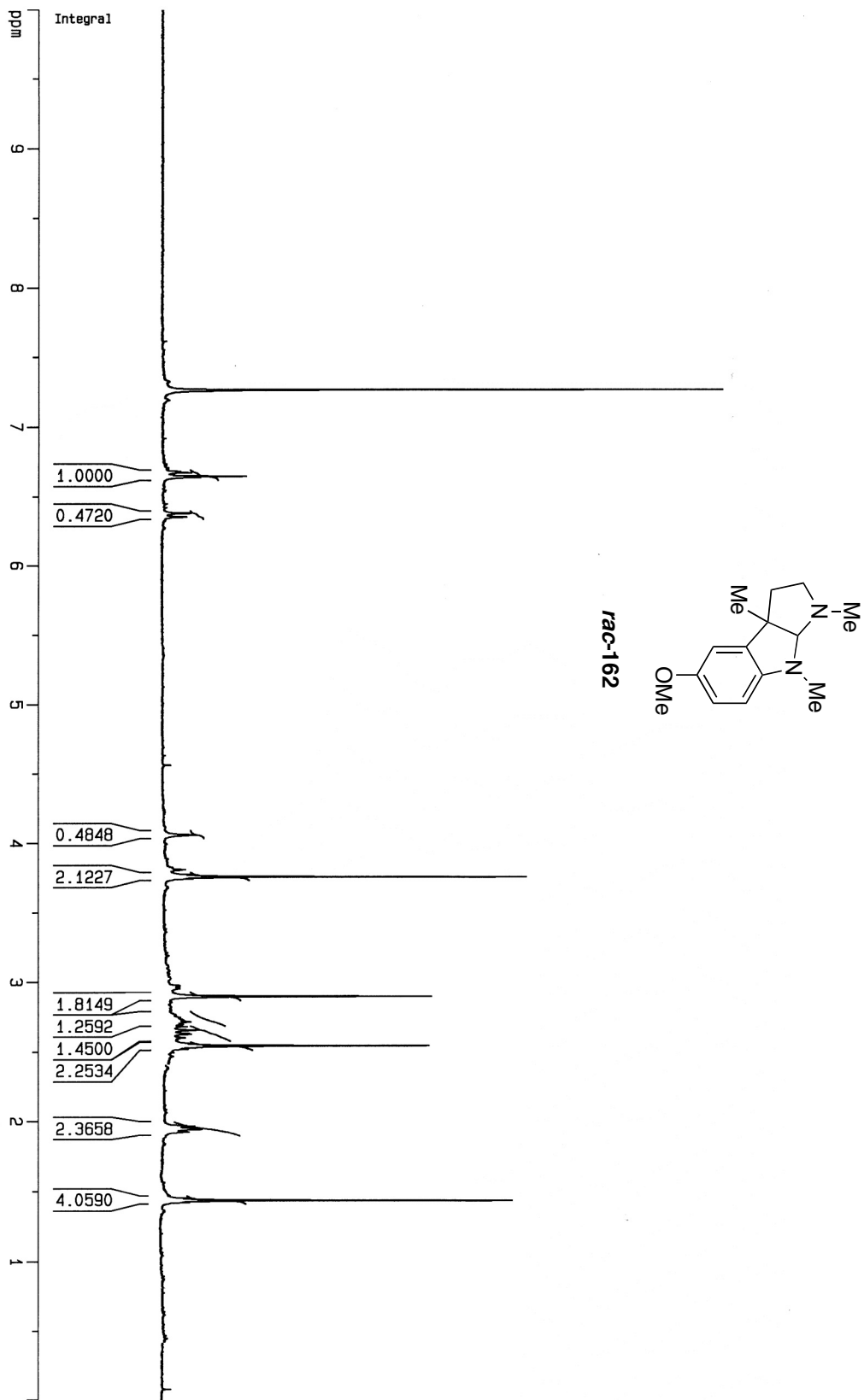


S-162









7.2. X-ray Crystallography Data

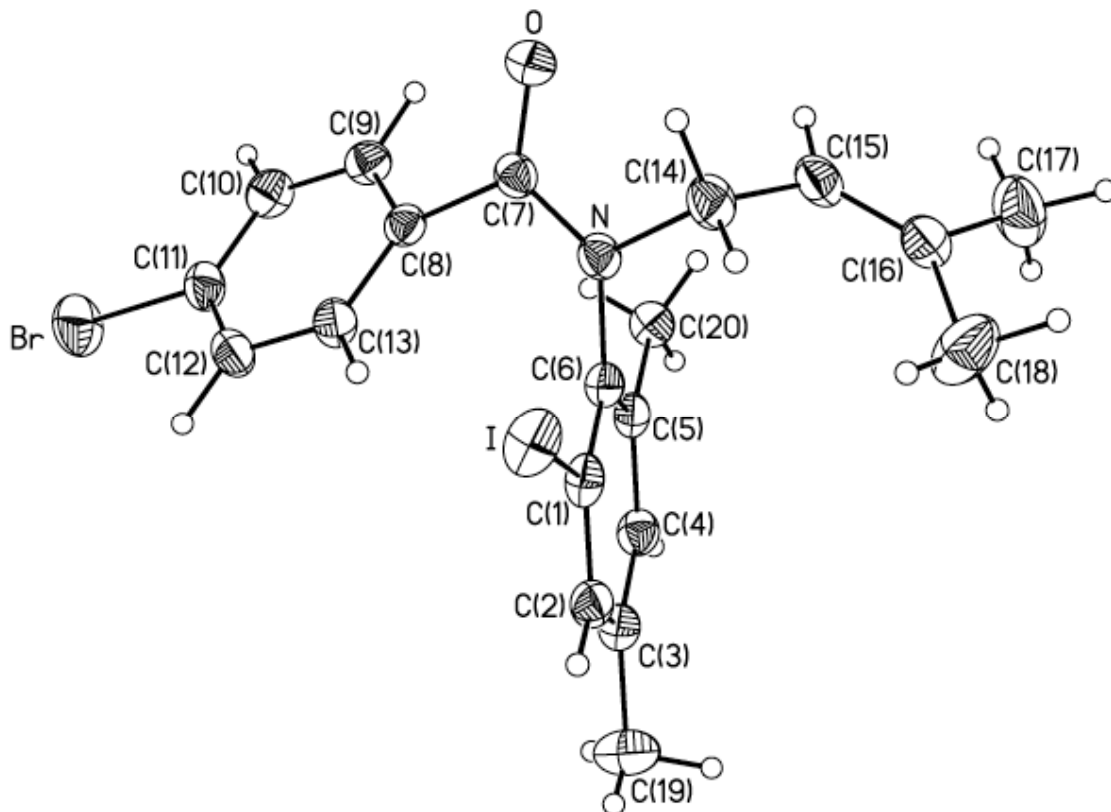


Figure 7.1 - ORTEP of (M)-56b

The corresponding CIF file for (M)-56b is found below, between the lines of '+' symbols.

```
+++++  
data_al0331  
  
_audit_creation_method          SHELXL-97  
_chemical_name_systematic  
;  
?  
;  
_chemical_name_common           ?  
_chemical_melting_point         ?  
_chemical_formula_moiety        ?  
_chemical_formula_sum           'C20 H21 Br I N O'  
_chemical_formula_weight        498.19  
  
loop_  
  _atom_type_symbol  
  _atom_type_description
```

```

_atom_type_scatter_dispersion_real
_atom_type_scatter_dispersion_imag
_atom_type_scatter_source
'C' 'C' 0.0033 0.0016
'International Tables Vol C Tables 4.2.6.8 and 6.1.1.4'
'H' 'H' 0.0000 0.0000
'International Tables Vol C Tables 4.2.6.8 and 6.1.1.4'
'N' 'N' 0.0061 0.0033
'International Tables Vol C Tables 4.2.6.8 and 6.1.1.4'
'O' 'O' 0.0106 0.0060
'International Tables Vol C Tables 4.2.6.8 and 6.1.1.4'
'Br' 'Br' -0.2901 2.4595
'International Tables Vol C Tables 4.2.6.8 and 6.1.1.4'
'I' 'I' -0.4742 1.8119
'International Tables Vol C Tables 4.2.6.8 and 6.1.1.4'

_symmetry_cell_setting ?
_symmetry_space_group_name_H-M ?

loop_
_symmetry_equiv_pos_as_xyz
'x, y, z'
'-y, x-y, z+1/3'
'-x+y, -x, z+2/3'

_cell_length_a 14.0919(6)
_cell_length_b 14.0919(6)
_cell_length_c 8.7408(5)
_cell_angle_alpha 90.00
_cell_angle_beta 90.00
_cell_angle_gamma 120.00
_cell_volume 1503.21(12)
_cell_formula_units_Z 3
_cell_measurement_temperature 150(2)
_cell_measurement_reflns_used ?
_cell_measurement_theta_min ?
_cell_measurement_theta_max ?

_exptl_crystal_description ?
_exptl_crystal_colour ?
_exptl_crystal_size_max 0.14
_exptl_crystal_size_mid 0.14
_exptl_crystal_size_min 0.08
_exptl_crystal_density_meas ?
_exptl_crystal_density_diffraction 1.651
_exptl_crystal_density_method 'not measured'
_exptl_crystal_F_000 732
_exptl_absorption_coefficient_mu 3.597
_exptl_absorption_correction_type ?
_exptl_absorption_correction_T_min 0.6328
_exptl_absorption_correction_T_max 0.7618
_exptl_absorption_process_details ?

_exptl_special_details
;
?
;

```

```

_diffrn_ambient_temperature      150(2)
_diffrn_radiation_wavelength     0.71073
_diffrn_radiation_type           MoK\alpha
_diffrn_radiation_source         'fine-focus sealed tube'
_diffrn_radiation_monochromator  graphite
_diffrn_measurement_device_type  ?
_diffrn_measurement_method      ?
_diffrn_detector_area_resol_mean ?
_diffrn_standards_number        ?
_diffrn_standards_interval_count ?
_diffrn_standards_interval_time ?
_diffrn_standards_decay_%       ?
_diffrn_reflns_number           19491
_diffrn_reflns_av_R_equivalents 0.0304
_diffrn_reflns_av_sigmaI/netI   0.0426
_diffrn_reflns_limit_h_min      -20
_diffrn_reflns_limit_h_max      20
_diffrn_reflns_limit_k_min      -20
_diffrn_reflns_limit_k_max      20
_diffrn_reflns_limit_l_min      -13
_diffrn_reflns_limit_l_max      13
_diffrn_reflns_theta_min        1.67
_diffrn_reflns_theta_max        32.46
_reflns_number_total            6981
_reflns_number_gt               6216
_reflns_threshold_expression     >2sigma(I)

_computing_data_collection      ?
_computing_cell_refinement      ?
_computing_data_reduction       ?
_computing_structure_solution   'SHELXS-97 (Sheldrick, 1990)'
_computing_structure_refinement 'SHELXL-97 (Sheldrick, 1997)'
_computing_molecular_graphics   ?
_computing_publication_material ?

```

_refine_special_details

```

;
Refinement of F2 against ALL reflections. The weighted R-factor wR and
goodness of fit S are based on F2, conventional R-factors R are based
on F, with F set to zero for negative F2. The threshold expression of
F2 > 2sigma(F2) is used only for calculating R-factors(gt) etc. and is
not relevant to the choice of reflections for refinement. R-factors based
on F2 are statistically about twice as large as those based on F, and R-
factors based on ALL data will be even larger.

```

```

;
_refine_ls_structure_factor_coef Fsqd
_refine_ls_matrix_type          full
_refine_ls_weighting_scheme     calc
_refine_ls_weighting_details
'calc w=1/[s2(Fo2)+(0.0172P)2+0.0000P] where P=(Fo2+2Fc2)/3'
_atom_sites_solution_primary    direct
_atom_sites_solution_secondary  difmap
_atom_sites_solution_hydrogens  geom
_refine_ls_hydrogen_treatment   mixed
_refine_ls_extinction_method    none
_refine_ls_extinction_coef      ?
_refine_ls_abs_structure_details

```

```
'Flack H D (1983), Acta Cryst. A39, 876-881'
_refine_ls_abs_structure_Flack    0.005(6)
_refine_ls_number_reflns         6981
_refine_ls_number_parameters      302
_refine_ls_number_restraints      1
_refine_ls_R_factor_all           0.0314
_refine_ls_R_factor_gt            0.0269
_refine_ls_wR_factor_ref          0.0514
_refine_ls_wR_factor_gt           0.0505
_refine_ls_goodness_of_fit_ref    0.922
_refine_ls_restrained_S_all       0.922
_refine_ls_shift/su_max           0.033
_refine_ls_shift/su_mean          0.002
```

loop_

```
_atom_site_label
_atom_site_type_symbol
_atom_site_fract_x
_atom_site_fract_y
_atom_site_fract_z
_atom_site_U_iso_or_equiv
_atom_site_adp_type
_atom_site_occupancy
_atom_site_symmetry_multiplicity
_atom_site_calc_flag
_atom_site_refinement_flags
_atom_site_disorder_assembly
_atom_site_disorder_group
N N 0.84912(16) 0.14757(15) -0.5811(2) 0.0247(4) Uani 1 1 d . . .
O O 0.89348(14) 0.08208(14) -0.78871(19) 0.0328(4) Uani 1 1 d . . .
I I 0.664422(13) 0.221534(12) -0.558141(17) 0.03436(4) Uani 1 1 d . . .
Br Br 0.48424(2) -0.41967(2) -0.58354(4) 0.04741(8) Uani 1 1 d . . .
C1 C 0.72829(17) 0.16129(17) -0.3912(3) 0.0252(4) Uani 1 1 d . . .
C2 C 0.68774(19) 0.14885(19) -0.2439(3) 0.0270(4) Uani 1 1 d . . .
H2 H 0.638(3) 0.170(3) -0.230(4) 0.051(9) Uiso 1 1 d . . .
C3 C 0.72476(19) 0.10790(19) -0.1294(3) 0.0288(5) Uani 1 1 d . . .
C4 C 0.80318(19) 0.07989(19) -0.1662(3) 0.0266(4) Uani 1 1 d . . .
H4 H 0.828(2) 0.054(2) -0.095(3) 0.026(6) Uiso 1 1 d . . .
C5 C 0.84524(17) 0.09059(17) -0.3135(2) 0.0236(4) Uani 1 1 d . . .
C6 C 0.80653(17) 0.13207(17) -0.4286(2) 0.0225(4) Uani 1 1 d . . .
C7 C 0.83634(17) 0.06437(18) -0.6751(2) 0.0240(4) Uani 1 1 d . . .
C8 C 0.74811(17) -0.05080(18) -0.6406(2) 0.0231(4) Uani 1 1 d . . .
C9 C 0.77183(19) -0.13309(19) -0.6765(3) 0.0272(4) Uani 1 1 d . . .
H9 H 0.847(2) -0.110(2) -0.722(3) 0.032(7) Uiso 1 1 d . . .
C10 C 0.6933(2) -0.2426(2) -0.6608(3) 0.0308(5) Uani 1 1 d . . .
H10 H 0.707(2) -0.299(2) -0.685(3) 0.033(7) Uiso 1 1 d . . .
C11 C 0.59060(19) -0.26961(18) -0.6078(3) 0.0289(5) Uani 1 1 d . . .
C12 C 0.56442(19) -0.1895(2) -0.5725(3) 0.0321(5) Uani 1 1 d . . .
H12 H 0.490(3) -0.210(3) -0.534(4) 0.046(8) Uiso 1 1 d . . .
C13 C 0.64347(18) -0.08030(19) -0.5889(3) 0.0278(4) Uani 1 1 d . . .
H13 H 0.625(3) -0.029(3) -0.562(3) 0.043(8) Uiso 1 1 d . . .
C14 C 0.9305(2) 0.26142(19) -0.6267(3) 0.0324(5) Uani 1 1 d . . .
H14A H 0.901(2) 0.310(2) -0.596(3) 0.036(7) Uiso 1 1 d . . .
H14B H 0.926(2) 0.260(2) -0.742(4) 0.041(8) Uiso 1 1 d . . .
C15 C 1.0426(2) 0.30104(19) -0.5622(3) 0.0323(5) Uani 1 1 d . . .
H15 H 1.078(2) 0.267(2) -0.605(3) 0.038(8) Uiso 1 1 d . . .
C16 C 1.0924(2) 0.3785(2) -0.4578(3) 0.0323(5) Uani 1 1 d . . .
C17 C 1.2058(3) 0.4123(3) -0.4028(5) 0.0524(8) Uani 1 1 d . . .
```

H17C H 1.233(3) 0.367(3) -0.451(4) 0.052(9) Uiso 1 1 d . . .
H17A H 1.259(4) 0.494(4) -0.414(6) 0.096(14) Uiso 1 1 d . . .
H17B H 1.214(4) 0.395(4) -0.298(5) 0.084(14) Uiso 1 1 d . . .
C18 C 1.0439(3) 0.4402(3) -0.3840(5) 0.0551(9) Uani 1 1 d . . .
H18A H 0.978(4) 0.418(3) -0.411(5) 0.071(13) Uiso 1 1 d . . .
H18B H 1.099(4) 0.527(4) -0.410(5) 0.082(13) Uiso 1 1 d . . .
H18C H 1.054(3) 0.447(3) -0.287(5) 0.053(10) Uiso 1 1 d . . .
C19 C 0.6809(3) 0.0953(3) 0.0307(3) 0.0443(7) Uani 1 1 d . . .
H19B H 0.637(3) 0.112(3) 0.041(5) 0.063(12) Uiso 1 1 d . . .
H19C H 0.672(4) 0.025(4) 0.074(5) 0.090(14) Uiso 1 1 d . . .
H19A H 0.740(4) 0.155(4) 0.090(6) 0.084(13) Uiso 1 1 d . . .
C20 C 0.9303(2) 0.0584(2) -0.3479(3) 0.0274(5) Uani 1 1 d . . .
H20B H 0.948(2) 0.046(2) -0.263(3) 0.031(7) Uiso 1 1 d . . .
H20B H 0.903(2) 0.001(2) -0.407(3) 0.028(7) Uiso 1 1 d . . .
H20A H 0.989(3) 0.105(3) -0.409(4) 0.054(10) Uiso 1 1 d . . .

loop_

_atom_site_aniso_label
_atom_site_aniso_U_11
_atom_site_aniso_U_22
_atom_site_aniso_U_33
_atom_site_aniso_U_23
_atom_site_aniso_U_13
_atom_site_aniso_U_12
N 0.0242(9) 0.0209(9) 0.0256(9) 0.0021(7) 0.0010(7) 0.0088(8)
O 0.0317(9) 0.0324(9) 0.0283(8) 0.0008(7) 0.0058(7) 0.0115(7)
I 0.04048(9) 0.03306(8) 0.03904(7) -0.00609(7) -0.01360(7) 0.02551(8)
Br 0.04288(16) 0.02426(12) 0.05994(17) 0.00140(12) 0.00297(13) 0.00542(12)
C1 0.0231(10) 0.0193(10) 0.0322(11) -0.0049(8) -0.0070(8) 0.0100(8)
C2 0.0231(10) 0.0233(10) 0.0350(12) -0.0056(8) -0.0008(9) 0.0119(9)
C3 0.0271(11) 0.0258(11) 0.0278(11) -0.0029(9) -0.0003(9) 0.0088(9)
C4 0.0266(11) 0.0273(11) 0.0237(10) 0.0002(8) -0.0037(8) 0.0118(9)
C5 0.0205(9) 0.0204(9) 0.0276(10) -0.0040(8) -0.0041(8) 0.0085(8)
C6 0.0221(10) 0.0192(9) 0.0244(10) -0.0015(8) -0.0013(8) 0.0089(8)
C7 0.0211(10) 0.0253(10) 0.0240(10) 0.0021(8) -0.0010(8) 0.0104(8)
C8 0.0234(10) 0.0250(10) 0.0212(10) -0.0017(8) -0.0020(8) 0.0123(8)
C9 0.0274(11) 0.0314(12) 0.0273(11) -0.0012(8) -0.0005(8) 0.0180(10)
C10 0.0355(12) 0.0275(11) 0.0344(12) -0.0029(9) -0.0013(10) 0.0194(10)
C11 0.0273(11) 0.0222(10) 0.0316(11) 0.0003(8) -0.0021(9) 0.0083(9)
C12 0.0217(11) 0.0298(12) 0.0398(13) -0.0043(10) 0.0029(9) 0.0091(10)
C13 0.0237(10) 0.0248(11) 0.0360(12) -0.0051(9) -0.0015(9) 0.0131(9)
C14 0.0334(12) 0.0223(11) 0.0338(13) 0.0053(9) 0.0028(10) 0.0080(10)
C15 0.0265(11) 0.0222(11) 0.0446(14) 0.0029(10) 0.0095(10) 0.0096(9)
C16 0.0275(11) 0.0287(12) 0.0397(13) 0.0029(10) 0.0040(9) 0.0134(10)
C17 0.0273(14) 0.0458(18) 0.078(2) -0.0067(17) -0.0031(14) 0.0136(13)
C18 0.054(2) 0.065(2) 0.060(2) -0.0281(18) -0.0161(17) 0.0399(19)
C19 0.0496(18) 0.060(2) 0.0337(14) 0.0000(13) 0.0072(13) 0.0351(17)
C20 0.0266(11) 0.0293(12) 0.0286(12) 0.0011(10) -0.0017(9) 0.0157(10)

_geom_special_details

;

All esds (except the esd in the dihedral angle between two l.s. planes) are estimated using the full covariance matrix. The cell esds are taken into account individually in the estimation of esds in distances, angles and torsion angles; correlations between esds in cell parameters are only used when they are defined by crystal symmetry. An approximate (isotropic) treatment of cell esds is used for estimating esds involving l.s. planes.

;

```

loop_
  _geom_bond_atom_site_label_1
  _geom_bond_atom_site_label_2
  _geom_bond_distance
  _geom_bond_site_symmetry_2
  _geom_bond_publ_flag
N C7 1.368(3) . ?
N C6 1.433(3) . ?
N C14 1.486(3) . ?
O C7 1.223(3) . ?
I C1 2.103(2) . ?
Br C11 1.896(2) . ?
C1 C2 1.384(3) . ?
C1 C6 1.395(3) . ?
C2 C3 1.382(3) . ?
C3 C4 1.385(3) . ?
C3 C19 1.503(4) . ?
C4 C5 1.393(3) . ?
C5 C6 1.404(3) . ?
C5 C20 1.508(3) . ?
C7 C8 1.501(3) . ?
C8 C13 1.392(3) . ?
C8 C9 1.394(3) . ?
C9 C10 1.384(3) . ?
C10 C11 1.380(3) . ?
C11 C12 1.386(3) . ?
C12 C13 1.384(3) . ?
C14 C15 1.498(4) . ?
C15 C16 1.323(4) . ?
C16 C18 1.495(4) . ?
C16 C17 1.500(4) . ?

```

```

loop_
  _geom_angle_atom_site_label_1
  _geom_angle_atom_site_label_2
  _geom_angle_atom_site_label_3
  _geom_angle
  _geom_angle_site_symmetry_1
  _geom_angle_site_symmetry_3
  _geom_angle_publ_flag
C7 N C6 124.22(18) . . ?
C7 N C14 117.66(19) . . ?
C6 N C14 116.89(18) . . ?
C2 C1 C6 121.2(2) . . ?
C2 C1 I 117.62(16) . . ?
C6 C1 I 121.17(16) . . ?
C3 C2 C1 120.6(2) . . ?
C2 C3 C4 118.2(2) . . ?
C2 C3 C19 120.3(2) . . ?
C4 C3 C19 121.5(2) . . ?
C3 C4 C5 122.8(2) . . ?
C4 C5 C6 118.3(2) . . ?
C4 C5 C20 120.7(2) . . ?
C6 C5 C20 120.99(19) . . ?
C1 C6 C5 118.96(19) . . ?
C1 C6 N 120.36(19) . . ?
C5 C6 N 120.65(19) . . ?

```

O C7 N 121.4(2) . . ?
 O C7 C8 119.3(2) . . ?
 N C7 C8 119.28(18) . . ?
 C13 C8 C9 118.9(2) . . ?
 C13 C8 C7 124.7(2) . . ?
 C9 C8 C7 116.14(19) . . ?
 C10 C9 C8 121.0(2) . . ?
 C11 C10 C9 119.0(2) . . ?
 C10 C11 C12 121.3(2) . . ?
 C10 C11 Br 118.73(18) . . ?
 C12 C11 Br 119.96(18) . . ?
 C13 C12 C11 119.2(2) . . ?
 C12 C13 C8 120.6(2) . . ?
 N C14 C15 113.7(2) . . ?
 C16 C15 C14 126.4(2) . . ?
 C15 C16 C18 124.7(3) . . ?
 C15 C16 C17 121.7(3) . . ?
 C18 C16 C17 113.6(3) . . ?

_diffraction_measured_fraction_theta_max 0.984
 _diffraction_refl_theta_full 32.46
 _diffraction_measured_fraction_theta_full 0.984
 _refine_diff_density_max 1.456
 _refine_diff_density_min -0.459
 _refine_diff_density_rms 0.081

+++++

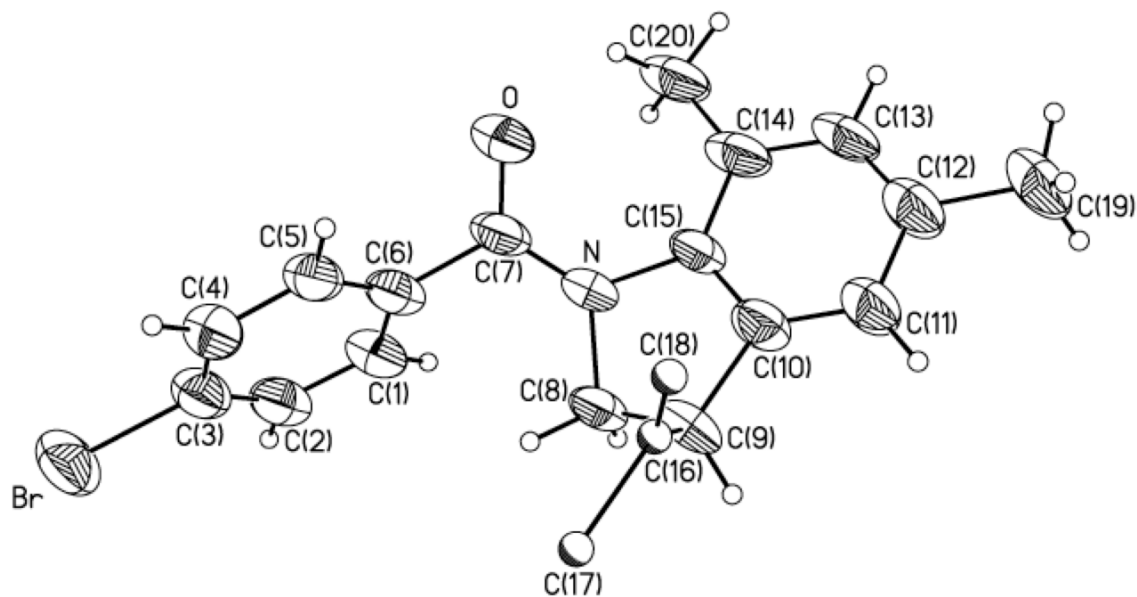


Figure 7.2 - ORTEP of (R)-57b

The corresponding CIF file for (R)-57b is found below, between the lines of '+' symbols.

+++++

data_cur602s

```

_audit_creation_method          SHELXL-97
_chemical_name_systematic
;
?
;
_chemical_name_common          ?
_chemical_melting_point        ?
_chemical_formula_moiety       ?
_chemical_formula_sum          'C20 H22 Br N O'
_chemical_formula_weight       372.30

loop_
  _atom_type_symbol
  _atom_type_description
  _atom_type_scatter_dispersion_real
  _atom_type_scatter_dispersion_imag
  _atom_type_scatter_source
  'C' 'C' 0.0033 0.0016
  'International Tables Vol C Tables 4.2.6.8 and 6.1.1.4'
  'H' 'H' 0.0000 0.0000
  'International Tables Vol C Tables 4.2.6.8 and 6.1.1.4'
  'N' 'N' 0.0061 0.0033
  'International Tables Vol C Tables 4.2.6.8 and 6.1.1.4'
  'O' 'O' 0.0106 0.0060
  'International Tables Vol C Tables 4.2.6.8 and 6.1.1.4'
  'Br' 'Br' -0.2901 2.4595
  'International Tables Vol C Tables 4.2.6.8 and 6.1.1.4'

_symmetry_cell_setting         Orthorhombic
_symmetry_space_group_name_H-M P2(1)2(1)2(1)

loop_
  _symmetry_equiv_pos_as_xyz
  'x, y, z'
  '-x+1/2, -y, z+1/2'
  '-x, y+1/2, -z+1/2'
  'x+1/2, -y+1/2, -z'

_cell_length_a                 9.0591(7)
_cell_length_b                 9.9088(8)
_cell_length_c                 19.8827(16)
_cell_angle_alpha              90.00
_cell_angle_beta               90.00
_cell_angle_gamma              90.00
_cell_volume                   1784.8(2)
_cell_formula_units_Z          4
_cell_measurement_temperature  200(2)
_cell_measurement_reflns_used  3545
_cell_measurement_theta_min    2.30
_cell_measurement_theta_max    20.94

_exptl_crystal_description     ?
_exptl_crystal_colour         ?
_exptl_crystal_size_max       0.34
_exptl_crystal_size_mid       0.20
_exptl_crystal_size_min       0.20
_exptl_crystal_density_meas    0

```

```

_exptl_crystal_density_diffn      1.386
_exptl_crystal_density_method     'not measured'
_exptl_crystal_F_000              768
_exptl_absorpt_coefficient_mu     2.307
_exptl_absorpt_correction_type    none
_exptl_absorpt_correction_T_min   0.5076
_exptl_absorpt_correction_T_max   0.6554
_exptl_absorpt_process_details    ?

_exptl_special_details
;
?
;

_diffn_ambient_temperature        200(2)
_diffn_radiation_wavelength       0.71073
_diffn_radiation_type             MoK\alpha
_diffn_radiation_source           'fine-focus sealed tube'
_diffn_radiation_monochromator     graphite
_diffn_measurement_device_type     'CCD area detector'
_diffn_measurement_method         'phi and omega scans'
_diffn_detector_area_resol_mean    ?
_diffn_standards_number           ?
_diffn_standards_interval_count    ?
_diffn_standards_interval_time    ?
_diffn_standards_decay_%          ?
_diffn_reflns_number              14269
_diffn_reflns_av_R_equivalents     0.0477
_diffn_reflns_av_sigmaI/netI      0.0576
_diffn_reflns_limit_h_min         -10
_diffn_reflns_limit_h_max         10
_diffn_reflns_limit_k_min         -11
_diffn_reflns_limit_k_max         11
_diffn_reflns_limit_l_min         -23
_diffn_reflns_limit_l_max         23
_diffn_reflns_theta_min           2.05
_diffn_reflns_theta_max           25.00
_reflns_number_total              3132
_reflns_number_gt                 1993
_reflns_threshold_expression       >2sigma(I)

_computing_data_collection         'Bruker SMART'
_computing_cell_refinement         'Bruker SMART'
_computing_data_reduction          'Bruker SAINT'
_computing_structure_solution      'SHELXS-97 (Sheldrick, 1990)'
_computing_structure_refinement    'SHELXL-97 (Sheldrick, 1997)'
_computing_molecular_graphics     'Bruker SHELXTL'
_computing_publication_material    'Bruker SHELXTL'

```

```
_refine_special_details
```

```
;
```

Refinement of F^2 against ALL reflections. The weighted R-factor wR and goodness of fit S are based on F^2 , conventional R-factors R are based on F , with F set to zero for negative F^2 . The threshold expression of $F^2 > 2\sigma(F^2)$ is used only for calculating R-factors(gt) etc. and is not relevant to the choice of reflections for refinement. R-factors based on F^2 are statistically about twice as large as those based on F , and R-factors based on ALL data will be even larger.

;

```
_refine_ls_structure_factor_coef  Fsqd
_refine_ls_matrix_type            full
_refine_ls_weighting_scheme       calc
_refine_ls_weighting_details
'calc w=1/[\s^2^(Fo^2^)+(0.0553P)^2^+0.0000P] where P=(Fo^2^+2Fc^2^)/3'
_atom_sites_solution_primary      direct
_atom_sites_solution_secondary    difmap
_atom_sites_solution_hydrogens    geom
_refine_ls_hydrogen_treatment     mixed
_refine_ls_extinction_method      none
_refine_ls_extinction_coef        ?
_refine_ls_abs_structure_details
'Flack H D (1983), Acta Cryst. A39, 876-881'
_refine_ls_abs_structure_Flack    0.013(15)
_refine_ls_number_reflns          3132
_refine_ls_number_parameters      218
_refine_ls_number_restraints      0
_refine_ls_R_factor_all           0.0802
_refine_ls_R_factor_gt            0.0440
_refine_ls_wR_factor_ref          0.1177
_refine_ls_wR_factor_gt           0.1067
_refine_ls_goodness_of_fit_ref    0.998
_refine_ls_restrained_S_all       0.998
_refine_ls_shift/su_max           0.049
_refine_ls_shift/su_mean          0.004
```

loop_

```
_atom_site_label
_atom_site_type_symbol
_atom_site_fract_x
_atom_site_fract_y
_atom_site_fract_z
_atom_site_U_iso_or_equiv
_atom_site_adp_type
_atom_site_occupancy
_atom_site_symmetry_multiplicity
_atom_site_calc_flag
_atom_site_refinement_flags
_atom_site_disorder_assembly
_atom_site_disorder_group
Br Br -0.90041(7) -0.18939(6) 0.50262(3) 0.1134(3) Uani 1 1 d . A 1
O O -0.5675(4) -0.0370(4) 0.20368(14) 0.0868(9) Uani 1 1 d . A 1
N N -0.3825(4) -0.1669(4) 0.24743(14) 0.0764(10) Uani 1 1 d . A 1
C1 C -0.6203(5) -0.2559(5) 0.3423(2) 0.0802(13) Uani 1 1 d . A 1
H1A H -0.5662 -0.3304 0.3251 0.096 Uiso 1 1 calc R A 1
C2 C -0.7092(6) -0.2731(5) 0.3984(2) 0.0832(14) Uani 1 1 d . A 1
H2A H -0.7190 -0.3597 0.4184 0.100 Uiso 1 1 calc R A 1
C3 C -0.7831(5) -0.1640(6) 0.4250(2) 0.0826(13) Uani 1 1 d . A 1
C4 C -0.7728(5) -0.0391(5) 0.3947(2) 0.0809(13) Uani 1 1 d . A 1
H4A H -0.8235 0.0360 0.4133 0.097 Uiso 1 1 calc R A 1
C5 C -0.6894(6) -0.0234(5) 0.3380(2) 0.0763(12) Uani 1 1 d . A 1
H5A H -0.6855 0.0619 0.3162 0.092 Uiso 1 1 calc R A 1
C6 C -0.6094(5) -0.1327(5) 0.31158(19) 0.0720(11) Uani 1 1 d . A 1
C7 C -0.5185(6) -0.1073(5) 0.2496(2) 0.0759(12) Uani 1 1 d . A 1
C8 C -0.2946(5) -0.1925(5) 0.30970(18) 0.0812(13) Uani 1 1 d . A 1
H8A H -0.2652 -0.2885 0.3129 0.097 Uiso 1 1 calc R A 1
```

H8B H -0.3511 -0.1675 0.3505 0.097 Uiso 1 1 calc R A 1
C9 C -0.1592(6) -0.1009(5) 0.30061(18) 0.0768(14) Uani 1 1 d . A 1
H9A H -0.0701 -0.1437 0.3213 0.092 Uiso 1 1 calc R A 1
C10 C -0.1441(6) -0.0985(5) 0.22394(19) 0.0772(13) Uani 1 1 d . A 1
C11 C -0.0238(6) -0.0668(5) 0.1855(2) 0.0855(14) Uani 1 1 d . A 1
H11A H 0.0667 -0.0408 0.2059 0.103 Uiso 1 1 calc R A 1
C12 C -0.0371(7) -0.0734(5) 0.1160(2) 0.0919(15) Uani 1 1 d . A 1
C13 C -0.1692(7) -0.1169(5) 0.08830(19) 0.0877(15) Uani 1 1 d . A 1
H13A H -0.1749 -0.1251 0.0408 0.105 Uiso 1 1 calc R A 1
C14 C -0.2945(6) -0.1495(5) 0.1260(2) 0.0856(13) Uani 1 1 d . A 1
C15 C -0.2783(6) -0.1365(5) 0.1961(2) 0.0764(13) Uani 1 1 d . A 1
C16 C -0.1825(13) 0.0375(7) 0.3292(3) 0.151(3) Uani 1 1 d . A 1
H16A H -0.0793 0.0726 0.3255 0.181 Uiso 1 1 calc R A 1
C17 C -0.1959(11) 0.0330(6) 0.4074(2) 0.152(3) Uani 1 1 d . A 1
H17A H -0.2002 0.1252 0.4250 0.227 Uiso 1 1 calc R A 1
H17B H -0.1099 -0.0135 0.4262 0.227 Uiso 1 1 calc R A 1
H17C H -0.2860 -0.0156 0.4199 0.227 Uiso 1 1 calc R A 1
C18 C -0.2475(11) 0.1320(12) 0.3051(5) 0.073(3) Uani 0.50 1 d P A 1
H18A H -0.2318 0.1332 0.2563 0.110 Uiso 0.50 1 calc PR A 1
H18B H -0.2102 0.2161 0.3247 0.110 Uiso 0.50 1 calc PR A 1
H18C H -0.3532 0.1235 0.3146 0.110 Uiso 0.50 1 calc PR A 1
C18' C -0.1176(16) 0.1514(11) 0.3018(5) 0.095(3) Uani 0.50 1 d P B 2
C19 C 0.0942(6) -0.0398(7) 0.0712(2) 0.1101(18) Uani 1 1 d . A 1
H19A H 0.0659 -0.0504 0.0239 0.165 Uiso 1 1 calc R A 1
H19B H 0.1761 -0.1008 0.0816 0.165 Uiso 1 1 calc R A 1
H19C H 0.1250 0.0537 0.0793 0.165 Uiso 1 1 calc R A 1
C20 C -0.4336(6) -0.1951(6) 0.0936(2) 0.0966(16) Uani 1 1 d . A 1
H20A H -0.4209 -0.1959 0.0447 0.145 Uiso 1 1 calc R A 1
H20B H -0.5138 -0.1331 0.1056 0.145 Uiso 1 1 calc R A 1
H20C H -0.4579 -0.2862 0.1092 0.145 Uiso 1 1 calc R A 1

loop_

_atom_site_aniso_label
_atom_site_aniso_U_11
_atom_site_aniso_U_22
_atom_site_aniso_U_33
_atom_site_aniso_U_23
_atom_site_aniso_U_13
_atom_site_aniso_U_12
Br 0.1200(4) 0.1490(5) 0.0713(3) 0.0176(4) 0.0239(3) -0.0174(4)
O 0.101(2) 0.105(2) 0.0542(16) 0.0219(17) -0.0054(17) -0.0026(19)
N 0.088(3) 0.104(3) 0.0369(16) 0.0152(18) -0.0008(17) 0.003(2)
C1 0.100(3) 0.090(3) 0.051(2) 0.011(2) -0.003(2) 0.002(3)
C2 0.100(3) 0.089(3) 0.061(3) 0.014(2) -0.012(3) -0.018(3)
C3 0.087(3) 0.101(4) 0.059(2) 0.015(3) -0.004(2) -0.012(3)
C4 0.082(3) 0.098(4) 0.063(3) 0.005(3) -0.005(2) 0.000(3)
C5 0.088(3) 0.093(3) 0.048(2) 0.012(2) -0.009(2) -0.007(3)
C6 0.085(3) 0.083(3) 0.048(2) 0.013(2) -0.009(2) -0.007(3)
C7 0.095(3) 0.094(3) 0.039(2) 0.013(2) -0.010(2) -0.006(3)
C8 0.100(3) 0.105(3) 0.039(2) 0.009(2) -0.001(2) 0.011(3)
C9 0.099(4) 0.092(3) 0.039(2) 0.004(2) 0.008(2) -0.004(3)
C10 0.096(4) 0.092(3) 0.043(2) -0.002(2) 0.004(2) 0.000(3)
C11 0.089(3) 0.116(4) 0.051(2) -0.007(2) 0.011(2) -0.006(3)
C12 0.119(4) 0.109(4) 0.048(2) -0.002(3) 0.023(3) 0.014(3)
C13 0.136(4) 0.094(3) 0.034(2) 0.002(2) 0.005(3) 0.015(3)
C14 0.113(4) 0.105(3) 0.040(2) 0.005(2) -0.006(3) 0.005(3)
C15 0.098(4) 0.091(3) 0.040(2) 0.012(2) 0.003(2) 0.003(3)
C16 0.301(10) 0.097(4) 0.056(3) -0.006(3) 0.063(5) -0.016(7)

C17 0.283(10) 0.122(5) 0.050(3) -0.014(3) 0.046(4) -0.020(6)
C18 0.062(6) 0.095(8) 0.063(5) -0.019(6) -0.006(4) 0.011(5)
C18' 0.109(9) 0.092(8) 0.083(7) -0.020(6) 0.000(7) -0.024(7)
C19 0.123(4) 0.140(5) 0.067(3) 0.007(3) 0.029(3) 0.004(4)
C20 0.126(4) 0.121(4) 0.042(2) 0.010(3) -0.009(2) 0.000(4)

_geom_special_details

;

All esds (except the esd in the dihedral angle between two l.s. planes) are estimated using the full covariance matrix. The cell esds are taken into account individually in the estimation of esds in distances, angles and torsion angles; correlations between esds in cell parameters are only used when they are defined by crystal symmetry. An approximate (isotropic) treatment of cell esds is used for estimating esds involving l.s. planes.

;

loop_

_geom_bond_atom_site_label_1
_geom_bond_atom_site_label_2
_geom_bond_distance
_geom_bond_site_symmetry_2
_geom_bond_publ_flag

Br C3 1.891(4) . ?
O C7 1.232(5) . ?
N C7 1.366(6) . ?
N C15 1.423(5) . ?
N C8 1.494(5) . ?
C1 C6 1.369(6) . ?
C1 C2 1.386(7) . ?
C2 C3 1.377(7) . ?
C3 C4 1.379(7) . ?
C4 C5 1.367(6) . ?
C5 C6 1.404(7) . ?
C6 C7 1.503(6) . ?
C8 C9 1.537(7) . ?
C9 C16 1.500(8) . ?
C9 C10 1.531(5) . ?
C10 C11 1.368(6) . ?
C10 C15 1.388(6) . ?
C11 C12 1.388(6) . ?
C12 C13 1.386(7) . ?
C12 C19 1.523(7) . ?
C13 C14 1.398(7) . ?
C14 C15 1.408(6) . ?
C14 C20 1.485(7) . ?
C16 C18 1.206(11) . ?
C16 C17 1.559(7) . ?

loop_

_geom_angle_atom_site_label_1
_geom_angle_atom_site_label_2
_geom_angle_atom_site_label_3
_geom_angle
_geom_angle_site_symmetry_1
_geom_angle_site_symmetry_3
_geom_angle_publ_flag

C7 N C15 122.0(3) . . ?
C7 N C8 121.8(3) . . ?

C15 N C8 106.0(3) . . ?
 C6 C1 C2 120.7(5) . . ?
 C3 C2 C1 119.6(4) . . ?
 C2 C3 C4 120.3(4) . . ?
 C2 C3 Br 118.8(4) . . ?
 C4 C3 Br 120.9(4) . . ?
 C5 C4 C3 120.0(5) . . ?
 C4 C5 C6 120.4(4) . . ?
 C1 C6 C5 118.9(4) . . ?
 C1 C6 C7 123.7(5) . . ?
 C5 C6 C7 117.4(4) . . ?
 O C7 N 123.1(4) . . ?
 O C7 C6 120.3(5) . . ?
 N C7 C6 116.6(4) . . ?
 N C8 C9 103.2(3) . . ?
 C16 C9 C10 112.1(4) . . ?
 C16 C9 C8 112.5(5) . . ?
 C10 C9 C8 101.4(4) . . ?
 C11 C10 C15 122.5(4) . . ?
 C11 C10 C9 129.1(5) . . ?
 C15 C10 C9 108.3(4) . . ?
 C10 C11 C12 118.4(5) . . ?
 C13 C12 C11 119.0(5) . . ?
 C13 C12 C19 120.6(4) . . ?
 C11 C12 C19 120.2(6) . . ?
 C12 C13 C14 124.0(4) . . ?
 C13 C14 C15 115.1(5) . . ?
 C13 C14 C20 121.8(4) . . ?
 C15 C14 C20 123.1(5) . . ?
 C10 C15 C14 120.7(5) . . ?
 C10 C15 N 110.7(3) . . ?
 C14 C15 N 128.4(5) . . ?
 C18 C16 C9 128.9(8) . . ?
 C18 C16 C17 112.4(8) . . ?
 C9 C16 C17 111.3(5) . . ?

<u>_diffn_measured_fraction_theta_max</u>	0.999
<u>_diffn_reflns_theta_full</u>	25.00
<u>_diffn_measured_fraction_theta_full</u>	0.999
<u>_refine_diff_density_max</u>	0.301
<u>_refine_diff_density_min</u>	-0.171
<u>_refine_diff_density_rms</u>	0.046

+++++


```

loop_
  _atom_type_symbol
  _atom_type_description
  _atom_type_scatter_dispersion_real
  _atom_type_scatter_dispersion_imag
  _atom_type_scatter_source
  'C' 'C' 0.0033 0.0016
  'International Tables Vol C Tables 4.2.6.8 and 6.1.1.4'
  'H' 'H' 0.0000 0.0000
  'International Tables Vol C Tables 4.2.6.8 and 6.1.1.4'
  'N' 'N' 0.0061 0.0033
  'International Tables Vol C Tables 4.2.6.8 and 6.1.1.4'
  'O' 'O' 0.0106 0.0060
  'International Tables Vol C Tables 4.2.6.8 and 6.1.1.4'
  'I' 'I' -0.4742 1.8119
  'International Tables Vol C Tables 4.2.6.8 and 6.1.1.4'

```

```

_symmetry_cell_setting          Orthorhombic
_symmetry_space_group_name_H-M P2(1)2(1)2(1)

```

```

loop_
  _symmetry_equiv_pos_as_xyz
  'x, y, z'
  '-x+1/2, -y, z+1/2'
  '-x, y+1/2, -z+1/2'
  'x+1/2, -y+1/2, -z'

```

```

_cell_length_a          9.166(2)
_cell_length_b          10.794(3)
_cell_length_c          17.987(4)
_cell_angle_alpha       90.00
_cell_angle_beta        90.00
_cell_angle_gamma       90.00
_cell_volume            1779.6(7)
_cell_formula_units_Z   4
_cell_measurement_temperature 295(2)
_cell_measurement_reflns_used 5854
_cell_measurement_theta_min 2.49
_cell_measurement_theta_max 29.83

```

```

_exptl_crystal_description ?
_exptl_crystal_colour     ?
_exptl_crystal_size_max   0.15
_exptl_crystal_size_mid   0.12
_exptl_crystal_size_min   0.10
_exptl_crystal_density_meas 0
_exptl_crystal_density_diffn 1.430
_exptl_crystal_density_method 'not measured'
_exptl_crystal_F_000      768
_exptl_absorpt_coefficient_mu 1.796
_exptl_absorpt_correction_type none
_exptl_absorpt_correction_T_min 0.7744

```

```
_exptl_absorpt_correction_T_max 0.8408
_exptl_absorpt_process_details ?
```

```
_exptl_special_details
```

```
;  
?  
;
```

```
_diffrn_ambient_temperature 295(2)  
_diffrn_radiation_wavelength 0.71073  
_diffrn_radiation_type MoK\alpha  
_diffrn_radiation_source 'fine-focus sealed tube'  
_diffrn_radiation_monochromator graphite  
_diffrn_measurement_device_type 'CCD area detector'  
_diffrn_measurement_method 'phi and omega scans'  
_diffrn_detector_area_resol_mean ?  
_diffrn_standards_number ?  
_diffrn_standards_interval_count ?  
_diffrn_standards_interval_time ?  
_diffrn_standards_decay_% ?  
_diffrn_reflns_number 14104  
_diffrn_reflns_av_R_equivalents 0.0799  
_diffrn_reflns_av_sigmaI/netI 0.0620  
_diffrn_reflns_limit_h_min -11  
_diffrn_reflns_limit_h_max 11  
_diffrn_reflns_limit_k_min -14  
_diffrn_reflns_limit_k_max 14  
_diffrn_reflns_limit_l_min -22  
_diffrn_reflns_limit_l_max 23  
_diffrn_reflns_theta_min 2.20  
_diffrn_reflns_theta_max 27.50  
_reflns_number_total 3953  
_reflns_number_gt 2737  
_reflns_threshold_expression >2sigma(I)
```

```
_computing_data_collection 'Bruker SMART'  
_computing_cell_refinement 'Bruker SMART'  
_computing_data_reduction 'Bruker SAINT'  
_computing_structure_solution 'SHELXS-97 (Sheldrick, 1990)'  
_computing_structure_refinement 'SHELXL-97 (Sheldrick, 1997)'  
_computing_molecular_graphics 'Bruker SHELXTL'  
_computing_publication_material 'Bruker SHELXTL'
```

```
_refine_special_details
```

```
;
```

Refinement of F^2 against ALL reflections. The weighted R-factor wR and goodness of fit S are based on F^2 , conventional R-factors R are based on F , with F set to zero for negative F^2 . The threshold expression of $F^2 > 2\sigma(F^2)$ is used only for calculating R-factors(gt) etc. and is not relevant to the choice of reflections for refinement. R-factors based on F^2 are statistically about twice as large as those based on F , and R-

factors based on ALL data will be even larger.

;

```
_refine_ls_structure_factor_coef Fsqd
_refine_ls_matrix_type full
_refine_ls_weighting_scheme calc
_refine_ls_weighting_details
'calc w=1/[\s^2^(Fo^2^)+(0.0851P)^2^+0.0000P] where P=(Fo^2^+2Fc^2^)/3'
_atom_sites_solution_primary direct
_atom_sites_solution_secondary difmap
_atom_sites_solution_hydrogens geom
_refine_ls_hydrogen_treatment mixed
_refine_ls_extinction_method SHELXL
_refine_ls_extinction_coef 0.030(2)
_refine_ls_extinction_expression
'Fc^*=kFc[1+0.001xFc^2^\l^3^/sin(2\q)]^-1/4^'
_refine_ls_abs_structure_details
'Flack H D (1983), Acta Cryst. A39, 876-881'
_refine_ls_abs_structure_Flack 0.05(6)
_refine_ls_number_reflns 3953
_refine_ls_number_parameters 185
_refine_ls_number_restraints 0
_refine_ls_R_factor_all 0.0829
_refine_ls_R_factor_gt 0.0532
_refine_ls_wR_factor_ref 0.1511
_refine_ls_wR_factor_gt 0.1306
_refine_ls_goodness_of_fit_ref 1.032
_refine_ls_restrained_S_all 1.032
_refine_ls_shift/su_max 0.065
_refine_ls_shift/su_mean 0.002
```

loop_

```
_atom_site_label
_atom_site_type_symbol
_atom_site_fract_x
_atom_site_fract_y
_atom_site_fract_z
_atom_site_U_iso_or_equiv
_atom_site_adp_type
_atom_site_occupancy
_atom_site_symmetry_multiplicity
_atom_site_calc_flag
_atom_site_refinement_flags
_atom_site_disorder_assembly
_atom_site_disorder_group
I1 I 0.84204(6) 1.12850(5) 0.17685(3) 0.0622(2) Uani 1 1 d . . .
O1 O 1.1184(6) 0.7858(6) 0.1860(4) 0.0695(16) Uani 1 1 d . . .
N1 N 0.9155(7) 0.8426(6) 0.1200(3) 0.0509(15) Uani 1 1 d . . .
C1 C 0.7333(9) 1.0586(9) -0.0562(5) 0.063(2) Uani 1 1 d . . .
C2 C 0.7678(11) 0.9307(10) -0.0667(5) 0.071(2) Uani 1 1 d . . .
H2 H 0.7506 0.8932 -0.1124 0.085 Uiso 1 1 calc R . .
C3 C 0.8274(9) 0.8622(8) -0.0084(4) 0.0580(17) Uani 1 1 d . . .
H3 H 0.8515 0.7795 -0.0161 0.070 Uiso 1 1 calc R . .
C4 C 0.8516(8) 0.9154(6) 0.0616(4) 0.0496(15) Uani 1 1 d . . .
```

C5 C 0.8132(8) 1.0403(7) 0.0704(4) 0.0492(17) Uani 1 1 d . . .
 C6 C 0.7553(8) 1.1101(8) 0.0129(5) 0.060(2) Uani 1 1 d . . .
 H6 H 0.7309 1.1926 0.0210 0.073 Uiso 1 1 calc R . . .
 C8 C 1.0630(8) 0.8492(7) 0.1370(4) 0.0519(18) Uani 1 1 d . . .
 C9 C 1.1530(10) 0.9386(8) 0.0922(4) 0.0585(18) Uani 1 1 d . . .
 H9 H 1.1101 0.9827 0.0536 0.070 Uiso 1 1 calc R . . .
 C10 C 1.2934(9) 0.9550(10) 0.1077(5) 0.068(2) Uani 1 1 d . . .
 H10 H 1.3317 0.9098 0.1471 0.082 Uiso 1 1 calc R . . .
 C11 C 1.3969(12) 1.0407(12) 0.0666(7) 0.088(3) Uani 1 1 d . . .
 H11A H 1.4825 0.9956 0.0521 0.133 Uiso 1 1 calc R . . .
 H11B H 1.4242 1.1080 0.0986 0.133 Uiso 1 1 calc R . . .
 H11C H 1.3494 1.0729 0.0231 0.133 Uiso 1 1 calc R . . .
 C12 C 0.6708(15) 1.1366(13) -0.1190(7) 0.103(4) Uani 1 1 d . . .
 H12A H 0.6891 1.2226 -0.1092 0.155 Uiso 1 1 calc R . . .
 H12B H 0.5675 1.1229 -0.1223 0.155 Uiso 1 1 calc R . . .
 H12C H 0.7162 1.1135 -0.1650 0.155 Uiso 1 1 calc R . . .
 C13 C 0.8261(9) 0.7500(7) 0.1617(4) 0.0569(18) Uani 1 1 d . . .
 H13 H 0.8632 0.7484 0.2128 0.068 Uiso 1 1 calc R . . .
 C15 C 0.6635(10) 0.7833(10) 0.1661(6) 0.072(2) Uani 1 1 d . . .
 H15A H 0.6528 0.8650 0.1879 0.087 Uiso 1 1 calc R . . .
 H15B H 0.6228 0.7857 0.1163 0.087 Uiso 1 1 calc R . . .
 C16 C 0.5807(13) 0.6905(12) 0.2121(7) 0.089(3) Uani 1 1 d . . .
 H16A H 0.4777 0.7111 0.2110 0.107 Uiso 1 1 calc R . . .
 H16B H 0.6133 0.6960 0.2633 0.107 Uiso 1 1 calc R . . .
 C17 C 0.6012(13) 0.5552(12) 0.1843(8) 0.096(4) Uani 1 1 d . . .
 H17A H 0.5560 0.4984 0.2192 0.115 Uiso 1 1 calc R . . .
 H17B H 0.5536 0.5453 0.1365 0.115 Uiso 1 1 calc R . . .
 C18 C 0.7588(13) 0.5254(10) 0.1771(8) 0.093(3) Uani 1 1 d . . .
 H18A H 0.7689 0.4441 0.1546 0.112 Uiso 1 1 calc R . . .
 H18B H 0.8020 0.5218 0.2262 0.112 Uiso 1 1 calc R . . .
 C19 C 0.8412(11) 0.6183(8) 0.1309(6) 0.072(2) Uani 1 1 d . . .
 H19A H 0.8047 0.6162 0.0803 0.087 Uiso 1 1 calc R . . .
 H19B H 0.9436 0.5956 0.1297 0.087 Uiso 1 1 calc R . . .

loop_

_atom_site_aniso_label
 _atom_site_aniso_U_11
 _atom_site_aniso_U_22
 _atom_site_aniso_U_33
 _atom_site_aniso_U_23
 _atom_site_aniso_U_13
 _atom_site_aniso_U_12
 I1 0.0706(3) 0.0498(3) 0.0662(3) -0.0077(2) 0.0029(3) -0.0030(3)
 O1 0.065(3) 0.072(4) 0.072(4) 0.020(3) -0.011(3) 0.002(3)
 N1 0.050(3) 0.045(4) 0.057(3) 0.004(3) -0.002(3) -0.005(3)
 C1 0.050(4) 0.073(6) 0.064(5) 0.022(4) -0.006(4) -0.010(4)
 C2 0.075(6) 0.085(7) 0.053(4) 0.008(4) -0.008(4) -0.009(5)
 C3 0.066(4) 0.049(4) 0.059(4) 0.001(3) -0.001(4) -0.004(5)
 C4 0.049(4) 0.042(3) 0.058(4) 0.003(3) -0.003(3) 0.001(3)
 C5 0.054(4) 0.052(4) 0.042(3) -0.011(3) 0.000(3) -0.005(3)
 C6 0.058(4) 0.050(5) 0.074(5) 0.013(4) -0.010(4) -0.002(4)
 C8 0.046(4) 0.050(5) 0.060(4) -0.004(3) 0.000(3) 0.003(3)
 C9 0.049(4) 0.059(4) 0.068(5) 0.010(3) -0.004(4) -0.002(4)
 C10 0.056(5) 0.072(6) 0.077(5) -0.010(5) -0.002(4) 0.000(4)
 C11 0.067(6) 0.096(8) 0.102(8) -0.009(7) 0.021(6) -0.020(6)
 C12 0.104(8) 0.105(9) 0.100(7) 0.046(7) -0.028(7) 0.007(10)
 C13 0.062(5) 0.042(4) 0.066(5) 0.006(3) -0.002(4) -0.004(4)

```

C15 0.058(4) 0.076(6) 0.083(6) 0.011(5) 0.012(5) -0.002(5)
C16 0.076(6) 0.095(8) 0.096(8) 0.021(6) 0.015(6) -0.015(6)
C17 0.089(7) 0.093(8) 0.106(8) 0.043(8) -0.014(7) -0.033(6)
C18 0.096(7) 0.060(6) 0.124(9) 0.021(7) -0.015(8) -0.013(5)
C19 0.073(5) 0.047(4) 0.098(6) 0.007(5) -0.010(5) -0.002(5)

```

```
_geom_special_details
```

```

;
All esds (except the esd in the dihedral angle between two l.s. planes)
are estimated using the full covariance matrix. The cell esds are taken
into account individually in the estimation of esds in distances, angles
and torsion angles; correlations between esds in cell parameters are only
used when they are defined by crystal symmetry. An approximate (isotropic)
treatment of cell esds is used for estimating esds involving l.s. planes.
;

```

```

loop_
  _geom_bond_atom_site_label_1
  _geom_bond_atom_site_label_2
  _geom_bond_distance
  _geom_bond_site_symmetry_2
  _geom_bond_publ_flag
I1 C5 2.154(6) . ?
O1 C8 1.226(9) . ?
N1 C8 1.388(10) . ?
N1 C4 1.436(9) . ?
N1 C13 1.495(9) . ?
C1 C6 1.375(12) . ?
C1 C2 1.429(14) . ?
C1 C12 1.521(12) . ?
C2 C3 1.395(12) . ?
C3 C4 1.401(10) . ?
C4 C5 1.403(10) . ?
C5 C6 1.386(11) . ?
C8 C9 1.504(12) . ?
C9 C10 1.329(13) . ?
C10 C11 1.517(14) . ?
C13 C19 1.532(12) . ?
C13 C15 1.536(12) . ?
C15 C16 1.505(14) . ?
C16 C17 1.554(18) . ?
C17 C18 1.486(19) . ?
C18 C19 1.505(14) . ?

```

```

loop_
  _geom_angle_atom_site_label_1
  _geom_angle_atom_site_label_2
  _geom_angle_atom_site_label_3
  _geom_angle
  _geom_angle_site_symmetry_1
  _geom_angle_site_symmetry_3
  _geom_angle_publ_flag
C8 N1 C4 122.1(7) . . ?

```

C8 N1 C13 117.2(7) . . ?
 C4 N1 C13 120.6(6) . . ?
 C6 C1 C2 118.5(8) . . ?
 C6 C1 C12 120.1(10) . . ?
 C2 C1 C12 121.3(10) . . ?
 C3 C2 C1 119.9(9) . . ?
 C2 C3 C4 121.4(8) . . ?
 C3 C4 C5 117.1(7) . . ?
 C3 C4 N1 119.8(6) . . ?
 C5 C4 N1 123.1(6) . . ?
 C6 C5 C4 122.3(7) . . ?
 C6 C5 I1 118.1(6) . . ?
 C4 C5 I1 119.6(5) . . ?
 C1 C6 C5 120.8(8) . . ?
 O1 C8 N1 122.3(8) . . ?
 O1 C8 C9 121.1(7) . . ?
 N1 C8 C9 116.6(7) . . ?
 C10 C9 C8 120.3(8) . . ?
 C9 C10 C11 125.8(10) . . ?
 N1 C13 C19 113.0(7) . . ?
 N1 C13 C15 113.7(7) . . ?
 C19 C13 C15 108.9(8) . . ?
 C16 C15 C13 111.2(8) . . ?
 C15 C16 C17 112.8(10) . . ?
 C18 C17 C16 110.5(10) . . ?
 C17 C18 C19 113.1(10) . . ?
 C18 C19 C13 111.9(9) . . ?

_diffn_measured_fraction_theta_max 0.968
 _diffn_reflns_theta_full 27.50
 _diffn_measured_fraction_theta_full 0.968
 _refine_diff_density_max 0.674
 _refine_diff_density_min -1.170
 _refine_diff_density_rms 0.120

+++

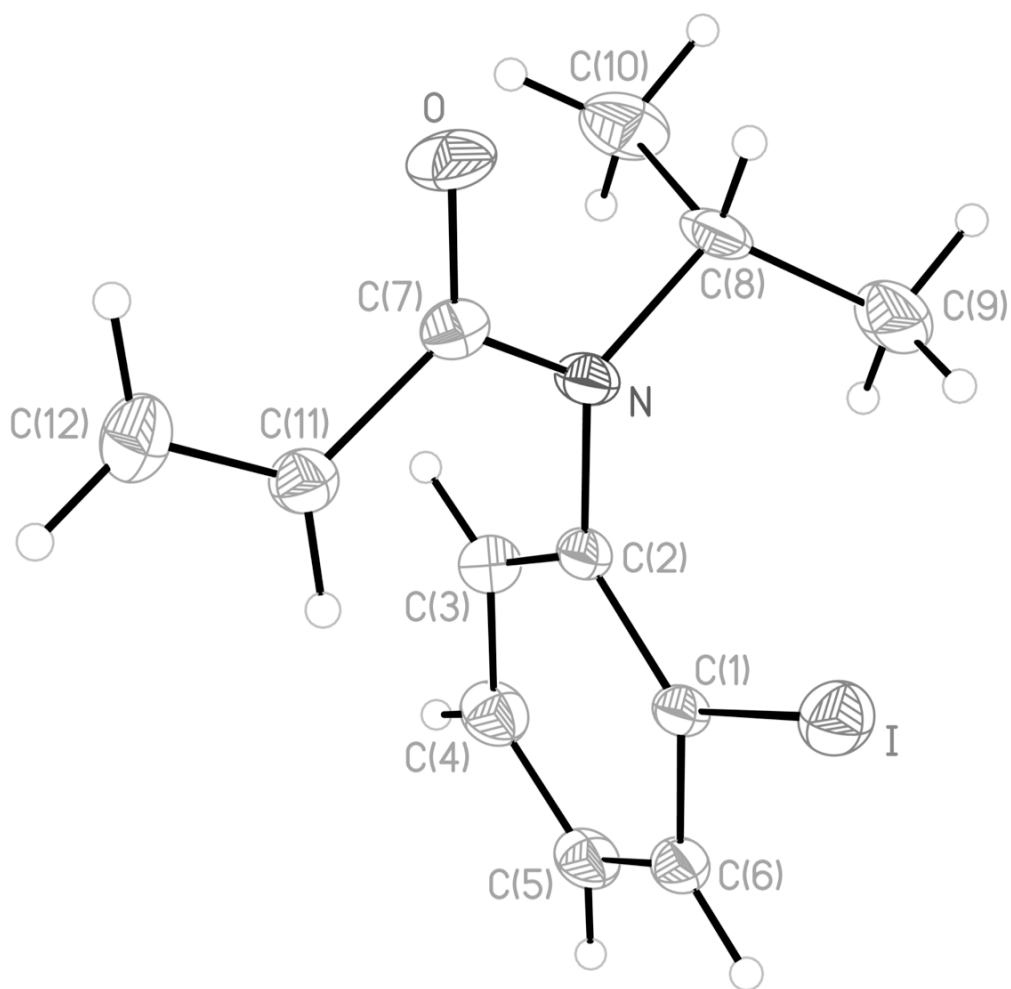


Figure 7.4 - ORTEP of (M)-112

The corresponding CIF file for (M)-112 is found below, between the lines of '+' symbols.

```

+++++
data_al428

_audit_creation_method          SHELXL-97
_chemical_name_systematic
;
?
;
_chemical_name_common           ?
_chemical_melting_point         ?
_chemical_formula_moiety        ?
_chemical_formula_sum           'C12 H14 I N O'
_chemical_formula_weight        315.14

loop_
  _atom_type_symbol

```

```

_atom_type_description
_atom_type_scatter_dispersion_real
_atom_type_scatter_dispersion_imag
_atom_type_scatter_source
'C' 'C' 0.0033 0.0016
'International Tables Vol C Tables 4.2.6.8 and 6.1.1.4'
'H' 'H' 0.0000 0.0000
'International Tables Vol C Tables 4.2.6.8 and 6.1.1.4'
'N' 'N' 0.0061 0.0033
'International Tables Vol C Tables 4.2.6.8 and 6.1.1.4'
'O' 'O' 0.0106 0.0060
'International Tables Vol C Tables 4.2.6.8 and 6.1.1.4'
'I' 'I' -0.4742 1.8119
'International Tables Vol C Tables 4.2.6.8 and 6.1.1.4'

_symmetry_cell_setting Monoclinic
_symmetry_space_group_name_H-M P2(1)

loop_
_symmetry_equiv_pos_as_xyz
'x, y, z'
'-x, y+1/2, -z'

_cell_length_a 7.0983(7)
_cell_length_b 11.0402(12)
_cell_length_c 8.6438(9)
_cell_angle_alpha 90.00
_cell_angle_beta 112.212(2)
_cell_angle_gamma 90.00
_cell_volume 627.12(11)
_cell_formula_units_Z 2
_cell_measurement_temperature 100(2)
_cell_measurement_reflns_used 7181
_cell_measurement_theta_min 0.00
_cell_measurement_theta_max 0.00

_exptl_crystal_description ?
_exptl_crystal_colour ?
_exptl_crystal_size_max 0.32
_exptl_crystal_size_mid 0.24
_exptl_crystal_size_min 0.22
_exptl_crystal_density_meas 0
_exptl_crystal_density_diffraction 1.669
_exptl_crystal_density_method 'not measured'
_exptl_crystal_F_000 308
_exptl_absorption_coefficient_mu 2.529
_exptl_absorption_correction_type none
_exptl_absorption_correction_T_min 0.4983
_exptl_absorption_correction_T_max 0.6062
_exptl_absorption_process_details ?

_exptl_special_details
;
?
;

_diffraction_ambient_temperature 100(2)
_diffraction_radiation_wavelength 0.71073

```

```

_diffrn_radiation_type           MoK\alpha
_diffrn_radiation_source         'fine-focus sealed tube'
_diffrn_radiation_monochromator   graphite
_diffrn_measurement_device_type  'CCD area detector'
_diffrn_measurement_method       'phi and omega scans'
_diffrn_detector_area_resol_mean ?
_diffrn_standards_number         ?
_diffrn_standards_interval_count ?
_diffrn_standards_interval_time  ?
_diffrn_standards_decay_%        ?
_diffrn_reflns_number            7969
_diffrn_reflns_av_R_equivalents  0.0195
_diffrn_reflns_av_sigmaI/netI    0.0283
_diffrn_reflns_limit_h_min       -10
_diffrn_reflns_limit_h_max       10
_diffrn_reflns_limit_k_min       -16
_diffrn_reflns_limit_k_max       16
_diffrn_reflns_limit_l_min       -13
_diffrn_reflns_limit_l_max       12
_diffrn_reflns_theta_min         2.55
_diffrn_reflns_theta_max         32.49
_reflns_number_total             4296
_reflns_number_gt                4169
_reflns_threshold_expression      >2sigma(I)

_computing_data_collection       'Bruker SMART'
_computing_cell_refinement       'Bruker SMART'
_computing_data_reduction        'Bruker SAINT'
_computing_structure_solution    'SHELXS-97 (Sheldrick, 1990)'
_computing_structure_refinement  'SHELXL-97 (Sheldrick, 1997)'
_computing_molecular_graphics    'Bruker SHELXTL'
_computing_publication_material  'Bruker SHELXTL'

```

```
_refine_special_details
```

```
;
```

Refinement of F^2 against ALL reflections. The weighted R-factor wR and goodness of fit S are based on F^2 , conventional R-factors R are based on F , with F set to zero for negative F^2 . The threshold expression of $F^2 > 2\sigma(F^2)$ is used only for calculating R-factors(gt) etc. and is not relevant to the choice of reflections for refinement. R-factors based on F^2 are statistically about twice as large as those based on F , and R-factors based on ALL data will be even larger.

```
;
```

```

_refine_ls_structure_factor_coef  Fsqd
_refine_ls_matrix_type           full
_refine_ls_weighting_scheme       calc
_refine_ls_weighting_details
'calc w=1/[\s^2^(Fo^2^)+(0.0414P)^2^+0.0000P] where P=(Fo^2^+2Fc^2^)/3'
_atom_sites_solution_primary     direct
_atom_sites_solution_secondary   difmap
_atom_sites_solution_hydrogens   geom
_refine_ls_hydrogen_treatment    mixed
_refine_ls_extinction_method     none
_refine_ls_extinction_coef       ?
_refine_ls_abs_structure_details
'Flack H D (1983), Acta Cryst. A39, 876-881'
_refine_ls_abs_structure_Flack    0.00(2)

```



```

_atom_site_aniso_U_11
_atom_site_aniso_U_22
_atom_site_aniso_U_33
_atom_site_aniso_U_23
_atom_site_aniso_U_13
_atom_site_aniso_U_12
I 0.02712(8) 0.02363(8) 0.02876(8) -0.00226(10) 0.00872(6) 0.00017(11)
O 0.0245(10) 0.0381(12) 0.0170(8) 0.0040(8) -0.0015(7) -0.0004(8)
N 0.0138(9) 0.0273(11) 0.0173(9) 0.0017(8) 0.0036(7) 0.0001(8)
C1 0.0131(10) 0.0296(13) 0.0157(10) -0.0018(9) 0.0043(8) 0.0001(8)
C2 0.0138(9) 0.0262(12) 0.0152(10) -0.0003(9) 0.0046(8) 0.0010(8)
C3 0.0212(11) 0.0255(12) 0.0227(11) -0.0017(9) 0.0069(10) -0.0009(9)
C4 0.0236(12) 0.0311(14) 0.0265(13) 0.0050(11) 0.0070(10) 0.0053(10)
C5 0.0184(11) 0.0380(16) 0.0188(11) 0.0047(10) 0.0040(9) 0.0052(10)
C6 0.0172(10) 0.0324(13) 0.0169(10) -0.0014(9) 0.0061(9) -0.0004(9)
C7 0.0204(11) 0.0233(12) 0.0179(10) -0.0001(9) 0.0042(9) -0.0002(9)
C8 0.0101(9) 0.0373(15) 0.0262(12) 0.0019(11) 0.0044(9) -0.0007(9)
C9 0.0235(13) 0.065(3) 0.0351(16) -0.0028(16) 0.0170(13) -0.0051(14)
C10 0.0236(13) 0.0370(18) 0.048(2) -0.0010(15) 0.0102(13) -0.0091(12)
C11 0.0211(11) 0.0271(13) 0.0198(11) 0.0000(10) 0.0068(9) -0.0016(10)
C12 0.0368(16) 0.0318(16) 0.0248(13) -0.0009(10) 0.0158(12) -0.0010(12)

```

_geom_special_details

```

;
All esds (except the esd in the dihedral angle between two l.s. planes)
are estimated using the full covariance matrix. The cell esds are taken
into account individually in the estimation of esds in distances, angles
and torsion angles; correlations between esds in cell parameters are only
used when they are defined by crystal symmetry. An approximate (isotropic)
treatment of cell esds is used for estimating esds involving l.s. planes.
;

```

```

loop_
  _geom_bond_atom_site_label_1
  _geom_bond_atom_site_label_2
  _geom_bond_distance
  _geom_bond_site_symmetry_2
  _geom_bond_publ_flag
I C1 2.103(3) . ?
O C7 1.233(3) . ?
N C7 1.362(3) . ?
N C2 1.438(3) . ?
N C8 1.487(3) . ?
C1 C6 1.389(4) . ?
C1 C2 1.396(4) . ?
C2 C3 1.394(4) . ?
C3 C4 1.389(4) . ?
C3 H3 0.9500 . ?
C4 C5 1.386(5) . ?
C4 H4 0.9500 . ?
C5 C6 1.387(4) . ?
C5 H5 0.9500 . ?
C6 H6 0.9500 . ?
C7 C11 1.491(4) . ?
C8 C9 1.523(5) . ?
C8 C10 1.525(5) . ?
C8 H8 1.0000 . ?
C9 H9A 0.9800 . ?

```

C9 H9B 0.9800 . ?
C9 H9C 0.9800 . ?
C10 H10A 0.9800 . ?
C10 H10B 0.9800 . ?
C10 H10C 0.9800 . ?
C11 C12 1.323(4) . ?
C11 H11 0.9500 . ?
C12 H12A 0.9500 . ?
C12 H12B 0.9500 . ?

loop_

_geom_angle_atom_site_label_1
_geom_angle_atom_site_label_2
_geom_angle_atom_site_label_3
_geom_angle
_geom_angle_site_symmetry_1
_geom_angle_site_symmetry_3
_geom_angle_publ_flag
C7 N C2 122.6(2) . . ?
C7 N C8 118.3(2) . . ?
C2 N C8 118.7(2) . . ?
C6 C1 C2 120.4(3) . . ?
C6 C1 I 119.1(2) . . ?
C2 C1 I 120.39(18) . . ?
C3 C2 C1 119.0(2) . . ?
C3 C2 N 119.3(2) . . ?
C1 C2 N 121.7(2) . . ?
C4 C3 C2 120.5(3) . . ?
C4 C3 H3 119.7 . . ?
C2 C3 H3 119.7 . . ?
C5 C4 C3 119.9(3) . . ?
C5 C4 H4 120.1 . . ?
C3 C4 H4 120.1 . . ?
C4 C5 C6 120.2(3) . . ?
C4 C5 H5 119.9 . . ?
C6 C5 H5 119.9 . . ?
C5 C6 C1 119.9(3) . . ?
C5 C6 H6 120.0 . . ?
C1 C6 H6 120.0 . . ?
O C7 N 121.6(3) . . ?
O C7 C11 121.3(3) . . ?
N C7 C11 117.1(2) . . ?
N C8 C9 111.9(2) . . ?
N C8 C10 110.9(3) . . ?
C9 C8 C10 111.6(3) . . ?
N C8 H8 107.4 . . ?
C9 C8 H8 107.4 . . ?
C10 C8 H8 107.4 . . ?
C8 C9 H9A 109.5 . . ?
C8 C9 H9B 109.5 . . ?
H9A C9 H9B 109.5 . . ?
C8 C9 H9C 109.5 . . ?
H9A C9 H9C 109.5 . . ?
H9B C9 H9C 109.5 . . ?
C8 C10 H10A 109.5 . . ?
C8 C10 H10B 109.5 . . ?
H10A C10 H10B 109.5 . . ?
C8 C10 H10C 109.5 . . ?

```

H10A C10 H10C 109.5 . . ?
H10B C10 H10C 109.5 . . ?
C12 C11 C7 121.3(3) . . ?
C12 C11 H11 119.3 . . ?
C7 C11 H11 119.3 . . ?
C11 C12 H12A 120.0 . . ?
C11 C12 H12B 120.0 . . ?
H12A C12 H12B 120.0 . . ?

```

```

_diffrn_measured_fraction_theta_max    0.967
_diffrn_reflns_theta_full              32.49
_diffrn_measured_fraction_theta_full   0.967
_refine_diff_density_max                1.911
_refine_diff_density_min               -0.702
_refine_diff_density_rms               0.115

```

+++++

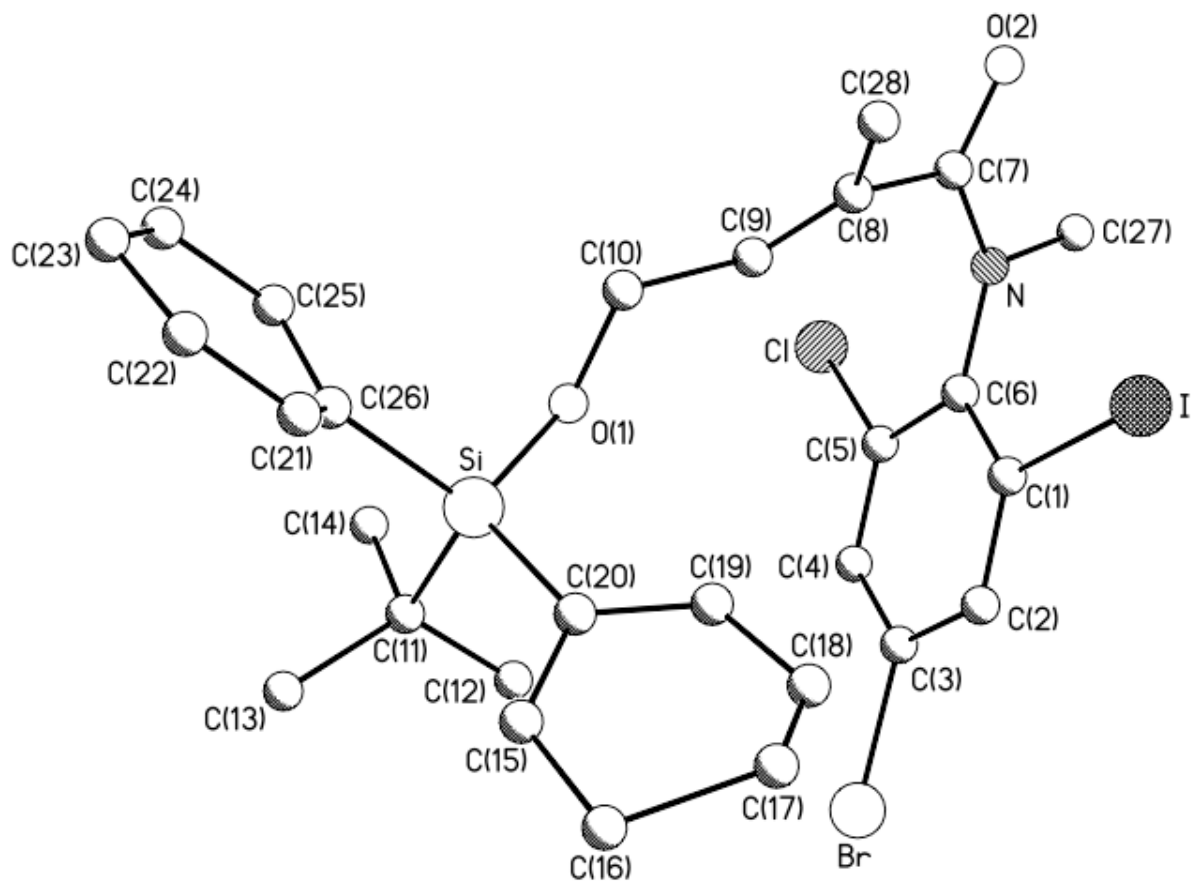


Figure 7.5 - ORTEP of *rac*-164

The corresponding CIF file for *rac*-164 is found below, between the lines of '+' symbols.

+++++

data_andrel

_audit_creation_method SHELXL-97

```

_chemical_name_systematic
;
?
;
_chemical_name_common          ?
_chemical_melting_point        ?
_chemical_formula_moiety       ?
_chemical_formula_sum
'C28 H30 Br Cl I N O2 Si'
_chemical_formula_weight       682.88

loop_
  _atom_type_symbol
  _atom_type_description
  _atom_type_scatter_dispersion_real
  _atom_type_scatter_dispersion_imag
  _atom_type_scatter_source
  'C' 'C' 0.0033 0.0016
  'International Tables Vol C Tables 4.2.6.8 and 6.1.1.4'
  'H' 'H' 0.0000 0.0000
  'International Tables Vol C Tables 4.2.6.8 and 6.1.1.4'
  'Br' 'Br' -0.2901 2.4595
  'International Tables Vol C Tables 4.2.6.8 and 6.1.1.4'
  'Cl' 'Cl' 0.1484 0.1585
  'International Tables Vol C Tables 4.2.6.8 and 6.1.1.4'
  'I' 'I' -0.4742 1.8119
  'International Tables Vol C Tables 4.2.6.8 and 6.1.1.4'
  'N' 'N' 0.0061 0.0033
  'International Tables Vol C Tables 4.2.6.8 and 6.1.1.4'
  'O' 'O' 0.0106 0.0060
  'International Tables Vol C Tables 4.2.6.8 and 6.1.1.4'
  'Si' 'Si' 0.0817 0.0704
  'International Tables Vol C Tables 4.2.6.8 and 6.1.1.4'

_symmetry_cell_setting          Monoclinic
_symmetry_space_group_name_H-M P2(1)

loop_
  _symmetry_equiv_pos_as_xyz
  'x, y, z'
  '-x, y+1/2, -z+1/2'
  '-x, -y, -z'
  'x, -y-1/2, z-1/2'

_cell_length_a                  14.9577(13)
_cell_length_b                  8.6493(8)
_cell_length_c                  24.7343(18)
_cell_angle_alpha               90.00
_cell_angle_beta                108.827(4)
_cell_angle_gamma               90.00
_cell_volume                    3028.8(4)
_cell_formula_units_Z           4
_cell_measurement_temperature    295(2)
_cell_measurement_reflns_used   3527
_cell_measurement_theta_min     2.51
_cell_measurement_theta_max     21.05

_exptl_crystal_description      ?

```

```

_exptl_crystal_colour          ?
_exptl_crystal_size_max       0.25
_exptl_crystal_size_mid       0.08
_exptl_crystal_size_min       0.08
_exptl_crystal_density_meas    0
_exptl_crystal_density_diffn   1.498
_exptl_crystal_density_method  'not measured'
_exptl_crystal_F_000          1360
_exptl_absorpt_coefficient_mu  2.528
_exptl_absorpt_correction_type none
_exptl_absorpt_correction_T_min 0.5706
_exptl_absorpt_correction_T_max 0.8233
_exptl_absorpt_process_details ?

_exptl_special_details
;
?
;

_diffn_ambient_temperature     295(2)
_diffn_radiation_wavelength    0.71073
_diffn_radiation_type          MoK\alpha
_diffn_radiation_source        'fine-focus sealed tube'
_diffn_radiation_monochromator  graphite
_diffn_measurement_device_type  'CCD area detector'
_diffn_measurement_method      'phi and omega scans'
_diffn_detector_area_resol_mean ?
_diffn_standards_number        ?
_diffn_standards_interval_count ?
_diffn_standards_interval_time ?
_diffn_standards_decay_%       ?
_diffn_reflns_number           23683
_diffn_reflns_av_R_equivalents 0.1084
_diffn_reflns_av_sigmaI/netI   0.0932
_diffn_reflns_limit_h_min      -17
_diffn_reflns_limit_h_max      17
_diffn_reflns_limit_k_min      -10
_diffn_reflns_limit_k_max      10
_diffn_reflns_limit_l_min      -29
_diffn_reflns_limit_l_max      29
_diffn_reflns_theta_min        1.44
_diffn_reflns_theta_max        25.00
_reflns_number_total           5342
_reflns_number_gt              2978
_reflns_threshold_expression    >2sigma(I)

_computing_data_collection      'Bruker SMART'
_computing_cell_refinement      'Bruker SMART'
_computing_data_reduction       'Bruker SAINT'
_computing_structure_solution   'SHELXS-97 (Sheldrick, 1990)'
_computing_structure_refinement 'SHELXL-97 (Sheldrick, 1997)'
_computing_molecular_graphics   'Bruker SHELXTL'
_computing_publication_material 'Bruker SHELXTL'

_refine_special_details
;
Refinement of F2 against ALL reflections. The weighted R-factor wR and
goodness of fit S are based on F2, conventional R-factors R are based

```

on F , with F set to zero for negative F^2 . The threshold expression of $F^2 > 2\sigma(F^2)$ is used only for calculating R-factors(gt) etc. and is not relevant to the choice of reflections for refinement. R-factors based on F^2 are statistically about twice as large as those based on F , and R-factors based on ALL data will be even larger.

;

```

_refine_ls_structure_factor_coef Fsqd
_refine_ls_matrix_type full
_refine_ls_weighting_scheme calc
_refine_ls_weighting_details
'calc w=1/[\s^2^(Fo^2^)+(0.0780P)^2^+0.0000P] where P=(Fo^2^+2Fc^2^)/3'
_atom_sites_solution_primary direct
_atom_sites_solution_secondary difmap
_atom_sites_solution_hydrogens geom
_refine_ls_hydrogen_treatment mixed
_refine_ls_extinction_method none
_refine_ls_extinction_coef ?
_refine_ls_number_reflns 5342
_refine_ls_number_parameters 316
_refine_ls_number_restraints 0
_refine_ls_R_factor_all 0.2076
_refine_ls_R_factor_gt 0.1444
_refine_ls_wR_factor_ref 0.3800
_refine_ls_wR_factor_gt 0.3673
_refine_ls_goodness_of_fit_ref 2.315
_refine_ls_restrained_S_all 2.315
_refine_ls_shift/su_max 0.061
_refine_ls_shift/su_mean 0.006

```

loop_

```

_atom_site_label
_atom_site_type_symbol
_atom_site_fract_x
_atom_site_fract_y
_atom_site_fract_z
_atom_site_U_iso_or_equiv
_atom_site_adp_type
_atom_site_occupancy
_atom_site_symmetry_multiplicity
_atom_site_calc_flag
_atom_site_refinement_flags
_atom_site_disorder_assembly
_atom_site_disorder_group
I I 0.45188(11) 0.22816(18) 0.01639(8) 0.0907(7) Uani 1 1 d . . .
Br Br 0.14257(16) -0.1818(2) 0.01288(13) 0.0926(9) Uani 1 1 d . . .
Cl Cl 0.0542(2) 0.4273(4) -0.06221(18) 0.0436(10) Uani 1 1 d . . .
Si Si 0.2199(3) 0.2505(6) 0.2070(2) 0.0518(13) Uani 1 1 d . . .
N N 0.2731(9) 0.4549(16) -0.0329(6) 0.049(4) Uani 1 1 d . . .
O1 O 0.2104(9) 0.3591(15) 0.1518(5) 0.065(3) Uani 1 1 d . . .
C1 C 0.3112(11) 0.1873(18) 0.0020(7) 0.043(4) Uani 1 1 d . . .
C2 C 0.2798(12) 0.041(2) 0.0093(7) 0.052(5) Uani 1 1 d . . .
H2A H 0.3230 -0.0395 0.0216 0.063 Uiso 1 1 calc R . .
O2 O 0.3562(9) 0.6759(13) -0.0093(5) 0.063(3) Uani 1 1 d . . .
C3 C 0.1825(16) 0.013(2) -0.0018(8) 0.063(5) Uani 1 1 d . . .
C4 C 0.1181(12) 0.127(2) -0.0224(8) 0.054(5) Uani 1 1 d . . .
H4A H 0.0537 0.1083 -0.0317 0.065 Uiso 1 1 calc R . .
C5 C 0.1519(12) 0.2715(17) -0.0289(7) 0.050(4) Uani 1 1 d . . .

```

C6 C 0.2465(11) 0.3064(16) -0.0208(7) 0.044(4) Uani 1 1 d . . .
C7 C 0.3235(11) 0.563(2) 0.0069(8) 0.049(4) Uani 1 1 d . . .
C8 C 0.3389(12) 0.5401(17) 0.0679(8) 0.051(5) Uani 1 1 d . . .
C9 C 0.2763(14) 0.4937(19) 0.0870(8) 0.059(5) Uani 1 1 d . . .
H9A H 0.2201 0.4680 0.0588 0.070 Uiso 1 1 calc R . .
C10 C 0.2735(16) 0.470(2) 0.1492(8) 0.069(6) Uani 1 1 d . . .
H10A H 0.3359 0.4413 0.1739 0.083 Uiso 1 1 calc R . .
H10B H 0.2566 0.5671 0.1631 0.083 Uiso 1 1 calc R . .
C11 C 0.0950(15) 0.153(3) 0.1888(10) 0.083(7) Uani 1 1 d . . .
C12 C 0.083(2) 0.053(4) 0.1387(14) 0.157(14) Uani 1 1 d . . .
H12A H 0.0220 0.0034 0.1286 0.235 Uiso 1 1 calc R . .
H12B H 0.1314 -0.0235 0.1474 0.235 Uiso 1 1 calc R . .
H12C H 0.0859 0.1151 0.1071 0.235 Uiso 1 1 calc R . .
C13 C 0.0821(19) 0.085(4) 0.2430(12) 0.129(11) Uani 1 1 d . . .
H13A H 0.0212 0.0372 0.2336 0.194 Uiso 1 1 calc R . .
H13B H 0.0865 0.1668 0.2701 0.194 Uiso 1 1 calc R . .
H13C H 0.1304 0.0101 0.2592 0.194 Uiso 1 1 calc R . .
C14 C 0.029(2) 0.275(6) 0.1693(17) 0.27(3) Uani 1 1 d . . .
H14A H -0.0338 0.2343 0.1592 0.409 Uiso 1 1 calc R . .
H14B H 0.0385 0.3221 0.1364 0.409 Uiso 1 1 calc R . .
H14C H 0.0385 0.3503 0.1990 0.409 Uiso 1 1 calc R . .
C15 C 0.3362(14) -0.003(2) 0.2568(10) 0.080(6) Uani 1 1 d . . .
H15A H 0.3049 0.0023 0.2837 0.096 Uiso 1 1 calc R . .
C16 C 0.405(2) -0.126(3) 0.2633(15) 0.161(18) Uani 1 1 d . . .
H16A H 0.4201 -0.2049 0.2905 0.193 Uiso 1 1 calc R . .
C17 C 0.450(2) -0.096(6) 0.211(2) 0.20(3) Uani 1 1 d . . .
H17A H 0.5049 -0.1483 0.2129 0.236 Uiso 1 1 calc R . .
C18 C 0.420(3) -0.019(5) 0.1753(14) 0.16(2) Uani 1 1 d . . .
H18A H 0.4366 -0.0289 0.1424 0.189 Uiso 1 1 calc R . .
C19 C 0.3591(18) 0.088(3) 0.1787(11) 0.093(7) Uani 1 1 d . . .
H19A H 0.3460 0.1632 0.1504 0.112 Uiso 1 1 calc R . .
C20 C 0.3143(12) 0.104(2) 0.2160(9) 0.057(5) Uani 1 1 d . . .
C21 C 0.3246(18) 0.358(3) 0.3193(9) 0.082(7) Uani 1 1 d . . .
H21A H 0.3667 0.2785 0.3197 0.099 Uiso 1 1 calc R . .
C22 C 0.341(2) 0.451(4) 0.3647(10) 0.112(10) Uani 1 1 d . . .
H22A H 0.3920 0.4274 0.3966 0.135 Uiso 1 1 calc R . .
C23 C 0.290(2) 0.573(3) 0.3681(14) 0.100(9) Uani 1 1 d . . .
H23A H 0.2988 0.6307 0.4012 0.120 Uiso 1 1 calc R . .
C24 C 0.232(3) 0.601(3) 0.322(2) 0.136(13) Uani 1 1 d . . .
H24A H 0.2012 0.6956 0.3211 0.164 Uiso 1 1 calc R . .
C25 C 0.1993(16) 0.513(3) 0.2687(12) 0.105(10) Uani 1 1 d . . .
H25A H 0.1519 0.5451 0.2359 0.127 Uiso 1 1 calc R . .
C26 C 0.2483(13) 0.378(2) 0.2733(8) 0.057(5) Uani 1 1 d . . .
C27 C 0.2559(14) 0.492(2) -0.0931(8) 0.066(5) Uani 1 1 d . . .
H27A H 0.2214 0.4089 -0.1164 0.100 Uiso 1 1 calc R . .
H27B H 0.3151 0.5054 -0.0998 0.100 Uiso 1 1 calc R . .
H27C H 0.2197 0.5855 -0.1025 0.100 Uiso 1 1 calc R . .
C28 C 0.4379(14) 0.587(3) 0.1069(10) 0.086(7) Uani 1 1 d . . .
H28A H 0.4426 0.5685 0.1460 0.129 Uiso 1 1 calc R . .
H28B H 0.4483 0.6942 0.1016 0.129 Uiso 1 1 calc R . .
H28C H 0.4846 0.5260 0.0975 0.129 Uiso 1 1 calc R . .

loop_
_atom_site_aniso_label
_atom_site_aniso_U_11
_atom_site_aniso_U_22
_atom_site_aniso_U_33
_atom_site_aniso_U_23

```

  _atom_site_aniso_U_13
  _atom_site_aniso_U_12
I 0.0728(11) 0.0825(12) 0.1171(15) -0.0095(9) 0.0308(9) 0.0003(8)
Br 0.0731(16) 0.0433(12) 0.168(3) 0.0157(13) 0.0472(16) -0.0016(9)
Cl 0.032(2) 0.0166(17) 0.072(3) 0.0099(17) 0.0037(18) 0.0018(14)
Si 0.047(3) 0.067(3) 0.042(3) 0.004(2) 0.017(2) 0.002(2)
N 0.038(8) 0.063(9) 0.049(10) 0.004(7) 0.016(7) -0.010(7)
O1 0.058(8) 0.072(9) 0.068(9) 0.021(7) 0.024(7) -0.003(6)
C1 0.039(9) 0.042(9) 0.042(10) -0.011(7) 0.002(8) -0.010(7)
C2 0.041(11) 0.055(11) 0.057(12) -0.003(8) 0.011(9) 0.024(8)
O2 0.074(9) 0.053(8) 0.068(9) 0.023(6) 0.034(7) -0.003(6)
C3 0.095(17) 0.044(11) 0.048(12) -0.008(9) 0.020(11) -0.001(10)
C4 0.043(10) 0.053(11) 0.064(12) 0.005(9) 0.015(9) 0.011(8)
C5 0.047(11) 0.029(9) 0.064(12) 0.005(8) 0.003(9) 0.012(7)
C6 0.042(10) 0.023(8) 0.052(10) -0.002(7) -0.003(8) -0.002(7)
C7 0.043(10) 0.056(11) 0.049(12) 0.009(9) 0.017(8) -0.015(8)
C8 0.046(11) 0.033(9) 0.073(14) 0.000(8) 0.020(10) -0.015(7)
C9 0.060(13) 0.048(11) 0.057(13) -0.029(9) 0.003(10) -0.001(9)
C10 0.097(16) 0.066(13) 0.040(12) 0.001(9) 0.016(11) -0.025(11)
C11 0.071(15) 0.086(16) 0.079(17) 0.009(13) 0.007(12) -0.020(12)
C12 0.12(3) 0.24(4) 0.12(3) -0.08(3) 0.04(2) -0.04(2)
C13 0.11(2) 0.16(3) 0.11(2) 0.040(19) 0.027(18) -0.051(19)
C14 0.07(2) 0.54(9) 0.18(4) 0.07(5) 0.02(2) 0.18(4)
C15 0.054(13) 0.080(15) 0.080(16) -0.009(13) -0.014(11) 0.008(11)
C16 0.10(2) 0.087(18) 0.17(3) -0.024(18) -0.12(2) 0.040(15)
C17 0.059(19) 0.34(7) 0.19(4) -0.22(5) 0.04(3) -0.02(3)
C18 0.21(5) 0.15(3) 0.07(2) 0.02(2) -0.01(2) 0.09(3)
C19 0.094(18) 0.098(19) 0.092(19) -0.020(14) 0.037(16) 0.013(14)
C20 0.048(11) 0.069(13) 0.053(12) -0.007(10) 0.015(10) 0.009(9)
C21 0.12(2) 0.078(15) 0.051(14) -0.012(12) 0.030(14) 0.022(13)
C22 0.14(3) 0.13(3) 0.046(15) -0.001(16) -0.003(15) -0.06(2)
C23 0.11(2) 0.071(19) 0.11(2) 0.004(16) 0.016(19) -0.003(16)
C24 0.12(3) 0.08(2) 0.25(5) -0.02(3) 0.12(3) 0.002(19)
C25 0.064(15) 0.103(19) 0.14(2) -0.074(18) 0.020(14) 0.018(12)
C26 0.051(12) 0.072(12) 0.046(12) -0.004(9) 0.015(10) -0.004(9)
C27 0.076(14) 0.076(13) 0.047(13) 0.001(10) 0.019(10) -0.026(10)
C28 0.067(14) 0.084(16) 0.087(16) -0.028(12) -0.002(12) -0.024(11)

```

```

_geom_special_details

```

```

;
```

All esds (except the esd in the dihedral angle between two l.s. planes) are estimated using the full covariance matrix. The cell esds are taken into account individually in the estimation of esds in distances, angles and torsion angles; correlations between esds in cell parameters are only used when they are defined by crystal symmetry. An approximate (isotropic) treatment of cell esds is used for estimating esds involving l.s. planes.

```

;
```

```

loop_

```

```

  _geom_bond_atom_site_label_1

```

```

  _geom_bond_atom_site_label_2

```

```

  _geom_bond_distance

```

```

  _geom_bond_site_symmetry_2

```

```

  _geom_bond_publ_flag

```

```

I C1 2.049(16) . ?

```

```

Br C3 1.861(18) . ?

```

```

Cl C5 1.963(15) . ?

```

```

Si O1 1.626(13) . ?

```

Si C20 1.856(18) . ?
Si C26 1.908(19) . ?
Si C11 1.97(2) . ?
N C7 1.39(2) . ?
N C6 1.406(18) . ?
N C27 1.46(2) . ?
O1 C10 1.36(2) . ?
C1 C2 1.38(2) . ?
C1 C6 1.40(2) . ?
C2 C3 1.41(2) . ?
C2 H2A 0.9300 . ?
O2 C7 1.217(17) . ?
C3 C4 1.36(2) . ?
C4 C5 1.38(2) . ?
C4 H4A 0.9300 . ?
C5 C6 1.40(2) . ?
C7 C8 1.46(2) . ?
C8 C9 1.24(2) . ?
C8 C28 1.54(2) . ?
C9 C10 1.56(3) . ?
C9 H9A 0.9300 . ?
C10 H10A 0.9700 . ?
C10 H10B 0.9700 . ?
C11 C14 1.42(4) . ?
C11 C12 1.47(3) . ?
C11 C13 1.53(3) . ?
C12 H12A 0.9600 . ?
C12 H12B 0.9600 . ?
C12 H12C 0.9600 . ?
C13 H13A 0.9600 . ?
C13 H13B 0.9600 . ?
C13 H13C 0.9600 . ?
C14 H14A 0.9600 . ?
C14 H14B 0.9600 . ?
C14 H14C 0.9600 . ?
C15 C20 1.33(3) . ?
C15 C16 1.46(3) . ?
C15 H15A 0.9300 . ?
C16 C17 1.66(6) . ?
C16 H16A 0.9300 . ?
C17 C18 1.08(7) . ?
C17 H17A 0.9300 . ?
C18 C19 1.32(4) . ?
C18 H18A 0.9300 . ?
C19 C20 1.31(3) . ?
C19 H19A 0.9300 . ?
C21 C22 1.34(3) . ?
C21 C26 1.34(3) . ?
C21 H21A 0.9300 . ?
C22 C23 1.32(4) . ?
C22 H22A 0.9300 . ?
C23 C24 1.21(4) . ?
C23 H23A 0.9300 . ?
C24 C25 1.47(5) . ?
C24 H24A 0.9300 . ?
C25 C26 1.36(3) . ?
C25 H25A 0.9300 . ?
C27 H27A 0.9600 . ?

C27 H27B 0.9600 . ?
C27 H27C 0.9600 . ?
C28 H28A 0.9600 . ?
C28 H28B 0.9600 . ?
C28 H28C 0.9600 . ?

loop_

_geom_angle_atom_site_label_1
_geom_angle_atom_site_label_2
_geom_angle_atom_site_label_3
_geom_angle
_geom_angle_site_symmetry_1
_geom_angle_site_symmetry_3
_geom_angle_publ_flag
O1 Si C20 110.6(8) . . ?
O1 Si C26 108.8(8) . . ?
C20 Si C26 110.0(8) . . ?
O1 Si C11 103.7(8) . . ?
C20 Si C11 111.4(10) . . ?
C26 Si C11 112.2(9) . . ?
C7 N C6 126.1(14) . . ?
C7 N C27 116.9(13) . . ?
C6 N C27 116.6(14) . . ?
C10 O1 Si 125.0(12) . . ?
C2 C1 C6 120.5(14) . . ?
C2 C1 I 120.5(12) . . ?
C6 C1 I 118.7(11) . . ?
C1 C2 C3 120.2(14) . . ?
C1 C2 H2A 119.9 . . ?
C3 C2 H2A 119.9 . . ?
C4 C3 C2 120.6(17) . . ?
C4 C3 Br 119.9(16) . . ?
C2 C3 Br 119.5(14) . . ?
C3 C4 C5 117.5(17) . . ?
C3 C4 H4A 121.3 . . ?
C5 C4 H4A 121.3 . . ?
C4 C5 C6 125.0(14) . . ?
C4 C5 C1 114.8(12) . . ?
C6 C5 C1 119.6(11) . . ?
C5 C6 N 120.7(13) . . ?
C5 C6 C1 115.8(14) . . ?
N C6 C1 123.4(14) . . ?
O2 C7 N 119.2(16) . . ?
O2 C7 C8 120.2(16) . . ?
N C7 C8 120.5(14) . . ?
C9 C8 C7 123.2(17) . . ?
C9 C8 C28 122(2) . . ?
C7 C8 C28 114.3(16) . . ?
C8 C9 C10 132.7(18) . . ?
C8 C9 H9A 113.7 . . ?
C10 C9 H9A 113.7 . . ?
O1 C10 C9 112.1(15) . . ?
O1 C10 H10A 109.2 . . ?
C9 C10 H10A 109.2 . . ?
O1 C10 H10B 109.2 . . ?
C9 C10 H10B 109.2 . . ?
H10A C10 H10B 107.9 . . ?
C14 C11 C12 105(3) . . ?

C14 C11 C13 108(3) . . ?
 C12 C11 C13 120(2) . . ?
 C14 C11 Si 105(2) . . ?
 C12 C11 Si 107.3(18) . . ?
 C13 C11 Si 110.0(15) . . ?
 C11 C12 H12A 109.5 . . ?
 C11 C12 H12B 109.5 . . ?
 H12A C12 H12B 109.5 . . ?
 C11 C12 H12C 109.5 . . ?
 H12A C12 H12C 109.5 . . ?
 H12B C12 H12C 109.5 . . ?
 C11 C13 H13A 109.5 . . ?
 C11 C13 H13B 109.5 . . ?
 H13A C13 H13B 109.5 . . ?
 C11 C13 H13C 109.5 . . ?
 H13A C13 H13C 109.5 . . ?
 H13B C13 H13C 109.5 . . ?
 C11 C14 H14A 109.4 . . ?
 C11 C14 H14B 109.5 . . ?
 H14A C14 H14B 109.5 . . ?
 C11 C14 H14C 109.5 . . ?
 H14A C14 H14C 109.5 . . ?
 H14B C14 H14C 109.5 . . ?
 C20 C15 C16 126(3) . . ?
 C20 C15 H15A 117.0 . . ?
 C16 C15 H15A 117.0 . . ?
 C15 C16 C17 104(3) . . ?
 C15 C16 H16A 127.9 . . ?
 C17 C16 H16A 128.0 . . ?
 C18 C17 C16 125(4) . . ?
 C18 C17 H17A 117.6 . . ?
 C16 C17 H17A 117.4 . . ?
 C17 C18 C19 119(5) . . ?
 C17 C18 H18A 120.4 . . ?
 C19 C18 H18A 120.4 . . ?
 C20 C19 C18 130(3) . . ?
 C20 C19 H19A 115.1 . . ?
 C18 C19 H19A 115.1 . . ?
 C19 C20 C15 114(2) . . ?
 C19 C20 Si 122.0(18) . . ?
 C15 C20 Si 123.9(17) . . ?
 C22 C21 C26 120(2) . . ?
 C22 C21 H21A 119.8 . . ?
 C26 C21 H21A 119.8 . . ?
 C23 C22 C21 126(3) . . ?
 C23 C22 H22A 117.1 . . ?
 C21 C22 H22A 117.1 . . ?
 C24 C23 C22 111(3) . . ?
 C24 C23 H23A 124.5 . . ?
 C22 C23 H23A 124.5 . . ?
 C23 C24 C25 132(3) . . ?
 C23 C24 H24A 114.1 . . ?
 C25 C24 H24A 114.1 . . ?
 C26 C25 C24 111(3) . . ?
 C26 C25 H25A 124.6 . . ?
 C24 C25 H25A 124.5 . . ?
 C21 C26 C25 118.2(19) . . ?
 C21 C26 Si 123.2(15) . . ?

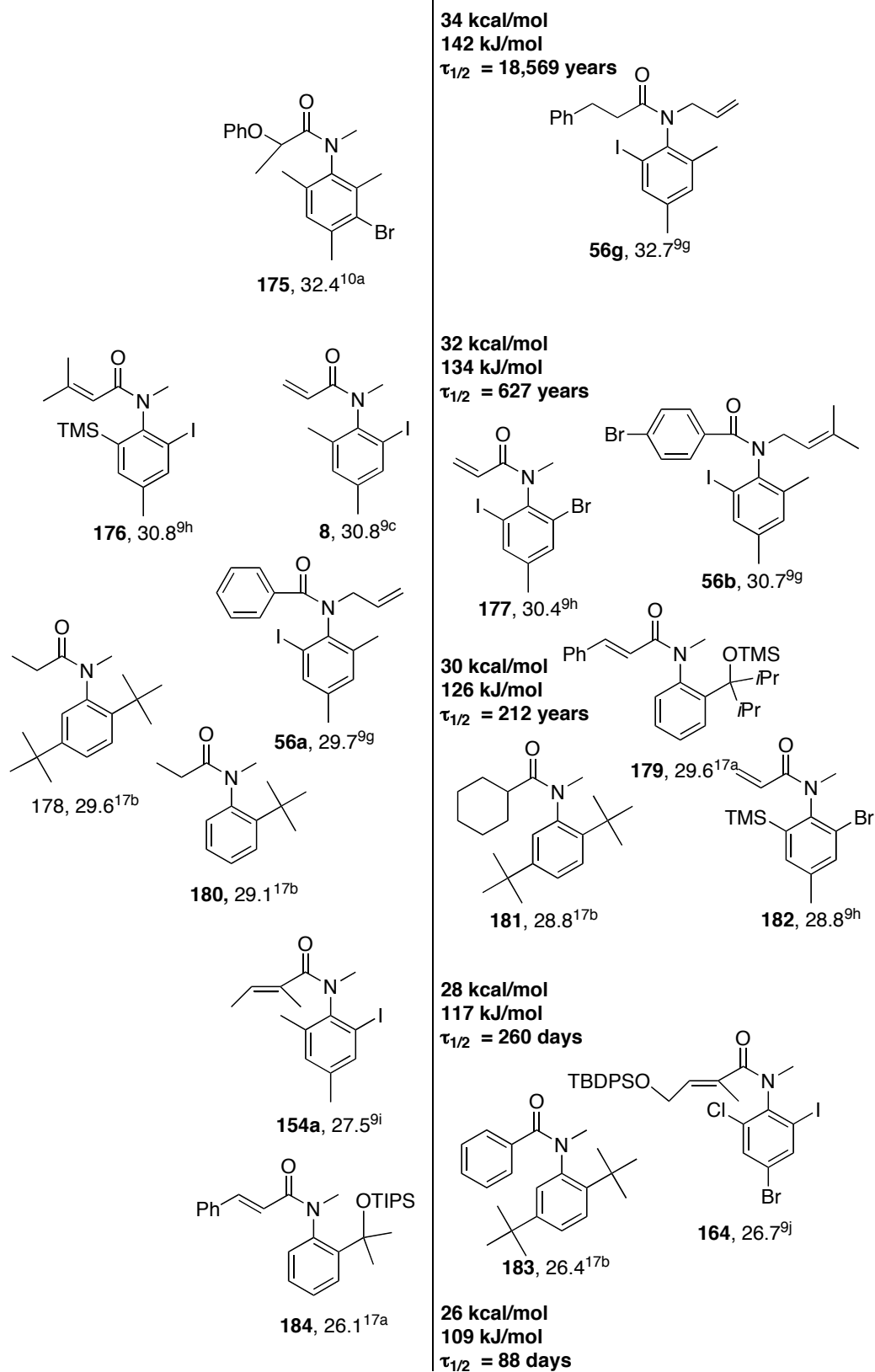
C25 C26 Si 117.3(16) . . ?
N C27 H27A 109.5 . . ?
N C27 H27B 109.5 . . ?
H27A C27 H27B 109.5 . . ?
N C27 H27C 109.5 . . ?
H27A C27 H27C 109.5 . . ?
H27B C27 H27C 109.5 . . ?
C8 C28 H28A 109.5 . . ?
C8 C28 H28B 109.5 . . ?
H28A C28 H28B 109.5 . . ?
C8 C28 H28C 109.5 . . ?
H28A C28 H28C 109.5 . . ?
H28B C28 H28C 109.5 . . ?

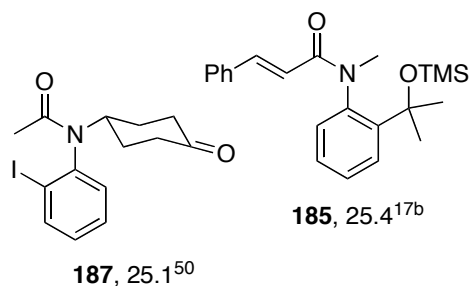
_diffn_measured_fraction_theta_max 1.000
_diffn_refl_theta_full 25.00
_diffn_measured_fraction_theta_full 1.000
_refine_diff_density_max 2.577
_refine_diff_density_min -1.750
_refine_diff_density_rms 0.248

+++++

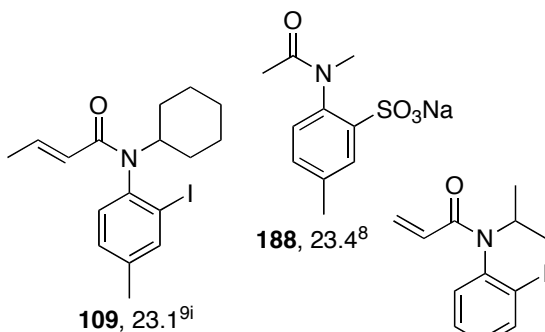
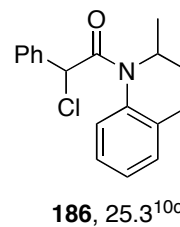
APPENDIX

N-Aryl Rotation Barriers
($\tau_{1/2}$ at 23 °C)

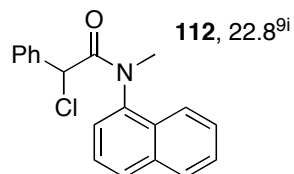
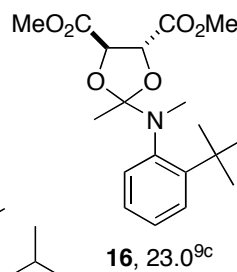




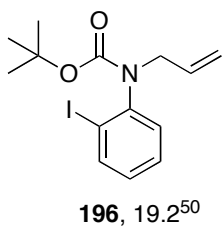
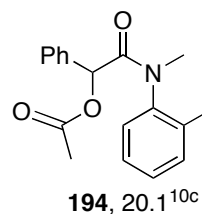
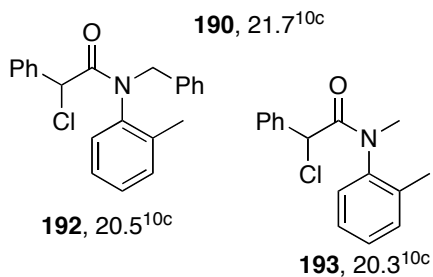
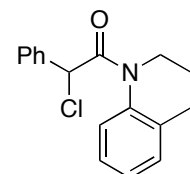
26 kcal/mol
109 kJ/mol
 $\tau_{1/2} = 88$ days



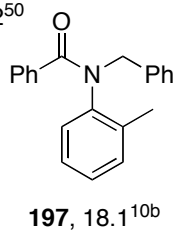
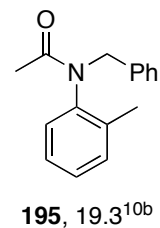
24 kcal/mol
100 kJ/mol
 $\tau_{1/2} = 7$ hours



22 kcal/mol
92 kJ/mol
 $\tau_{1/2} = 14$ minutes



20 kcal/mol
84 kJ/mol
 $\tau_{1/2} = 29$ seconds



18 kcal/mol
75 kJ/mol
 $\tau_{1/2} = 986$ milliseconds

BIBLIOGRAPHY

- ¹ Eliel, E. L.; Wilen, S. H. in *Stereochemistry of Organic Compounds*; Wiley-Interscience: New York, **1994**, p 1119.
- ² *ibid*, p 1193.
- ³ Christie, G. H.; Kenner, J. J. *J. Chem. Soc.* **1922**, 614–620.
- ⁴ Oki, M. *Top. Stereochem.* **1983**, *14*, 1–76.
- ⁵ Pedersen, B. F.; Pedersen, B. *Tetrahedron Lett.* **1956**, 2995–3001.
- ⁶ (a) Boeyens, J. C. A.; Denner, L.; Painter, S.; Staskun, B. S. *Afr. J. Chem.* **1987**, *40*, 60–64. (b) Solans, X.; Miravittles, C.; Gali, S.; Plans, F. *Crystal. Struct. Commun.* **1977**, *6*, 351–357. (c) Pedersen, B. F. *Acta Chem. Scand.* **1967**, *21*, 1415–1424. (d) Singh, P.; Ahmed, F. R. *Acta Crystallogr., Sect. B* **1969**, *25*, 1901–1910. (e) Saito, S.; Toriumi, Y.; Tomioka, N.; Itai, A. *J. Org. Chem.* **1995**, *60*, 4715–4720.
- ⁷ Adams, R.; Yuan, H. C. *Chem. Rev.* **1933**, *12*, 261–338.
- ⁸ Mills, W. H.; Kelham, R. M. *J. Chem. Soc.* **1937**, 274–278.
- ⁹ (a) Curran, D. P.; Qi, H.; Geib, S. J.; DeMello, N. C. *J. Am. Chem. Soc.* **1994**, *116*, 3131–3132. (b) Curran, D. P.; Geib, S.; DeMello, N. *Tetrahedron* **1999**, *55*, 5681–5704. (c) Curran, D. P.; Liu, W. D.; Chen, C. H.-T. *J. Am. Chem. Soc.* **1999**, *121*, 11012–11013. (d) Kondru, R. K.; Chen, C. H. T.; Curran, D. P.; Beratan, D. N.; Wipf, P. *Tetrahedron: Asymmetry* **1999**, *10*, 4143–4150. (e) Ates, A.; Curran, D. P. *J. Am. Chem. Soc.* **2001**, *123*, 5130–5131. (f) Terauchi, J.; Curran, D. P. *Tetrahedron: Asymmetry* **2003**, *14*, 587–592. (g) Curran, D. P.; Chen, C. H.-T.; Geib, S. J.; Lapierre, A. J. B. *Tetrahedron*, **2004**, *60*, 4413–4424. (h) Petit, M.; Geib, S. J.; Curran, D. P. *Tetrahedron* **2004**, *60*, 7543–7552. (i) Petit, M.; Lapierre, A. J. B.; Curran, D. P. *J. Am. Chem. Soc.* **2005**, *127*, 14994–14995. (j) Andre Lapierre, unpublished results.
- ¹⁰ (a) Siddall III, T. H. *Tetrahedron Lett.* **1965**, *6*, 4515–4522. (b) Price, B. J.; Eggleston, J. A.; Sutherland, I. O. *J. Chem. Soc. B* **1967**, 922–925. (c) Siddall III, T. H.; Stewart, W. E. *J. Phys. Chem.* **1969**, *73*, 40–46.
- ¹¹ (a) Price, B. J.; Eggleston, J. A.; Sutherland, I. O. *J. Chem. Soc. B* **1967**, 922–925. (b) Shvo, Y.; Taylor, E. C.; Mislow, K.; Raban, M. *J. Am. Chem. Soc.* **1967**, *89*, 4910–4917.
- ¹² (a) Kitagawa, O.; Izawa, H.; Taguchi, T.; Shiro, M. *Tetrahedron Lett.* **1997**, *38*, 4447–4450. (b) Kitagawa, O.; Izawa, H.; Sato, K.; Dobashi, A.; Taguchi, T.; Shiro, M. *J. Org. Chem.* **1998**, *63*, 2634–2640.
- ¹³ (a) Hughes, A. D.; Simpkins, N. S. *Synlett* **1998**, 967–968. (b) Hughes, A. D.; Price, D. A.; Simpkins, N. S. *J. Chem. Soc., Perkin Trans. 1* **1999**, 1295–1304.
- ¹⁴ (a) Hata, T.; Koide, H.; Taniguchi, N.; Uemura, M. *Org. Lett.* **2000**, *2*, 1907–1910. (b) Hata, T.; Koide, H.; Uemura, M. *Synlett* **2000**, 1145–1147. Koide, H.; (c) Hata, T.; Uemura, M. *J. Org. Chem.* **2002**, *67*, 1929–1935. (d) Koide, H.; Hata, T.; Yoshihara, K.; Kamikawa, K.; Uemura, M. *Tetrahedron* **2004**, *20*, 4527–4541.
- ¹⁵ Kitagawa, O.; Kohriyama, M.; Taguchi, T. *J. Org. Chem.* **2002**, *67*, 8682–8684.
- ¹⁶ Kitagawa, O.; Takahashi, M.; Yoshikawa, M.; Taguchi, T. *J. Am. Chem. Soc.* **2005**, *127*, 3676–3677.
- ¹⁷ (a) Cass, Q. B.; Degani, A. L. G.; Tiritan, M. E.; Matlin, S. A.; Curran, D. P.; Balog, A. *Chirality* **1997**, *9*, 109–112. (b) Curran, D. P.; Hale, G. R.; Geib, S. J.; Balog, A.; Cass, Q. B.;

- Degani, A. L. G.; Hernandez, M. Z.; Freitas, L. C. G. *Tetrahedron: Asymmetry* **1997**, *8*, 3955–3975.
- ¹⁸ Pirkle, W. H.; Welch, C. J. *Tetrahedron: Asymmetry* **1994**, *5*, 777–780.
- ¹⁹ (a) Leuchs, H. *Ber.* **1913**, *46*, 2435–2443. (b) Leuchs, H. *Ber.* **1915**, *48*, 1015–1020.
- ²⁰ Ronteix, M. J.; Marquet, A. *Tetrahedron Lett.* **1966**, *7*, 5801–5806.
- ²¹ Seebach, D.; Wasmuth, D. *Angew. Chem. Int. Ed.* **1981**, *20*, 971.
- ²² Kawabata, T.; Yahiro, K.; Fuji, K. *J. Am. Chem. Soc.* **1991**, *113*, 9694–9696.
- ²³ Kawabata, T.; Wirth, T.; Yahiro, K.; Suzuki, H.; Fuji, K. *J. Am. Chem. Soc.* **1994**, *116*, 10809–10810.
- ²⁴ Fuji, K.; Kawabata, T. *Chem. Eur. J.* **1998**, *4*, 373–376.
- ²⁵ New Oxford American Dictionary
- ²⁶ (a) Kawabata, T.; Fuji, K. In *Topics in Stereochemistry*, Vol. 23; Denmark, S. E., Ed.; John Wiley & Sons: New York, **2003**, 175–205. (b) Zhao, H. W.; Hsu, D. C.; Carlier, P. R. *Synthesis* **2005**, 1–16.
- ²⁷ Schmalz, H.-G.; de Koning, C. B.; Bernicke, D.; Siegel, S.; Pfletschinger, A. *Angew. Chem. Int. Ed.* **1999**, *38*, 1620–1623.
- ²⁸ (a) Giese, B.; Wettstein, P.; Stahelin, C.; Barbosa, F.; Neuburger, M.; Zehnder, M.; Wessig, P. *Angew. Chem., Int. Ed.* **1999**, *38*, 2586–2587. (b) Seiler, M.; Schumacher, A.; Lindemann, U.; Barbosa, F.; Giese, B. *Synlett* **1999**, 1588–1590. (c) Sinicropi, A.; Barbosa, F.; Basosi, R.; Giese, B.; Olivucci, M. *Angew. Chem. Int. Ed.* **2005**, *44*, 2390–2393.
- ²⁹ Kochi, J. K. *Adv. Free Radical Chem.* **1975**, *5*, 189–317.
- ³⁰ (a) Buckmelter, A. J.; Powers, J. P.; Rychnovsky, S. D. *J. Am. Chem. Soc.* **1998**, *120*, 5589–5590. (b) Buckmelter, A. J.; Kim, A. I.; Rychnovsky, S. D. *J. Am. Chem. Soc.* **2000**, *122*, 9386–9390. (c) Rychnovsky, S. D.; Hata, T.; Kim, A. I.; Buckmelter, A. J. *Org. Lett.* **2001**, *3*, 807–810. (d) Dalgard, J. E.; Rychnovsky, S. D. *Org. Lett.* **2004**, *6*, 2713–2716.
- ³¹ Christine H.-T. Chen. In *Transfer of Chirality in Asymmetric Radical Cyclizations* M. Sc. thesis, University of Pittsburgh, 2000.
- ³² Giese, B.; Kopping, B.; Göbel, T.; Dickhaut, J.; Thoma, G.; Kulicke, K. J.; Trach, F. in *Organic Reactions*, Vol. 48, John Wiley & Sons: New York, **1996**, p 301–856.
- ³³ Miura, K.; Ichinose, Y.; Nozaki, K.; Oshima, K.; Utimoto, K. *Bull. Chem. Soc. Jpn.* **1989**, *62*, 143–147.
- ³⁴ Bowman, W. R.; Heaney, H.; Jordan, B. M. *Tetrahedron Lett.* **1988**, *29*, 6657–6660.
- ³⁵ Dittami, J. P.; Ramanathan, H. *Tetrahedron Lett.* **1988**, *29*, 45–48.
- ³⁶ Jones, K.; Storey, J. M. D. *J. Chem. Soc., Chem. Commun.* **1992**, 1766–1767.
- ³⁷ (a) Togo, H.; Kikuchi, O. *Tetrahedron Lett.* **1988**, *29*, 4133–4137. (b) Togo, H.; Kikuchi, O. *Heterocycles* **1989**, *28*, 373–381. (c) Jones, K.; Wilkinson, J.; Ewin, R. *Tetrahedron Lett.* **1994**, *35*, 7673–7676. (d) Brunton, S. A.; Jones, K. *J. Chem. Soc., Perkin Trans. 1* **2000**, 763–768. (e) Ozaki, S.; Matsushita, H.; Ohmori, H. *J. Chem. Soc., Perkin Trans. 1* **1993**, 2339–2344. (f) Ishibashi, H.; Kobayashi, T.; Machida, N.; Tamura, O. *Tetrahedron* **2000**, *56*, 1469–1473. (g) Munusamy, R.; Dhathathreyan, K. S.; Balasubramanian, K. K.; Venkatachalam, C. S. *J. Chem. Soc., Perkin Trans. 2* **2001**, 1154–1166. (h) Ganguly, A.; Wang, C. H.; David, M.; Bartner, P.; Chan, T. M. *Tetrahedron Lett.* **2002**, *43*, 6865–6868.
- ³⁸ Similar preferences are seen for reactions on the *N*-acyl side of many anilide radicals. See: (a) Curran, D. P.; Abraham, A. C. *Tetrahedron* **1993**, *49*, 4821–4840. (b) Beckwith, A. L. J.; Storey,

- J. M. D. *J. Chem. Soc., Chem. Commun.* **1995**, 977–978. (c) Ganguly, A. K.; Wang, C. H.; Chan, T. M.; Ing, Y. H.; Buevich, A. V. *Tetrahedron Lett.* **1989**, *30*, 2657–2660.
- ³⁹ Curran, D. P.; Demello, N. C. *J. Chem. Soc., Chem. Commun.* **1993**, 1314–1317.
- ⁴⁰ Ha, C.; Horner, J. H.; Newcomb, M.; Varick, T. R.; Arnold, B. R.; Luszytk, J. *J. Org. Chem.* **1993**, *58*, 1194–1198.
- ⁴¹ (a) Sibi, M. P.; Manyem, S.; Zimmerman, S. *Chem. Rev.* **2003**, *103*, 3263–3295. (b) Bar, G.; Parsons, A. F. *Chem. Soc. Rev.* **2003**, *32*, 251–263. (c) Curran, D. P.; Porter, N. A.; Giese, B. in *Stereochemistry of Radical Reactions: Concepts, Guidelines and Synthetic Applications*, **1996**, VCH: Weinheim.
- ⁴² Porter, N. A.; Giese, B.; Curran, D. P. *Acc. Chem. Res.* **1991**, *24*, 296–304.
- ⁴³ Porter, N. A.; Lacher, B.; Chang, V. H.; Magmin, D. R. *J. Am. Chem. Soc.* **1989**, *111*, 8309–8310.
- ⁴⁴ (a) Whitesell, J. K. *Chem. Rev.* **1989**, *89*, 1581–1590.
- ⁴⁵ Jones, K.; Wilkinson, J. *J. Chem. Soc., Chem. Comm.* **1992**, *24*, 1767–1769.
- ⁴⁶ Jones, K.; McCarthy, C. *Tetrahedron Lett.* **1989**, *30*, 2657–2660.
- ⁴⁷ Marti, C.; Carreira, E.; *Eur. J. Org. Chem.* **2003**, 2209–2219.
- ⁴⁸ Lindley, J. *Tetrahedron* **1984**, *40*, 1433–1456.
- ⁴⁹ Ma, D.; Zhang, H. *Org. Lett.* **2003**, *5*, 2453–2455.
- ⁵⁰ (a) Barluenga, J.; González, J. M.; García-Martín, M. A.; Campos, P. J.; *Tetrahedron Lett.* **1993**, *34*, 3893–3896. (b) Barluenga, J.; González, J. M.; García-Martín, M. A.; Campos, P. J.; Asensio, G. *J. Org. Chem.* **1993**, *58*, 2058–2060.
- ⁵¹ Adler, T.; Bonjoch, J.; Clayden, J.; Font-Bardia, M.; Pickworth, M.; Solans, X.; Solé, D.; Vallverdú, L. *Org. Biomol. Chem.* **2005**, *3*, 3173–3183.
- ⁵² Mizoroki, T.; Mori, K.; Ozaki, A. *Bull. Chem. Soc. Jpn.* **1971**, *44*, 581.
- ⁵³ Heck, R. F.; Nolley, J. P. *J. Org. Chem.* **1972**, *14*, 2320–2322.
- ⁵⁴ (a) Patel, P. A.; Ziegler, C. B.; Ziegler, Plevyak, J. E.; Zebovitz, T. C.; Terpko, M.; Heck, R. F. *J. Org. Chem.*, **1977**, *42*, 3903–3907. (b) Ziegler, C. B.; Heck, R. F. *J. Org. Chem.* **1978**, *43*, 2941–2946. (c) Heck, R. F. *Organic React.* **1982**, *27*, 345.
- ⁵⁵ Sato, Y.; Sodeoka, M.; Shibasaki, M. *J. Org. Chem.* **1989**, *54*, 4738 – 4739.
- ⁵⁶ (a) Sato, Y.; Watanabe, S.; Shibasaki, M. *Tetrahedron Lett.* **1992**, *33*, 2589 – 2592. (b) Kojima, A.; Boden, C. D. J.; Shibasaki, M. *Tetrahedron Lett.* **1997**, *38*, 3459 – 3460. (c) Sato, Y.; Sodeoka, M.; Shibasaki, M. *Chem. Lett.* **1990**, 1953 – 1954.
- ⁵⁷ Sato, Y.; Honda, T.; Shibasaki, M. *Tetrahedron Lett.* **1992**, *33*, 2593 – 2596.
- ⁵⁸ (a) Nukui, S.; Sodeoka, M.; Shibasaki, M. *Tetrahedron Lett.* **1993**, *34*, 4965 – 4968. (b) Sato, Y.; Nukui, S.; Sodeoka, M.; Shibasaki, M. *Tetrahedron* **1994**, *50*, 371 – 382.
- ⁵⁹ (a) Kagechika, K.; Shibasaki, M. *J. Org. Chem.* **1991**, *56*, 4093 – 4094. (b) Kagechika, K.; Oshima, T.; Shibasaki, M. *Tetrahedron* **1993**, *49*, 1773 – 1782.
- ⁶⁰ Carpenter, N. E.; Kucera, D. J.; Overman, L. E. *J. Org. Chem.* **1989**, *54*, 5846–5848.
- ⁶¹ (a) Ashimori, A.; Overman, L. E. *J. Org. Chem.* **1992**, *57*, 4571–4572. (b) Ashimori, A.; Matsuura, T.; Overman, L. E.; Poon, D. J. *J. Org. Chem.* **1993**, *58*, 6949–6951.
- ⁶² (a) Ashimori, A.; Bachand, B.; Overman, L. E.; Poon, D. J. *J. Am. Chem. Soc.* **1998**, *120*, 6477 – 6487. (b) Ashimori, A.; Bachand, B.; Calter, M. A.; Govek, S. P.; Overman, L. E.; Poon, D. J. *J. Am. Chem. Soc.* **1998**, *120*, 6488 – 6499.
- ⁶³ Jutand, A.; Mosleh, A. *Organometallics* **1995**, *14*, 1810–1817.

-
- ⁶⁴ Stambuli, J. P.; Stauffer, S. R.; Shaughnessy, K. H.; Hartwig, J. F. *J. Am. Chem. Soc.* **2001**, *123*, 2677–2678.
- ⁶⁵ Unpublished results, Marc Petit.
- ⁶⁶ Takano, S.; Ogasawara, K. In *The Alkaloids*; Brossi, A., Ed.; Academic: New York, 1989; Vol. 36, pp 224–251.
- ⁶⁷ Node, M.; Itoh, A.; Masaki, Y.; Fuji, K. *Heterocycles* **1991**, *32*, 1705–1707.
- ⁶⁸ Zumburn, A.; Uebelhart, P.; Eugster, C. H. *Helv. Chim. Acta* **1985**, *68*, 1519–1539.
- ⁶⁹ Artman III, G. D.; Weinreib, S. M. *Org. Lett.* **2003**, *5*, 1523–1526.
- ⁷⁰ Sakamoto, M.; Takahashi, M.; Fujita, T.; Watanabe, S.; Nishio, T.; Iiad, I.; Aoyama, H. *J. Org. Chem.* **1997**, *62*, 6298–6308.
- ⁷¹ Beckwith, A. L. J.; Goh, S. H. *J. Chem. Soc., Chem. Comm.* **1983**, 905–906.
- ⁷² (a) Luo, W.; Yu, Q.-S.; Zhan, M.; Parrish, D.; Deschamps, J. R.; Kulkarni, S. S.; Holloway, H. W.; Alley, G. M.; Lahiri, D. K.; Brossi, A.; Greig, N. H. *J. Med. Chem.* **2005**, *48*, 986–994. (b) Yu, Q.-S.; Attack, J. R.; Rapoport, S. I.; Brossi, A. *J. Med. Chem.* **1998**, *31*, 2297–2300. (c) Tanaka, K.; Taniguchi, T.; Ogasawara, K. *Tetrahedron Lett.* **2001**, *42*, 1049–1048.
- ⁷³ Kosynkin, D. V.; Tour, J. M. *Org. Lett.* **2001**, *3*, 991–992.
- ⁷⁴ Yang, S.-C.; Chung, W.-H. *Ind. J. Chem. Sect. B.* **1999**, *38*, 897–904.
- ⁷⁵ Odle, R.; Blevins, B. *J. Org. Chem.* **1980**, *45*, 2709–2710.
- ⁷⁶ Curran, D. P.; Chang, C. T. *J. Org. Chem.* **1989**, *54*, 3140–3157.
- ⁷⁷ (a) Procedure adapted from Ezquerra J.; Pedregal, C.; Lamas, C.; Barluenga, J.; Pérez, M.; García-Martín, M. A.; González, J. M. *J. Org. Chem.* **1996**, *61*, 5804–5812. (b) This compound has been previously synthesized.
- ⁷⁸ Procedure adapted from: Parlow, J. J.; Stevens, A. M.; Stegeman, R. A.; Stallings, W. C.; Kurumbail, R. G.; South, M. S. *J. Med. Chem.*, **2003**, *46*, 4297–4312.
- ⁷⁹ This compound has been previously synthesized: Reddy, T. J.; Leclair, M.; Proulx, M. *Synlett* **2005**, *4*, 583–586.
- ⁸⁰ Sy, W.-W. *Synth. Comm.* **1992**, *22*, 3215–3219.
- ⁸¹ Roche, D.; Prasad, K.; Repic, O.; Blacklock, T. J. *Tetrahedron Lett.*, **2000**, *41*, 2083–2085.
- ⁸² Artman, G. D.; Weinreib, S. M. *Org. Lett.* **2003**, *5*, 1523–1526.
- ⁸³ Eliel, E. L.; Wilen, S. H. In *Stereochemistry of Organic Compounds*; Wiley-Interscience: New York, 1994, p 54.